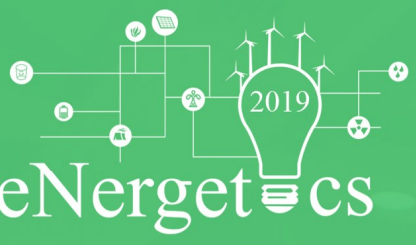

Proceedings of the 5th Jubilee Virtual International Conference on Science, Technology and Management in Energy

Editors:
Stajić, Z. and Velimirović, L. Z.

Publishers:
Research and Development Center
"ALFATEC", Niš, Serbia
Complex System Research Center, Niš, Serbia

Serbia, Niš, October 28-29, 2019

Editors
Stajić, Z.
Velimirović, L. Z.

eNergetics 2019

5th Jubilee Virtual International Conference on Science, Technology and Management in Energy

Proceedings

Publishers
Research and Development Center “ALFATEC”, Niš, Serbia
Complex System Research Centre, Niš, Serbia

Serbia, Niš, October 28-29, 2019

Proceedings of the
5th Jubilee Virtual International Conference
on Science Technology and Management in Energy

Serbia, Niš, October 28-29, 2019

Editors:
Prof. Dr. Zoran Stajić and Dr. Lazar Z. Velimirović

Technical Editor:
Dr. Petar Vranić

Published by:
Research and Development Center “ALFATEC”, Niš, Serbia, and
Complex System Research Centre, Niš, Serbia

Printed by:
Blue Copy, Niš, Serbia

Number of copies printed: 100
The publishing year: 2019

Printing of this edition has been financially supported by
Serbian Ministry of Education, Science and Technological Development

ISBN 978-86-80616-04-9

CIP - Каталогизација у публикацији
Народна библиотека Србије, Београд

620.9(082)(0.034.2)

VIRTUAL International Conference on Science Technology and Management in Energy (5 ; 2019 ; Niš)
Energetics 2019 [Elektronski izvor] : proceedings / 5th Jubilee Virtual International Conference on Science Technology and Management in Energy, Niš, October 28-29, 2019 ; editors Stajić Z.[Zoran], Velimirović, L.[Lazar] Z. - Niš : Research and Development Centar "Alfatec" : Complex System Research Centre, 2019 (Niš : Blue Copy). - 1 elektronski optički disk (DVD) ; 12 cm

Sistemski zahtevi: Nisu navedeni. - Nasl. sa naslovne strane dokumenta. - Tiraž 100.
- Bibliografija uz svaki rad.

ISBN 978-86-80616-04-9 (RDCA)

a) Енергетика -- Зборници

COBISS.SR-ID 281895180

eNergetics 2019

5th Jubilee Virtual International Conference on Science Technology and Management in Energy

Organizer:
Research and Development Center “ALFATEC”

Co-organizers:

- Mathematical Institute of the Serbian Academy of Sciences and Arts
- Faculty of Technical Sciences, UKLO University St. Climent Ohridski
- Complex System Research Centre
- Academy of Sciences and Arts of the Republika Srpska
- Faculty of Mining and Geology, University of Belgrade

Supported by:
Serbian Ministry of Education, Science and Technological Development

Program Committee

Chair:

Prof. Dr. Zoran Stajić, Faculty of Electronic Engineering, Serbia

Members:

Dr. Lazar Velimirović, Mathematical Institute of the Serbian Academy of Sciences and Arts, Serbia

Prof. Dr. Aleksandar Janjić, Faculty of Electronic Engineering, Serbia

Prof. Dr. Gorazd Stumberger, Faculty of Electrical Engineering and Computer Science, Slovenia

Prof. Dr. Detelin Markov, Faculty of Power Engineering and Power Machines, Bulgaria

Prof. Dr. Marko Serafimov, Faculty of Mechanical Engineering, Macedonia

Prof. Dr. Mileta Janjić, Faculty of Mechanical Engineering, Montenegro

Prof. Dr. Miomir Stanković, Faculty of Occupational Safety, Serbia

Prof. Dr. Enver Agić, Public Enterprise Electric Utility of Bosnia and Herzegovina, Bosnia and Herzegovina

Prof. Dr. Niko Majdandžić, Faculty of Mechanical Engineering, Croatia

Prof. Dr. Serkan Abbasoglu, Cyprus International University, Turkey

Prof. Dr. Bojan Srđević, Faculty of Agriculture, Serbia

Dr. K. Lenin, PVP Siddhartha Institute of Technology, India

Prof. Dr. Abdelhak Djoudi, National Polytechnic School, Algeria

Dr. Elson Avallone, Federal Institute of Education, Science and Technology of São Paulo, Brazil

Prof. Dr. Zdravko Milovanović, Faculty of Mechanical Engineering, Bosnia and Herzegovina

Prof. Dr. Miloš Jelić, Research and Development Center Alfatec, Serbia

Prof. Dr. Zoran Markov, Faculty of Mechanical Engineering, Macedonia

Dr. Sasa Milic, Institute Nikola Tesla, Serbia

Prof. Dr. Krsto Miljanović, Agromediterranean Faculty, Bosnia and Herzegovina

Organizing Committee

Chair:

Prof. Dr. Miomir Stanković, Faculty of Occupational Safety, Serbia

Members:

Prof. Dr. Zoran Stajić, Faculty of Electronic Engineering, Serbia

Dr. Lazar Velimirović, Mathematical Institute of the Serbian Academy of Sciences and Arts, Serbia

Dr. Petar Vranić, Mathematical Institute of the Serbian Academy of Science and Arts, Serbia

M.Sc. Ljubiša Stajić, Research and Development Center "ALFATEC", Serbia

M.Sc. Radmila Janković, Mathematical Institute of the Serbian Academy of Science and Arts, Serbia

M.Sc. Jelena Velimirović, Mathematical Institute of the Serbian Academy of Sciences and Arts, Serbia

M.Sc. Biserka Mijucić, Research and Development Center "ALFATEC", Serbia

M.Sc. Ivana Velickovska, Mathematical Institute of the Serbian Academy of Sciences and Arts, Serbia

Table of Contents

The Marginal Economic Benefits of Centrally Controlled and Maintained Virtual Power Plants

Kurt Walkom, Mark Diesendorf, Benjamin McCoy

UNSW Sydney, Australia, kurt.walkom@unsw.edu.au; m.diesendorf@unsw.edu.au; benjamin.mccoy@student.unsw.edu.au

Abstract — **Virtual power plants (VPPs) are expected to be integral components of nascent, intelligent, large-scale electricity systems, enabling the integration of distributed energy resources (DERs) to form a coalition to trade in wholesale markets, maximize profits and stabilize grids. This investigation develops a new, internationally replicable model to estimate the economic outcome when a central body (e.g. electricity retailer, community organization or utility) owns, deploys, co-ordinates and maintains DERs in a market. Australia's National Electricity Market (NEM) is used as a case study to analyze the marginal economic benefit a body receives when DER systems (i.e. solar array, battery, smart inverter and smart meter) are deployed across multiple locations within the NEM. The analysis shows eight of the ten locations can expect to earn an internal rate of return (IRR) greater than industry benchmarks and have commercial potential. The system's ability to conduct arbitrages by charging and discharging DERs during price peaks and troughs accounts for most of the economic benefit. Wholesale price profiles, wholesale price projections, capital expenditure projections and solar data sets are the inputs with greatest impact on IRR. The maximum IRR that can be attributed to renewable energy support schemes was small, indicating that VPP returns are likely to surpass industry benchmarks even in the absence of direct legislative support.**

Keywords – distributed energy resource, virtual power plant; renewable energy, scenario analysis

I. INTRODUCTION

Virtual power plants (VPPs) are recent innovations that are rapidly attracting global interest due to their ability to trade in wholesale markets by integrating renewable distributed energy resources (DERs) to form a coalition to trade in wholesale markets in a profit-maximizing, system-stabilizing, and sustainable manner [1, 2]. These outcomes far surpass that of passive, independent, and non-market orientated DER operation modes. VPPs have the capacity to significantly impact the generation mix, contribute to building the nascent, intelligent energy infrastructure and supply systems globally, and to progress the international renewable generation agenda [1-3].

A VPP is an aggregation of small generating units of different technologies connected to an electricity distribution network. These operate as a single power plant via central control of the aggregated units [3-5]. VPPs are modular and incremental deployments consist of the following elements: distributed generation (DG) units, energy storage (ES) units, and information and communication systems. This investigation uses the term 'DER system' to refer to one module of a VPP, as illustrated in Fig. 1.

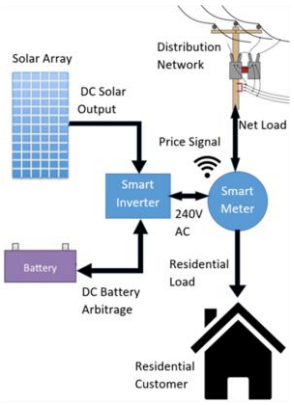

Figure 1. One DER system.

ISBN: 978-86-80616-04-9

VPPs present an opportunity for central bodies such as companies, community organizations and governments to lucratively progress the international renewable generation agenda. There is significant existing literature on the technical optimization of DG systems, determining the optimal schedules, sites, and sizes to reduce losses, improve voltage profiles, and optimize generation [6-13]. Recent literature reviews highlight the many scheduling problems that have been investigated and the associated frameworks developed to solve them, including multi-objective optimization methods [14, 15]. The most common commercial objectives are maximization of self-supply and maximization of market revenue [16].

VPPs are not confined to scholarly literature, they are operational globally [2]. In Australia, at least four VPPs are already operational [17], and pressure from community organizations and the renewable energy industry is encouraging the transition to a more renewable generation mix [18, 19]. There is substantial research into the technical implementation and optimization of VPPs, however, few economic optimizations and no economic implementation models were found during this investigation's literature review.

This investigation is the first study into the marginal economic benefit that a central body could expect if they were to own, deploy, co-ordinate and maintain a VPP. Specifically, this structure studies daily arbitrages by charging and discharging DERs during price troughs and peaks, the purchase of wholesale electricity from the grid, and sales to residential consumers.

This investigation uses Australia's National Electricity Market (NEM) as a test market, and analyses the marginal economic benefit attained when additional DER modules are deployed across each of the six wholesale markets within the NEM. Public institution source data and MATLAB were used to conduct this analysis.

This paper is organized as follows: Section 2 outlines data sources; Section 3 describes the investigation method; Section 4 outlines results; Section 5 discusses results; Section 6 concludes.

II. Data Sources

Location-specific time-varying data sourced from public institution reports was used for this analysis. This data was converted into four seasonal daily profiles, broken into 30-minute intervals for each component of the analysis. Specifically, annual distribution network load profiles, zoned solar irradiance profiles and regional wholesale price profiles were each converted into four representative 24-hour profiles with each profile representing a season. Data sources are tabulated in Table I.

TABLE I. Data Sources

Dataset	**Source**	**Ref.**
Capital costs	CSIRO	[20]
Maintenance costs	CSIRO	[20]
Installation costs	CSIRO	[20]
Load profiles	AEMO	[21]
Irradiance profiles	BOM	[22]
Wholesale price profiles	AEMO	[23]
Wholesale price projections	AEMC	[24]
Transmission network tariffs	AEMC	[24]
Distribution network tariffs	AEMC	[24]
Network tariff projections	NA*	[25]
Daily average residential loads	AEMC	[24]
Annual average load projections	AEMO	[26]

*Legislative uncertainty made network tariff projections difficult to forecast. They were assumed to remain constant.

The analysis was conducted across ten locations which spanned the six wholesale markets within the NEM. The analysis used location-specific datasets, as shown in Table II.

TABLE II. Datasets for each location studied

Location	**Solar Dataset**	**Load Data**	**Market, Price & Network Charge Datasets**
Canberra	Adelaide	ActewAGL	ACT/NSW
Sydney	Adelaide	Ausgrid	NSW
Wagga Wagga	Wagga Wagga	Essential Energy	NSW
Bourke	Rockhampton	Essential Energy	NSW
Brisbane	Rockhampton	Energex	QLD
Longreach	Longreach	Ergon	QLD
Townsville	Townsville	Ergon	QLD
Adelaide	Adelaide	SA Power	SA
Hobart	Cape Grim	Aurora	TAS
Melbourne	Melbourne	Powercor	VIC

III. Method

A. Assumptions

This analysis evaluated DER systems of the following solar array sizes: 2.5kW, 3kW, 3.5kW, 4kW, 4.5kW, 5kW, 7.5kW, 10kW, 15kW and 20kW at each location. The analysis made the assumptions shown in Table III.

In this model, array size determines how much energy is generated by the DER system, and therefore the amount and rate at which energy is exported and/or stored. For simplicity, this analysis has assumed battery sizes and

inverter limits for each system will be determined by array size. This assumption is rational as the minimum charge and discharge capabilities of the battery will need to accommodate power generated by the array [20].

Investigations have shown that solar output can be approximated by including a derating factor that reduces the generation output to account for effects of soiling, wiring losses and nameplate inaccuracies, as well as sub-optimal tilt and azimuth angles if they are not separately accounted for [27, 28]. As this investigation applies a standard system to a variety of locations, optimal tilt and azimuth angles vary and therefore a simplified derating factor is used. When tilt and azimuth were accounted for, the derating factor in Australia was calculated to be 0.92 [28]. When all factors were accounted for in the Carolinas, USA, a derating factor of 0.85 was calculated [27, 28], thus an all-encompassing derating factor of 0.85 is deemed a reasonable assumption for this investigation.

The Australian Commonwealth Scientific and Industrial Research Organisation's (CSIRO) Future Energy Storage Trends Report [20] reviewed the datasheets of a cross-section of available battery systems in 2015. A Li-Ion battery round-trip efficiency of 90% and a depth of discharge of 90% was determined.

This investigation has been conservative in assuming that the DER system lifetime matches the expected warranty of the subcomponents. Therefore, a constant 10-year lifetime for each iteration of DER system analysis is assumed.

The September 2017 LGC spot price was used as the assumed rate of legislative renewable support for the lifetime of this study. LGCs are Large-scale Generation Certificates, Australia's commercial renewable rebate. This assumption predicts legislative support of $82.30/MWh will remain for the proposed system lifetime, regardless of scheme name or jurisdiction.

DER systems used the same components in each location except for the battery sizes, which varied according to the cumulative net surplus solar output. This was determined as the amount of solar energy generated between the time the battery was discharged one morning, until it was discharged in the afternoon, minus the energy consumed by the household during summer. This cumulative amount was then rounded up to the nearest kWh to 'size' the battery, at a specific location for a specific size system. For example, for the Canberra analysis the storage requirement and corresponding battery sizes selected for each system are shown in Table IV.

TABLE III. SYSTEM ASSUMPTIONS

System Component	Assumption
Solar array size	1.5kW – 20kW
Inverter size	1.5kW – 20kW
Battery size	Net energy surplus storage requirement
Battery charge/discharge time	30mins (one interval)
Solar derating factor	0.85 [27, 28]
Battery round-trip efficiency	0.90 [20]
Battery depth of discharge (DoD)	0.9 [20]
DER system warranty	10 years [20]
DER system life	10 years (warranty)
LGC price (Sep 2017)	$82.30/MWh
Yearly maintenance cost	$60 per annum [20]
Installation cost	$400 for <7kWh: function of kWh for >7kWh [20]
Daily average residential load	Regional: 0.460kW – 0.979kW [29]

TABLE IV. ASSUMED BATTERY SIZES FOR CANBERRA

PV and Inverter Size (kW)	Storage Requirement (kWh)	Battery (kWh)
2.5	7.7	8
3	10.5	11
3.5	13.5	14
4	16.5	17
4.5	19.5	20
5	22.5	23
7.5	37.0	38
10	53.5	54
15	84.9	85
20	116.2	117

During a sensitivity analysis, the capital expenditure (CapEx) for a complete DER system, as well as the component standalone ES and standalone PV systems were evaluated for each location. The cashflow assumptions made for each of these are highlighted in Table V.

TABLE V. CAPEX & CASHFLOW ASSUMPTIONS

System Type	CapEx	Cashflows
DER System	PV array, battery, inverter, installation	Wholesale energy exports, transmission and distribution network charge reduction, battery arbitrage, LGCs, ongoing maintenance
PV System	PV array, inverter, installation	Wholesale energy exports, transmission and distribution network charge reduction, LGCs, ongoing maintenance
ES System	Battery, inverter, installation	Battery arbitrage, ongoing maintenance

B. Procedure

The Global and Local Learning Model (GALLM) produced by CSIRO, was used as the basis for CapEx projections ranging from 2017 to 2035. The GALLM is an endogenous technological learning model, that accounts for complex changes in global and local environments. The GALLM projects that PV prices, Li-ion prices, and smart inverter prices will continue to fall due to technological maturity and scale benefits, with the greatest drop being the least mature technology, Li-ion batteries [20]. Projections made by alternative investigations in other jurisdictions, whilst lacking the same robust methodology and proximity to the Australian market, are within the max and min bounds of the GALLM projections [30]. The GALLM also projects no real change in cost of installation or on-going maintenance, as these are largely manual tasks with established processes [20]. This analysis uses the projected minimum, base, and maximum case prices produced by the GALLM as its CapEx projections.

The Australian Energy Market Operator (AEMO) is responsible for conducting the market activities within the NEM. AEMO reports 30-minute interval wholesale price data by state, and 30-minute interval load data by DNSP [23]. AEMO predicts annual average loads and consumption profiles to remain steady over the long term, therefore they were assumed constant from 2016 onwards in this analysis.

The Bureau of Meteorology (BOM) provides national 1-minute interval mean global irradiance levels at key regional centers [22]. For each location, annual data sets were processed and averaged across seasonal 30-minute intervals (2014, 2015 and 2016 data sets when available). For locations where no specific data stations were present, stations in the same solar exposure zone were used. This study considered solar irradiance forecasting as outside its scope. Seasonal mean global irradiance profiles from the BOM were converted into seasonal mean solar output profiles using (1), where PV_{output} is energy output from the system, pv_c is nameplate capacity of the system, I_m is incident solar radiation and 0.85 is the derating factor.

$$PV_{Output} = 0.85 \times pv_c \left(\frac{I_m}{1000 w / m^2} \right) (kW) \ . \quad (1)$$

The value of solar output was calculated by converting 30-minute interval solar output data to kWh, and then multiplying by the corresponding seasonal wholesale price intervals. This data was used to calculate the annual solar output profiles.

The value of LGCs generated were then calculated. An LGC is created each time eligible, low-carbon generation systems produce 1MWh of electricity. For a VPP, this is equal to the cumulative solar output (in MWh) and is calculated by averaging seasonal cumulative daily solar output and multiplying by 365/1000.

Historical average 30-minute spot pricing for each jurisdiction in the NEM is published online by AEMO [23] and FY2016-17 data was used to aggregate a seasonal mean daily wholesale price profile across each region. Wholesale pricing profiles use only FY2016-17 data for two reasons: 1) Material changes in volume-weighted average wholesale price have occurred over the past 3 years; 2) the volatility of the profile would be substantially reduced by averaging data sets. This volatility is critical to approximating the value of the battery arbitrage opportunity. Calculating seasonal mean daily prices by seasonally averaging a year's data still materially reduces the day-to-day volatility of the pricing profile and masks the revenue opportunities presented by extreme movements. The prevalence of these extreme wholesale price peaks has been rising steadily over the past five years in the NEM [31]. Therefore, the economic analysis conducted by this investigation likely understates the financial potential of the battery arbitrage. Regional indexed pricing projections from 2017 to 2037 [24] were used as a proxy for forecasted changes in baseline wholesale electricity prices, as well as volatility. Cash flows from each of the system component elements were adjusted yearly to reflect these projected changes in wholesale prices. A minimum, base and maximum case were analyzed.

As Australia's generation mix progressively contains more wind and solar PV, Australia's electricity supply becomes increasingly variable and so the rising prevalence of extreme price peaks is expected to continue in coming the decade [24]. While increasing volatility was not directly accounted for, regional indexed pricing projections developed by a government-commissioned study [24] were used as a proxy for forecasted changes in baseline electricity prices and volatility. Minimum, maximum and

base case price projections by distribution network region for 2015 to 2037 were made. Cashflows from 2037 onwards were assumed constant for the remaining system lifetime. These projections use the DOGMMA (Distributed On-site Generation Market Model Australia) which is robust, reliable and forms the basis of electricity demand forecasting reports by AEMO and retail competition reports by the Australian Energy Market Commission (AEMC) [24, 29].

In Australia, there is significant legislative uncertainty surrounding transmission and distribution network charges in both the short and long-term [24, 25]. This investigation has therefore used FY2016-17 regional transmission and distribution network charges [24], and has projected these as constant rates throughout the analysis. The value of network charge reductions were calculated, these are dependent on the residential load that is displaced by the solar output, as network charges are priced as cents per kWh. Since solar output and residential load are assumed to be constant over the analysis lifetime for each array size, displaced load and reductions in transmission and distribution network charges are also constant.

After inspection of the mean wholesale price profiles of each region, a morning peak and trough, and an afternoon peak and trough were consistently found. Thus, it was determined that two battery arbitrage cycles (morning and afternoon), where the battery is fully charged at the trough, and fully discharged at the peak, was an appropriate assumption. For each season at each location, both arbitrage cycles were first tested for viability. The morning and/or afternoon price differential (*PD*) had to overcome battery efficiency limits, as well as the distribution network charge (*DNC*) that would be incurred, and is shown by (2), where *RTE* is Round trip efficiency and *DoD* is depth of discharge:

$$\frac{PD}{RTE \times DoD} > DNC \quad . \tag{2}$$

After calculating the threshold limits of the energy arbitrage differential, arbitrage profit was calculated for a stand-alone ES system and for complete DER system (batteries and solar combined). The DER system unlocked greater value as the solar energy supplied did not have to be purchased at the morning minimum and was not subject to the distribution network charge hurdle. Note that any local price minimum followed by local price maximum that creates a price differential larger than the distribution network charge threshold is a potential arbitrage opportunity. Thus, the potential number of arbitrages is restricted only by the frequency that the pricing differential crosses the threshold in a day. The mean calculation of the wholesale price profile and consequent 'double peak' arbitrage method understates the daily volatility of the wholesale price curve. In practice, the arbitrage value realized would likely be larger.

Economic analyses require financial calculations to compare the value of projects over time. Internal rate of return (IRR) was chosen as it allows a company with a set capital budgeting hurdle rate to accept or reject a project, or compare projects competing for the same financial resources. The cashflow re-investment assumption is considered reasonable over the projection timeline as it is unlikely the market would reach saturation. In this case, IRR was used to explicitly benchmark DER system returns against industry return on capital invested for DNSPs (6.2% [25]) and electricity retailers (12% [29]) to determine the commercial viability of the proposed VPP. Payback period was also evaluated because it is industry standard.

MATLAB was used to execute each of these calculations and applied iteratively for each location. Once cashflows were calculated, the IRR and payback periods for commissioned systems in years 2017 to 2035 were calculated for maximum, minimum and base cases. Finally, the analysis assumptions were tested by an iterative process of input assumption variation and result comparison.

IV. Results

Using the assumptions specified in Tables III-V, analyses were conducted for each location. The Canberra IRR analysis results for the complete DER system under base case assumptions are shown in Fig. 2 and the payback period results are shown in Fig. 3.

For each location, IRR and payback period follow consistent trends, specifically IRR increases with system size up to a limit and IRR tends to increase with year commissioned. Thus, representative systems were compared from each location in results tables. Specifically, the following comparative analyses were conducted:

1) IRR and payback period results between locations for 5kW systems were compared. This ranked locations on a yearly basis and highlighted component system values (Table VI).

2) Differences in expected cashflow compositions between locations were compared. This highlights the added value the DER system creates, or the 'system synergy' (Table VII).

The comparative expected return on capital invested for the DER system and its component systems is highlighted in Fig. 4. This figure also details the sources of value for each system.

TABLE VI. IRR RESULTS FOR A REPRESENTATIVE 5KW ARRAY SYSTEM (BASE CASE)

Location	2017 IRR (%)	2035 IRR (%)	Avg. IRR (%)
Longreach	16.7	33.9	28.9
Townsville	15.7	32.3	27.5
Brisbane	13.9	28.7	26.1
Adelaide	17.4	28.7	25.5
Bourke	12.5	28.2	24.1
Canberra	11.5	27.1	23.1
Wagga Wagga	11.0	25.8	21.9
Sydney	11.0	25.6	21.8
Melbourne	3.3	13.1	8.9
Hobart	-2.3	5.1	2.2

TABLE VII. CUMULATIVE SYSTEM REVENUES FOR A REPRESENTATIVE 5KW ARRAY SYSTEM

Location	Average system revenue ($)	Proportion of DER system revenue (% of total)		
		PV System	ES System	Added value
Melbourne	32,664	60.0	3.3	36.7
Bourke	54,427	47.4	31.0	21.7
Hobart	21,507	75.9	2.9	21.3
Wagga Wagga	50,892	47.1	33.1	19.8
Adelaide	58,735	39.8	41.0	19.3
Sydney	50,707	47.6	33.2	19.2
Brisbane	58,808	39.6	42.5	18.0
Longreach	65,435	41.6	41.6	18.0
Townsville	62,007	42.1	42.1	17.9
Canberra	53,450	44.0	41.0	15.1

V. DISCUSSION

The results reveal that eight out of the ten locations analyzed have commercial potential, as the estimated IRR significantly exceeds the benchmark industry returns over the warranted-life of the system, i.e. 6% for DNSPs [25] and 12% for electricity retailers [29]. For each of these locations, the average estimated payback period is also below five years. The subsequent comparison and extrapolation of the results regionally, suggests system potential is greatest in South Australia in the short-term, and in northern Queensland in the medium to long-term, as shown in Table VI.

The expected cumulative revenues generated by a representative 5kW DER system during its 10-year lifetime for each location range from $21,500 (Hobart) to $65,400 (Longreach), as illustrated in Table VII. The locations that benefit the greatest proportionately from a complete DER system are locations where threshold arbitrage price limits restrict battery arbitrages. These threshold arbitrage limits are a direct result of both DNSP charges and wholesale electricity price differentials. In areas with high DNSP

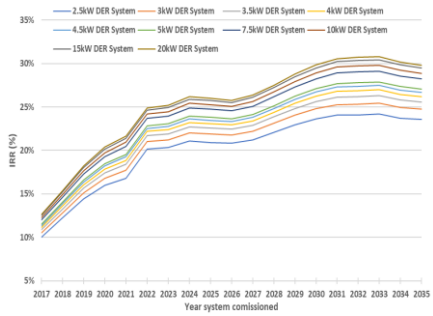

Figure 2. Canberra IRR Analysis (Complete DER system, base case).

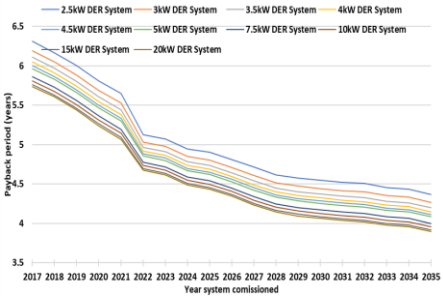

Figure 3. Canberra payback period analysis (complete DER system, base case).

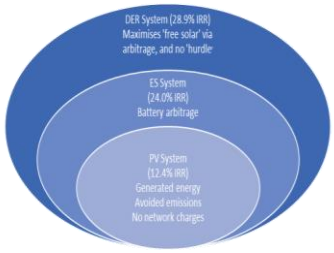

Figure 4. IRR comparison of the DER system and its component systems for Longreach.

charges and low price differentials the threshold price limits are higher. Therefore, the system synergy of a complete DER system is higher at these locations too since solar energy being sold back to the grid will not have to be purchased from the grid. When the converse conditions apply, threshold values are low, and the synergies created by a complete DER system decrease as a proportion of total system revenues.

As Table VII shows, the benefit of the DER system is superior to the sum of its parts. There is significant value created by having the opportunity to store surplus solar energy, and then sell it in the wholesale market at the price peak. This is despite the opportunity cost of the battery arbitrage forgone by storing the solar energy. A stand-alone battery system simply creates value by load-shifting, i.e. charging during price troughs and discharging during price peaks. A stand-alone PV system creates value through the energy it generates, the emissions it avoids (LGCs) and the network charges it avoids. While stand-alone PV systems generate significantly more revenue than stand-alone ES systems, their IRR is substantially inferior due to the greater investment. Overall, the DER system is the configuration that maximizes return on investment, as highlighted in Fig. 4.

Further comparative analyses were used to evaluate the investigation's sensitivity to input datasets. Wholesale price profiles, wholesale price projections, CapEx projections and solar data sets are the inputs with greatest impact on the expected IRR (more than 10%). Distribution network tariffs, and average annual load estimates have minor impacts on expected IRR (1% - 2%), while load profiles are immaterial

VI. Conclusion

This paper provides a novel, globally replicable framework to estimate the expected economic benefit of centrally operated VPPs for a specific geography or customer type in an accessible means.

VPP business models are already technically feasible, regulatory compliant, and commencing implementation in some markets, however a readily accessible investment evaluation framework did not previously exist. This evaluation is critical in the early decision-making stages of the capital budgeting process and the lack of a replicable investment evaluation framework was a barrier to VPP adoption.

It is the authors' hope that by making it easier for decision-makers to develop economic appraisals of VPPs, this paper contributes to progressing their adoption, and accelerates the transition to a renewable energy future.

This investigation conservatively calculates that a central body in the Australian NEM coordinating a VPP could expect to receive a sustained marginal economic benefit of greater than 20% return on investment for eight of the ten locations analyzed, beating industry benchmarks for DNSPs and electricity retailers. These results support the commercial viability of centrally controlled and maintained VPPs.

Moreover, as the maximum IRR contribution from legislative support schemes was calculated to be 3.64%, DER system returns on investment would continue to surpass industry benchmarks in their absence. The eight locations were representative of Queensland, New South Wales, South Australia and the Australian Capital Territory, which account for 60% of Australia's population. Therefore, the commercial potential of a VPP to facilitate the growth of decentralized renewable energy generation in Australia is independent of public policy support.

Acknowledgment

This research did not receive any specific grant from funding agencies in the public, commercial or not-for-profit sectors.

References

[1] M. Loßner, D. Böttger, and T. Bruckner, "Economic assessment of virtual power plants in the German energy market — A scenario-based and model-supported analysis," Energy Economics, vol. 62, 2017, pp. 125-138.

[2] I. Perez-Arriaga et al., "Utility of the future: An MIT Energy Initiative response to an industry in transition," MIT 2015.

[3] K. E. Bakari and W. L. Kling, "Virtual power plants: An answer to increasing distributed generation," in 2010 IEEE PES Innovative Smart Grid Technologies Conference Europe (ISGT Europe), 2010, pp. 1-6.

[4] M. M. Othman, Y. G. Hegazy, and A. Y. Abdelaziz, "Electrical energy management in unbalanced distribution networks using virtual power plant concept," Electric Power Systems Research, vol. 145, 2017, pp. 157-165.

[5] D. Pudjianto, C. Ramsay, and G. Strbac, "Virtual power plant and system integration of distributed energy resources," IET Renewable Power Generation, vol. 1, no. 1, pp. 10-16, 2007.

[6] R. Viral and D. Khatod, "An analytical approach for sizing and siting of DGs in balanced radial distribution networks for loss minimization," Int. J. Electr. Power Energy Syst., vol. 67, no. C, 2015, pp. 191-201.

[7] A. Forooghi Nematollahi, A. Dadkhah, O. Asgari Gashteroodkhani, and B. Vahidi, "Optimal sizing and siting of DGs for loss reduction using an iterative-analytical method," Journal of Renewable and Sustainable Energy, vol. 8, no. 5, 2016.

[8] H. Pandzic, Y. Yishen Wang, D. S. Ting Qiu, D. S. Dvorkin, and D. S. Kirschen, "Near-Optimal Method for Siting and Sizing of Distributed Storage in a Transmission Network," Power Systems, IEEE Transactions on, vol. 30, no. 5, 2015, pp. 2288-2300.

[9] M. A. Darfoun and M. E. El-Hawary, "Multi-objective Optimization Approach for Optimal Distributed Generation Sizing and Placement," Electric Power Components and Systems, vol. 43, no. 7, 2015, pp. 828-836.

[10] E. Galvan, P. Mandal, A. U. Haque, and T.-L. Tseng, "Optimal Placement of Intermittent Renewable Energy Resources and Energy Storage System in Smart Power Distribution Networks," Electric Power Components and Systems, vol. 45, no. 14, 2017, pp. 1543-1553.

[11] Y. M. Atwa, E. F. El-Saadany, M. M. A. Salama, and R. Seethapathy, "Optimal Renewable Resources Mix for Distribution System Energy Loss Minimization," Power Systems, IEEE Transactions on, vol. 25, no. 1, 2010, pp. 360-370.

[12] A. F. P. Posada, J. G. Villegas, and J. M. López-Lezama, "A scatter search heuristic for the optimal location, sizing and contract pricing of distributed generation in electric distribution systems," Energies, vol. 10, no. 10, 2017.

[13] S. Daud, A. F. A. Kadir, C. K. Gan, A. Mohamed, and T. Khatib, "A comparison of heuristic optimization techniques for optimal placement and sizing of photovoltaic based distributed generation in a distribution system," Solar Energy, vol. 140, 2016, pp. 219-226.

[14] S. M. Nosratabadi, R. Hooshmand, and E. Gholipour, "A comprehensive review on microgrid and virtual power plant concepts employed for distributed energy resources scheduling in power systems," in Renew. Sust. Energ. Rev. vol. 67, ed, 2017, pp. 341-363.

[15] A. Y. Abdelaziz, Y. G. Hegazy, W. El-Khattam, and M. M. Othman, "A Multi-objective Optimization for Sizing and Placement of Voltage-controlled Distributed Generation Using Supervised Big Bang–Big Crunch Method," Electric Power Components and Systems, vol. 43, no. 1, 2015, pp. 105-117.

[16] K. Dietrich, J. M. Latorre, L. Olmos, and A. Ramos, "Modelling and assessing the impacts of self supply and market-revenue driven Virtual Power Plants," Electric Power Systems Research, vol. 119, 2015, pp. 462-470.

[17] B. Potter. (2018, 15/05/2018). *Powershop, Reposit Power join 'virtual power plant' stampede*. Available at: https://www.afr.com/news/powershop-reposit-power-join-virtual-power-plant-stampede-20180313-h0xe3s

[18] A. Finkel, K. Moses, C. Munro, T. Effene, and M. O'Kane, *Independent Review into the Future Security of the National Electricity Market: Blueprint for the Future*, 2017, Available at : https://www.energy.gov.au/publications/independent-review-future-security-national-electricity-market-blueprint-future.

[19] R. Sharp et al., *Smart Grid, Smart City: Shaping Australia's Energy Future: Executive Report*, 2014. Avaliable at: http://smartcitiesappg.com/wp-content/uploads/PDF/SmartGrid.pdf

[20] T. Brinsmead et al., *Future Energy Storage Trends: An Assessment of the Economic Viability, Potential Uptake and Impacts of Electrical Energy Storage on the NEM 2015 - 2035*., EP155039, 2015, Available at: https://publications.csiro.au/rpr/pub?pid=csiro:EP155039.

[21] Australian Energy Market Operator. (2017). *Load Profiles*. Available at: https://www.aemo.com.au/Electricity/NationalElectricity-Market-NEM/Data/Metering/LoadProfiles.

[22] Bureau of Meteorology. (2017). *About one minute solar data*. Available at: http://www.bom.gov.au/climate/data/oneminsolar/about-IDCJAC0022.shtml

[23] Australian Energy Market Operator. (2017). *Data Dashboard*. Available at: https://www.aemo.com.au/Electricity/National-Electricity-Market-NEM/Data-dashboard

[24] Australian Energy Market Commission, *2016 Residential Electricity Price Trends: Final Report*, EPR0049,2016, Available at: https://www.aemc.gov.au/markets-reviews-advice/2016-residential-electricity-price-trends.

[25] Australian Energy Regulator, *State of the Energy Market*, 2017. Available at: https://www.aer.gov.au/publications/state-of-the-energy-market-reports/state-of-the-energy-market-may-2017.

[26] Australian Energy Market Operator, 2016, *National Electricity Forecasting Report 2016*, Available at: https://www.aemo.com.au/Electricity/National-Electricity-Market-NEM/Planning-and-forecasting/National-Electricity-Forecasting-Report.

[27] B. J. Alqahtani, K. M. Holt, D. Patiño-Echeverri, and L. Pratson, "Residential Solar PV Systems in the Carolinas: Opportunities and Outcomes," Environmental Science & Technology, vol. 50, no. 4, 2016, pp. 2082-2091.

[28] V. D. Ruelle, M. Jeppesen, and M. Brear, *Rooftop PV Model Technical Report*, 2016, Available at: https://www.aemo.com.au/-/media/Files/Electricity/NEM/Planning_and_Forecasting/NEFR/2016/UoM-Rooftop-PV-Model-Technical-Report.pdf.

[29] Australian Energy Market Commission, *2017 AEMC Retail Energy Competition Review: Final*, RPR0005, 2017, Available at: https://www.aemc.gov.au/markets-reviews-advice/2017-retail-energy-competition-review.

[30] P. Bronski et al., The Economics of Load Defection: How Grid-Connected Solar-Plus-Battery Systems Will Compete With Traditional Electric Service, Why It Matters, and Possible Paths Forward, Rocky Mountain Institute, 2015.

[31] Australian Energy Regulator. (2017). *Trading intervals above $5000/MWh (annual) 2017*. Available at: https://www.aer.gov.au/wholesale-markets/wholesale-statistics/trading-intervals-above-5000-mwh-annual

Utilization of Raw Glycerol from Biodiesel Industry for Production of Microbial Biocontrol Agents

Ivana Pajčin, Jovana Grahovac, Jelena Dodić, Vanja Vlajkov, Siniša Dodić, Zorana Rončević, Ivana Mitrović

University of Novi Sad, Faculty of Technology Novi Sad, Serbia, paj@tf.uns.ac.rs

Abstract — **A promising alternative for utilization of fossil fuels, whose reserves are near depletion and whose usage represents a growing problem for the environment, is production and utilization of biofuels, such as bioethanol, biogas and biodiesel. Biodiesel represents a mixture of alkyl esters emerged during transesterification reaction between triglycerides and alcohol, where glycerol is the major byproduct of this reaction. Scientific community on global level is included in solving the problem of raw glycerol surplus, whose amount increases with increase of biodiesel global market. One of the suggestions for its utilization is microbial conversion to different value added products. The aim of this study was to investigate the suitability of raw glycerol from biodiesel production as substrate for production of biocontrol agents effective against phytopathogenic *Xanthomonas* strains, which represent a significant threat to the agricultural production of economically important crops in the Republic of Serbia, such as cabbage, pepper and tomato. The results of this study have confirmed the ability of the producing strain *Bacillus velezensis* to successfully metabolize raw glycerol from biodiesel production, simultaneously producing value-added products, which in this case could be utilized as biocontrol agents against black rot and bacterial spot causers.**

Keywords – *Bacillus velezensis*, raw glycerol, biodiesel, *Xanthomonas*, biological control

I. INTRODUCTION

Utilization of fossil fuels in all sectors of industry and transport, as well as for production of electric energy and heat in households and public objects, hasn't been a sustainable system for a while, mostly because of the depletion of fossil fuels' reserves and due to their negative effect on environment and human health. A promising alternative is production and utilization of biofuels, mostly obtained from natural resources or waste materials [1], with a special emphasis on biofuels produced from plant biomass, whose production is characterized by several advantages: availability of raw materials, the fact they are completely renewable, as well as the fact that utilization of plant biomass in biofuels' production does not emit additional CO_2 in the atmosphere [2]. The most utilized biofuels nowadays are bioethanol, biogas and biodiesel.

Biodiesel is biofuel whose production and consumption has greatly expanded in the last decade and which can be used as a substitute for diesel fuel produced from oil in conventional diesel engines. It is fourth generation biofuel, therefore the strategy of its production anticipates generating minimal amount of waste streams [1]. Biodiesel represents a mixture of alkyl esters emerged during transesterification reaction between triglycerides and alcohol, where glycerol is the major byproduct of this reaction in an amount of 10% (w/w) compared to biodiesel amount [3]. Commonly used raw materials for biodiesel production are plant oils and animal fats, such as rapeseed, sunflower and soy oil [4]. In the last few years there has been an emerging trend of utilization of waste oils and fats from the frying process in restaurants or households as raw material for biodiesel production. Methanol is usually used for transesterification reaction due to its low price. Furthermore, this reaction requires presence of alkali catalyst (KOH or NaOH). During transesterification reaction it is possible to obtain some undesired reaction products, such as soaps [5]. All of these impurities,

ISBN: 978-86-80616-04-9

including undesired reaction products, remains of methanol, catalyst, salts, fatty acids, as well as the impurities arising from the raw material, remain in raw glycerol as the major byproduct after biodiesel separation [6].

Raw glycerol from biodiesel production, according to the results of elementary analysis, contains around 25% (w/w) of carbon, sodium (more than 1% (w/w)), other metals, such as potassium, calcium, magnesium (4-163 ppm), and nonmetals (phosphorus, nitrogen and sulfur). It also contains proteins (0.06–0.44%, w/w), fats (1-13%, w/w) and carbohydrates (75-83%) [7]. Glycerol content in raw glycerol ranges from 65% to 85% (w/w) [8].

Due to large amount of impurities, simple deposition of raw glycerol in the environment isn't possible, while the procedure of its purification is expensive, complex and unprofitable considering the price of commercial glycerol [9]. Therefore solving the problem of present raw glycerol surplus will significantly affect the future of biodiesel industry on the global market. Due to the rising amount of raw glycerol on the global market, its price keeps decreasing. There's an estimation that biodiesel production cost increases for 0.021 $/L for each decrease of raw glycerol price of 0.22 $/kg [10]. However, global biodiesel market continues to rise, with an estimated value of 40.5 billion liters in 2026 [11]. Therefore, the amount of available raw glycerol on global market will continue to increase. Hence, scientific community on global level is included in solving the problem of raw glycerol surplus. One of the suggestions for its utilization is microbial conversion to different value added products, where raw glycerol could be used as carbon source and one of the main components of cultivation medium.

Utilization of raw glycerol as carbon source in different types of microbial conversion represents a new field of scientific interest. The present excess of raw glycerol from biodiesel production makes usage of glucose as carbon source very expensive. Besides, glucose has also been applied in the production of food and feed, which is not the case when it comes to raw glycerol [12]. Glycerol also shows higher degree of reduction comparing to sugars [13]. During glycerol fermentation the yield of ethanol and formic acid (or ethanol and hydrogen) is doubled comparing to glucose fermentation because the half of the sugar amount is lost during fermentation to produce carbon dioxide [14]. Numerous microorganisms can metabolize glycerol aerobically, and also there are microorganisms capable to metabolize glycerol anaerobically [15]. The microorganisms that can convert glycerol to value added products belong to the following genera: *Escherichia*, *Klebsiella*, *Clostridium*, *Enterobacter*, *Gluconobacte*r, *Citrobacter*, *Propionibacterium*, *Bacillus*, *Lactobacillus*, *Pseudomonas*, *Candida*, *Aspergillus* etc. [1, 16, 17]. Utilization of raw glycerol as carbon source in microbial conversions has resulted in producing 1,2-propanediol, 1,3-propanediol, 2,3-butanediol, ethanol, butanol, hydrogen, dihydroxyacetone, propionic acid, citric acid, succinic acid, lactic acid, polyhydroxybutirate, polyhydroxyalkanoate, pigments and biosurfactants [1, 10, 14, 18].

Microbial conversion of raw glycerol by bacteria of the genus *Bacillus* has been investigated in the production of fengycin [19], biosurfactants [20, 21], 2,3-butanediol [22], polyhydroxybutirate [23] and polyhydroxyalkanoate [24].

Biological control represents usage of beneficial organisms or their products to suppress or prevent plant diseases caused by different phytopathogens. It has been emerged as potential alternative to agrochemicals, whose utilization represents a significant burden for the environment and also potential risk for human health [25]. Microorganisms, with a special emphasis on genera *Bacillus*, *Streptomyces* and *Trichoderma*, are amongst most usually used biocontrol agents. Bacteria of the genus *Bacillus* have several characteristics making them suitable candidates for biological control of plant pests: rapid growth and multiplication, ability to adjust to different ecological conditions, sporulation ability, and most of all, production of wide spectra of different antimicrobial metabolites, including antibiotics, enzymes, lipopeptides and volatile organic compounds [26-30]. However, due to high cost of biocontrol agents' production, different approaches have been investigated to reduce the production cost, and therefore the final product price. Therefore, the aim of this study was to investigate the suitability of raw glycerol from biodiesel production as substrate for production of biocontrol agents effective against phytopathogenic *Xanthomonas* strains, which represent a significant threat to the agricultural production of economically important crops in

the Republic of Serbia, such as cabbage, pepper and tomato, by using *Bacillus velezensis*, strain with proven antimicrobial activity, as the producing microorganism.

II. Material and Methods

A. Microorganisms

The producing microorganism in this study was *Bacillus velezensis*, a strain isolated from fresh cheese and identified using 16s rDNA sequencing. Test microrganisms in this study were *Xanthomonas campestris* Mn 7-2, isolated from cabbage with black rot symptoms, and two strains isolated from pepper with bacterial spot symptoms: *Xanthomonas euvesicatoria* PAP LIST 1 and PAP LIST 2, which have also been identified using 16s rDNA sequencing.

B. Inoculum Preparation

The producing microorganism was cultivated on nutrient agar slant for 48 h at 28°C in order to regain its physiological activity. After that, biomass of the producing microorganism was transferred to nutrient broth (50 mL) and incubated at 28°C for 24 h on a laboratory shaker (150 rpm). After that, the obtained liquid was transferred to higher volume of nutrient broth (150 mL) and incubated under the same conditions as in the previous phase. The obtained inoculum (200 mL) after 48 h of incubation was used for inoculation of cultivation medium based on raw glycerol in the laboratory-scale bioreactor.

C. Cultivation Medium and Conditions

Production of microbial biocontrol agents effective against phytopathogenic *Xanthomonas* spp. using *Bacillus velezensis* as the producing microorganism was performed in a laboratory-scale bioreactor with working volume of 2 L (Biostat® Aplus, Sartorius AG, Göttingen, Germany). Cultivation conditions were the following: temperature 28°C, agitation rate 250 rpm, aeration rate 1 vvm (volume of air/volume of liquid/min), duration 96 h. Raw glycerol from biodiesel production, obtained from the company BIODIZEL CO d.o.o. (Belgrade, Serbia), was used as the main carbon source in the cultivation medium for production of microbial biocontrol agents, which consisted of 16.67 g/L of raw glycerol, 4.66 g/L of K_2HPO_4 and 0.3 g/L of $MgSO_4 \cdot 7H_2O$. During cultivation, cultivation broth was sampled in 12 hour-intervals in order to determine *Bacillus velezensis* biomass content, residual nutrients' content and antimicrobial activity of cultivation broth samples against the tested phytopathogenic *Xanthomonas* strains.

D. Analytical Methods

Bacillus velezensis biomass content was determined using the gravimetric method. After centrifugation of cultivation broth sample (20 mL, 10 min, 10000 rpm) (Rotina 380R, Hettich, Tuttlingen, Germany), the obtained biomass pellet was dried at 105°C and measured until reaching the constant weight. Biomass concentration (g/L) was calculated using the measured dry weight value and initial sample volume (20 mL).

Residual content of the main nutrients (glycerol, total nitrogen and total phosphorus) was determined using the supernatants of cultivation broth samples obtained after the biomass separation by centrifugation (10 min, 10000 rpm; Rotina 380R, Hettich, Tuttlingen, Germany). HPLC method was employed to determine residual glycerol content [31]. Residual total nitrogen content was determined using the Kjeldahl method [32], while residual total phosphorus content was determined using the spectrophotometric method [33].

Antimicrobial activity assaying was performed using the diffusion disc method, where cultivation broth samples, containing biomass of *Bacillus velezensis* and the produced metabolites, were tested against three phytopathogenic *Xanthomonas* strains. Test microorganisms were incubated at 26°C during 48 h on yeast maltose agar (glucose 15 g/L, yeast extract 3 g/L, peptone 5 g/L, malt extract 3 g/L, agar 20 g/L). Suspensions of test microorganisms were prepared using the sterile saline to contain 10^8 CFU/mL. These suspensions were used for inoculation of melted and tempered (50±1°C) media (yeast maltose agar) used for antimicrobial activity testing. Samples of cultivation broth (15 µL) were tested in three replicates against each test microorganism. Incubation was carried out at 26°C during 72 h and afterwards inhibition zone diameters were measured.

III. Results and Discussion

One of the potential solutions for utilization of the present excess of raw glycerol from biodiesel production is its microbial conversion into different value added products. However, since raw glycerol contains around 60-85% (w/w) of glycerol, and the rest are different

impurities, the major problem when it comes to its utilization in microbial bioprocesses is potential inhibitory effect of those impurities on microbial metabolic pathways [17]. In our previous study [34], different strains of the genus *Bacillus* were investigated for production of biocontrol agents using medium based on raw glycerol from biodiesel production. All of the tested strains have showed certain antimicrobial activity, indicating the ability of the investigated *Bacillus* strains to metabolize raw glycerol. Among the tested strains, *Bacillus velezensis* has showed the highest antimicrobial potential, therefore this strain was employed as the producing microorganism in this study where cultivation was carried out in a larger volume of cultivation medium, i.e. in a laboratory-scale bioreactor. During the bioprocess, cultivation broth samples were analyzed in 12 hour-intervals in order to determine *Bacillus velezensis* biomass content, residual content of the main nutrients (glycerol, total nitrogen and total phosphorus), as well as antimicrobial activity against phytopathogenic *Xanthomonas* strains isolated from diseased plants (cabbage and pepper).

Biomass content of the producing microorganism *Bacillus velezensis* during cultivation in a laboratory-scale bioreactor using medium based on raw glycerol was determined by the gravimetric method (Fig. 1). Since inoculum of the producing microorganism was prepared using commercial medium (nutrient broth), which contains mostly simple sugars and amino acids as the main nutrients to support microbial growth, the producing microorganism required certain time to adjust to metabolizing different nutrients after transferring the inoculum in the medium based on raw glycerol. Therefore, during the first 24 hours of cultivation only slight change of biomass content could be observed, due to lag or adaptation growth phase of *Bacillus velezensis*. After that, exponential or log growth phase could be noticed between 24th and 48th hour of cultivation, with sharp increase in biomass content, indicating the ability of the producing microorganism to successfully metabolize raw glycerol as carbon source necessary for synthesis of cell components. Also, since during preparation of the cultivation medium none of the nitrogen sources has been added, it can be concluded that raw glycerol from biodiesel production also contains nitrogen compounds, since nitrogen is essential nutrient for synthesis of DNA and proteins as the major cell components, which is indicated by the significant increase in biomass content during exponential growth phase. Other studies which had investigated the composition of raw glycerol from biodiesel production have also confirmed the presence of nitrogen in raw glycerol [7]. After 60th hour of cultivation, stationary growth phase could be observed with only slight changes in biomass content until the end of cultivation. Also, it can be noticed that *Bacillus velezensis* biomass content has increased almost nine folds during the cultivation.

During cultivation of the producing microorganism *Bacillus velezensis* in a laboratory-scale bioreactor using medium based on raw glycerol residual content of the main nutrients (glycerol, total nitrogen and total phosphorus) was determined using the appropriate analytical methods in order to monitor nutrients' consumption and its relation to *Bacillus velezensis* growth and antimicrobial activity. Based on the results presented in Fig. 2, it can be concluded that consumption of glycerol, nitrogen and phosphorus was in a strong correlation with *Bacillus velezensis* growth (Fig. 1) and antimicrobial activity (Fig. 3). The most intense consumption of nutrients was observed during the exponential growth phase, due to utilization of these nutrients for building cell components, while in the stationary growth phase (after 60th hour of cultivation) only moderate consumption of nutrients could be noticed. When it comes to conversion of nutrients, it can be concluded that 76.73% of glycerol was converted to biomass and microbial metabolites during cultivation of *Bacillus velezensis*, which represents a

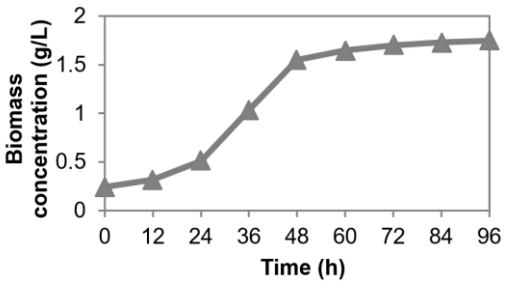

Figure 1. *Bacillus velezensis* biomass concentration during cultivation in a laboratory-scale bioreactor using medium based on raw glycerol

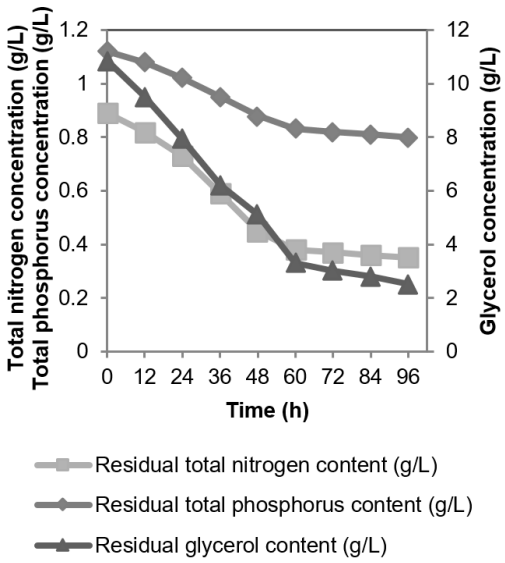

Figure 2. Residual content of the main nutrients during cultivation of *Bacillus velezensis* in a laboratory-scale bioreactor using medium based on raw glycerol

satisfying value for utilization of this waste material as carbon source, suggesting the potential of raw glycerol utilization even in a larger scale bioprocess of this type. The presence of nitrogen compounds in raw glycerol is also confirmed by observing residuals of this nutrient in cultivation broth samples, while 60.67% of this nutrient was consumed during the cultivation. When it comes to phosphorus, a significantly lower conversion coefficient was observed (28.57%), which indicates the need to further optimize cultivation medium composition in terms of phosphorus content, or to decrease the initial concentration of the phosphorus source in the cultivation medium, which also contributes to the reduction of the cultivation medium cost.

Antimicrobial activity of the cultivation broth samples, containing biomass of *Bacillus velezensis* and the metabolites produced during the cultivation in a laboratory-scale bioreactor using medium based on raw glycerol, was tested in vitro against three phytopathogenic *Xanthomonas* strains using the diffusion disc method. Inhibition zone diameters, as the main indicators of antimicrobial activity, were measured (Fig. 3). The results have indicated that antimicrobial activity of the cultivation broth samples is also in good correlation with *Bacillus velezensis* growth (Fig. 1). This result is supported by numerous scientific reports claiming that competition for nutrients and growth space, where living cells of biocontrol agent have the most important role in suppressing phytopathogenic microorganisms, is one of the most common mechanisms of antimicrobial activity [35]. Also, a slight increase in inhibition zone diameters could be observed even during the stationary growth phase (after 60th hour of cultivation). Since *Bacillus velezensis* is well known for producing different types of secondary metabolites, many of which express antimicrobial activity [36], it is justified to assume that this producing strain also possesses the ability to synthesize some of the metabolites expressing antimicrobial activity against phytopathogenic *Xanthomonas* strains. While the antifungal activity of *Bacillus velezensis* has been thoroughly investigated [37], it has also been proven that compounds from surfactin and locillomycin families express antibacterial activity [36, 38]. Therefore, further research in the field of identification of antimicrobial compounds produced by *Bacillus velezensis* strain used in this study and using medium based on raw glycerol will be conducted, with a special emphasis on investigation of lipopeptide compounds production.

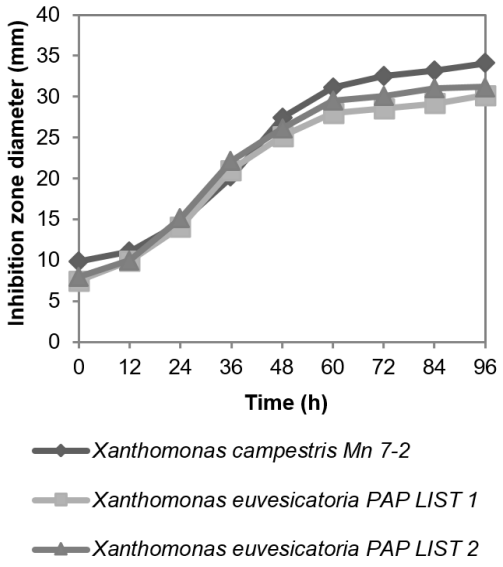

Figure 3. Antimicrobial activity of *Bacillus velezensis* cultivation broth samples against phytopathogenic *Xanthomonas* spp. during cultivation in a laboratory-scale bioreactor using medium based on raw glycerol

IV. CONCLUSIONS

The results of this study have confirmed the ability of the producing strain *Bacillus velezensis* to successfully metabolize raw glycerol from biodiesel production, simultaneously producing value-added products, which in this case could be utilized as biocontrol agents against black rot and bacterial spot causers. Considering the potential of this bioprocess in contributing to solving the problem of the raw glycerol surplus, further research will focus on precise identification of the produced biocontrol agents and their mechanisms of action, as well as on optimization of bioprocess conditions in order to obtain viable and sustainable bioprocess solution applicable at larger production scale.

ACKNOWLEDGMENT

This study was financially supported by the Ministry of Education, Science and Technological Development of the Republic of Serbia through the project TR 31002.

REFERENCES

[1] V. K. Garlapati, U. Shankar, and A. Budhiraja, "Bioconversion technologies of crude glycerol to value added industrial products," Biotechnol. Rep., vol. 9, 2016, pp. 9-14.

[2] J. S. de Castro, L. D. Nguyen, and J. Seppala, "Bioconversion of commercial and waste glycerol into value-added polyhydroxyalkanoates by bacterial strains," J. Microb. Biochem. Technol., vol. 6, 2014, pp. 337-345.

[3] M. F. Milazzo, F. Spina, A. Vinci, C. Espro, and J. C. J. Bart, "Brassica biodiesels: past, present and future," Renew. Sust. Energ. Rev., vol. 18, 2013, pp. 350–389.

[4] C. H. Zhou, J. N. Beltramini, Y. X. Fan, and G. Q. Lu, "Chemoselective catalytic conversion of glycerol as a biorenewable source to valuable commodity chemicals," Chem. Soc. Rev., vol. 37, 2008, pp. 527–549.

[5] H. W. Tan, A. R. Abdul Aziz, and M. K. Aroua, "Glycerol production and its applications as a raw material: A review," Renew. Sust. Energ. Rev., vol. 27, 2013, pp. 118–127.

[6] F. Yang, M. A. Hanna, and R. Sun, "Value-added uses for crude glycerol – a byproduct of biodiesel production," Biotechnol. Biofuels, vol. 5, 2012, pp. 1-10.

[7] J. C. Thompson and B. B. He, "Characterization of crude glycerol from biodiesel production from multiple feed stocks," Appl. Eng. Agric., vol. 22, 2006, pp. 261–265.

[8] M. Gonzalez-Pajuelo, I. Meynial-Salles, F. Mendes, J. C. Andrade, I. Vasconcelos, and P. Soucaille, "Metabolic engineering of *Clostridium acetobutylicum* for the industrial production of 1,3-propanediol from glycerol," Metab. Eng., vol. 7, 2005, pp. 329–336.

[9] M. Ayoub and A. Z. Abdullah, "Critical review on the current scenario and significance of crude glycerol resulting from biodiesel industry towards more sustainable renewable energy industry," Renew. Sust. Energ. Rev., vol. 16, 2012, pp. 2671–2686.

[10] C. Li, K. L. Lesnik, and H. Liu, "Microbial conversion of waste glycerol from biodiesel production into value-added products," Energies, vol. 6, 2013, pp. 4739-4768.

[11] OECD/FAO, OECD-FAO Agricultural Outlook 2017-2026, Paris, France: OECD Publishing, 2017.

[12] C. E. Nakamura and G. M. Whited, "Metabolic engineering for the microbial production of 1,3-propanediol," Curr. Opin. Biotech., vol. 14, 2003, pp. 454–459.

[13] Y. Dharmadi, A. Murarka, and R. Gonzalez, "Anaerobic fermentation of glycerol by *Escherichia coli*: a new platform for metabolic engineering," Biotechnol. Bioeng., vol. 94, 2006, pp. 821–829.

[14] G. P. da Silva, M. Mack, and J. Contiero, "Glycerol: A promising and abundant carbon source for industrial microbiology," Biotechnol. Adv., vol. 27, 2009, pp. 30-39.

[15] S. S. Yazdani and R. Gonzalez, "Anaerobic fermentation of glycerol: a path to economic viability for the biofuels industry," Curr. Opin. Biotech., vol. 18, 2007, pp. 213-219.

[16] P. F. F. Amaral, T. F. Ferreira, G. C. Fontes, and M. A. Z. Coelho, "Glycerol valorization: New biotechnological routes," Food Bioprod. Process., vol. 87, 2009, pp. 179–186.

[17] A. B. Leoneti, V. Aragão-Leoneti, and S. V. W. G. de Oliveira, "Glycerol as a by-product of biodiesel production in Brazil: Alternatives for the use of unrefined glycerol," Renew. Energ., vol. 45, 2012, pp. 138-145.

[18] J. A. Posada, L. E. Rincón, and C. A. Cardona, "Design and analysis of biorefineries based on raw glycerol: Addressing the glycerol problem," Bioresour. Technol., vol. 111, 2012, pp. 282–293.

[19] A. F. de Faria, D. Stéfani, B. G. Vaz, Í. S. Silva, J. S. Garcia, M. N. Eberlin, M. J. Grossman, O. L. Alves, and L. R. Durrant, "Purification and structural characterization of fengycin homologues produced by *Bacillus subtilis* LSFM-05 grown on raw glycerol," J. Ind. Microbiol. Biotechnol., vol. 38, 2011a, pp. 863-871.

[20] A. F. de Faria, D. S. Teodoro-Martinez, G. N. de Oliveira Barbosa, B. G. Vaz, Í. S. Silva, J. S. Garcia, M. R. Tótola, M. N. Eberlin, M. Grossman, O. L. Alves, and L. R. Durrant, "Production and structural characterization of surfactin (C14/Leu7) produced by *Bacillus subtilis* isolate LSFM-05 grown on raw glycerol from the biodiesel industry," Process Biochem., vol. 46, 2011b, pp. 1951-1957.

[21] M. de Sousa, I. T. Dantas, A. K. N. Felix, H. B. de Sant'Ana, V. M. M. Melo, and L. R. B. Gonçalves, "Crude glycerol from biodiesel industry as substrate for biosurfactant production by *Bacillus subtilis* ATCC 6633," Braz. Arch. Biol. Technol., vol. 57, 2014, pp. 295-301.

[22] T. W. Yang, Z. M. Rao, X. Zhang, M. J. Xu, Z. H. Xu, and S. T. Yang, "Fermentation of biodiesel-derived glycerol by *Bacillus amyloliquefaciens*: effects of co-substrates on 2,3-butanediol production." Appl. Microbiol. Biot., vol. 97, 2013, pp. 7651-7658.

[23] P. Moreno, C. Yañez, N. S. M. Cardozo, H. Escalante, M. Y. Combariza, and C. Guzman, "Influence of nutritional and physicochemical variables on PHB production from raw glycerol obtained from a Colombian biodiesel plant by a wild-type *Bacillus megaterium strain*," New Biotechnol., vol. 32, 2015, pp. 682-689.

[24] P. L. L. Ribeiro, G. S. Silva, and J. I. Druzian, "Evaluation of the effects of crude glycerol on the production and properties of novel polyhydroxyalkanoate copolymers containing high 11-hydroxyoctadecanoate by *Cupriavidus necator* IPT 029 and *Bacillus megaterium* IPT 429," Polym. Adv. Technol.,vol. 27, 2016, pp. 542-549.

[25] D. Spadaro and M. L. Gullino, "State of the art and future prospects of the biological control of postharvest fruit diseases," Int. J. Food Microbiol., vol. 91, 2004, pp. 185– 194.

[26] P. Zhao, Y. Xue, W. Gao, J. Li, X. Zu, D. Fu, X. Bai, Y. Zuo, Z. Hu, and F. Zhang, "Bacillaceae-derived peptide antibiotics since 2000," Peptides, vol. 101, 2018, pp. 10-16.

[27] E. Z. Gomaa, "Antimicrobial activity of a biosurfactant produced by *Bacillus licheniformis* strain M104 grown on whey," Braz. Arch. Biol. Technol., vol. 56, 2013, pp. 259-268.

[28] M. J. Torres, C. P. Brandan, D. C. Sabaté, G. Petroselli, R. Erra-Balsells, and M. C. Audisio, "Biological activity of the lipopeptide-producing *Bacillus amyloliquefaciens* PGPBacCA1 on common bean *Phaseolus vulgaris* L. pathogens," Biol. Control, vol. 105, 2017, pp. 93-99.

[29] A. Gotor-Vila, N. Teixidó, A. Di Francesco, J. Usall, L. Ugolini, R. Torres, and M. Mari, "Antifungal effect of volatile organic compounds produced by *Bacillus amyloliquefaciens* CPA-8 against fruit pathogen decays of cherry," Food Microbiol., vol. 64, 2017, pp. 219-225.

[30] J. Shafi, H. Tian, and M. Ji, "*Bacillus* species as versatile weapons for plant pathogens: a review," Biotechnol. Biotec. Eq., vol. 31, 2017, pp. 446-459.

[31] I. Pajčin, Z. Rončević, J. Dodić, S. Dodić, A. Jokić, and J. Grahovac, "Production of biocontrol agents using *Bacillus* sp. in a laboratory scale bioreactor," Journal on Processing and Energy in Agriculture, vol. 22, 2018, pp. 138-142.

[32] K. Herlich, Official Methods of Analysis of the Association of Official Analytical Chemists (15th ed.). Association of Official Analytical Chemists, Virginia, USA: Arlington, 1990.

[33] M. E. J. Gales, E. C. Julian, and R. C. Kroner, "Method for quantitative determination of total phosphorus in water," J. Am. Water Works Assoc., vol. 58, 1966, pp. 1363-1368.

[34] I. Pajčin, Z. Rončević, S. Dodić, A. Jokić, J. Dodić, and J. Grahovac, "Ispitivanje mogućnosti iskorišćenja sirovog glicerola za proizvodnju antimikrobnih agenasa primenom *Bacillus* spp.," VI Memorijalni naučni skup iz zaštite životne sredine „Docent dr Milena Dalmacija", Novi Sad, Serbia, March 29-30, 2018, UO-02.

[35] K. K. Pal and B. McSpadden Gardener, "Biological control of plant pathogens," Plant Health Instr., 2006.

[36] M. Ongena and P. Jacques, "*Bacillus* lipopeptides: versatile weapons for plant disease biocontrol," Trends Microbiol., vol. 16, 2008, pp. 115–125.

[37] S. M. Lim, M.- Y. Yoon, G. J. Choi, Y. H. Choi, K. S. Jang, T. S. Shin, H. W. Park, N. H. Yu, Y. H. Kim, and J.- C. Kim, "Diffusible and volatile antifungal compounds produced by an antagonistic *Bacillus velezensis* G341 against various phytopathogenic fungi," Plant Pathol. J., vol. 33, 2017, pp. 488-498.

[38] C. Luo, X. Liu, H. Zhou, X. Wang, and Z. Chen, "Nonribosomal peptide synthase gene clusters for lipopeptide biosynthesis in *Bacillus subtilis* 916 and their phenotypic functions," Appl. Environ. Microbiol., vol. 81, 2015, pp. 422–431.

Impact of Energy Storage Systems on the Power Grid

Ognjen Lukačević, Martin Ćalasan

Faculty of Electrical engineering - Universyty of Montenegro, Podgorica, Montenegro, ognjen.lukacevic96@gmail.com; martinc@ucg.ac.me

Abstract — **This paper describes the impact of the Energy Storage Systems (ESS) on the power grid. The ESS are installed on power grid to ensure more reliable power supply for consumers during rush hours, and at the same time to ensure a more economical operation of the system. In that goal, this paper deals with optimal allocation of ESS in order to minimize power losses in power grid. For that purpose, software GAMS has been used and the IEEE 24 - test buss network. It is shown that by installing ESS in the power grid, power losses can be reduced.**

Keywords – ESS, AC power flow, IEEE 24-test buss network

I. INTRODUCTION

One of the most common topics regarding to the power systems are sustainable sources. They are attractive to large number of different perspectives, for their low cost of energy production, their green effect, etc. However, the main problem with sustainable sources is that they depend on natures conditions. In order to solve that problem, in the last couple of years, solutions like Energy Storage Systems (ESS), has been offered [1].

The idea behind ESS is to store the energy, produced by sustainable sources during low demands, and use it when it is needed. By this method, significant amounts of energy could be saved and with proper energy management, power system could be more stable. At this moment, there are many types of ESSs like: Pumped Hydroelectric Storage (PHS), Compressed Air Energy Storage (CAES), Conventional Batteries and Flow Batteries, Hydrogen-Based Energy Storage System (HESS), Flywheel Energy Storage System (FESS), Superconducting Magnetic Energy Storage (SMES), Supercapacitor Energy Storage System, etc. [1].

On the other hand, many papers that describes how ESSs can contribute and improve power systems, can be found. In [2] by using Particle Swarm Optimization (PSO) algorithm, it is shown how ESS in low voltage distributed network can affect power loss reduction. Namely, in mentioned paper, CIGRÉ low voltage network has been selected to evaluate the effectiveness of the method. In paper [3], authors explained how ESS can maximize utilization of wind power with minimal investment cost of ESS. In that purpose, they used PSO algorithm as well. Furthermore, the storage capacity optimization of case system indicates that the model could smooth wind power by smaller cost and larger utilization of wind power. In [4], the objective of the optimization is the minimization of operation and capital costs in the complete lifespan considering the constraints. In this paper, nonlinear programming (NLP) is used in General Algebraic Modelling Software (GAMS) to solve the optimization problem. The results obtained henceforth are studied and then compared with the results obtained by optimizing the HESS system with particle swarm optimization (PSO) technique. Furthermore, in [5] problem of optimal sizing and allocation of ESS in power grid is solved. As a test network is used IEEE 24-test bus network and DC power flow problem is solved by using GAMS. On the other hand, paper [6] considers a specific aspect of the applications of ESS in power systems – improvement of power system stability. The mentioned paper then further presents an example of a simple power system installed with a BESS to improve power system oscillations.

This paper deals with optimal allocation of ESS in large power grids, in order to minimize power losses. In order to solve this problem, we used IEEE 24 – test bus network. The proposed algorithm will be written in software GAMS [8-9].

ISBN: 978-86-80616-04-9

The paper is organized as follows. In the second section, problem of allocation is described and presented. Third section is reserved for case study. In this section numerical results are presented. In the fourth section we will give shorty summary of our paper.

II. PROBLEM FORMULATION

This chapter presents mathematical model which describes AC power flow of power system. Namely, AC power flow model describes the energy flow through each transmission line considering active and reactive power.

However, this mathematical model has nonlinear nature. The reason why it is nonlinear is because the power flow into load impedances is a function of the square of the applied voltages. In many cases non-linearity can be avoided by using DC power flow model, but it should be mentioned that DC model is not accurate as AC power flow model. Therefore, DC power flow model is used when faster calculations are needed, or like in case, it is used for calculations of starting values of AC power flow variables. General AC power flow model is given on Fig. 1.

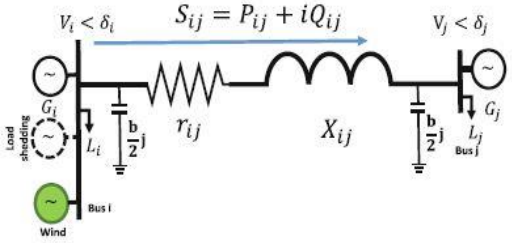

Figure 1. AC power flow

This model can be described by using the following equations:

$$P_{i,t}^{g} + P_{i,t}^{LS} + P_{i,t}^{W} - P_{i,t}^{L} - P_{i,t}^{c} + P_{i,t}^{d} = \sum_{j} P_{i,j,t} \quad (1)$$

$$Q_{i,t}^{g} + Q_{i,t}^{LS} + Q_{i,t}^{W} - Q_{i,t}^{L} = \sum_{j} Q_{i,j,t} \quad . \quad (2)$$

In equations (1) and (2), $P_{i,t}^{g}$ and $Q_{i,t}^{g}$ are active and reactive power that thermal generating units produce in buss i at time t, respectively. $P_{i,t}^{LS}$ and $Q_{i,t}^{LS}$ represents active and reactive power of load shedding in buss i at time t, $P_{i,t}^{W}$ and $Q_{i,t}^{W}$ are active and reactive power produced by wind farms in buss i at time t, while $P_{i,t}^{L}$ and $Q_{i,t}^{L}$ are active and reactive power of load in buss i at time t, respectively. $P_{i,t}^{c}$ is active power of charging of ESS, and $P_{i,t}^{d}$ is active power of discharging of ESS, in buss i at time t. $P_{i,j,t}$ is active power through the transmission line between busses i and j, at time t.

Furthermore, the current trough transmission lines is calculated by following equation:

$$I_{i,j,t} = \frac{V_{i,t}\angle\delta_{i,t} - V_{j,t}\angle\delta_{j,t}}{Z_{i,j}\angle\theta_{i,j}} + \frac{bV_{i,t}}{2}\angle\left(\delta_{i,t} + \frac{\pi}{2}\right), \quad (3)$$

where $I_{i,j,t}$ represents current trough transmission lines between busses i and j at time t, $V_{i,t}$ and $V_{j,t}$ are voltages in busses i and j at time t, respectively $\delta_{i,t}$ and $\delta_{j,t}$ represents voltage angles and busses i and j, at time t respectively. $Z_{j,t}$, is impedance of the branch between busses i and j, with following angle $\theta_{i,j}$. b represents susceptance between node i and j. Using equation (3), apparent power can be calculated with the following equation:

$$S_{i,j,t} = V_{i,t}\angle\delta_{bus,t} \cdot I_{i,j,t}^{*}. \quad (4)$$

Furthermore, active and reactive power can be calculated as follows:

$$P_{i,j,t} = rael\{S_{i,j,t}\} = \frac{V_{i,j}^{2}}{Z_{i,j}}\cos(\theta_{i,j}) - \frac{V_{i,t}\cdot V_{j,t}}{Z_{i,j}}\cos(\delta_{i,t} - \delta_{j,t} + \theta_{i,j}), \quad (5)$$

$$Q_{i,j,t} = imag\{S_{i,j,t}\} = \frac{V_{i,j}^{2}}{Z_{i,j}}\sin(\theta_{i,j}) - \frac{V_{i,t}\cdot V_{j,t}}{Z_{i,j}}\sin(\delta_{i,t} - \delta_{j,t} + \theta_{i,j}) - \frac{bV_{i,t}^{2}}{2}. \quad (6)$$

In order to have accurate optimization, this model has to be expanded with network and other limitations. Thermal units' limits are given as follows:

$$\begin{aligned} P_g^{\min} &\le P_{g,t} \le P_g^{\max} \\ Q_g^{\min} &\le Q_{g,t} \le Q_g^{\max} \\ P_{g,t} - P_{g,t-1} &\le RU_g \\ P_{g,t-1} - P_{g,t} &\le RD_g, \end{aligned} \quad (7)$$

where $P^g_{\min}$ and $P^g_{\max}$ are minimum and maximum active power that thermal unit can produce, respectively. $Q^g_{\min}$ and $Q^g_{\max}$ are minimum and maximum reactive power of thermal units, respectively. Only these 2 limitations are not enough to model real system, so limitations for ramp rates are also added in (7) where RU_g represents ramp-up and RD_g represents ramp-down.

Network limitations are given with following equation:

$$-S^{\max}_{i,j} \le S_{i,j,t} \le S^{\max}_{i,j} \ . \quad (8)$$

Since in this case we take into consideration load shedding and wind curtailment, their limitations are presented in following equations:

$$\begin{aligned} 0 &\le P^{LS}_{i,t} \le P^{L}_{i,t} \\ P^{WC}_{i,t} &= w_{i,t}\lambda_i^w - P^w_{i,t} \\ 0 &\le P^w_{i,t} \le w_{i,t}\lambda_i^w, \end{aligned} \quad (9)$$

where $w_{i,t}$ is wind turbine availability in buss *i* at time *t*. λ_i^w is capacitance of wind turbine.

To describe *State Of Charge* (SOC) of ESS, limitations of charging and discharging power and limit of number of ESSs are given with following equations:

$$SOC_{i,t} = SOC_{i,t-1} + (P^c_{i,t} \cdot \eta_c - \frac{P^d_{i,t}}{\eta_d})\Delta t, \quad (10)$$

$$P^c_{i,\min} \le P^c_i \le P^c_{i,\max} \ , \quad (11)$$

$$P^d_{i,\min} \le P^d_i \le P^d_{i,\max} \ , \quad (12)$$

$$N_k \cdot SOC_{i,\min} \le SOC_{i,t} \le N_k \cdot SOC_{i,\max} \ , \quad (13)$$

$$\sum_k N_k \le N_{\max} \ . \quad (14)$$

In equations (13), N_k is integer variable that has value different from 0 when there is ESS at bus *i*. With equation (14) maximal number of ESS in power grid is limited.

Optimal function for minimization of power lost in transmission lines is formulated as follows:

$$OF = \sum_{i=1}^{k} [g_{mn}(V_m^2 + V_n^2 - 2V_m V_n \cos(\theta_{mn}))], \quad (15)$$

where g_{mn} is conductance of transmission line between busses *m* and *n*. V_m and V_n are voltages at busses *m* and *n*, *k* is number of lines and θ_{mn} is phase angle difference between busses *m* and *n*.

III. CASE STUDY

As it is said earlier, for our test network we used IEEE 24 – test network, which is shown on Fig 2.

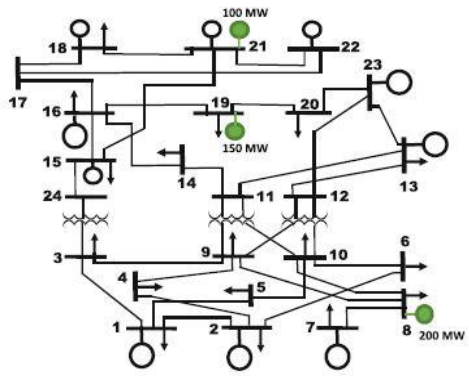

Figure 2. IEEE 24 – test network

In order to show impact of ESS on reductions of power losses, we first run the algorithm and calculate power losses in system without ESS. We obtained that the minimal value of losses is 0.987 [pu]. After that, in this paper we performed also two more cases:

- In non-generating nodes we put storages with different fixed power,
- Optimal allocation of ESS with different power.

A. *ESS with different fixed power in non-generating nodes*

In this case in non-generating nodes we used ESSs of different fixed value of power. The numerical results are given in Table 1. From these results it can be seen that if ESS is not

properly located and properly dimensioned its impact on power losses can be negligible. However, it can be seen, in this case, the minimal value of power losses can be obtained with 1000MW ESS connected in node 20.

TABLE I. NUMERICAL RESULTS FOR CASE A

Nodes	Power of ESS [MW]							
	100	***200***	***300***	***400***	***500***	***600***	***800***	***100***
4	0,987	0,987	0,987	0,987	0,987	0,987	0,987	0,987
5	0,987	0,987	0,987	0,987	0,987	0,987	0,987	0,987
6	0,987	0,987	0,987	0,987	0,987	0,987	0,987	0,987
10	0,987	0,987	0,987	0,987	0,987	0,987	0,987	0,987
9	0,987	0,987	0,987	0,987	0,987	0,987	0,987	0,987
3	0,987	0,987	0,987	0,987	0,987	0,987	0,987	0,987
24	0,987	0,987	0,987	0,987	0,987	0,987	0,987	0,987
12	0,985	0,984	0,984	0,983	0,982	0,981	0,98	0,979
11	0,986	0,986	0,986	0,986	0,986	0,986	0,986	0,986
14	0,987	0,987	0,987	0,987	0,987	0,987	0,987	0,987
20	0,982	0,978	0,974	0,971	0,967	0,964	0,958	0,952
17	0,986	0,986	0,985	0,985	0,985	0,984	0,984	0,984

B. Optimal allocation of ESS with different power

For the second case, we placed ESSs in optimal nodes, which are calculated with proposed algorithm, in order to minimize power losses in transmission network. When we compare results from Table 1 and Table 2, it can be seen that power losses are lower if we connect 50 ESS of 20MW located in optimal nodes (see Table 2). From the Table 2, we can also conclude that as we include more ESSs into the network, the optimal nodes are going to be spread through the network.

However, we can not say general rule about optimal nodes. This is multidimensional problem, and it is specific from case to case. It depends from many factors and some of them are: length of transmission lines in the network, load power, power and position of the thermal units as well as wind generators, etc.

TABLE II. NUMERICAL RESULTS FOR CASE B

Power of ESS [MW]	Minimal number of ESS in one node	Total number of ESS in grid	Total power losses	Optimal nodes
20	5	5	0,978	23-5
20	10	10	0,97	23-10
20	15	15	0,962	23-15
20	20	20	0,954	23-20
20	30	30	0,939	23-30
20	40	40	0,925	22 -1, 23-39
20	50	50	0,911	22 -4, 23-46

IV. CONCLUSION

In this paper we analyzed the impact of number and power of ESS on the value of total power losses in the network. For this purpose, we used program GAMS and IEEE 24 – test bust system.

The presented results show that with the proper analysis, for the specific network, ESS can have significant impact.

REFERENCES

[1] F. Díaz-González, A.Sumper, O. Gomis-Bellmunt, "Energy Storage in Power Systems", Wiley, may 2016.

[2] M. Farrokhifar, S. Grillo and E. Tironi, "Optimal placement of energy storage devices for loss reduction in distribution networks," IEEE PES ISGT Europe 2013, Lyngby, 2013, pp. 1-5.

[3] Z. Jiang, J. Feng, Y. Sun, B. Sun and N. Wu, "Wind farm energy storage capacity optimization based on PSO," 2013 Ninth International Conference on Natural Computation (ICNC), Shenyang, 2013, pp. 590-594.

[4] B. Das and A. Kumar, "Cost optimization of a hybrid energy storage system using GAMS," 2017 International Conference on Power and Embedded Drive Control (ICPEDC), Chennai, 2017, pp.89-92.

[5] M. A. Abdulgalil, A. M. Amin, M. Khalid and M. AlMuhaini, "Optimal Sizing, Allocation, Dispatch and Power Flow of Energy Storage Systems Integrated with Distributed Generation Units and a Wind Farm," 2018 IEEE PES Asia-Pacific Power and Energy Engineering Conference (APPEEC), Kota Kinabalu, 2018, pp. 680-684.

[6] W. Du, Z. Chen, H. F. Wang and Rod Dunn, "Energy storage systems applied in power system stability control," 2007 42nd International Universities Power Engineering Conference, Brighton, 2007, pp. 455-458.

[7] Q. A. Salih, D. M. Soomro and I. S. Saeh, "Optimal distributed generators location for power losses improvement using sensitivity based method," 2015 IEEE 3rd International Conference on Smart Instrumentation, Measurement and Applications (ICSIMA), Kuala Lumpur, 2015, pp. 1-4.

[8] A. Soroudi, Power System Optimization Modeling in GAMS. Springer, 2017.

[9] M. Calasan, L. Nikitovic, S. Mujovic, "Conopt solver embeded in GAMS for optimal power flow", Journal of Renewable and Sustainable Energy, accepted for publications, 2019.

Impacts of Climate Trends on Energy Production by Renewable Sources

Luiz Felipe Souza Fonseca, Victor Hugo Lobo Correia, Monica Carvalho

Federal University of Paraíba, João Pessoa, Brazil. luiz.fonseca@cear.ufpb.br; victorloboc@gmail.com; monica@cear.ufpb.br

Abstract — **Research on climate change is essential to carry out satisfactory energy planning, as it is necessary to know and understand local characteristics. Climate change can hinder energy planning efforts, as local variations can be present, even within the same region, and can lead to an increase or decrease in the output of a specific renewable energy technology. This study presents a bibliographical review regarding the impacts of climate change on the outputs of renewable energy-based technologies. A systematic search was carried out in the Google Scholar, CAPES journals, and Science Direct databases. The search resulted in 61 studies, within the 2001-2019 period, of which 26 were selected after titles and abstracts were read to verify whether the studies fulfilled inclusion criteria. Studies were then thoroughly read to identify those that addressed the variation explicitly in the outputs of renewable energy technologies due to climate change, which finally resulted in 20 studies. The results obtained herein demonstrate that there are scarce studies on the subject, and many resources are not even mentioned (tide, ocean, geothermal). The studies that employed climate trends presented mixed results, with significant changes detected for some types of renewable resources, and non-significant changes for others.**

Keywords – weather, wind power, temperature, solar radiation.

I. INTRODUCTION

The greenhouse effect is a natural phenomenon on Earth and essential for life. However, its intensification is not beneficial for the organisms that live here. According to the Intergovernmental Panel on Climate Change (IPCC), climate change refers to a change in the state of climate, identified by changes in its average and/or variability of its properties. The emissions of greenhouse gases (GHG) due to human activities can cause changes in air temperature and rain precipitation patterns, which are the main variations observed. These variations can be proven by statistics methods of meteorological series, as mentioned in [1]. Climate variation can be global or local, affecting energy generation, transmission, and distribution, for renewable or nonrenewable sources. The definition of renewable energy [2] involves sources with natural cycles of solar radiation conversion, practically inexhaustible, and that do not alter the planet's thermal balance. Wind energy, for example, as well as other climate aspects, is susceptible to long-term natural variability [3], and therefore, a small increase or decrease can become a much larger issue.

Combustion of nonrenewable resources (such as coal and oil) pollutes the environment with harmful particles, which spread across the world and influence global warming [4]. Therefore the utilization of renewable resources is the most viable way to reduce GHG emissions and, consequently, achieve sustainable development.

A more functional energy matrix is ideally constituted by more than one type of resource, but it is necessary to carefully analyze the different factors and impacts involved in the utilization of specific energy/natural resources.

Climatic changes significantly affect the outputs of renewable energy technologies. There is interference from the advance of global warming on renewable energy production, and a compilation of studies assessing climate effects on renewable energy production across the world was reported by [5].

A photovoltaic panel, for example, has its electrical conversion efficiency reduced when there is a significant temperature increase [6]. A wind turbine has a maximum wind speed limit

ISBN: 978-86-80616-04-9

in which it can operate without damaging its structure [7]. All renewable sources have pros and cons, and in the international context, the efforts to expand the participation of renewable energies are the subject of intense discussion [8]. The efficient use of available resources and renewable energy sources should be the main objective for regional development of the energy system [4].

It is still often the case that energy systems based on renewable sources consider the influential climatic parameters in their production to be constant, such as the incidence of solar radiation. However, climate trends analyzed and evaluated in various regions of the world have shown that it is no longer possible to consider these parameters as constant and stable values over the years [9]. Therefore, the understanding of climate dynamics is essential in determining the energy produced [1].

The objective of this study is to present how climate change affects the use and generation of renewable energy, based on a literature review of scholarly articles published on the subject.

II. Methodology

A search was conducted within the Google Scholar, CAPES Journals, and Science Direct databases. The following keywords were used: climate change, climate trends, climate and energy, electricity production, electricity generation, climate and electricity and their respective synonyms in Portuguese and Spanish (to maximize the number of studies identified).

- Inclusion criteria: the papers included in the analysis were those specifically addressing the generation, production, or use of renewable energy affected by climate change and published between 2001 and 2019.
- Exclusion criteria: The papers that addressed climate change without focusing on the consequences of renewable energy were excluded from the analysis. Also excluded were studies that reported in the forms of energy production through renewable sources.
- Analysis: First, systematic reading of the titles of the studies was performed. Papers with titles relevant to the theme were selected. The abstracts were read to filter the studies regarding their scope. Finally, the studies were entirely read to ensure the fulfillment of inclusion criteria. The references of the included studies were also analyzed, in case relevant studies could be found.

III. Results

After the initial bibliographical research, the search returned 47 studies. Also, the references cited in the selected studies were investigated, and 14 more papers were included, leading to a total of 61. Then, studies were screened by reading the abstracts, and then 26 were considered relevant according to the inclusion criteria.

After reading the full versions of the studies, 20 works were selected, all published between 2001 and 2019. It was verified that research on climate change that affects renewable energy power generation has been carried out in many countries around the world, including three continents: America, Europe, and Africa. Among them, Europe produced the most significant number of scientific studies published in this area. A brief explanation of each study and its results follows.

Reference [3] investigated scenarios of climate change impacts on wind power generation potential in five different regions of the Northwest United States. The authors compiled wind speed data from five airports within the study region, with a reference height of 10m, between 1964 and 2000. The annual average wind speed was collected for Boise (Idaho), Casper (Wyoming), Great Falls (Montana), Portland (Oregon) and Yakima (Washington). The wind speeds in the Northwest of United States, obtained with models applied to future climate scenarios, suggest that in warm weather such as summer and spring, the wind power resource may drop 5%-10%. During wintertime, the reduction may be slight or possibly increase like in Yakima, where a potential rise is indicated. However, the models presented a considerable inconsistency in statistics for this city. The study concluded that there is a high level of uncertainty about the impacts of future climate changes on wind power resource in Yakima, but data obtained for the other four Northwest cities are reliable.

Reference [10] employed two climate models: General Circulation Model (GCM) HadCM2 and Regional Climate Model (RCM) RegCM2. The objective of this study was to verify the potential change in wind power over the United States due to CO_2 emissions in the early and mid-21st century. The authors verified

that the difference in daily average wind power between an enhanced CO_2 scenario and a scenario in the actual period of the research decreased 10%-20% for all seasons in most of the United States. However, small areas of the country such as the south-central region, show possible increases of 0% - 30%.

In [11], the authors showed that the near-surface wind speeds are higher than projections made by IPCC for emissions scenarios A2 and B2. The study used the Regional Climate Model (RCM) with boundary conditions derived from ECHAM4/OPYC3 AOGCM, and the HadAM3H GCM with the control period of 1961-1990, and analyzed period of 2071-2100. The analyses focused on northern Europe and specifically on the Baltic region. In the simulations conducted using HadAM3H, the values were less expressive than in simulations with ECHAM4/OPYC3. However, the authors conclude that there is a possible increase of 10% in the wind speed and availability, during the latter portion of the 21st century.

The vulnerability of renewable energy power generation to climate change in Brazil was studied by [12]. The work analyzed hydropower generation and biofuels production, with IPCC emission scenarios A2 and B2. Regarding hydropower generation, both scenarios exhibit a descending trend in the 2071-2100 period. According to the authors, the impacts are lower in the south and southeast, while the more substantial impact occurs in the north and northeast regions of Brazil. The consequence in the latter will be lower flow inputs to hydropower reservoirs. São Francisco Basin is the most affected, where the decrease in energy production could reach more than 7% for the B2 scenario. Regarding biodiesel production, the temperature in the northeast and mid-west regions is expected to rise, which can directly affect soy production and hence fuel production. However, in the south and southeast regions, soy production is likely to improve as a result of climate change.

The effects of climate change on the wind energy resource of Ireland were evaluated in [14]. Through the Regional Climate Model (RCM) Rossby Center's RCM (RCA3), Nolan et al. found a possible increment of wind energy potential during winter months and a reduction for summer. All four simulated scenarios exhibited the changes through annual wind speeds analysis. The predictions show that in the winter, the annual energy content increases 4%-10% and decreases 5%-14% in summer months. Moreover, the wind directions changes were analyzed, and no meaningful changes were identified. Finally, the authors suggest that annual variability could occur due to cyclone activity over the studied regions.

The authors of [15] studied wind power development in the UK and the influence of climate change. The research shows that mean wind speed is higher over the winter and lower in summer. Also, there is a considerable variation in the mean wind speed across the country, with higher speeds in the coasts and northern areas. The period evaluated was 2081-2100. The authors concluded that the annual impact of wind speed increase is minimal, and thus a re-plan strategy to handle wind power development would not be necessary.

Climate change effects on renewable power generation in Germany's Northwest Metropolitan Region was analyzed in [16]. The research focuses on solar and wind power generation. Regarding solar energy, only photovoltaic power plants were considered. Global radiation could rise by 18.3% for the period 2071-2100. During the summer, this growth is due to less cloud cover. According to the authors, wind energy is much dependent on climate, especially on wind speeds. For the 2071-2100 period, the increment would be 12.3% and 12.9% for 2036-2065. Projections show that mean wind speeds decrease in summer and increase in winter. Although there will be a variation of global radiation within the studied region, solar power production is not considerably affected because of the broad range of the photovoltaic modules' tilt angles, which can improve efficiency. Nevertheless, wind energy is affected by its cubic dependence on wind speeds and changes of season that increase in fall and winter.

Reference [19] investigated future changes in the potential of wind power generation over Europe and in the effectiveness of wind power production from wind farms operating at the end of 2012 and expected by 2020. It is reported that future changes do not affect (either positively or negatively) wind power potential over a significant part of Europe. Nevertheless, a substantial reduction is noticed over the Mediterranean region, while a relevant rise is found in the Aegean Sea and Baltic Sea areas. The authors concluded that the variation of wind

power potential in Europe would remain between ±15% and ±20% by mid- and late- century, respectively.

The authors in [22] studied the influence of climate trends on future energy utilization in the hinterland area of the Paraíba state. Climate data from 1970 to 2014 was employed, obtained from two meteorological stations localized in the cities of Patos and São Gonçalo. The scenarios assessed the energy production of two renewable resources: solar photovoltaic and wind energy. It was found that there is more cloud cover during the first four months of the year, which is also the rainy season with the lowest wind speed. The analysis showed a temperature increase of 0.04 ^{o}C/year in Patos station, but the authors concluded that photovoltaic energy production was not considerably affected over the four decades analyzed. For wind energy, there was a relevant decrease when comparing the first ten years with the last ten years.

The average wind speed fields over Mozambique through the dynamic downscaling technique on the RAMS6.0 was simulated in [23]. The objective of this work was to verify the wind potential variation for the period 2079-2099 in comparison to 1985-2005. To this end, wind speeds were analyzed at three heights: 10, 50, and 100 meters. The results showed that the wind speed was stronger during the period of analysis due to the positive values obtained at all the heights. Regarding wind direction, there will be variation in each month when compared to the months of the reference period, with a 5% to 30% fluctuation throughout the year. The research concluded that the wind resources predicted for 2079-2099 are equally distributed and it indicates a mean increase in annual wind speed of 2-4% to 10 meters, 2-9% to 50 meters, and 1.5-7% to 100 meters. This increase is higher in the central and southern regions of the country during the winter.

The authors in [1] evaluated a set of scientific studies about the consequences of climate trends on photovoltaic energy generation in semiarid regions. The research shows a significant influence of climate change on electricity production. Although there is considerable solar potential, the temperature rise is an obstacle in photovoltaic production.

The EURO-CORDEX ensemble of high-resolution climate projections together with a PV power production model were employed to assess the impacts of climate change on photovoltaic power generation in Europe by [9]. The results show that the mean solar radiation pattern, for 1970-1999 versus 2070-2099 periods, is positive in Southern Mediterranean regions and negative in the north areas, reaching about 5W/m² for the former and -10W/m² to 20W/m² for the latter. The study indicates that by the end of the 21st century, changes in photovoltaic production compared with current climate conditions will be in the range of -14% to 2%, with northern countries presenting the most significant reductions.

The analysis conducted in [13] applied two climate models: HadGEM1 and HadCM3. The scenario used was the IPCC special report on emissions scenarios (SRES) A1B, and the study regions were California, Nevada, Spain, Algeria, Germany, Saudi Arabia, China, and Australia. The study indicated that temperature and insolation contributions are relevant to photovoltaic (PV) and concentrated solar power (CSP) production. The statistics show that Spain, Germany, and China present an increase in the photovoltaic power production of 3%, 4%, and 3.5%, respectively; whereas in California, Spain, Algeria, China, and Germany CSP production will grow between 4% for the first and 12% for the last. All data were assessed from 2010 to 2080.

The solar energy resource in the UK and the impact of climate change were investigated by [17]. The work utilized the UKCP09 probabilistic climate change projections and the baseline period of 1961-1990. Considering an intermediate emissions scenario, it was estimated that in 2050, summer months show solar irradiance rise of 7.9% in the southwest and a reduction of -2.9% in the north of Scotland. In Midwest Scotland, a decrease of -7.6% is expected for winter months. Solar energy resource will increase in most southern regions of the UK during the summer, while few regions will show a slight decrease. When considering a high-emission scenario, annual growth is expected, from 3.6% in 2050 to 4.4% in 2080. The study concluded that climate change would enhance solar energy resources in the south and slightly reduce in the northwest of the UK.

Climate change impact on photovoltaic energy generation in Greece was assessed by [18]. The authors obtained monthly means of temperature and irradiance for five regional climate models under the SRES A1B emission scenarios of the IPCC. The projection of change in photovoltaic energy generation was estimated

for two periods, 2011-2050 and 2061-2100. While in the first period the average variation of temperature is about 1.5 ºC and irradiance ranges between 2-3 W/m², in the 2061-2100 period these values reach 3-3.5ºC and 2-5W/m². For the latter, a more considerable increase is expected over Epirus and western Macedonia. The authors concluded that a considerable reduction is expected due to temperature rise, but this is compensated by irradiance increase, resulting in a 4% energy generation increment.

In [20], the authors assessed the impacts of climate change on wind and solar resources in southern Africa. The study used the MERRA dataset to represent the base climate for both resources. Variations in wind speeds and Global Horizontal Irradiance were predicted for southern Africa through data analysis over 11 years, from 2045 to 2055. December and January season presented the highest wind energy potential, while energy demand is higher from June to August. The fluctuation in wind speed would be relatively slight, around 1.5 m/s (positive or negative). In 2050, however, this fluctuation will be relevant in some regions, reaching ±20%. The authors conclude that wind and solar resources of southern Africa will remain unchanged, but with a small change probability of ±15%.

The research conducted by [21] applied eight climate models. The models contained solar radiation and air temperature datasets to analyze the impacts of climate change on photovoltaic energy production in West Africa between 2006-2100. Results show that trends of solar radiation are negative for seven models, except for the IPSL, which was the only model to predict a positive trend of 0.17 W/m²/year for Cape Verde. However, the MIROC model predicted a reduction of -0.18 W/m²/year for the same location. Regarding temperature, an increment between 0.02 ºC/year and 0.08 ºC/year was detected for all regions. The authors affirm that the trends are negative in all countries analyzed, except for Liberia and Sierra Leone, where photovoltaic production may increase.

Reference [24] examined the trends in temperature and rainfall nearby the artificial Sobradinho Lake, located in the state of Bahia, Northeast Brazil. Data for the period 1966 to 2014 were provided by the Brazilian Agricultural Research Corporation (EMBRAPA). The climatic indices were calculated through the software RClimDex, developed by Xuebin Zhang and Feng Yang for the Canadian Meteorological Service. The results indicate an increasing trend of temperature as well as warm days along the year for two stations assessed: Bebedouro – PE, and Mandacaru – BA. Nevertheless, it is not possible to ensure that the construction of the artificial lake of the Sobradinho Hydroelectric Plant affected local microclimate. Also, based on the Pettitt test [25], a rise in temperature and warm days cannot be attributed to the formation of the artificial lake.

The impact of climate trends on photovoltaic energy generation in the Brazilian semiarid was studied in [26]. The research utilized the characteristics of two solar panels: AXITEC AC-270P/156-60S and Panasonic VBHN240SJ25. Data from 1961 to 2014 were obtained from the Brazilian National Institute of Meteorology (INMET) and assessed through the Mann-Kendall method, which analyzes variables regarding increasing or decreasing trends. According to the authors, the monthly average temperatures throughout the year were about 25ºC and 28ºC in winter and summer, respectively, with higher cloud cover in winter months. However, annual trends were relevant, demonstrating temperature rise. Therefore, electricity generation decreased when comparing the first decade to the last decade of the considered period, but this reduction was slight, representing less than 1% for annual values. Finally, it was concluded that the influence on photovoltaic energy production was small for both solar panels, even with temperature increases.

The Sertão Paraibano mesoregion was analyzed in [27] to verify temperature variations, through data provided by INMET. The software Estima_T was used to study the spatial and temporal distribution of the air temperature of cities within the region. From 1950 to 2017, there was a significant increase in air temperature estimation for all locations, with a range of 0.008 to 0.0011ºC/year. The authors indicate a relevant alteration in air temperature, which is according to the temperature increase of up to 1ºC by 2040 for the semiarid Northeast region as forecasted by the Brazilian Panel on Climate Change (PBMC) and the Intergovernmental Panel on Climate Change. The temperatures vary between 21.9 to 27.8 ºC, with December and July being the hottest and coldest months, respectively.

TABLE I. DETAILS AND INFORMATION COMPILED FROM ANALIZED PAPERS

Author	Source	Expected energy production	Region	Scenario (s)	Climatic Model (s)	Spatial scope
Sailor et al. [3]	Wind	Decrease(summer), Increase (winter) [1]	Northwest United States	A1B and A2	ECHAM5/MPI-OM, GFDL-CM2.1, GIS-S-ER, MRI-CGCM2.3.2	Regional
Jerez et al. [9]	PV	Decrease	Europe	RCP4.5, RCP8.5	EURO-CORDEX [3]	Regional
Sengal et al. [10]	Wind	Decrease	United States	**	HadCM2, RegCM2	Country
Pryor et al. [11]	Wind	Increase [1]	Northern Europe	A2 and B2	RCAO	Regional
Lucena et al. [12]	Hydro, Biofuel	Decrease [1]	Brazil	A2 and B2	PRECIS	Country
Crook et al. [13]	PV and CSP	Increase	*	A1B	HadGEM, HadCM3	Country
Nolan et al. [14]	Wind	Increase (winter), Decrease (summer)	Ireland	A1B, A2, B1 and B2	RCA3	Country
Cradden et al. [15]	Wind	*no significant change*	United Kingdom	A1B, A2 and B1	ECHAM5	Country
Wachsmuth et al. [16]	Wind and PV	Increase [1]	Northwest Germany	A1B	REMO, CLM	Regional
Burnet et al. [17]	PV	Increase (South), Decrease (Northwest)	United Kingdom	n/a	UKCP09	Country
Panagea et al. [18]	PV	Increase	Greece	A1B	C4IRCA3, ETHZ-CLM, MPI-M-REMO, SMHIRCA, CNRM-RM5.1	Country
Tobin et al. [19]	Wind	Decrease	Europe	A1B	RCA3	Regional
Fant et al. [20]	Wind and PV	*Unchanged*	Southern Africa	IGSM	Statistical	Country
Bazyomo et al. [21]	PV	Decrease	West Africa	RCP8.5	**	Country
Abrahão et al. [22]	Wind and PV	Decrease [1]	Northwest Brazil	n/a	Mann-Kendall [2]	Regional
Silva et al. [23]	Wind	Increase	Mozambique	RCP8.5	RAMS6.0	Country
Silva et al. [26]	PV	*no significant change*	Brazil	n/a	Mann-Kendall [2]	Region

[1] see discussion for more information.
[2] non-parametric test of Mann-Kendall, for the analysis of climate change in time series.
[3] software package – ETCCDI climate change indices.
* regions: California, Nevada, Spain, Algeria, Germany, Saudi Arabia, China, and Australia.
** the climatic models are: NOAA, NCC, MPI, MIROC, IPSL, ICHEC, CNRM, CCCMA

Table 1 shows a compilation of information from the studies herein analyzed, which are further explained.

In [3], the impacts in scenario A2 were generally slightly higher than in scenario A1B, but difference is minimal. The use of different scenarios also showed a difference in the results of [11], using boundary conditions from ECHAM4/OPYC3 that indicate an increase in the control period of 1961-1990, but these changes are more pronounced in the A2 scenario than in B2. When compared to the 2071-2100 period, the differences are statistically significant.

The decrease in energy is higher in the B2 scenario, in [12], with 3.15% compared to 1.58% for the A2 scenario. The authors also mention that for the northeast and center regions

of the country, there is also a decrease in energy generation due to lower flow inputs to hydroelectric plants. Finally, the production of biofuel will also decrease due to the impact of temperature increase due to Global Climate Change.

In [16], the authors report no significant increase in energy production by solar photovoltaic. However, the slightly higher wind speeds affect wind power production, which is higher in the fall season until the mid-21st century and even higher in the winter season until the end of the century. Similarly, in [22], photovoltaic power production was not significantly affected in the period. However, the wind power production was considerably affected, with 38% and 88% less electricity produced in Patos and São Gonçalo stations, respectively.

Following the research line of [1, 5, 24-41], the need of further studies on historical climate behavior at the installation site of new energy systems is highlighted, including the identification of climate trends.

IV. CONCLUSION

The studies identified herein mainly address two types of renewable energy sources: wind and solar photovoltaic. Power generation by solar concentration and hydroelectric have also been studied, to a lower degree. However, other sources are not investigated regarding climate variations that affect the generation of electricity.

Future climate projections are very site-dependent and could be both advantageous and disadvantageous for the same region studied, differing only by the seasons of the year. In most studies, the winter season presented the most satisfactory results for wind power generation while summer presented the highest solar irradiation, which contributed to enhanced photovoltaic generation.

However, the amount of studies on this topic is still scarce. Climate analysis for future generation of electricity requires a considerable climate database, which is not evident in many countries, as weather stations do not count with long series of data, which hinders these analyses.

More studies are necessary on the influence of climatic factors on electricity generation by renewable sources. The studies included in the review presented herein were carried out in different parts of the world for specific, limited renewable electric power generation, showing the growing interest in this area of study and demonstrating growing demand for more research in the area.

REFERENCES

[1] J. M. S. Júnior, J. R. F. Neto, R. Abrahão, M. Carvalho and A. K. P. Oliveira, “Considerations on climate trends in photovoltaic power production in semiarid regions,” 1st National Congress of Semiarid Diversity, Natal, Brazil, Dec. 12−14, 2018, pp. 1−10. [In Portuguese]

[2] F. Pacheco, “Renewable energy: brief concepts,” Conjuncture and Planning, n. 149, SEI, 2006, pp. 4−11.

[3] D. J. Sailor, M. Smith and M. Hart, “Climate change implications for wind power resources in the Northwest United States”, Renewable Energy, vol. 33, 2008, pp. 2393–2406.

[4] V. Klevas, K. Brieksa and L. Murauskaitė, “Innovative method of RES integration into the regional energy development scenarios,” Energy Policy, vol. 64, 2014, pp. 324-336.

[5] J. R. F. Neto, J. M. S. Júnior, R. Abrahão and M. Carvalho, “How do climate change impact on renewable energy production?” VI Brazilian Congress on Environmental Management and Sustainability, João Pessoa, Brazil, Nov. 23−26, 2018, pp. 771-779. [In Portuguese]

[6] E. A. F. A. Fadigas, “Photovoltaic solar energy: fundamentals, conversion and technical and economic feasibility,” Energy group Polytechnic School University of São Paulo, pp. 22−92. [In Portuguese]

[7] E. A. F. A. Fadigas. Wind Energy, v. 1, São Paulo: Manole LTDA, 2011. [In Portuguese]

[8] C. Bermann, “Environmental crisis and renewable energies,” Energy, Environment and Society, vol. 60, 2008, pp. 20−29. [In Portuguese]

[9] S. Jerez, et al., “The impact of climate change on photovoltaic power generation in Europe,” Nature Communications, vol. 6, 2015, pp. 1−8.

[10] M. Sengal, Z. Pan, R. W. Arritt and E. S. Takle, “On the potencial change in wind power over the US due to increases of atmospheric greenhouse gases”, Renewable Energy, vol. 24, 2001, pp. 235–243.

[11] S. C. Pryor, R. J. Barthelmie and E. Kjellström, “Potential climate change impact on wind energy resources in northern Europe: analyses using a regional climate model”, Climate Dynamics, vol. 25, 2005, pp. 815–835.

[12] A. F. P. Lucena, et al., “The vulnerability of renewable energy to climate change in Brazil”, Energy Policy, vol. 37, 2008, pp. 879–889.

[13] J. A. Crook, L. A. Jones, P. M. Forster and R. Crook, “Climate change impacts on future photovoltaic and concentrated solar power energy output”, Energy & Environmental Science, vol. 4, no. 3101, 2011.

[14] P. Nolan, P. Lynch, R. McGrath, T. Semmler and S. Wang, “Simulating climate change and its effects on the wind energy resource of Ireland”, Wind Energy, vol. 15, 2011, pp. 593–608.

[15] L. C. Cradden, G. P. Harrison and J. P. Chick, “Will climate change impact on wind power development in the UK?”, Climatic Change, vol. 115, 2012, pp. 837–852.

[16] J. Wachsmuth, et al., “How will renewable power generation be affected by climate change? The case of a Metropolitan Region in Northwest Germany”, Energy, vol. 58, 2013, pp. 192–201.

[17] D. Burnett, E. Barbour and G. P. Harrison ,“The UK solar energy resource and the impact of climate change”, Renewable Energy, vol. 71, 2014, pp. 333–343.

[18] I. S. Panagea, I. K. Tsanis, A. G. Koutroulis, and M. G. Grillakis, “Climate Change Impact on Photovoltaic Energy Output: The Case of Greece”, Advances in Meteorology, vol. 2014, no. 264506, pp. 11.

[19] I. Tobin, R. Vautard and I. Balog, “Assessing climate change impacts on European wind energy from ENSEMBLES high-resolution climate projections”, Climatic Change, vol. 128, 2014, pp. 99–112.

[20] C. Fant, C. A. Schlosser and K. Strzepek, “The impact of climate change on wind and solar resources in southern Africa”, Applied Energy, vol. 161, 2015, pp. 556–564.

[21] S. D. Bazyomo, A. E. Lawin, O. Coulibaly and A. Ouedraogo, “Forecasted Changes in West Africa Photovoltaic Energy Output by 2045”, Climate, vol. 4, no. 53, 2016.

[22] R. Abrahão, I. M. B. M. Peixoto and M. Carvalho, “Solar or wind energy for the Brazilian semiarid? - Climatic characterization and future trends”, 30th Int. Conf. on Efficiency, Cost, Optimization, Simulation and Environmental Impact of Energy Systems, San Diego, USA, July 2-6, 2017, pp. 1–12.

[23] E. M. Silva, N. M. Banga and J. M. B. Alves, “Wind Resource Modeling on Mozambique Considering Climate Change Scenario”, Brazilian Journal of Meteorology, vol. 32, 2017, pp. 157–170. [In Portuguese]

[24] M. M. M. S. Melo, et al., “Trends in Temperature and Rainfall Extremes near the Artificial Sobradinho Lake, Brazil”, Brazilian Journal of Meteorology, vol. 33, 2018, pp. 426–440.

[25] A. N. Pettitt, “A non-parametric approach to the change-point problem”, Applied Statistics, vol. 28, 1979, pp. 126–135.

[26] L. P. Silva, S. E. Leite, W. K. M. Silva and R. Abrahão, “Climate trends in the Paraíba forest mesoregion and its influence on photovoltaic energy production”, Biosphere Encyclopedia, vol. 15, 2018, pp. 90–101. [In Portuguese]

[27] S. E. L. Medeiros, R. Abrahão, L. P. Silva and W. K. M. Silva, “Comparison between observed and estimated data to assess air temperature variability and trends in the Sertão Paraibano mesoregion (Brazil)”, Environmental Monitoring and Assessment, vol. 191, no. 63, 2019. [In Portuguese]

[28] R. Abrahão, “Understanding regional climate change by applying three statistical methods,” V Brazilian Congress of Solar Energy, Recife, Brasil, Mar. 31–April 03, 2014. [In Portuguese]

[29] R. Abrahão, “Group Comparison, Trends and Cluster Analysis to Understand Historical Precipitation,” 7th Global Conference on Global Warming, Athens, Greece, May 24−27, 2015, pp. 77−87.

[30] R. Abrahão, “Group Comparison, Trends and Cluster Analysis to Understand Historical Precipitation,” Energy, Transportation and Global Warming, vol. 1, P. Grammelis, Eds. Springer International Publishing, 2016, pp.77−87.

[31] R. Abrahão, L. P. Silva and I. M. B. M. Peixoto, “Interpretation of climate trends towards a better renewable energy use in the Brazilian semiarid,” X Cuba Industry 2016 - Reclien, La Havana, Cuba, 2016. [In Spanish]

[32] S. E. L. Medeiros, R. Abrahão, I. G. Garizabal, I. M. B. Peixoto and L. P. Silva, “Trend analysis of rainfall within the state of Paraíba (Brazil),” V International Symposium On Environmental Biotechnology And Engineering, Buenos Aires, Argentina, 2016. [In Spanish]

[33] I. M. B. M. Peixoto, L. P. Silva and R. Abrahão, “Initial observations of climate change for the Paraibano Sertão,” IV National Environmental Education Congress, João Pessoa, Brazil, 2016. [In Portuguese]

[34] L. P. Silva, I. M. B. M. Peixoto and R. Abrahão, “Initial analysis of climate change in the Paraíba coast,” IV National Environmental Education Congress, João Pessoa, Brazil, 2016. [In Portuguese]

[35] R. Abrahão, I. M. B. M. Peixoto and M. Carvalho, “Solar or wind energy for the Brazilian semiarid - Climatic characterization and future trends,” XXX International Conference On Efficiency, Cost, Optimization, Simulation And Environmental Impact Of Energy Systems, San Diego, California, 2017a, pp. 1–12.

[36] R. Abrahão, I. M. B. M. Peixoto, L. P. Silva and S. E. L Medeiros, “More heat for the Sertão? Perspectives of trends in the heat index of Sertão Paraibano,” XX Brazilian Congress of Agrometeorology, Petrolina, Pernambuco, 2017b. [In Portuguese]

[37] S. E. L. Medeiros, W. K. M. Silva, L. P. Silva, I. M. B. M. Peixoto and R. Abrahão, “Variability analysis and trends for the average air temperature in the Sertão Paraibano with real and estimated data,” II CONIDIS, Campina Grande, João Pessoa, 2017. [In Portuguese]

[38] S. E. L Medeiros, “Analysis of trends and weather patterns for the Paraíba backlands mesoregion with emphasis on renewable energies,” Masters dissertation, Universidade Federal da Paraíba, João Pessoa, Paraíba, 2018. [In Portuguese]

[39] S. E. L. Medeiros, R. Abrahão, I. G. Garizabal, I. M. B. M. Peixoto and L. P. Silva, “Assessment of Precipitation Trends in the Sertão Paraibano Mesoregion,” Brazilian Journal of Meteorology, vol. 33, 2018, pp. 344.

[40] L. P. Silva, S. E. Leite, W. K. M. Silva and R. Abrahão, “Climate trends in the Paraíba forest mesoregion and its influence on photovoltaic energy production,” Biosphere Encyclopedia, vol. 15, 2018, pp. 90-101. [In Portuguese]

[41] S. E. L. Medeiros, R. Abrahão, L. P. Silva and W. K. M. Silva, “Comparison between observed and estimated data to assess air temperature variability and trends in the *Sertão Paraibano* mesoregion (Brazil),” Environmental Monitoring and Assessment, vol. 191:63, 2019, pp. 1−1

Efficient Energy Trading Based on Blockchain Technology

Nenad Petrović, Đorđe Kocić

Faculty of Electronic Engineering, University of Niš, Niš, Serbia,
nenad.petrovic@elfak.ni.ac.rs; seriousdjoka@gmail.com

Abstract — **In this paper, we propose a framework for efficient energy trading within the Smart Grid. Backbone of the system is smart contract generator supported by blockchain technology. System also features load forecasting model based on deep learning and a linear model for optimal energy distribution.**

Keywords – blockchain, deep learning, linear optimization, smart contract, smart grid.

I. INTRODUCTION

Future of power distribution networks is the *smart grid*. It enables, from a technical perspective, a better, more efficient and more reliable way of utilizing the power grid. Traditionally main problems of the distribution power networks are variable consumer energy demand, power losses and faults [1, 2]. All of which are relatively well handled by the smart grid that provides adaptive demand response, smart power management and reliability-based maintenance [1, 2].

New challenges involve distributed power generation (relying mostly on renewable energy sources) in medium and low voltage networks. Distributed generation sources usually offer intermittent and non-constant power generation. That makes generation and load management more difficult. Energy trading contracts in smart grid are a possible new way of energy management [3, 4]. The goal of this concept would be to create a open market for energy trading on the local (regional) level, the level of distribution grid, which would in turn stimulate small private companies to invest in power accumulation and generation facilities and create a more constant supply of power on distribution level. The main benefits are [3, 4]: better usage of intermittent energy sources, possible lower cost of electrical energy for the utility companies.

In recent years, the blockchain technology has been adopted in various fields to ensure security and trust, especially when financial transactions are involved. This was also the case for energy trading. However, the existing solutions mainly focus on the trading itself and do not consider the problem of providing energy timely [5, 6, 7], which is contradictory to the main principles of smart grid architecture advocating that near real-time response is crucial [1, 2, 8].

For that reason, we decide to focus on developing a novel framework for efficient energy trading between the power generation and the consumers leveraging the load forecasting together with optimization to provide timely response to consumer demands. In this paper, the main aspects of the implemented framework are presented: architecture, optimization model, load forecasting mechanism and smart contract generator. Moreover, some evaluation aspects of the implemented framework are included: prediction performance evaluation and time necessary for smart contract generation.

II. BACKGROUND AND RELATED WORK

A. Linear programming

Linear programming (also known as *linear optimization*) is a method aiming to achieve the best outcome possible (such as maximum profit or lowest cost), based on a mathematical model whose requirements are represented by linear relationships [9]. More precisely, it refers to a technique for optimization of a linear objective function, subject to linear equality and inequality constraints. Problem which can be expressed in the canonical form such as the following is referred to as *linear program*:

ISBN: 978-86-80616-04-9

$$maximize\ c^T x\ . \quad (1)$$

$$subject\ to\ Ax \le b\ . \quad (2)$$

$$and\ x \ge 0\ . \quad (3)$$

In this case, x represents the vector of variables that have to be determined (*decision variable*). Moreover, c and b are vectors of known coefficients, while A is a known matrix of coefficients. Linear programming is widely adopted – from business and economics to engineering. In engineering, linear programming models are leveraged in transportation, energetics, telecommunications, manufacturing, especially when it comes to problems in planning, routing, scheduling, assignment and distribution. In electric grids, optimization is used in processes of production, transmission and consumption to minimize costs, reduce overall consumption, balance supply and demand [10].

In this paper, linear programming is adopted for optimal energy distribution across connected electric grids with respect to constraints related to maximum energy capacity and demand. The goal is to minimize the overall power transfer and generation cost. For that purpose, we used AMPL, an algebraic modeling language for mathematical programming [11]. It provides the ability to write linear programs using the expressions similar to traditional algebraic notation with extensions that provide support for definition of network flow constraints and piecewise linearities specific to optimization problems. However, AMPL itself is not a solver, but it offers an interface to other programs which are actually responsible for solving. In our case, CPLEX is used as a solver. Its implementation is based on simplex method [12].

B. Deep learning

Deep learning refers to a family of machine learning techniques and algorithms based on artificial neural networks. The learning process itself can be either supervised, semi-supervised or unsupervised. It has been applied in various areas, such as computer vision, speech recognition, natural language processing, audio recognition, bioinformatics.

Artificial neural network (ANN) is a group of nodes interconnected through weighted links. A node (also referred to as *neuron* or *perceptron*) is a computational unit containing one or more weighted input connections, a transfer function that combines the inputs, and an output connection [13]. It receives the signal, processes it and then forwards it to other nodes connected to it. In neural networks, three types of layers are identified [13, 14]: 1) *input layer*, which corresponds to the input variables 2) *hidden layers*, the nodes between input and output layers 3) *output layer*, that produces the output variables. A *deep neural network* (DNN) is an artificial neural network (ANN) with multiple layers between the input and output layers [14].

In our case, deep learning approach is used for load forecasting (consumer demand) within the electric grid, leveraging the historical data that consists of electrical and other measurements (temperature and rainfall). For implementation, we rely on TensorFlow [1] library for Python programming language that supports GPU execution on CUDA-compatible hardware. The work related to load forecasting builds upon our previous work presented in [15], while the information about daily rainfall was included beside the average daily temperature as including weather data can lead to better forecasts [16].

C. Blockchain and smart contracts

Since the breakthrough of Bitcoin [2] cryptocurrency in 2009, blockchain has been considered as one of the most influential technologies of the last decade [17, 18, 19]. Its main purpose was enabling the transfer of financial assets worldwide without intermediary and additional transfer costs. From music industry to healthcare, huge efforts are put to adopt blockchain within the existing information systems and applications in order to increase overall safety and trust. Blockchain refers to a data structure (also called *ledger*) that consists of append-only sequence of blocks holding the information about the executed transactions [19]. However, the same term is often used for a distributed system that stores copies of the previously mentioned data structure within the

[1] https://www.tensorflow.org/

[2] https://bitcoin.org/en/

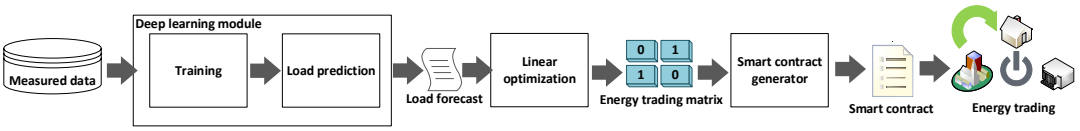

Figure 1. Framework architecture and working principle overview.

peer-to-peer network of nodes. Each node has alphanumeric address that enables both anonymity and transaction record transparency at the same time. Moreover, each block also contains a cryptographic hash of the previous block and timestamp in order to ensure that no one can modify or delete them, once they are recorded in ledger. The transaction itself represents transfer of value and ownership of digital tokens between sender and recipient recorded in the distributed ledger [18, 19]. Token can represent either tangible and intangible goods/assets, from cash and electrical energy to intellectual property.

When it comes to blockchain's adoption within the power grid systems, many interesting use cases have been presented in current literature. They can be summarized as follows [20, 21]: 1) operational status log of power grid 2) decentralized control of power transmission and distribution 3) energy trading. In this paper, we focus on blockchain adoption in energy trading.

Smart contracts are recognized as a key-enabler of this use case [21]. Smart contract is a protocol intended to digitally facilitate, verify, or enforce the execution of a particular contract [19]. In context of blockchain technology, it is a software code that defines and executes transactions on the target blockchain platform, while the performed transactions are trackable, irreversible and do not involve third parties. It can be implemented in any programming language and secured using encryption and digital signing. In case of Ethereum [3] [22] blockchain (considered in this paper), smart contracts are written using a high-level object-oriented language Solidity [4], developed by Ethereum Foundation. We decide to use Solidity due to fact that it is far more expressive and powerful than Bitcoin's original script language used for definition of smart contracts.

A similar approach to energy trading leveraging Solidity contracts within Ethereum blockchain network was used in [23]. The smart contract generation module used in this paper is a modified version of semantic-driven Solidity smart contract generator for Ethereum platform presented in [24], originally aiming contracts between the participants in music industry supply chain.

III. FRAMEWORK OVERVIEW

A. Architecture and working principle

In this subsection, we propose a novel framework for blockchain-based energy trading leveraging consumption demand forecasting. A complete overview of its architecture and working principle is illustrated in Fig. 1.

First, the measured electrical signals and other measurements are acquired and stored into the measurements database for a certain period. After that, the deep learning module performs training based on the historical data, so it becomes able to make predictions about the consumer demand within the electric in future. Furthermore, the load forecast produced by the deep learning module is forwarded to linear optimization component that is taking them as input, together with the other information in order to perform the optimal energy distribution. The energy trading matrix is produced as output of the optimization process, holding the information about the amount of energy that needs to be transferred between the grids. Finally, this matrix is used for generation of smart contract code that enables the execution of blockchain-based transactions.

B. Linear optimization model

Let us assume that there is a network of connected electric grids, where each grid is referred to as *node*, while the links between grids are referred to as *arcs*. Each $grid_i$ is characterized by the maximum capacity of electrical energy that can be produced, denoted as $capacity_i$ and consumer demand for electricity, denoted as $demand_i$, while both of them are given in megawatts. In cases when consumer demand is greater than the available

[3] https://www.ethereum.org/

[4] https://solidity.readthedocs.io/en/v0.5.5/

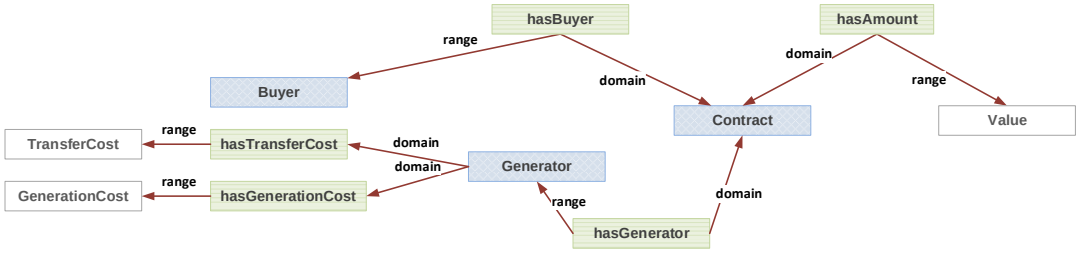

Figure 2. Energy trading ontology used for smart contract generation.

power that can be produced by the considered grid, the process of energy trading is performed. For each arc, we assign a decision variable indicating the amount of energy that will be exchanged between the nodes: $x[i,j] \geq 0$ if energy trading along $arc(i,j)$ will be performed, while $x[i,j]=0$ otherwise. For each arc, we assign the cost of energy transfer between $grid_i$ and $grid_j$ nodes, referred to as $transfer\_cost[i,j]$ given in dollars per megawatt. Moreover, the power generation cost for each $grid_j$ is denoted as $generation\_cost[j]$ and is given in the same unit as transfer cost. The principal constraint related to energy trade between grids is that the amount of overall energy available is equal or greater than the demand for each grid within the network. The overall energy available for each grid is a sum of its capacity, positive value of energy received from other nodes and negative value of energy sent to other nodes. This constraint is expressed as following: $capacity[i]+\sum_{j \in Grids} x[i,j]-x[j,i] \geq demand[i],\ i \in Grids$. When it comes to objective function, a possible approach would be to minimize the sum of costs, taking into account both the power generation and energy trading between the nodes to optimize the energy distribution: $minimize \sum_{i,j \in Grids} x[i,j]transfer\_cost[i,j]generation\_cost[j]$.

```
param numGrids;
set Grids:=1..numGrids;
param Transfer_Cost {i in Grids, j in Grids};
param Capacity {i in Grids};
param Demand {i in Grids};
param Generation_Cost {i in Grids};

# variable declaration
var X {i in Grids, j in Grids} >= 0;

# objective function
minimize cost:
       sum{i in Grids, j in Grids}
X[i,j]*Transfer_Cost[i,j]*Generation_Cost[j];

# constraints
subject to demand_satisfaction {i in Grids}:
      Capacity[i]+sum{j in Grids}(X[i,j]-X[j,i])>=Demand[i];
```

Figure 3. AMPL code of the proposed optimization model.

The AMPL code for the previously described linear program is given in Fig. 3.

C. Load forecasting

The input data is split into two disjoint datasets – training (75% of data) and test (25% of data). It consists of five variables, as shown in Table I. Grid is the identification number of power consumer. Day refers to the ordinal number of a day within the considered year. Rainfall refers to the amount of liquid precipitation over an area in that day. Temperature refers to average temperature recorded that day. Consumption is the amount of energy spent during the considered day by the given grid. Grid, day, rainfall and temperature are considered as independent variables, while the energy consumption is treated as dependent variable (that is predicted).

TABLE I. LOAD FORECASTING DATASET

Grid	Day	Rainfall [mm/m^2]	Temp [°C]	Consumption [MW]

The data is prepared by summing the value of consumption by all the households within the grid for each day. After that, the information

```
pragma solidity ^0.4.21;
contract EnergyTrade{
      event Sent(address buyer, address generator, uint amount, uint
transfer_cost, uint generation_cost);
      uint price;
      uint token_price;
      function trade() public {
      price=(amount*transfer_cost*generation_cost)/token_price;
            if (balances[buyer] < price) return;
            balances[buyer] -= price;
            balances[generator] += price;
            emit Sent(buyer, generator, amount, transfer_cost, generation_cost);
      }
}
```

Figure 4. Solidity smart contract for energy trading.

about the weather that day (temperature and rainfall) in the given geographic location of the grid is added to the dataset.

D. Smart contract generation

First, the cost matrices and energy trading matrix created as output of linear optimization process are used to generate the semantic representation of a smart contract, according to the domain ontology that we propose, as shown in Fig. 2.

Ontology represents the shared conceptualization of a particular domain. In this paper, RDF[5] is used for the representation of semantic data. It consists of classes, their properties and relationships expressed in forms of triplets (*subject, predicate, object*). SPARQL[6] is used for querying the RDF semantic triple stores and retrieval of information that is necessary for code generation. The main advantage of semantic representation is the ability to store the smart contracts in a form that is both human- and machine- readable. Moreover, it and can be used to enable interoperability between various blockchain technologies by developing the corresponding code generators.

Each smart contract for energy trading consists of two types of participants – *buyer* and *generator*. Buyer refers to a participant that will receive an amount of energy by paying the overall price of the trade. Generator is the participant that sends the given amount of energy, but, on the other side, receives the amount of tokens equivalent to the trade price of energy transferred. The trade price is defined as *(amount*transfer_cost*generation_cost)/token_price*. While transfer cost and generation cost are characteristics of the energy generator, token price refers to the current price of a cryptocurrency token in dollars.

Once the semantic representation is constructed, smart contract is generated by executing SPARQL queries that return results that are used to populate the parameters of a template. An example of energy trading smart contract template written in Solidity is given in Fig. 4.

IV. EVALUATION

In this section, several aspects of evaluation are presented. The execution was performed on a laptop equipped with Intel i7 7700-HQ quad core CPU running at 2.80GHz, 16GB of DDR4 RAM and GeForce GTX 1050 CUDA-enabled GPU with 2GB of VRAM.

A. Deep learning module evaluation

The deep learning-based forecasting module is evaluated with respect to mean relative error. For evaluation purposes, a public domain dataset about the household consumption was used [25]. In TensorFlow, a neural network with 4 hidden layers was created. The learning was performed in 10 epochs.

As average of 100 runs, the results presented in Table II were achieved. According to the achieved results, it can be seen that the relative error of predicted value decreases as the training set size becomes larger. Moreover, it was noticed that the prediction performance is improved (relative error is decreased for around 5%) with respect to our previous work [15], as we also included the rainfall data within the training set.

[5] https://www.w3.org/RDF/

[6] https://www.w3.org/TR/rdf-sparql-query/

In Fig. 5, the visualization of the last epoch is shown. The blue line is the expected load, the red line represents the predicted output, while the Y-axis is normalized to range [0,1].

TABLE II. DEEP LEARNING EVALUATION RESULTS

Training set size	Test set size	MRE [%]	Execution time [s]
75	25	11.08	0.39
750	250	8.02	0.57

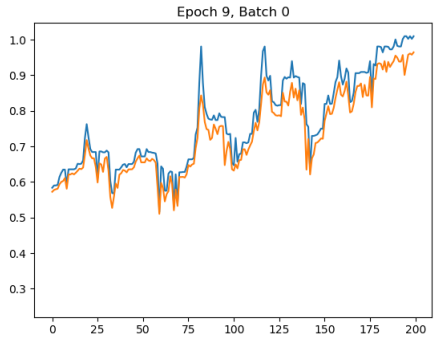

Figure 5. Load forecasting based on deep learning visualized in the last epoch.

B. *Smart contract generation time evaluation*

In Table III, the evaluation results for smart contract generator module are shown. The first column represents the overall number of grids considered. The second column denotes the number of energy trades needed according to the output of optimization process. The third column is the time needed for the execution of optimization algorithm. The fourth column shows the time needed to generate the semantic RDF representation of a smart contract using the values created as output of the optimization module. The fifth column is the time needed for the execution of SPARQL queries that are used to retrieve the contract parameters. Moreover, the sixth column shows the time needed to generate a smart contract from the semantic representation. Finally, the last column is the total time needed for the process of smart contract generation starting from energy trading matrices.

According to the achieved results, it can be seen that the overall time for smart contract generation increases, as the number of girds and trades increase. Moreover, the operations related to the semantic triple store are slower than the optimization and code generation due to fact that the semantic triple store used for the evaluation purposes was deployed in Cloud. In all the cases, the overall smart contract generation time is order of magnitude of 1. It can be concluded that the smart contract generation is comparable to [24]. However, in [24] there is a web page generation step, but there is no optimization process included.

In simulation environment based on [26], the solutions involving load forecasting and without it were compared. According to the results, the demand response was about 7% faster in the case when load forecasting was adopted.

TABLE III. SMART CONTRACT GENERATOR EVALUATION RESULTS

N_g	N	T_{opt} [s]	T_{rdf} [s]	T_{sparql} [s]	T_{gen} [s]	T_{tot} [s]
5	1	0.19	1.16	0.72	0.28	2.74
8	5	0.23	2.16	1.18	0.63	4.21
10	8	0.27	2.92	1.32	0.91	5.48

V. CONCLUSION AND FUTURE WORK

In this paper, a framework for efficient, blockchain-supported energy trading based on synergy of linear optimization and deep learning was presented. According to the achieved results, the approach seems promising, showing similar performance with slight improvements compared to previous work [15], while there are still many aspects to be considered in future. First, our plan is to work on integration of the presented framework with our existing IoT-based architecture for adaptive smart grids presented in [15, 27]. Once integrated, our goal will be to reduce the execution time of overall smart contract generation process in order to enable energy trading in real time. Moreover, another direction in our future work will be the adoption of blockchain technology to tackle the security issues in smart grids and smart contract verification [20, 21].

ACKNOWLEDGMENT

This work is partially supported by grant III44006 by the Ministry of Education, Science and Technological Development of the Republic of Serbia.

REFERENCES

[1] H. Gharavi, R. Ghafurian, “Smart Grid: The Electric Energy System of the Future [Scanning the Issue]”,

Proceedings of the IEEE, vol. 99, no. 6, 2011, pp. 917–921. https://doi.org/10.1109/jproc.2011.2124210

[2] A. H. Bagdadee, L. Zhang, "Smart Grid: A Brief Assessment of the Smart Grid Technologies for Modern Power System", Journal of Engineering Technology, vol. 8, no. 1, 2019. pp. 122- 142.

[3] I. S. Bayram, M. Z. Shakir, M. Abdallah, K. Qaraqe, "A survey on energy trading in smart grid", 2014 IEEE Global Conference on Signal and Information Processing (GlobalSIP), 2014, pp. 258-262, https://doi:10.1109/globalsip.2014.7032118

[4] R. Deng, Z. Yang, M.-Y. Chow, J. Chen, "A Survey on Demand Response in Smart Grids: Mathematical Models and Approaches", IEEE Transactions on Industrial Informatics, vol. 11, no. 3, 2015, pp. 570–582. https://doi.org/10.1109/tii.2015.2414719

[5] C. G. Lim, S. T. Lim, I. Aliyu, "Blockchain For Small Scale Energy Trading", 2018 Fall Conference - The Korea Institute of Electronic Communication Sciences, 2018, pp. 59-61.

[6] X. Dong et al., "ETSB: Energy Trading System Based on Blockchain", Advances in Intelligent Systems and Computing, 2019, pp. 673–684, https://doi.org/10.1007/978-3-030-16946-6_55

[7] S.-C. Oh, M.-S. Kim, Y. Park, G.-T. Roh, C.-W. Lee, "Implementation of blockchain-based energy trading system", Asia Pacific Journal of Innovation and Entrepreneurship, vol. 11, no. 3, 2017, pp. 322–334. https://doi.org/10.1108/apjie-12-2017-037

[8] E. Kabalci, Y. Kabalci, "Introduction to Smart Grid Architecture", Smart Grids and Their Communication Systems, 2018. pp. 3–45, https://doi.org/10.1007/978-981-13-1768-2_1

[9] G. B. Dantzig and M. N. Thapa, Linear Programming 1 - Introduction, Springer, 1997.

[10] M. Ahat, S. B. Amor, M. Bui, A. Bui, G. Guérard, C. Petermann, "Smart Grid and Optimization", American Journal of Operations Research, vol. 03, no. 01, 2013, pp. 196–206. https://doi.org/10.4236/ajor.2013.31A019

[11] R. Fourer, D. Gay, B. Kernighan, AMPL: A Modeling Language for Mathematical Programming, Duxbury Press, 2003.

[12] G. B. Dantzig, A. Orden and P. Wolfe, "The generalized simplex method for minimizing a linear form under linear inequality restraints", Pacific Journal of Mathematics, vol. 5, no. 2, 1955, pp. 183-195.

[13] R. Lippmann, "An introduction to computing with neural nets", IEEE ASSP Magazine, vol. 4, no. 2, 1987, pp. 4-22.

[14] Y. Bengio, "Learning Deep Architectures for AI", Foundations and Trends in Machine Learning, vol. 2, no. 1, 2009, pp. 1-127.

[15] N. Petrović, Đ. Kocić, "Podacima-vođena arhitektura za prilagodljive energetske mreže zasnovana na IoT uređajima", ETRAN 2019, Silver Lake, Serbia, 2019, pp. 880-885.

[16] A. B. M. S. Ali and S. Azad, "Demand Forecasting in Smart Grid", Green Energy and Technology, 2013, pp. 135–150. https://doi.org/10.1007/978-1-4471-5210-1_6

[17] A. Ushmani, "Blockchain Insight", International Journal of Computer Science Trends and Technology (IJCST), vol. 7, no. 2, 2019, pp. 1-3.

[18] A. Narayanan, J. Clark, "Bitcoin's academic pedigree", Communications of the ACM, vol. 60, no. 12, 2017, pp. 36–45.

[19] N. Balani and R. Hathi, Enterprise Blockchain: A Definitive Handbook, 2017.

[20] Z. Nehai, G. Guérard, "Integration of the Blockchain in a Smart Grid Model", CYSENI 2017, Kaunas, Lithuania, 2017, pp. 127-134.

[21] A. S. Musleh, G. Yao, S. M. Muyeen, "Blockchain Applications in Smart Grid - Review and Frameworks", IEEE Access, vol. 7, 2019, pp. 86746 – 86757. https://doi.org/10.1109/ACCESS.2019.2920682

[22] *A Next-Generation Smart Contract and Decentralized Application Platform*, Available at: https://github.com/ethereum/wiki/wiki/White-Paper . Last accessed: 24/03/2019.

[23] M. Uday, P. Devi Prasad, N. Jagadeesh Sai, "Energy Trading through Blockchain", International Journal of Scientific Research in Computer Science, Engineering and Information Technology, vol. 5, no. 2, 2019, pp. 800-803. https://doi.org/10.32628/CSEIT1952199

[24] N. Petrovic, "Adopting Semantic-Driven Blockchain Technology to Support Newcomers in Music Industry", CIIT 2019, Mavrovo, North Macedonia, 2019, pp. 1-6.

[25] Hourly Energy Consumption - *Over 10 years of hourly energy consumption data from PJM in Megawatts*. Available at: https://www.kaggle.com/robikscube/hourly-energy-consumption/. Last accessed: 21/08/2019.

[26] N. Petrović, "Approach to Dynamic Adaptivity Simulation in Fog Computing Scenarios" [accepted for publication], TELSIKS 2019, Nis, Serbia, 2019, pp. 1-4.

[27] Đ. Kocić, N. Petrović, "Application of Android Based Devices in Analog Electric Signal Measurement", YuInfo 2019, Kopaonik, Serbia, 2019, pp. 1-5.

Acridoidea Stimulated Artificial Bee Colony Algorithm for Solving Optimal Reactive Power Problem

Kanagasabai Lenin

Prasad V.Potluri Siddhartha Institute of Technology, Kanuru, Vijayawada, Andhra Pradesh 520007, gklenin@gmail.com

Abstract — **In this paper Acridoidea Stimulated Artificial Bee Colony (AAB) Algorithm is proposed to solve the optimal reactive power problem. Proposed AAB algorithm is based upon the jump occurrence of Acridoidea and it has been hybridized with Artificial Bee Colony Algorithm. Upgrading the position has been done based on the Acridoidea's jumping distance. With reference to Horizontal distance "*D*" which related to angle *θ*, velocity *V*, "*h*" is the increase of rate which occurs due to gravity Ballistic projectile travels. To enhance the range, the take off should at 45◦ to the horizontal and range is entirely dependent on the take-off velocity. Projected Acridoidea Stimulated Artificial Bee Colony (AAB) Algorithm has been tested in standard IEEE 14, 30 bus test systems and simulation results show the proposed algorithm reduced the real power loss efficiently.**

Keywords - optimal reactive power, transmission loss, acridoidea stimulated Artificial Bee Colony algorithm

I. INTRODUCTION

Reactive power problem plays an important role in secure and economic operations of power system. Numerous types of methods (Newton's method, interior point, successive quadratic programming method) [1-6] have been utilized to solve the optimal reactive power problem. However many scientific difficulties are found while solving problem due to an assortment of constraints. Evolutionary techniques (gravitational search, Ant Lion Optimizer, symbiotic organism search algorithm) [7-16] are applied to solve the reactive power problem. This paper proposes Acridoidea Stimulated Artificial Bee Colony (AAB) Algorithm to solve the optimal reactive power problem. In Artificial Bee Colony (ABC) algorithm has employed bee, onlooker bee, scout bee as formed groups. In the algorithm Employed bees solutions cannot be enhanced through a preset number of trials. Acridoidea which has a surprising ability of jumping on grass or in any other base when the consequence of air resistance has been overcome, then the motion of a jumping creature subsequent to it lifts-off from the base is alike to a bullet which came out from gun. This movement is termed as "ballistic movement", - equations portray the kinetics of such movements are well known. Proposed Acridoidea Stimulated Artificial Bee Colony (AAB) Algorithm is based upon the jumping phenomenon of Acridoidea and it hybridized with Artificial Bee Colony Algorithm. Modernization of position is computed from the Acridoidea jumping distance. Projected Acridoidea Stimulated Artificial Bee Colony (AAB) Algorithm has been tested in standard IEEE 14, 30, bus test systems and simulation results show the projected algorithm reduced the real power loss effectively.

II. PROBLEM FORMULATION

Objective of the problem is to reduce the true power loss:

$$F = P_L = \sum_{k \in Nbr} gk(V_i^2 + V_j^2 - 2V_iV_j \cos\theta_{ij}) \ , \quad (1)$$

$$F = Power\ loss + \omega_V \times VD \ , \quad (2)$$

$$Voltage\ Deviation\ (VD) = \sum_{i=1}^{N_{pq}} |V_i - 1| \ . \quad (3)$$

Constraint (Equality)

$$P_G = P_D + P_L \ . \quad (4)$$

Constraints (Inequality)

$$p_{gslack}^{\min} \le P_{gslack} \le p_{gslack}^{\max} , \quad (5)$$

$$Q_{gi}^{\min} \le Q_{gi} \le Q_{gi}^{\max}, i \in N_g , \quad (6)$$

$$V_i^{\min} \le V_i \le V_i^{\max}, i \in N_B , \quad (7)$$

$$T_i^{\min} \le T_i \le T_i^{\max}, i \in N_T \ , \quad (8)$$

$$Q_C^{\min} \le Q_C \le Q_C^{\max}, i \in N_C \ . \quad (9)$$

III. ACRIDOIDEA STIMULATED ARTIFICIAL BEE COLONY ALGORITHM

In Artificial Bee Colony (ABC) algorithm has employed bee, onlooker bee, scout bee as formed groups. In the algorithm Employed bees solutions cannot be enhanced through a preset number of trials. For self-organizing ,collective intelligence two leading modes of behaviour are designed [17].

Initialization stage: Through scout bees food sources (population "SN") are arbitrarily engendered. x_m (food source) is a vector to the problem, x_m have "*D*" variables and "*D*" is the dimension of exploration space of the objective function to be optimized.

$$x_m = l_i + rand(0.1) * (u_i - l_i) . \quad (10)$$

Employed Bee Phase: A employed bee discover a new-fangled food source inside the locality of the food source. The respectetive food source data will be accumulated by employed bee will be shared with onlooker bees.

$$V_{mi} = x_{mi} + \Phi_{mi}(x_{mi} - x_{\kappa i}) . \quad (11)$$

The fitness vaue is computed by,

$$fit_m(x_m) = \left\{ \begin{array}{l} \frac{1}{1+f_m(x_m)}, f_m(x_m) > 0 \\ 1+|f_m(x_m)|, f_m(x_m) < 0 \end{array} \right\} \quad (12)$$

Onlooker Bee Phase: through waggle dance Onlooker bees conpute the profitability of food sources, afterward arbitrarily choose a superior food source. Profitability (P_m) of all food sources;

$$P_m = \frac{fit_m(x_m)}{\sum_{m=1}^{SN} fit_m(x_m)} \ . \quad (13)$$

Onlooker bees explore the neighborhood of food source with reference to,

$$V_{mi} = x_{mi} + \Phi_{mi}(x_{mi} - x_{\kappa i}) \ . \quad (14)$$

Scout Phase: when the profitability of food source cannot be enhanced then the solutions will be discarded by scout bees. Subsequently, scouts begin to arbitrarily search the new-fangled solutions. When solution "xi" has been discarded, then the new-fangled solution x_m will be revealed by the scout. "x_m" is defined by

$$x_m = l_i + rand(0.1) * (u_i - l_i) \ . \quad (15)$$

Acridoidea which has a surprising ability of jumping on grass or in any other base when the consequence of air resistance has been overcome, then the motion of a jumping creature subsequent to it lifts-off from the base is alike to a bullet which came out from gun. This movement is termed as "ballistic movement", - equations portray the kinetics of such movements are well known.

$$D = \frac{V^2 \sin(2\theta)}{h} \ . \quad (16)$$

Ballistic projectile travels to a Horizontal distance "*D*" that is related to the take-off angle θ, velocity *V* at take-off: Where, "*h*" is the increase of rate which occurs due to gravity. To augment the range, the take off should at 45◦ to the horizontal and range is completely reliant on the take-off velocity.

Proposed Acridoidea stimulated Artificial Bee Colony (AAB) Algorithm is based upon the jumping phenomenon of Acridoidea and it hybridized with Artificial Bee Colony Algorithm. Modernization of position is computed from the Acridoidea jumping distance. Distance *D* in Eq. 16 will be utilized as a new-fangled position of the most excellent solution which is going to modernize its position during the exploration procedure.

$$x'_{bestj} = \sqrt{(x_{bestj})^2 + (x_{bestj} - x_{ij})^2} \times \sin(2\theta) . \quad (17)$$

Where, "*i*" is an arbitrarily chosen solution from the population, x'_{bestj} is the modernized position of the most excellent solution of the swarm in j^{th} direction, θ - symbolize the angle of rotation. $V^2 = \sqrt{(x_{bestj})^2 + (x_{bestj} - x_{ij})^2}$ is derived from the self -perseverance which arbitrarily chosen from the solution of the exploration space. "θ" vary from 0◦ to 360◦.

$$angel\ of\ rotation(\theta) = 10 \times t \ . \quad (18)$$

Parameters are initialized
While end criteria do
Step a: for engendering new-fangled food sources apply Employed bee phase
Step b: for modernization the food sources on the basis of nectar amounts apply Onlooker bee phase
Step c: in order to find out the new-fangled food sources in place of discarded food sources apply Scout bee phase
Step d: Minimization $f_{(x)}$;
Choose the most excellent solution x_{best} in the swarm which will alter its position;
Iter count =0
While $(t < T)$ do
Engender a new-fangled solution x'_{bestj} as follows;

i. Input the most excellent solution x_{best} from the population;
ii. Arbitrarily choose a solution x_i from the population;
iii. Value $\theta = 10 \times t / *t$ will be the present iteration counter
iv. For *j=1* to *D* do
v. If U(0, 1) < Cr then (Cr - perturbation rate (0, 1))
vi. $x'_{bestj} = x_{bestj}$
vii. Else
viii. $x'_{bestj} = \sqrt{(x_{bestj})^2 + (x_{bestj} - x_{ij})^2} \times \sin(2\theta)$
ix. End if
x. End for
xi. Return x'_{bestj}

Compute the objective value $f(x'_{bestj})$
If $f(x'_{bestj}) < f(x_{bestj})$ then $x_{best} = x'_{best}$
End if
$t = t + 1$;
End while
Produce most excellent solution

IV. SIMULATION RESULTS

At first in standard IEEE 14 bus system [18] the validity of the proposed Acridoidea Stimulated Artificial Bee Colony (AAB) Algorithm has been tested, Table I shows the constraints of control variables Table II shows the limits of reactive power generators and comparison of results with particle swarm optimization (PSO), modified particle swarm optimization (MPSO), self-adaptive real coded Genetic algorithm (SAGRA), Evolutionary Programming (EP) are presented in Table III.

TABLE I. CONSTRAINTS OF CONTROL VARIABLES

System	Variables	Min. (PU)	Max. (PU)
IEEE 14 Bus	Generator Voltage	0.95	1.1
	Transformer Tap	o.9	1.1
	VAR Source	0	0.20

TABLE II. CONSTRAINS OF REACTIVE POWER GENERATORS

System	Variables	Q Min. (PU)	Q Max. (PU)
IEEE 14 Bus	1	0	10
	2	-40	50
	3	0	40
	6	-6	24
	8	-6	24

.

TABLE III. SIMULATION RESULTS OF IEEE −14 SYSTEM

Control variables	Base case	MPSO [19]	PSO [19]	EP [19]	SARGA [19]	AAB
VG−1	1.060	1.100	1.100	NR*	NR*	1.019
VG−2	1.045	1.085	1.086	1.029	1.060	1.020
VG−3	1.010	1.055	1.056	1.016	1.036	1.016
VG−6	1.070	1.069	1.067	1.097	1.099	1.013
VG−8	1.090	1.074	1.060	1.053	1.078	1.029
Tap 8	0.978	1.018	1.019	1.04	0.95	0.936
Tap 9	0.969	0.975	0.988	0.94	0.95	0.929
TAP 10	0.932	1.024	1.008	1.03	0.96	0.930
QC−9	0.19	14.64	0.185	0.18	0.06	0.131
PG (MW)	272.39	271.32	271.32	NR*	NR*	271.64
QG (Mvar)	82.44	75.79	76.79	NR*	NR*	75.82
Reduction in PLoss (%)	0	9.2	9.1	1.5	2.5	26.19
Total PLoss (Mw)	13.550	12.293	12.315	13.346	13.216	10.001

NR* - Not reported.

.

TABLE IV. CONSTRAINTS OF CONTROL VARIABLES

System	Variables	Minimum (PU)	Maximum (PU)
IEEE 30 Bus	Generator Voltage	0.95	1.1
	Transformer Tap	o.9	1.1
	VAR Source	0	0.20

TABLE V. CONSTRAINS OF REACTIVE POWER GENERATORS

System	Variables	Q Minimum (PU)	Q Maximum (PU)
IEEE 30 Bus	1	0	10
	2	-40	50
	5	-40	40
	8	-10	40
	11	-6	24
	13	-6	24

Then the proposed Acridoidea stimulated Artificial Bee Colony (AAB) Algorithm has been tested, in IEEE 30 Bus system. Table IV shows the constraints of control variables, Table V shows the limits of reactive power generators and comparison of results with particle swarm optimization (PSO), modified particle swarm optimization (MPSO), self-adaptive real coded Genetic algorithm (SAGRA), Evolutionary Programming (EP) are presented in Table VI.

TABLE VI. SIMULATION RESULTS OF IEEE −30 SYSTEM

Control variables	Base case	MPSO [19]	PSO [19]	EP [19]	SARGA [19]	AAB
VG−1	1.060	1.101	1.100	NR*	NR*	1.018
VG−2	1.045	1.086	1.072	1.097	1.094	1.025
VG−5	1.010	1.047	1.038	1.049	1.053	1.019
VG−8	1.010	1.057	1.048	1.033	1.059	1.037
VG−12	1.082	1.048	1.058	1.092	1.099	1.039
VG-13	1.071	1.068	1.080	1.091	1.099	1.026
Tap11	0.978	0.983	0.987	1.01	0.99	0.936
Tap12	0.969	1.023	1.015	1.03	1.03	0.928
Tap15	0.932	1.020	1.020	1.07	0.98	0.942
Tap36	0.968	0.988	1.012	0.99	0.96	0.937
QC10	0.19	0.077	0.077	0.19	0.19	0.091
QC24	0.043	0.119	0.128	0.04	0.04	0.126
PG (MW)	300.9	299.54	299.54	NR*	NR*	297.67
QG (Mvar)	133.9	130.83	130.94	NR*	NR*	131.37
Reduction in PLoss (%)	0	8.4	7.4	6.6	8.3	19.82
Total PLoss (Mw)	17.55	16.07	16.25	16.38	16.09	14.070

NR* - Not reported.

V. CONCLUSION

In this paper Acridoidea Stimulated Artificial Bee Colony (AAB) Algorithm successfully solved the optimal reactive power problem. Projected AAB Algorithm is based upon the jumping phenomenon of Acridoidea and it hybridized with Artificial Bee Colony Algorithm. Modernization of position is computed from the Acridoidea jumping distance. Proposed Acridoidea Stimulated Artificial Bee Colony (AAB) Algorithm has been tested in standard IEEE 14, 30 bus test systems and simulation results show the projected algorithm reduced the real power loss. Percentage of real power loss reduction has been improved when compared to other standard algorithms.

REFERENCES

[1] K. Y. Lee, “Fuel-cost minimisation for both real and reactive-power dispatches,” Proceedings Generation, Transmission and Distribution Conference, vol.131, no. 3, 1984, pp. 85-93.

[2] N. I. Deeb, “An efficient technique for reactive power dispatch using a revised linear programming approach,” Electric Power System Research, vol. 15, no. 2, 1998, pp. 121–134.

[3] M. R. Bjelogrlic, M. S. Calovic, B. S. Babic, ”Application of Newton’s optimal power flow in voltage/reactive power control”, IEEE Trans Power System, vol. 5, no. 4, 1990, pp. 1447-1454.

[4] S. Granville, “Optimal reactive dispatch through interior point methods,” IEEE Transactions on Power System, vol. 9, no. 1, 1994, pp. 136–146. http://dx.doi.org/10.1109/59.317548

[5] N. Grudinin, “Reactive power optimization using successive quadratic programming method,” IEEE Transactions on Power System, vol. 13, no. 4, 1998, pp. 1219–1225. http://dx.doi.org/10.1109/59.736232.

[6] Ng Shin Mei, R.; Sulaiman, M.H.; Mustaffa, Z.; Daniyal, H.,"Optimal reactive power dispatch solution by loss minimization using moth-flame optimization technique", Appl. Soft Comput. vol. 59, 2017, pp. 210–222.

[7] Chen, G.; Liu, L.; Zhang, Z.; Huang, S. "Optimal reactive power dispatch by improved GSA-based algorithm with the novel strategies to handle constraints" Appl. Soft Comput. vol. 50, 2017, pp. 58–70.

[8] Naderi, E.; Narimani, H.; Fathi, M.; Narimani, M.R, "A novel fuzzy adaptive configuration of particle swarm optimization to solve large-scale optimal reactive power dispatch", Appl. Soft Comput. vol. 53, 2017, pp. 441–456.

[9] Heidari, A.A.; Ali Abbaspour, R.; Rezaee Jordehi, (2017) A. "Gaussian bare-bones water cycle algorithm for optimal reactive power dispatch in electrical power systems", Appl. Soft Comput. 2017, 57, pp. 657–671.

[10] Mahaletchumi Morgan, Nor Rul Hasma Abdullah, Mohd Herwan Sulaiman, Mahfuzah Mustafa, Rosdiyana Samad, "Benchmark Studies on Optimal Reactive Power Dispatch (ORPD) Based Multi-objective Evolutionary Programming (MOEP) Using Mutation Based on Adaptive Mutation Adapter (AMO) and Polynomial Mutation Operator (PMO)", Journal of Electrical Systems, 2016, pp. 12-1.

[11] Rebecca Ng Shin Mei, Mohd Herwan Sulaiman, Zuriani Mustaffa,"Ant Lion Optimizer for Optimal Reactive Power Dispatch Solution" , Journal of Electrical Systems, "Special Issue AMPE2015", 2016, pp. 68-74.

[12] P. Anbarasan; T. Jayabarathi, "Optimal reactive power dispatch problem solved by symbiotic organism search algorithm", Innovations in Power and Advanced Computing Technologies, 2016, DOI: 10.1109/IPACT.2017.8244970

[13] Gagliano A., Nocera F. "Analysis of the performances of electric energy storage in residential applications", International Journal of Heat and Technology", vol. 35, Special Issue 1, 2017, pp. S41-S48. DOI: 10.18280/ijht.35Sp0106.

[14] Caldera M., Ungaro P., Cammarata G., Puglisi G. "Survey-based analysis of the electrical energy demand in Italian households", Mathematical Modelling of Engineering Problems, vol. 5, no. 3, 2018, pp. 217-224. DOI: 10.18280/mmep.050313

[15] M. Basu, "Quasi-oppositional differential evolution for optimal reactive power dispatch", Electrical Power and Energy Systems, 2016, vol. 78, pp. 29-40.

[16] Gai-Ge Wang, Moth search algorithm: a bio-inspired metaheuristic algorithm for global optimization problems, Memetic Comp 2016, DOI 10.1007/s12293-016-0212-3.

[17] Karaboga, D., & Akay, B. (2011). A modified artificial bee colony (abc) algorithm for constrained optimization problems. Applied Soft Computing, vol. 11, no. 3, 2011, pp. 3021–3031.

[18] IEEE, "The IEEE-test systems", (1993), http://www.ee.washington.edu/trsearch/pstca/.

[19] Ali Nasser Hussain, Ali Abdulabbas Abdullah and Omar Muhammed Neda, "Modified Particle Swarm Optimization for Solution of Reactive Power Dispatch", Research Journal of Applied Sciences, Engineering and Technology vol. 15, no. 8, 2018, pp. 316-327. DOI:10.19026/rjaset.15.5917.

Cloud-Based Approach for Real-time Monitoring of Smart Grid Topology

Miodrag Forcan[1], Mirjana Maksimović[1], Jovana Forcan[2]

[1] University of East Sarajevo, Faculty of Electrical Engineering, East Sarajevo, BiH, miodrag.forcan@etf.ues.rs.ba; mirjana.maksimovic@etf.ues.rs.ba
[2]University of East Sarajevo, Faculty of Philosophy, Department of Mathematics, Informatics and Physics, East Sarajevo, BiH, jovanajankovic91@yahoo.com

Abstract — **This article is focused on the development of a real-time communication system for monitoring of Smart Grid (SG) topology using Cloud-based approach. Network topology processors are an integral part of the transmission network's state estimation and power flow analysis functions. Tracking of SG topology in real-time could be achieved using available local measurements from smart devices and Cloud-based control center, communicating with each other through the internet. Well-known IEEE test grid topology is modeled using MATLAB/Simulink software package and modified to support real-time communication with open source IoT platform ThingSpeak. As a result an interesting and novel model is proposed combining SG and Cloud-based communication system. Several simulation case studies, related to network reconfigurations, are defined to test the developed model. Obtained simulation results show all capabilities and benefits of the proposed Cloud-based monitoring approach.**

Keywords – smart grid, feeder reconfiguration, cloud computing, real-time monitoring

I. INTRODUCTION

Power system safe operation depends on the accurate knowledge of the electrical quantities in the grid [1]. State estimation algorithms use network topology data, power system elements data, available measurements, and pseudo-measurements (measurements from the past) [2]. Network topology processing is the first step in the state estimation function. During topology processing, the statuses of breakers/switches are first telemetered by the system network configurator [3] and then processed using a bus-section/switching-device network model [4].

Monitoring of network topology enables up to date information related to feeder reconfiguration (FRC) in distribution networks. FRC is a planning and real-time operational control process that changes the distribution network topology [5].

Traditional distribution networks are low observable systems with limited number of measurements available. The future transition from traditional to SG will be followed by the large amount of the new measurement data requiring to be processed in near real-time. The usage of novel and more efficient communication architectures is expected to enable distribution system operator functions in SG. Cloud-based communication approach could be an efficient and a low cost solution for monitoring of SG topology. Traditionally, processing, analyzing, and storing data from large-scale distributed system, such as SG, are handled by the Cloud architecture [6].

The rest of this article is organized as follows. Section II presents the basic objectives of FRC and describes the most common switching devices in distribution network. Cloud-based communication approach for monitoring of network topology is proposed and analyzed in Section III. Open source IoT platform ThingSpeak and MATLAB-based modeling and simulation setup is given is Section IV. Section V analysis obtained simulation results with main goal to verify expected capabilities of the proposed approach. The outcome of the research in this article is concluded in Section VI.

ISBN: 978-86-80616-04-9

II. DISTRIBUTION NETWORK RECONFIGURATION

Traditional distribution networks are mainly radially supplied, meaning that power flow is unidirectional. Power is transferred over the distribution feeders from the main substation to loads.

A. FRC major goals

The main goals of FRC are listed below [5]:

- Loss reduction – at each stage of the power distribution process, from the sources to the consumer, the delivery of power is followed with power losses. Power losses that occur in distribution networks due to many reasons, such as load imbalance, low voltages and long distribution lines, have a direct influence on the electricity costs and efficiency of the distribution system. Different methods for reducing power losses are mainly classified in three groups: organizational, technical and methods for enhancement of an accounting electricity system. Finding the configuration which minimizes overall power losses of the distribution system is a primary objective of FRC [7-10].

- Load balancing – to keep the power distribution system reliable and efficient it is crucial to maintain optimal balancing of loads. The overload in distribution network can cause the damage of power system and low voltage at the consumer side. Therefore, the overload should be prevented, and voltage of the system should be kept within acceptable range. Network reconfiguration can balance feeder loads and avoid overload by transferring partial loads from the heavily loaded feeders to the lightly loaded ones [11-14].

- Voltage profile enhancement – voltage instability in the distribution system can be the outcome of many causes. Hence, making a better voltage profile and avoiding the voltage drops across transmission lines is quite important in the distribution system. The utilization of voltage regulators and reactive power support can enable increasing or decreasing voltage at various points, therefore maintaining the node voltages within operating limits. Distribution network reconfiguration is a very useful in voltage stability improvement [15, 16].

- Service Restoration – is a group of objectives in emergency conditions such as fault when there is a need to isolate faulty parts from healthy ones. In this case switches are opened to isolate part of the system. Service restoration via network reconfiguration enable to revive as many loads as possible by transferring loads in inoperative areas to another distribution feeder via changing the switches status. During the restoration process following requirements should be accomplished: minimum switching operation, minimum losses and satisfying the voltage and current constraints [17, 18].

B. Switching devices in distribution network

The most efficient strategy to increase the reliability is network automation by installing switching devices. Selecting the optimal number, type and arrangement of automatic switching devices to be installed in the distribution networks is quite challenging [19]. The most common types of switching devices used in distribution networks are [20]:

- Circuit breaker - an automatically operated electrical switch designed to immediately isolate faulty part from the rest of the network. The circuit breaker contains a fixed contact and a moving contact (which are normally closed) and may be equipped with various protective relays. When a fault or overloaded is sensed by relays, the contacts of the circuit breakers open and in such way isolate the faulted feeder [21].

- Automatic recloser – high-voltage electric switch which is highly efficient in increasing network reliability. It acts as automatically closing circuit breaker and is also able to recognize and clear transient faults in addition to permanent faults. Automatic recloser shuts off electric power when fault occurs in an electric distribution network, and if the problem was only temporary, the recloser automatically resets itself and restores the electrical energy. If the fault is permanent automatic recloser remains off and isolates the electric distribution network [22].

- Sectionalizing switches – switches used to isolate healthy zones from faulted sections of distribution lines. Both manual and remotely controlled sectionalizing switches are effective in the fault management process and enable network reconfiguration in

normal as well as in abnormal conditions. Integration of Sectionalizing Switches into the system improves its reliability but at the same time their failure may initiate a system interruption [23, 24].

- Counter sectionalizer - used in conjunction with automatic recloser to automatically isolate faulted sections of feeders. They do not have fault interrupting capability, but do have a fault counter device that count the number of current interruptions made by the upstream automatic recloser. Hence, when a fault occurs, the automatic recloser iterates reclosing process and counter sectionalizer counts the number of interruptions. In the case of permanent fault, the counter sectionalizer will automatically open when the counter reaches the preset value. If a fault occurs downstream of the counter sectionalizer, the automatic recloser does not sense the fault current anymore. In this case the customers downstream the Counter sectionalizers are interrupted while the upstream customers are isolated from the fault and have power restored. If the fault occurs upstream of the counter sectionalizer, the automatic recloser operates and all customers are interrupted [24, 25].

III. CLOUD-BASED COMMUNICATION APPROACH FOR MONITORING OF SG TOPOLOGY

In the future SG an increased number of switching devices is expected to be deployed. The coordination of their operations is expected to be fully automated, but still supervised by SG operating center. Bidirectional near-real time communication system is going to be required to support previous coordination. The first step forward is likely to be the enabling of monitoring functions.

A Cloud-based IoT server is proposed as a low-cost solution for monitoring of SG topology in this article. Cloud computing is the one of possible solutions related to more efficient processing of Big Data emerging from SG measurement systems. Among large quantities of a very diverse measurement data, information on statuses of breakers'/switches' contacts is mandatory for topology monitoring and FRC control and analysis. The monitoring function requires unidirectional data flow (from switching devices to SG operating center). The application of the proposed approach is described using the example of a well-known IEEE 34-bus test grid case study. The simplified schematic illustration of the power and communication systems is given in Fig. 1.

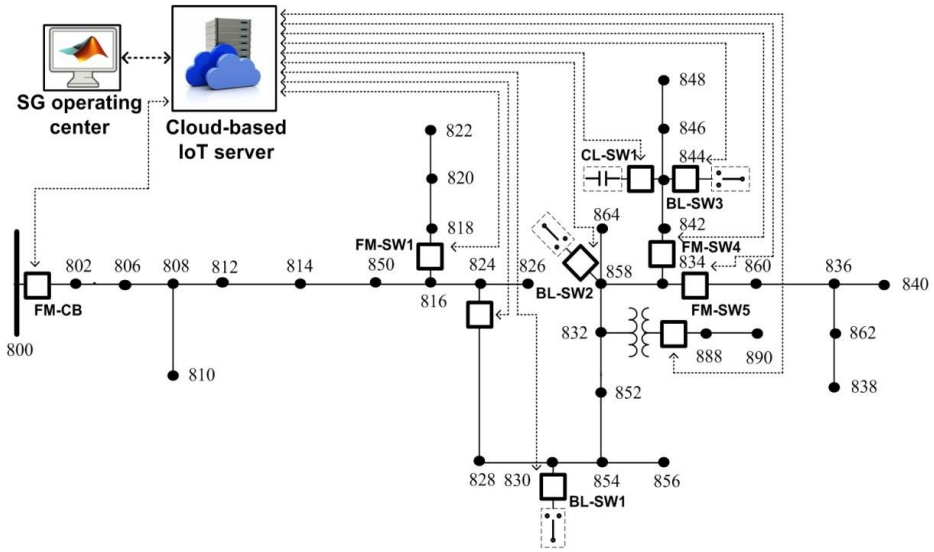

Figure 1. Cloud-based communication approach for monitoring of SG topology – IEEE 34-bus test grid case study.

It can be seen in Fig. 1 that future IEEE 34-bus test grid is assumed to be equipped with many switching devices (square symbols). According to their application these devices can be classified in three categories: load balancing (BL-SW1, BL-SW2 and BL-SW3), voltage regulation (CL-SW1) and fault management system (FM-CB, FM-SW1, FM-SW4, FM-SW5 and two remaining unnamed switches). Traditional distribution networks are often equipped only with circuit breaker in the main substation (FM-CB).

Even not required for monitoring purposes, communication medium in Fig. 1 is shown as bidirectional. The focus of this research is rather on communication architecture and not on communication medium types. As can be seen in Fig. 1, SG operating center is using Cloud-based IoT server for collecting and analyzing information on statuses of switching devices, thus continuously monitoring SG topology. Every switching device status change is captured in near real-time (allowing for data transfer delays depending on the speed of used communication medium).

IV. MODELING AND SIMULATION SETUP

To verify proposed SG topology monitoring approach a real-time simulation setup is developed using open source IoT platform ThingSpeak [26] and MATLAB/Simulink software package [27]. ThingSpeak supports real-time communication with Simulink-based models using Desktop Real-time Toolbox.

A. IEEE 34-bus test grid model

Using existing example of IEEE 13-bus test grid model embedded in MATLAB [28] a new Simulink-based IEEE 34-bus test grid model is developed. Detailed information on IEEE 34-bus test grid is available in [29]. This test grid represents the actual 24.9 kV radial distribution network located in Arizona. It is a long and lightly loaded grid with corresponding single line diagram shown in Fig. 1.

Distribution lines are modeled using distributed line models, while power source is modeled as ideal. Modeling of two in-line voltage regulating transformers is neglected, while distribution transformer connecting buses 832 and 888 is modeled without consideration of saturation characteristic. Capacitive load is considered only at bus 844. Previous modeling simplifications are not mandatory for analysis in this article. All switching devices are modeled as ideal and their positions are assumed as shown in Fig. 1.

B. Cloud-based communication model

Communication model enabling real-time data transfer between MATLAB/Simulink and ThingSpeak IoT platform is proposed in our previous article [30]. Proposed model communicates with ThingSpeak server using standard Transmission Control Protocol/Internet Protocol (TCP/IP). Simulations are performed on personal computer (PC) with the following characteristics: Intel(R) Core(TM) i7-7700 CPU @ 3.60 GHz processor, 8.00 GB installed RAM memory and 64-bit operating system.

During simulation data is periodically sent to ThingSpeak at 20 s rate in real-time via three private communication channels. Every monitored variable is received by its matching field. 10 fields are used for monitoring of the same number of switching devices. Communication security is reinforced using Application Programming Interface (API) keys. Interactive plotting tools automatically visualize monitored variables (statuses of switching devices).

V. SIMULATION RESULTS AND DISSCUSION

With aim to show and verify the capabilities of the proposed monitoring approach three case studies are defined: load balancing, voltage regulation and fault management system.

A. Load balancing

Balancing of loads is typically done by transferring selected loads from heavily to lightly loaded feeders. In this case study only one feeder is considered and it is assumed that some unbalanced loads are equipped with switches. Three single-phase loads are selected from IEEE 34-bus test grid and equipped with switches BL-SW1, BL-SW2 and BL-SW3, as shown in Fig. 1. Considered loads are initially connected to the most loaded phase A. SG operator initiates reconfiguration process with aim to transfer the loads from phase A to phase C. The proposed cloud-based communication system performs its real-time monitoring function with the corresponding results presented in Fig. 2. The first switch BL-SW1 operates 20 s after simulation start, the second BL-SW2 follows at 40 s and finally the third one BL-SW3 operates at 80 s.

Figure 2. Real-time monitoring of IEEE 34-bus test grid topology – load balancing case study.

According to results from Fig. 2 it can be seen that there are two field charts per every switch. All three considered switches consist of two parallel switches labeled as 11-12, 21-22, 31-32 for BL-SW1, BL-SW2 and BL-SW3, respectively. From field charts 1 and 2 it can be seen that reconfiguration event for BL-SW1 is detected between 20 and approximately 40 s, referenced to simulation starting time. Switch 11 disconnects the load from phase A and simultaneously switch 12 connects the load to phase C. Similar reconfiguration events for BL-SW2 and BL-SW3 are captured between approximately 40 and 60 s which can be seen from the remaining charts in Fig. 2.

During simulation negative sequence current is measured at bus 802 and corresponding results are presented in Fig. 3.

It can be noticed that negative sequence current magnitude is decreasing in steps which is caused by switching operations. The lower value of the negative sequence current magnitude is good indicator load unbalance decrease. The proposed system for real-time monitoring of SG topology proved to be successful in tracking and visualizing statuses of the switching devices. Up-to-date information on switching operations provides constant updating of bus-section/switching-device network model.

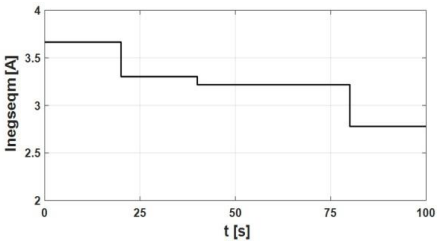

Figure 3. Negative sequence current magnitude changes at bus 802 - load balancing case study.

B. *Voltage regulation*

Reactive power compensation is commonly used for voltage regulation in distribution network. Connecting the capacitive loads at network buses leads to a local voltage magnitude increase. In this case study it is assumed that initially there is no capacitive load in test grid. 20 s after the simulation start switch CL-SW1 operates and connects capacitive load to bus 844 (Fig. 1). Real-time monitoring of the switch operation is shown in Fig. 4.

As can be seen in Fig. 4, the switch operation is successfully detected in time interval 20-40 s by the monitoring function. To show the effect of reactive power compensation on voltage profile the magnitudes of phase voltages at bus 802 are given in Fig. 5.

The results presented in Fig. 5 show the increase in voltage magnitudes caused by reactive power compensation. It can be concluded that proposed real-time monitoring system is able to successfully track operation of the switch CL-SW1 and consequently update the bus-section/switching-device network model.

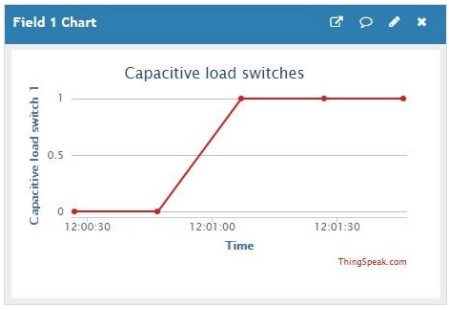

Figure 4. Real-time monitoring of IEEE 34-bus test grid topology – voltage regulation case study.

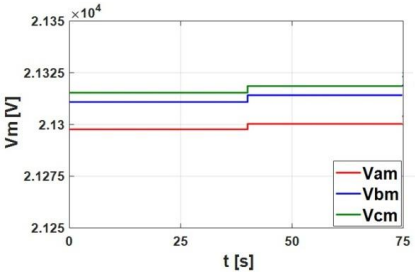

Figure 5. Voltage magnitude changes at bus 802 - voltage regulation case study.

C. *Fault management system*

Fault management system is the most complex considered case study in this analysis. The permanent three-phase fault is initiated at time t_1 = 39 s after the simulation start, on the half-length of the line connecting buses 860 and 836. The following sequence of switching events happened: (1) the main breaker FM-CB initially disconnected feeder and interrupted the fault current at time t_2 = 40 s; (2) the switch FM-SW1 disconnected the lateral from the bus 816 at time t_3 = 45 s; (3) FM-CB reconnected and immediately again disconnected the feeder, since the fault is not cleared - (t_4 = 70-71 s); (4) FM-SW1 reconnected the lateral at time t_5 = 75 s; (5) FM-SW4 disconnected the lateral from the bus 834 at time t_6 = 75 s; (6) FM-CB reconnected and immediately again disconnected the feeder, since the fault is not cleared - (t_7 = 100-101 s); (7) FM-SW4 reconnected the lateral at time t_8 = 105 (8) FM-SW5 disconnected the feeder's section from the bus 834 at time t_9 = 105 s; (9) FM-CB permanently reconnected the feeder at time t_{10} = 130 s, since the fault is now cleared.

Previous sequence of the events during fault management process is monitored by the proposed approach and the corresponding results are presented in Fig.6. FM-CB operation status is shown in field 1 chart, while statuses of FM-SW1, FM-SW4 and FM-SW5 are shown in fields 2, 5 and 6 charts, respectively.

From field 1 chart it could be noticed that only two FM-CB operations are detected. These operations correspond to times t_{2m} = 40 s and t_{9m} = 140 s. Reclosing operations at times t_4 and t_7 are not detected since they are too fast for the monitoring system.

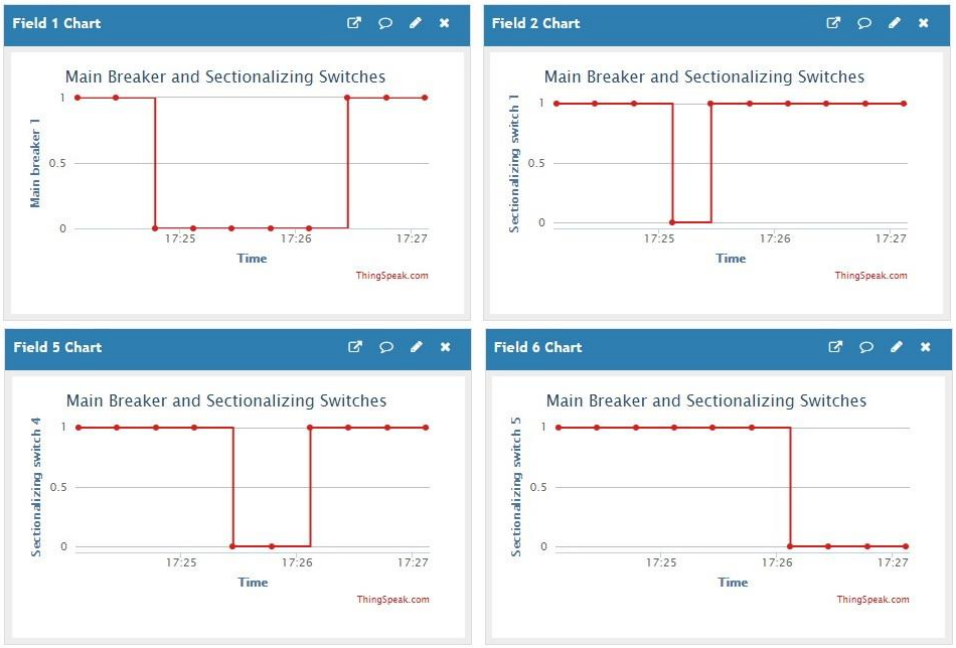

Figure 6. Real-time monitoring of IEEE 34-bus test grid topology – fault management system case study.

According to results presented in field 4 chart it can be seen that operation of FM-SW1 is detected at time t_{3m} = 60 s (actual event occurred at time t_3 = 45 s). The event of lateral reconnection is detected at time t_{5m} = 80 s. Similarly, from the field 5 chart it can be seen that operation of FM-SW4 is detected at time t_{6m} = 80 s (actual event occurred at time t_6 = 75 s) and the event of lateral reconnection is detected at time t_{8m} = 120 s. Finally, according to results presented in field 6 chart it is noticeable that operation of FM-SW5 is detected at time t_{9m} = 120 s (actual event occurred at time t_9 = 105 s). The last event is detected in field 1 chart at time t_{10m} = 140 s representing feeder permanent reconnection by FM-CB.

The proposed monitoring system managed to successfully track operations of switching devices during fault management process within its resolution limits.

VI. Conclusion

Real-time monitoring of network's topology is considered to be one of the basic functions in future SG operating center. In this article a Cloud-based communication approach is proposed as a low-cost and easy implementable solution for monitoring of statuses of switching devices, thus enabling up-to-date forming of bus-section/switching-device network model which is the basis for many other applications, such as state estimation and load flow. The proposed approach's capabilities are tested and verified using combined power and communication system model. Obtained simulation results show that proposed approach is capable of real-time tracking of SG topology in the cases of load balancing, voltage regulation and fault management system. All models given in this article can be easily upgraded to support testing of other important future operating activities in SG.

References

[1] G. Celli, P.A. Pegoraro, F. Pilo et al., Pisano G., "DMS cyberphysical simulation for assessing the impact of state estimation and communication media in smart grid operation," IEEE Trans. Power Syst., vol. 29, no. 5, 2014, pp. 2436–2446.

[2] M. Maksimović and M. Forcan, "Internet of Things and Big data Recommender Systems to support Smart Grid" in Big Data Recommender Systems: Recent trends and advances, vol. 2, Application Paradigms, O. Khalid, S. U. Khan and A. Y. Zomaya (eds.), Stevenage, United Kingdom: Institution of Engineering and Technology (IET), 2019, pp. 145-172.

[3] Clerk I. S. Costa and J. A. Leao, "Identification of topology errors in power system state estimation," IEEE Trans. Power Syst., vol. 8, no. 4, 1993, pp. 1531-1538.

[4] A. Monticelli, “Electric power system state estimation,” in Proceedings of the IEEE, vol. 88, no. 2, . 2000, pp. 262-282.

[5] L. Tang, F. Yang and J. Ma, “A survey on distribution system feeder reconfiguration: Objectives and solutions,” 2014 IEEE Innovative Smart Grid Technologies - Asia (ISGT ASIA), Kuala Lumpur, 2014, pp. 62-67.

[6] F.Y. Okay and S. Ozdemir, “A Fog computing based smart grid model,” International Symposium on Networks, Computers and Communications (ISNCC), Tunisia, 2016.

[7] Y. Al-Mahroqi, I.A. Metwally, A. Al-Hinai, A. Al-Badi, “Reduction of power losses in distribution systems,” World Academy of Science, Engineering and Technology International Journal of Computer and Systems Engineering, vol. 6, no. 3, 2012, pp. 315-322.

[8] G. Vulasala, S. Sirigiri, R. Thiruveedula, “Feeder reconfiguration for loss reduction in unbalanced distribution system using genetic algorithm,” World Academy of Science, Engineering and Technology, vol. 28, 2009, pp. 745-753.

[9] A.D.T. Le, K.A. Kashem, M. Negnevitsky, G. Ledwich, “Minimising power losses in distribution systems with distributed resources,” in Australasian Universities Power Engineering Conference, 2005.

[10] Y. Wilms, S. Fedorovich, N.A. Kachalov, “Methods of reducing power losses in distribution systems,” MATEC Web of Conferences 141, 01050, Smart Grid 2017, doi: 10.1051/matecconf/201714101050

[11] M.A. Kashem, V. Ganapathy, G.G. Jasmon, “Network reconfiguration for load balancing in distribution networks,” IEE Proceedings - Generation, Transmission and Distribution, vol. 146, no. 6, 1999, pp. 563-567.

[12] H. J. Kim and Y. T. Yoon, “Reconfiguration for load balancing of feeder in distribution system including distributed generation,” Journal of International Council on Electrical Engineering, vol. 6, no. 1, 2016, pp. 166–170.

[13] T. Lantharthong and N. Rugthaicharoencheep, “Network reconfiguration for load balancing in distribution system with distributed generation and capacitor placement,” World Academy of Science, Engineering and Technology International Journal of Electrical and Computer Engineering, vol. 6, no. 4, 2012, pp. 409-414.

[14] W. M. Siti, A.A. Jimoh, D. V. Nicolae, “Load balancing in distribution feeder through reconfiguration,” 31st Annual Conference of IEEE Industrial Electronics Society, IECON 2005, doi:10.1109/iecon.2005.1568914

[15] A. Onlam, D. Yodphet, R. Chatthaworn, et al., “Power loss minimization and voltage stability improvement in electrical distribution system via Network Reconfiguration and Distributed Generation placement using novel adaptive shuffled frogs leaping algorithm,” Energies, vol. 12, no. 3, 2019. doi:10.3390/en12030553

[16] A. Landeros, Smart reconfiguration of electric power distribution networks for power loss minimization and voltage profile optimization, Master of Science Thesis in Sustainable Energy Engineering. Reykjavík University, 2018.

[17] S. Sivanagaraju and T. Ramana, “A simple method for feeder reconfiguration and service restoration of distribution networks,” Electric Power Components and Systems, vol. 32, no. 9, 2004, pp. 883–892.

[18] M. F. Sulaima, N. Baharin, A. A. Ahmad, “Distribution network reconfiguration via service restoration by using iabc algorithm considering distributed generation,” ARPN Journal of Engineering and Applied Sciences, vol. 13, no. 11, 2018, pp. 3820-3827.

[19] Z. Popovic, S. Knezevic, B. Brbaklic, “Optimal number, type and location of automatic devices in distribution networks with distribution generation,” CIRED Workshop, paper no 0023, Helsinki, Finland, 2016.

[20] M. Izadi, M. Farajollahi, A. Safdarian, “Switch deployment in distribution networks,” in Electric Distribution Network Management and Control Power Systems, A. Arefi et al. (eds.), Springer Nature Singapore Pte Ltd. 2018, pp. 172-233.

[21] P. S. R. Murty, “Circuit Breakers,” Electrical Power Systems. 2017, pp. 383–416. doi:10.1016/b978-0-08-101124-9.00016-4

[22] Eaton’s Cooper Power Systems, “What is a Recloser?” *Recloser Technical data TD280027EN*, 2017. Available at: https://www.eaton.com/content/dam/eaton/products/medium-voltage-power-distribution-control-systems/reclosers/recloser-definition-information-td280027en.pdf

[23] M. Farajollahi, M. Fotuhi-Firuzabad, A. Safdarian, “Sectionalizing switch placement in distribution networks considering switch failure,” IEEE Trans. Smart Grid, vol. 10, no. 1, 2019, pp. 1080–1082.

[24] Eaton’s Cooper Power Systems, “Sectionalizers,” *Technical Data 270-10*, 2014. Available at: http://www.xn--qoqr9h9y2eevh.xn--iqs8s/ecm/groups/public/@pub/@electrical/documents/content/pct_1130878.pdf

[25] R.E. Brown, Electric Power Distribution Reliability. 2nd Edition, CRC Press, 2008.

[26] ThingSpeak, Available at: https://thingspeak.com/

[27] MATLAB R2017b, The MathWorks, Inc., Natick, Massachusetts, United States.

[28] Mathworks, Available at: https://www.mathworks.com/help/physmod/sps/examples/ieee-13-node-test-feeder.html

[29] IEEE PES, Available at: http://sites.ieee.org/pes-testfeeders/resources/

[30] M. Forcan and M. Maksimović, „Cloud-Fog-based approach for Smart Grid monitoring,“ Simulation Modelling Practice and Theory, 2019, 101988, ISSN 1569-190X, doi: 10.1016/j.simpat.2019.101988

Time Series Vector Autoregression Prediction of the Ecological Footprint Based on Energy Parameters

Radmila Janković[1], Ivan Mihajlović[2], Alessia Amelio[3]

[1]Mathematical Institute of the SASA, Belgrade, Serbia, rjankovic@mi.sanu.ac.rs
[2]University of Belgrade, Technical Faculty in Bor, Bor, Serbia, imihajlovic@tfbor.bg.ac.rs
[3]DIMES, University of Calabria, Rende (CS), Italy, aamelio@dimes.unical.it

Abstract — **Sustainability became the most important component of world development, as countries worldwide fight the battle against the climate change. To understand the effects of climate change, the ecological footprint, along with the biocapacity should be observed. The big part of the ecological footprint, the carbon footprint, is most directly associated with the energy, and specifically fuel sources. This paper develops a time series vector autoregression prediction model of the ecological footprint based on energy parameters. The objective of the paper is to forecast the EF based solely on energy parameters and determine the relationship between the energy and the EF. The dataset included global yearly observations of the variables for the period 1971-2014. Predictions were generated for every variable that was used in the model for the period 2015-2024. The results indicate that the ecological footprint of consumption will continue increasing, as well as the primary energy consumption from different sources. However, the energy consumption from coal sources is predicted to have a declining trend.**

Keywords – time series, ecological footprint, energy, vector autoregression, forecasting

I. INTRODUCTION

According to the OECD (The Organisation for Economic Co-operation and Development) report [1], the industrial production and construction involving mining, manufacturing, electricity, gas, and air-conditioning sectors in 2018 had an increasing trend, compared to 2015. Moreover, in the first quarter of 2019, global manufacturing increased by 2.5 percent compared to the first quarter of 2018 [2]. At the same time, in 2018, global primary energy consumption grew by 2.9 percent comparing to the year before, which was the fastest observed growth since 2010 [3]. In terms of the fuel type, all fuels had a highly increasing trend compared to their 10-year averages, except for renewable sources [3], which clearly indicates the need for new sustainability policies which will solely focus on increasing renewable source usage and decreasing fossil fuel production. This rapid economic growth highly affects the natural capital of the planet, by decreasing it and lowering the possibility of maintaining a healthy environment.

The latest review of world energy [3] indicates the growth in primary energy consumption in all world continents, with the highest consumption values generated in 2018 in Asia Pacific area (5985.8 mtoe), followed by North America (2832 mtoe), and Europe (2050.7 mtoe). In terms of the fuel type, North America, South America, Europe and Africa mostly use energy from oil sources, while the CIS (The Commonwealth of Independent States) and Middle East countries focus on using primary energy from natural gas [3]. In Asia, a prevalent use of energy from coal sources is observed [3].

In order to maintain the life-supporting systems of the planet, the sustainability concept has been introduced. Sustainability involves the "development that meets the needs of the present without compromising the ability of future generations to meet their own needs" [4], and involves three dimensions: (1) economical, (2) social, and (3) environmental dimension, which are completely interdependent [5]. If properly applied by creating sustainable policies and laws, the sustainability concept should preserve the

ISBN: 978-86-80616-04-9

Earth's ecosystems and allow optimized natural resource allocation. Unfortunately, human activities today exhaust the nature faster than it can regenerate, hence the ecological deficit arises as a critical problem when dealing with the climate change. As humans highly depend on nature, it is clear that such deficit should be handled in the near time future.

There is a clear need to use nature's resources in accordance to their regenerative capacity, and to dispose waste in accordance to the speed of its absorption [6]. But in order to do so, the availability of nature's resources and human requirements for natural resources should be estimated, hence the Ecological Footprint (EF) term has been introduced. The EF has been developed by Rees and Wackernagel [7, 8] and presents "the tool that enables us to estimate the resource consumption and waste assimilation requirements of a defined human population or economy in terms of a corresponding productive land area" [6]. It can also be interpreted as the demand of the population on the nature [9]. In these terms, another concept is very closely connected to the EF and must be observed and analyzed in order to fully understand the state of natural resources and biosphere. Biocapacity shows the amount of biologically productive land and water area which can be used to provide humanity [9]. Both measures are expressed in global hectares (gha) and are comparable.

The EF and biocapacity in their calculations include several land use types, in particular: (1) cropland, (2) graying land, (3) fishing grounds, (4) forests, (5) uptake land, and (6) built-up land [9]. Cropland includes the land area required to produce the agricultural products such as crop, livestock feeds, fish meals, oil crops and rubber [9]. Grazing land involves the land area covered in grass, i.e. grassland, used to provide foods for livestock, in addition to feeds from cropland area [9]. Fishing grounds involve fishery and aquaculture, while forest land involves the area covered in forests and used for harvesting fuelwoods and timber in order to supply forest products [9]. Carbon uptake land refers to the land used for carbon dioxide (CO_2) emissions absorption. As most of carbon uptake happens in forests, this is a subcategory of forest land [9]. Lastly, the built-up land involves the area covered in infrastructure such as housing, transportation, industrial buildings and reservoirs for hydroelectric power generation [9]. Furthermore, there are two types of the EF: (1) the EF of production, and (2) the EF of consumption [10]. The first presents the primary demand for natural resources [9], while the latter includes the area used to produce products to support an observed population's consumption habits [10].

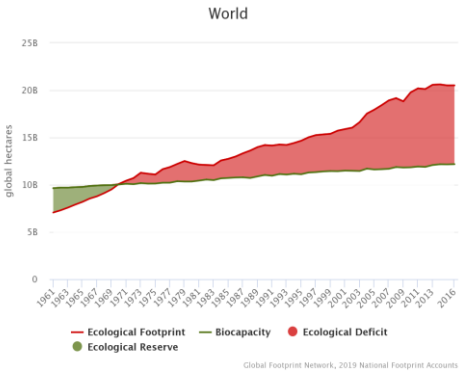

Figure 1. EF and Biocapacity (source: [11]).

The importance of the EF is reflected in the fact that it mainly focuses on the needs of the planet and provides clear approximation of the impact of human demand for natural resources. Natural capital is very much limited and should be carefully and efficiently used, but not abused. Based on the last available data [11], there is a global biocapacity deficit, while EF is on the rise (Fig. 1). It can be observed that there is a very small rising trend of ecological reserves, but in order to achieve bigger increases, the pressure human activities put on the nature should weaken and allow nature to regenerate.

In [12] the EF of Slovenia was investigated, and the values of the EF were predicted based on the energy consumption growth in terms of fossil fuels, electric energy, biomass, import and export of electrical energy and embodied energy in exported products. Energy consumption growth was calculated by predicting the ratio of industrial growth which was then used as a weighting factor for energy forecasting [12]. The predictions indicated an increase in energy consumption in Slovenia, followed by the increase of the EF [12]. In [13] an urban EF prediction model based on the Markov chain was developed. Some of the indicators used in developing the model involve population, urbanization rate, total energy consumption, consumer price index, contribution share of third strata industries, and contribution share of total retail sales of consumer goods to the gross domestic product [13]. It was shown that the energy consumption widely contributes the

urban EF [13]. In [14] the environmental Kuznets curve for EF was investigated from the aspect of energy and financial development. It was found that high levels of energy use generate higher values of the EF and increase the environmental degradation [14].

The novelty of this approach is presented in the fact that the forecasting of the EF is based specifically and only on energy parameters, in particular on the primary energy consumption values. The developed prediction model gives some estimates in terms of future values of observed variables and can help policy makers to create efficient and sustainable decisions. Moreover, the model makes predictions based on the values of all variables, hence the relations between the variables are also considered when forecasting.

This paper is organized as follows. Section 2 presents the data and methodology used in this research. Section 3 shows the obtained results and predictions of the developed model. Lastly, section 4 presents the conclusions of this research.

II. METHODOLOGY

The dataset used in this research was obtained from several sources [11, 15, 16] and involves global yearly data for the period 1971-2014. One dependent variable and eight independent variables were analyzed. The dependent variable represents the total EF of consumption, while the independent variables represent the primary energy consumption from different sources, in particular: natural gas, coal, oil, nuclear, hydroelectric, wind, solar photovoltaic (PV), and other renewable sources. The dependent variable, the total EF of consumption, is expressed in gha, while all independent variables are expressed in terawatt-hours. All analyses and modellings were performed using R programming language for statistical computing on a 1.7GHz dual-core Windows machine.

The first step, after importing the variables, was to identify correlations between the dependent and independent variables. Correlations were calculated based on the Pearson's correlation coefficient (denoted r) which shows the strength of the relationship between the variables, if such exists [17]. The values of the Pearson's correlation can be in the range [-1,1], where the value of 1 represents the strong, linear, relationship, while 0 shows no linear correlation. Depending on the sign, correlation can be positive or negative.

The next step included data preprocessing, where each variable was separately log transformed. Because the primary energy consumption from solar PV sources, and from wind sources, included zero values, the log10 transformation was used to transform these variables, with added constant of 1. Other variables included values higher than 0, hence the standard log10 transformation was used in order to prepare the variables for time series prediction. After fitting the model and generating predictions, an inverse log transformation was performed in order to generate real-value predictions.

The next step involved creating and fitting the Vector Autoregression model (VAR). The optimal number of lags was estimated based on the Akaike Information Criterion (AIC), and a value of 2 lags was used for creating the model. The AIC technique estimates the quality of a model when predicting the future values in terms that it compares each model to the other models. The AIC is calculated as follows [18]:

$$AIC = (-2)\log(L) + 2k \ . \qquad (1)$$

TABLE 1. CORRELATION BETWEEN THE VARIABLES

		Solar PV	Oil	Gas	Coal	Nuclear	Hydroelectric	Wind	Other Renewables
Total EF of consumption	t	5.141	36.276	63.092	37.77	11.042	38.149	8.6884	12.208
	df	42	42	42	42	42	42	42	42
	p-value	<0.001	<0.001	<0.001	<0.001	<0.001	<0.001	<0.001	<0.001
	r	0.621	0.984	0.995	0.986	0.862	0.986	0.802	

t – t test value, df – degrees of freedom, r – Pearson's coefficient

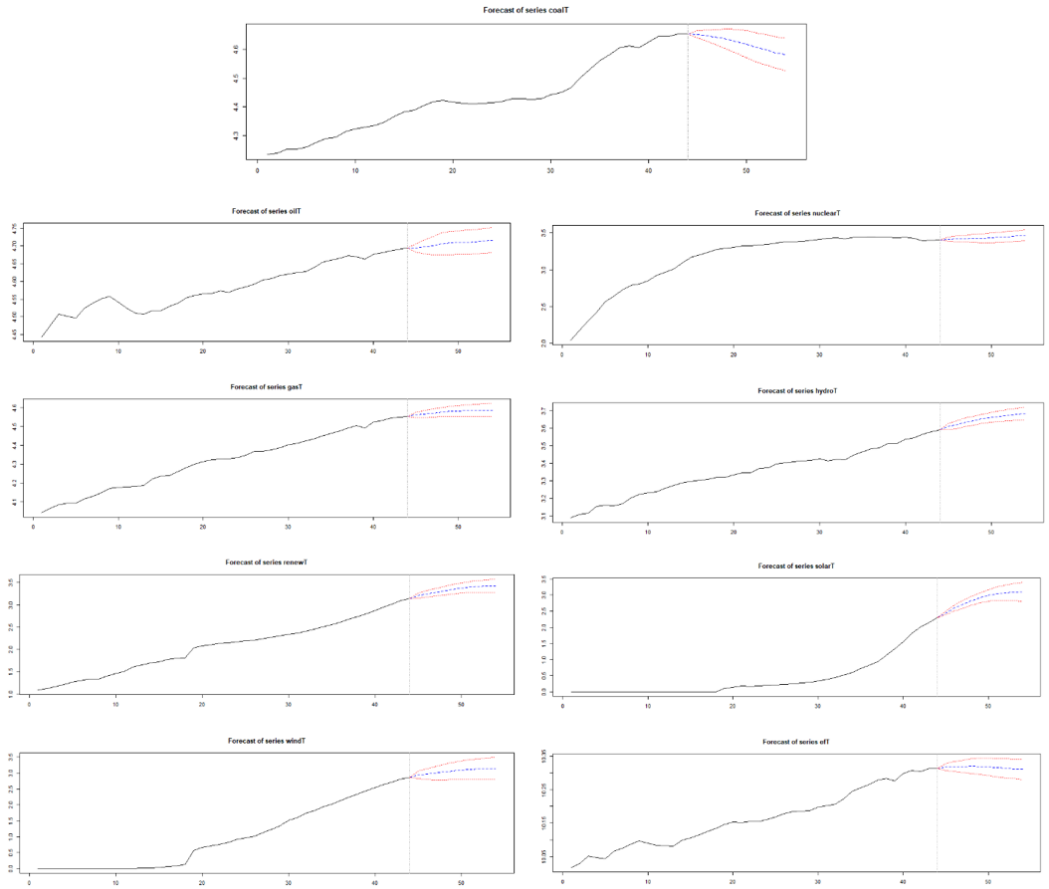

Figure 2. VAR forecast for each variable (log transformed values for oil sources, nuclear sources, gas sources, hydro sources, coal sources, other renewable sources, solar sources, wind sources, and the total EF of consumption).

where L is the maximum likelihood value, and k is the number of estimated parameters [18].

The VAR is a linear model consisting of n-variables, in which every variable is explained by its own lagged values, and the values of other variables [6]. Therefore, VAR is used to model interdependencies between multiple time series, hence it represents a multivariate model. A p-lag VAR can be represented as follows [19, 20]:

$$y_t = c + A_{1y_{t-1}} + A_{2y_{t-2}} + \cdots + A_{py_{t-p}} + e_t\,, \qquad (2)$$

where c represents a vector of constants, Ai represents the coefficient matrix, y_{t-i} is the *i-th* lag of y, and et is the vector of errors.

After fitting the model, predictions were generated for the period 2015-2024.

III. RESULTS AND DISCUSSION

Before performing the time series vector autoregression, a correlation analysis was executed. The obtained results are presented in Table I, where it can be observed that the variables total EF of consumption and primary energy consumption from gas sources have the highest, positive correlation, with a value of r=0.995, followed by the correlation value obtained for the total EF of consumption and coal sources (r=0.986). The same value of correlation is also observed between the total EF of consumption and primary energy consumption from hydroelectric sources (r=0.986). For all other variables correlation coefficients are also found to be high, except for the primary energy consumption from Solar Photovoltaic sources (r=0.621). All correlations are found to be significant ($p<0.001$).

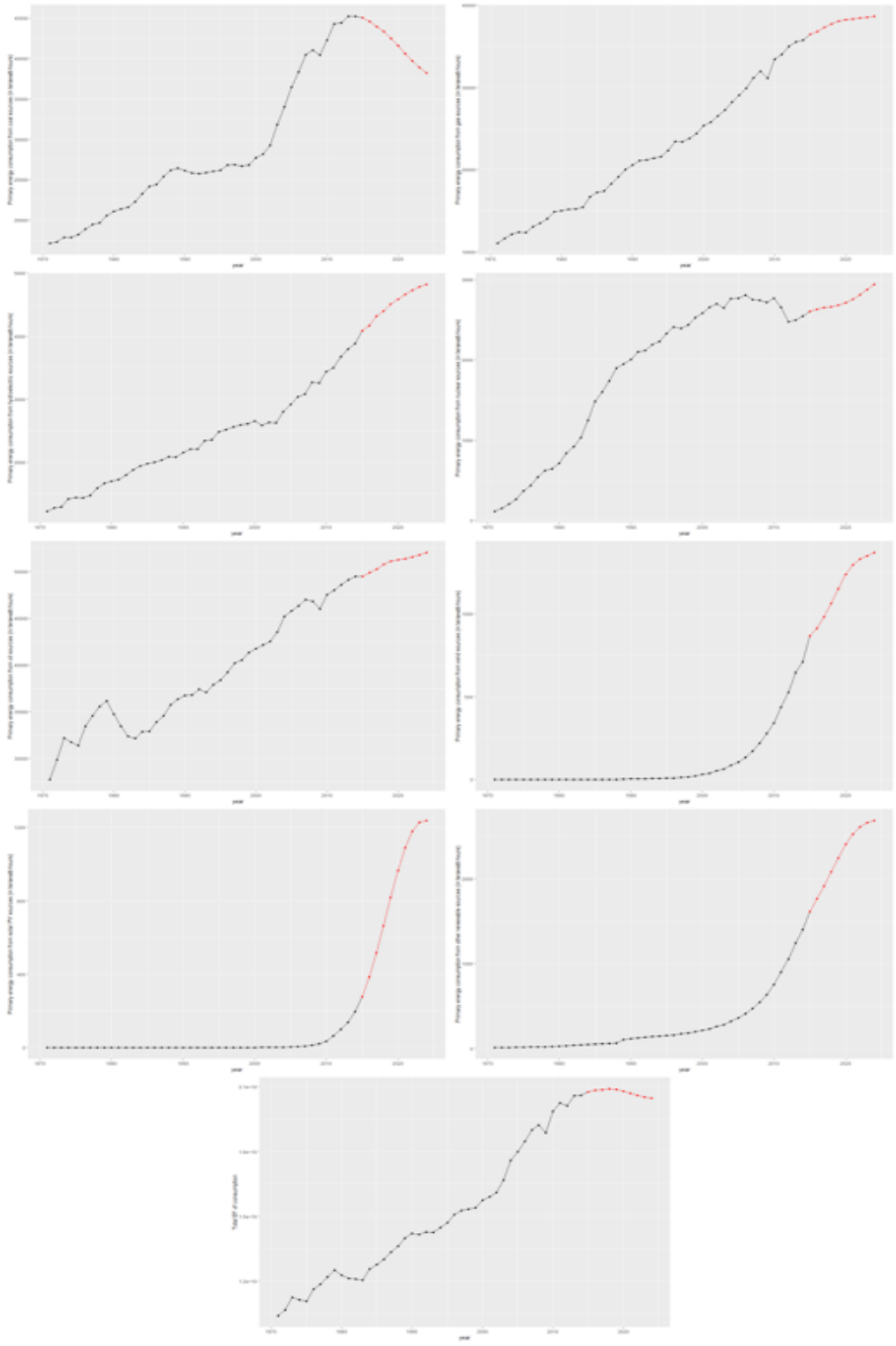

Figure 3. Real value predictions generated by the VAR model for each variable

After log-transforming each variable, the data was fitted to the VAR model, and the graphs showing the real values, upper and lower prediction limits, and forecasted values were generated (Fig. 2). Lastly, the predicted values were inverse log-transformed, and the results are shown in Fig. 3. For each variable, the prediction trend is shown in Fig. 3

The predictions in Fig. 3 indicate that the amount of primary energy consumption from gas, hydroelectric, oil, nuclear, and wind sources will have an increasing trend in the upcoming years. These predictions support previous findings by other authors, such as the use of oil as an energy source which is predicted to increase in the future [21, 22, 23]. Moreover, from Fig. 3 it is observable that the amount of primary energy consumption from coal sources will decrease in the following years, supporting the findings in [21, 22, 23]. The use of energy from solar PV sources, and from other renewable sources will increase by the year of 2023, after which it will have a more stable trend. Lastly, considering the total EF of consumption is predicted to increase until 2019, when a slow decrease occurs.

The obtained findings indicate a strong relationship between the energy and the ecological footprint, as with the decrease of fossil fuel consumption, the EF also decreases.

IV. CONCLUSIONS

This paper analyzed the relationship between the total EF of consumption and the primary energy consumption from coal, hydroelectric, nuclear, oil, natural gas, wind, solar PV, and other renewable sources. The objective of the paper was to create a forecasting model for the EF prediction based only on energy parameters. The prediction model was developed using vector autoregression, where the values of each of the variables were predicted for the period 2015-2024.

The results showed a high correlation between the EF of consumption and the primary energy consumption from all sources. Moreover, the prediction model suggests that the global EF will maintain an increasing trend until 2020, when it slowly starts to decline. Energy sources will maintain a high level of use in the future, with exception of the coal. Based on the predictions, global primary energy consumption from coal sources will decrease until 2024. As coal produces the highest concentrations of carbon dioxide, such predictions are positive.

As more countries set sustainable goals and work towards accomplishing them, further action is still needed. Natural capital should be appropriated on a rational level, considering its boundaries. In terms of energy, the carbon footprint should be of special importance as it considers the effects of each phase of the life cycle of fuel on the environment.

ACKNOWLEDGMENT

This research was financially supported by the Mathematical Institute of the Serbian Academy of Sciences and Arts (Project III44006) and through the project of the Ministry of Education, Science and Technological Development of Serbia – TR34023.

REFERENCES

[1] OECD. (2019). Industrial production (indicator). doi: 10.1787/39121c55-en

[2] United Nations Industrial Development Organization. (2019). *World Manufacturing Production. Statistics for Quarter 1*, 2019. Available at: https://www.unido.org/sites/default/files/files/2019-06/World_manufacturing_production_2019_q1.pdf

[3] British Petroleum Company. (2019). *BP statistical review of world energy. London.* Available at: https://www.bp.com/content/dam/bp/business-sites/en/global/corporate/pdfs/energy-economics/statistical-review/bp-stats-review-2019-primary-energy.pdf

[4] United Nations General Assembly, Report of the World Commission on Environment and Development: Our Common Future. Transmitted to the General Assembly as an Annex to document A/42/427 – Development and International Co-operation: Environment, 1987.

[5] United Nations General Assembly, 2005 World Summit Outcome, Resolution A/60/1, adopted by the General Assembly, 15 September 2005.

[6] M. Wackernagel and W. Rees, Our ecological footprint: reducing human impact on the earth. New Society Publishers, 1998.

[7] W. E. Rees, "Ecological footprints and appropriated carrying capacity: what urban economics leaves out, " Environment and urbanization, vol. 4, no. 2, 1992, pp. 121-130.

[8] M. Wackernagel, How big is our ecological footprint? A handbook for estimating a community's appropriated carrying capacity. Verlag nicht ermittelbar, 1993.

[9] M. Borucke, et al., "Accounting for demand and supply of the biosphere's regenerative capacity: The National Footprint Accounts' underlying methodology and framework," Ecological indicators, vol. 24, 2013, pp. 518-533.

[10] D. Lin, “Ecological footprint accounting for countries: updates and results of the national footprint accounts, 2012–2018, “. Resources, vol. 7, no. 3, 2018, pp. 58.

[11] *Global Footprint Network*, Available at: data.footprintnetwork.org.

[12] S. Medved, "Present and future ecological footprint of Slovenia - The influence of energy demand scenarios," Ecological Modelling, vol. 192, no. 1-2, 2006, pp. 25-36.

[13] Y. Lu and B. Chen, "Urban ecological footprint prediction based on the Markov chain," Journal of cleaner production, vol. 163, 2017, pp. 146-153.

[14] M.A. Destek and S.A. Sarkodie, "Investigation of environmental Kuznets curve for ecological footprint: the role of energy and financial development," Science of the Total Environment, vol. 650, 2019, pp. 2483-2489.

[15] British Petroleum Company. (2017). *BP statistical review of world energy*, London, Available at: http://www.bp.com/en/global/corporate/energy-economics/statistical-review-of-world-energy.html

[16] H. Ritchie and M. Roser. (2019). *Energy Production & Changing Energy Sources*. Available at: OurWorldInData.org,

[17] K. Pearson, “Determination of the coefficient of correlation”. Science, vol. 30, no. 757, 1909, pp. 23-25.

[18] H. Akaike, “A new look at the statistical model identification,” in Selected Papers of Hirotugu Akaike, New York, NY: Springer, 1974, pp. 215-222.

[19] J.H. Stock and M.W. Watson, “Vector autoregressions,” Journal of Economic perspectives, vol. 15, no. 4, 2001, pp. 101-115.

[20] E. Zivot and J. Wang, “Vector autoregressive models for multivariate time series,” Modeling Financial Time Series with S-Plus®, 2006, pp. 385-429.

[21] British Petroleum Company. (2019). *BP Energy Outlook*, 2019 edition, Available at: https://www.bp.com/content/dam/bp/business-sites/en/global/corporate/pdfs/energy-economics/energy-outlook/bp-energy-outlook-2019.pdf

[22] National Research Council, *Coal: Research and development to support national energy policy.* National Academies Press, 2007, Available at: https://www.nap.edu/read/11977/chapter/4

[23] R.G. Newell, D. Raimi, and G. Aldana, Global Energy Outlook 2019: The Next Generation of Energy, Resources for the future (RFF), July 2019, Available at: https://media.rff.org/documents/GEO_Report_8-22-19.pdf

A Management Proposal for Requirements of Process and Product on Ethanol Production Chain

Paulo Henrique Palota[1], Murilo Secchieri de Carvalho[1], Elson Avallone[1], Paulo César Mioralli[1], Manoel Fernando Martins[2]

[1]Federal Institute of Education, Science and Technology of São Paulo, Catanduva-SP, Brazil, palota@ifsp.edu.br
[2]Federal University of São Carlos, São Carlos, Brazil, manoelf@dep.ufscar.br

Abstract — **The main objective of this work is to investigate the main products and processes requirements on the ethanol production chain in order to propose a framework that facilitates the attainment of these requirements on this chain. To meet this objective, an empirical research of multiple cases was performed in the ethanol production chain in order to find these requirements and investigate the use of practices of the element "process management" from the "internal process" theory. The field study showed that, in most cases, there is a lack of a system of continuous improvement on the agents of the ethanol production chain. The proposal helps meeting the requirements of ethanol production and presents solutions to eliminate gaps on the agents of the ethanol chain related to the element "process management". Besides it can corroborate towards the attendance of the requirements of ethanol production by this chain agents, resulting in ethanol production chain more quality.**

Keywords – Ethanol Production; Products and Process Requirement; Process Management; Internal Process.

I. INTRODUCTION

Sugar cane generates foreign exchange for Brazil through the production of sugar, ethanol and more recently the cogeneration of electric energy that has been gaining prominence as an alternative source in the Brazilian energy matrix. The ethanol production chain plays a very important role in Brazilian once it is used as a fuel in the biofuel.

With the advent of open markets, globalization and the prices of sugarcane main products are tied to commodity exchange and futures; the Brazilian sugarcane agribusiness needs to be competitive. The competitiveness and survival of the sugar-energy chain is subject to a management that add value to this chain through the improvement of the quality of its products and its processes for obtaining more competitive costs for the production chain. Each agent of the ethanol production chain has to attend the products requirements. In order to realize the attainment of the Quality Management (QM) requirements of each step of production must be realized. This could be supported by internal process (IP). According to [1], a successful implementation of supply chain quality management needs add the internal process (IP), compound by the following elements: product/service design, process management (PM) and logistics. However, this work considers the element "process management" from the "internal process", once they are related with the management of the quality requirements of the chain.

The main objective of this work is to investigate the main products and processes requirements on the ethanol production chain and the (PM) practices in order to identify agreement and disagreement for proposing a framework that facilitates the attainment of these requirements on this chain. Within this context, the research aims to answer the following question:

ISBN: 978-86-80616-04-9

- How to manage the product and process requirements of the ethanol production chain?

To achieve this work proposal, some specific objectives are considered:

- Identify IP management in the literature;
- Find the main elements of this topic.
- Find the main practices of this element in the literature;
- Investigate these practices on the ethanol production chain in field research.
- Investigate in field research the process requirements demanded by the ethanol production chain;
- Present a proposal based on what was identified in the previous steps.

II. INTERNAL PROCESS/ETHANOL PRODUCTION CHAIN

The internal process (IP) refers to all the activities of a company. This concept includes three elements: product and service design, process management and logistics. The successful implementation of the practices of these elements can generate a significant impact on the operational performance [1]. The IP, when properly managed, facilitates the integration and rationalization of the internal operational activities of a company [2]. The authors state that internal process management has positive effects on both external and internal operating performance.

As the objective of this work is to propose a model for managing the necessary requirements for ethanol chain production, the focus in this work is on the element "Process Management", which will be addressed in the next topic.

A. Process Management

According to [3], PM can generate quality for the final product in addition to improving the efficiency, effectiveness, and flexibility of production. IP management has positive effects on internal and external operating performance. However, external process management has a positive effect on external operational performance [2].

When IP has standardization, clear instructions and statistically controlled, they assist in the delivery of products and services that improve a company's operational performance [2]. Practices like Kanban, inventory reduction and lean management are all part of Toyota's internal processes [4]. The process control is critical to the success of supply chain and can be achieved through performance measurement of supply chain [5]. Companies can identify weaknesses in its internal supply chain to maximize process performance [6]. Organizations need to review and improve processes continuously in order to reduce errors [7]. A synchronous connection between different processes and/or operations is considered critical for an efficient supply chain [8]. PM refers to the use of statistical techniques, which increases the level of process and error-proofing process design and minimizes the chance of employees' mistakes [9].

Summarizing, it can be identified the following main practices related to the PM element:

- Control and improve continuously the processes.
- Use of statistical techniques.
- Use of fool-proof for process design.
- Use of automatic processes.
- Use of the preventive equipment maintenance.
- Clarity of work or process instruction.

B. Ethanol Production Chain

The configuration of the ethanol production chain can be seen in Fig. 1, where the main agents that make up the sugarcane production chain are showed, as follow:

- Seedlings growers: the companies and/or institutions responsible for the development of new cultivars for sugarcane farms.
- Agricultural inputs: the industries of correctives, fertilizers, agricultural defenses and irrigation systems for the farms of the sugarcane growers.
- Manufacturers of machinery and equipment: the harvesters, tractors,

TABLE I. THE RESEARCH PLANNING METHOD.

Topic	Steps	Description	Results for the research
Literature review	S1	Internal process	Definition of the theory of IP and explanation of the element PM with its practices
Field research	S2	Establishment of criteria for case selection	Identification and selection of companies for cases
	S3	Elaboration and evaluation of the research protocol	Better understanding of theme, validation and improvement of the questionnaire
	S4	Conducting the interviews	Field verification of the PM element of the IP theory for the cases
Analysis of Results	S5	Case report, cases analysis and solution proposal	Comparative analysis of the existing practices and the missing ones investigated in the cases. Proposal solution

trucks, trailers, sprayers and various implements used for the cultivation of land (subsoilers, plows, furrows, among others).

- Farms: the growers that supply sugarcane to the millings, which can be both independent suppliers and integrated into the milling itself.
- Milling: the industry manufacturer of products, such as: ethanol, various types of sugar, electric power from cogeneration, yeast and additives.

The study object selected for field research, indicated in Fig. 1, covers only the raw material-related agents for the production of ethanol, that is, sugarcane (seedling and sugarcane growers and the processing of sugarcane in order to produce ethanol).

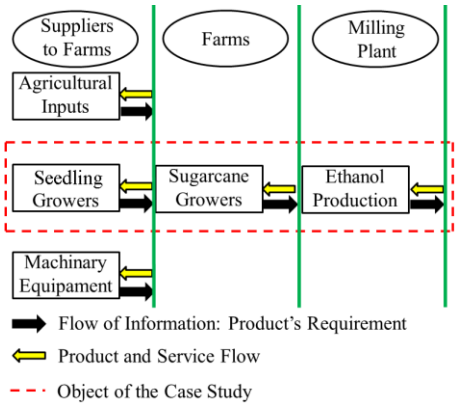

Figure 1. Production chain of ethanol.

III. METHODOLOGY

The research method used in this work is the study of multiple cases, as it investigates deeply the phenomenon of the object of analysis.

The research is aimed at the elaboration of a proposal through the verification of the PM element from the IP theory for different approaches and with replication of it in the agents that holds part of the production chain of ethanol as: seedling growers, sugarcane growers and millings. The field research seeks investigating the practices of the PM element, and the product and QM requirements that are used on the agents of the ethanol production chain.

A. Overview Planning

The Table 1 shows a method of research planning for the conduction of the field research showing three phases and five steps. Each step is identified by the letter "S".

The elaborated research protocol aimed at, in overall way, to investigate the following questions:

- What are the main quality product and QM requirements for ethanol production chain?
- What practices of the PM element on the ethanol production chain agents (seedlings and sugarcane growers), and milling are executed?

TABLE II. QM REQUIREMENTS TO SEEDLINGS.

Seeding Production		
Grower's production process steps	**QM requirements**	**Product's Requirements**
Crossing	Construct a database containing the characterization of the whole germplasm	Use on different soil condition
	Test the germline capacity of caryopses	Seeding production with capacity of germination
Seeding	Meet good seeding production practices	Ensuring sprouting and agronomic characteristics of seedlings
Transplanting	Respect from 3 to 5 centimeters tall seedlings	Tall of seedlings
	Weekly pruning	Decrease leaf perspiration
	Get good stapling	Need for plants with good compaction and profiling
Selection	Achieve natural field conditions such as soil tillage, furrow spacing	Meet the agronomic characteristics
Multiplication	Phytopathological tests of coal and mosaic and technological analyses	To be approved on phytopathological tests
	Obtain the correct rate of: Brix of broth, POL% of broth, POL% of cane and fiber%	Necessity of agronomic characteristics of seedlings
	Perform tests in different climates	Seedlings need to adapt on different climates
	Perform heat treatment on seedlings	Control of ratoon stunting disease on seedlings
Commercial testing	Perform tests of health risks	Seedlings need to be free of health risks

TABLE III. QM REQUIREMENTS TO SUGARCANE.

Sugarcane Production		
Grower's production process steps	**QM requirements**	**Product's Requirements**
Soil preparation and cultural treatment	Application of correct dosage of limestone/plaster for soil correction	High Total Recoverable Sugar (TRS)
	Application of correct dosage of fertilizers and insecticides	High Total Recoverable Sugar (TRS) and low shoot borer rates
Plantation	Choice of the seedling variety suitable for soil type	High Total Recoverable Sugar (TRS) Vegetal impurities and low shoot borer rates
	Planning for the use of suitable seedling: super early, early, middle and late varieties	High Total Recoverable Sugar (TRS)
Harvesting	Low soil moisture at harvest	Low mineral and vegetal impurities
	Proper adjustment of the harvester's cutting base	Low mineral impurities
	Proper adjustment of the harvester fans	Low vegetal impurities
	Meet useful period of industrialization for variety of types in the field	High Total Recoverable Sugar (TRS)
Sugarcane transportation to milling	Low time from harvest to extraction	High Total Recoverable Sugar (TRS)

The interviews were conducted on the seedling grower, sugarcane grower and milling.

IV. CASE STUDIES AND PROPOSAL FOR REQUIRIMENT'S MANAGEMENT IN THE CHAIN

In this topic, the analysis of the results from the cases of seedling grower, sugarcane grower and milling are presented. Besides of a proposal regarding the gaps found based on the practices of the element PM.

A. Seedling Grower

1) Process Management.

The producer develops seedlings of commercial varieties with genetic and phytosanitary purity of early, medium and late maturation to be able to meet the total harvest period from the beginning of April to November of each year.

The development stages of the varieties of seedlings follow a standard with agronomic and phytosanitary characterization, whose analysis in comparison with the standard varieties defines discarded or released as new cultivars. In the validation process of the cultivars, statistical tests are performed in at least eight different regions in order to better adapt the cultivar to a given environment.

The processes of obtaining the seedlings follow standardization with control and when any deviation occurs, it is evaluated, which can be discarded or maintained. However, actions are more corrective than preventive.

2) Seedling's Requirements

The development of a certain attribute of the cultivar is based on a market need, as is the case of energy cogeneration through sugarcane bagasse or sugar and/or ethanol production. Today there are varieties that contain 24% of fiber used for cogeneration, but there is no commercial interest due to the necessity of the millings in extracting the broth for later production of sugar or ethanol.

The goal of the seedlings developer is to balance the attributes of sucrose and fiber contents in cultivars, as there is a negative correlation between these parameters, that is, by increasing the sugar content of the cultivar, the fiber content of the cultivar is decreased and vice versa.

The requirement of the Ministry of Agriculture, Livestock and Food Supply of Brazil for the release of a new variety is based only on a morphological characterization of the sugarcane (color, stem diameter etc.). In Table 2, follow the QM requirements necessary to meet the requirements of the seedlings on its production phases.

B. Sugarcane Grower

1) Process Management

The sugarcane grower has specific production processes, controlled and monitored to take corrective actions for deviations, in which there is no dissemination of a culture of a preventive nature. He seeks to have a customer-oriented relationship, seeking to involve him in actions to improve the quality of the sugarcane that arrives at the milling. However, performance indicators of cane quality requirements, involving the client, are used in an informative way, that is, they are not used to generate actions for improvement. The grower does not have structured planning for dissemination of the continuous improvement culture on the farm. The cane harvest is mechanized.

2) Product and QM Requirements

The sugar cane quality requirements of the producer are: the highest possible sucrose content represented by the ATR, the lowest mineral (soil) and vegetable (straw, wax, etc.) impurities and the lowest incidence of shoot borer, one of the plague of sugar cane which decreases the sucrose content and is detrimental to the juice, decreasing productivity.

In Table 3, follow the QM requirements necessary to meet the requirements of sugar cane on its production phases.

C. Milling

1) Process Management

The milling has criteria to manage and control the various processes of ethanol production, which are formalized, where the deviations are measured and monitored for the proper corrective action, but there is no culture of actions for preventive improvement.

There is a sharing of information on the status of ethanol production processes internally at the milling.

TABLE IV. QM REQUIREMENTS TO ETHANOL.

Ethanol		
Milling's ethanol production steps	**QM requirements**	**Ethanol's Requirements**
Sugarcane juice treatment	Obtaining the correct Ph range correction in sugarcane	Ph range
	Polymer dosage control in sugarcane juice	Residual lead and iron rates
Fermentation of sugarcane	Brix control of must	Alcohol rate
	Dosing control of sulfuric acid	PH; residual lead and iron rates; electric conductivity rate
Destination	Ph range control	Ph range
	Alcohol level control	Alcohol rate
	Total acid control	Total acidity rate
	Electric conductivity control	Electric conductivity rate

2) Anidro Ethanol's Requirements

The National Petroleum Agency (NPA) of Brazil rules that anhydrous ethanol needs to be clear and free of impurities, but it differs in relation to its color since an orange-colored pigment must be added to the blend in order to differentiate it of hydrated ethanol. Anhydrous ethanol must have an alcoholic rate of at least 99,6%.

3) Hidrato Ethanol's Requirements

The NPA of Brazil establishes several quality criteria for the product to be marketed. Hydrous ethanol needs to be clear and free of purity with respect to its appearance which means that the liquid must be uniform, of the same color, and with no solid residue in its mixture. The method to define the quality is only visual, without having to submit the ethanol to other tests, which is used for the certification of the quality of its color. Because hydrated ethanol is a mixture made primarily of alcohol and water, it does not have coloration, which makes it transparent. The ANP stipulates the alcoholic content of hydrated ethanol between 95.1 and 96 INPM, (unit of measure equivalent to the percentage of alcohol in the mixture). The pH must be between 6 and 8, that is, it can neither be very basic nor very acid, remaining neutral. The minimum ethanol that the blend needs to have is between 94.5% volume, while the water can have a maximum of 4.9%.

In Table 4, follow the QM requirements necessary to meet the requirements of the ethanol on its production phases.

D. Proposal for Ethanol Production Chain Requirements

1) Meeting the requirements

All of the products requirements of the ethanol production chain must be accomplished by each one of its agents (seedling grower, sugarcane grower and milling). Then, the quality of sugarcane needs of a management that enables the attainment of these requirements identified and also the gaps related to the practices of the PM element of the internal process theory in the ethanol production chain, mainly to the practice "control and improve continuously the processes", where there is the control, but lack

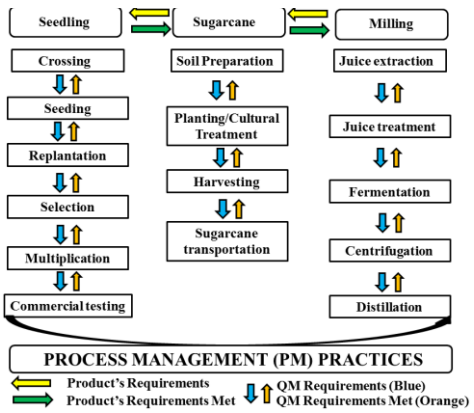

Figure 2. Illustration for managing the product requirements of the ethanol production chain.

of a system of continuous improvement implement in the three agents of the ethanol production chain. To perform these needs, a QM proposal is presented, which seeks to fill the cited gaps through the agents that forms the ethanol production chain. This model, once implemented, could help the main agents of this chain attain the product quality requirements, having the PM practices, as a basis for the implementation of the proposal. An illustration of the proposal to manage the product requirements in the ethanol production chain is shown Fig. 2.

The proposal is based on meeting the product requirements demanded by customers in the ethanol production chain (yellow arrows). To meet these requirements, suppliers must meet the QM requirements (orange arrows). If at each stage of ethanol production the requirements of QM are met (blue arrows), consequently the product requirements of the agents will be met (green arrows).

Product requirements must be defined for all agents in the production chain in order to develop and produce products that meet customer needs. These requirements are obtained both from regulatory agencies and by specifications of chain customers.

QM requirements must be defined and specified for each agent to meet the ethanol product requirements. These requirements are those used and necessary for the definition of the management procedures with the objective of achieving the expected quality of the product, also contemplating the reduction of costs and losses in ethanol production.

2) Process Management (PM)

The execution of the practices of the PM element is a basis to support the quality management model.

In order to meet the PM element practices in the ethanol production chain, discussed in the previous topic, it is necessary to identify, investigate and update these practices in order to improve transparency and trust among the agents of the chain through actions that compliance with QM requirements. This is to improve product quality and efficiency in the activities of the ethanol production chain. An evaluation of the PM practices regarding their

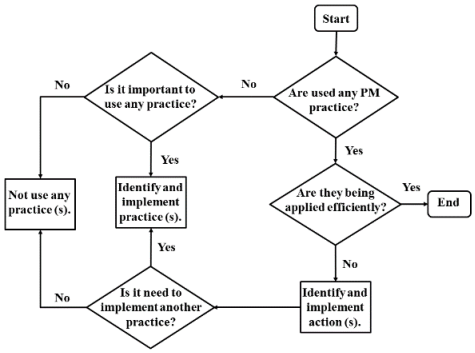

Figure 3. Flowchart of the information flow of the practices of the PM element.

effectiveness in the timeline should be undertaken. If they are effective, they should be maintained. If they are ineffective, the cause of ineffectiveness must be identified and eliminated. Fig. 3 is shown a flowchart that assists in the evaluation of PM element practices.

V. CONCLUSION

The PM element from IP theory and its main practices were identified in the literature. The empirical research of multiple cases investigated the use of the practices of this element in the ethanol production chain. The product requirements were identified on the agents of this chain as well QM requirements demanded by each internal process of the agents. Some shortcomings were identified regarding to this agents, such as the lack of quality preservation actions to lead to actions of continuous improvement. To fill these gaps and to meet the requirements of the chain, a proposal was presented, establishing a flow of information to meet the QM requirements, based on the PM practices that support it. This proposal could corroborate the improvement on the quality of product requirements among agents in the ethanol chain, which could result on the attainment of the products requirements of the agents.

The main objective of this work, which is to present a proposal to manage the requirements of the ethanol chain was performed. However, the proposal does not address aspects related to the external activities of this chain. This is a suggestion for a future work.

ACKNOWLEDGMENT

To the Federal Institute of Education, Science and Technology .of São Paulo, Catanduva-SP, Brazil for the support and incentive. To the University Federal of São Carlos for the support.

REFERENCES

[1] H. T. Quang, P. Sampaio, M. S. Carvalho, A. C. Fernandes, D. T. Binh An, and E. Vilhenac, "An extensive structural model of supply chain quality management and firm performance", Int. J. Qual. Reliab. Manag., vol. 33, no. 4, 2016, pp. 444–464.

[2] D. Prajogo, J. Toy, A. Bhattacharya, A. Oke, and T. C. E. Cheng, "The relationships between information management, process management and operational performance: Internal and external contexts", Int. J. Prod. Econ., vol. 199, 2018, pp. 95–103,.

[3] A. Chiarini and E. Vagnoni, "World-class manufacturing by Fiat. Comparison with Toyota Production System from a Strategic Management, Management Accounting, Operations Management and Performance Measurement dimension", Int. J. Prod. Res., vol. 53, no. 2, 2015, pp. 590–606.

[4] Z. Cai, Q. Huang, H. Liu, and L. Liang, "The moderating role of information technology capability in the relationship between supply chain collaboration and organizational responsiveness: Evidence from China", Int. J. Oper. Prod. Manag., vol. 36, no. 10, 2016, pp. 1247–1271.

[5] A. Gunasekaran, C. Patel, and R. E. McGaughey, "A framework for supply chain performance measurement", Int. J. Prod. Econ., vol. 87, no. 3, 2004, pp. 333–347.

[6] X. Brusset, "Does supply chain visibility enhance agility?", Int. J. Prod. Econ., vol. 171, 2016, pp. 46–59.

[7] Wing S. Chow and King. H. Lui, "A structural analysis of the significance of a set of the original TQM measurement items in information systems function", J. Comput. Inf. Syst., vol. 43, no. 3, 2003, pp. 81–91.

[8] C. J. Robinson and M. K. Malhotra, "Defining the concept of supply chain quality management and its relevance to academic and industrial practice", Int. J. Prod. Econ., vol. 96, no. 3, 2005, pp. 315–337.

[9] H. Kaynak, "The relationship between total quality management practices and their effects on firm performance", J. Oper. Manag., vol. 21, no. 4, 2003, pp. 405–435.

Effects of Change of L/D Ratio With Variation of Mach Number and Temperature For Tandem Dual Cavity in Scramjet Combustion Engine

Krishna Murari Pandey[1*], Kumari Ambe Verma[1], Anjali[2], Mukul Ray[3],

[1]Department of Mechanical Engineering, National Institute of Technology Silchar, Assam-788010, India, *kmpandey2001@yahoo.com
[2]Environmental Hydrology Division, National Institute of Hydrology Roorkee, Pin-247667, Uttarakhand, India
[3]Public Works Department, Government of Tripura, Agartala- 799006, India

Abstract — **The objective of the paper is to explore the typical tandem dual cavity scramjet combustor with the help of changing parametric conditions of incoming air. Many experiments are going on all over the world on scramjet combustion to make them suitable for travelling and to improve the overall efficiency. Hydrogen as a fuel has been chosen to get higher effective results compared to other hydrocarbon fuels. To reduce the computational cost, two dimensional model is chosen to simulate the model in ANSYS Fluent solver. Validation has been completed through open literature paper and is found to be in good agreement between experimental and computational simulation. From the shadowgraph comparison, similar trends have been identified in contour plot of computational work. So based on these results, Ansys fluent is selected for further work in this paper. Also less computational time was identified in Reynold Average Navier Stokes based equation model. The computational outcomes show that effect of Mach number variations show that good combustion characteristics are achieved in the ranges of Mach number 2.75 and 3 as the combustion phenomena remains limited to the regions around the combustor cavity walls.**

Keywords - cavity, length to depth ratio, mach number, static pressure, temperature, total pressure loss

I. INTRODUCTION

Supersonic ramjet engine i.e. scramjet is most promising air breathing engine in the aircraft application. All the operations are performed by taking oxygen from the atmosphere thus making the machine lighter and faster. Also since there is no need to carry oxygen, it makes the scramjet lighter. Scramjet are designed to perform operations in supersonic zone. Above Mach 3, turbomachinery cannot be used and ram style compression is preferred. Since there is no turbomachinery, so scramjet cannot start from the initial stage all alone and sufficient compression is achieved during supersonic flight. In the present work two dimensional tandem dual cavity scramjet combustor with single step chemical reaction is performed with steady Reynolds Average Navier-Stokes (RANS) coupled with k-epsilon turbulence model. Validation of present work is done and compared with the research work of Yang et al. [2] which shows good agreement towards results. Numerical simulations with the help of ANSYS 16-Fluent code is selected to identify the effect of variation of parametric variables on the flow-field.

ISBN: 978-86-80616-04-9

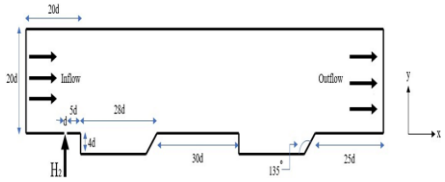

Figure 1. Schematic diagram of the model.

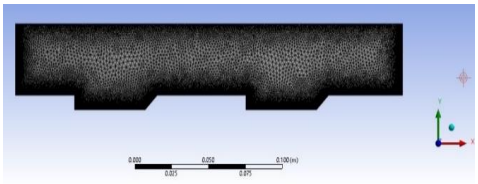

Figure 2. Meshing of 2D computational model.

II. GEOMETRY AND GRID GENERATION

CFD is one of the most fascinating technique for analysis and design of scramjet application [1]. Here the 2D model of tandem dual cavity scramjet combustor model is made. The experimental model is studied by Yang et al. [2] and is selected for this article shown in Fig. 1. Fig. 2 shows the meshing of 2D computational model. In this analysis, triangular mesh is used with unstructured grid.

To check the grid independence test of the combustor, three types of meshing have been utilized. Satisfactory agreement can be seen in pressure graph depicted in the Fig. 3 compared with experimental data available in open literature. Similar shock wave behavior is observed from the contour plot obtained from the simulation, which shows similar trends.

Ansys 16 – Fluent based solver has been chosen to simulate the steady, two dimensional tandem dual cavity combustor to explore the performance characteristics with the help of parametric variation. Reynolds Average Navier-Stokes (RANS) model has been selected to complete the computational work. Two equation based k-epsilon turbulence model [4] has been taken into consideration.

The governing equations of the selected model are explained as Continuity equation:

$$\frac{\partial \rho}{\partial t}+\frac{\partial(\rho u_k)}{\partial x_k}=0;\ \mathrm{k}=1,2,3\ . \qquad (1)$$

Momentum equation:

$$\frac{\partial(\rho u_i)}{\partial t}+\frac{\partial(\rho u_i u_j)}{\partial x_k}+\frac{\partial \rho}{\partial x_i}= =\frac{\partial \tau_{ik}}{\partial x_k};\ \mathrm{i,k}=1,2,3 \qquad (2)$$

Energy equation:

$$\frac{\partial(\rho H)}{\partial t}+\frac{\partial(\rho u_k H)}{\partial x_k}= =-\frac{\partial(u_j \tau_{jk})}{\partial x_k}+\frac{\partial q_k}{\partial x_k};\ \mathrm{j,k}=1,2,3 \qquad (3)$$

Turbulence kinetic energy k equation:

$$\frac{\partial(\rho k)}{\partial t}+\frac{\partial(\rho u_k H)}{\partial x_k}= =\frac{\partial}{\partial x_k}\left(\left(\frac{\mu_t}{\mathrm{Pr}}+\frac{\mu_t}{\sigma_k}\right)\frac{\partial k}{\partial x_k}\right)+S_k \qquad (4)$$

Rate of dissipation of turbulence energy (ε) equation:

$$\frac{\partial(\rho Y_n)}{\partial t}+\frac{\partial(\rho Y_n u_k)}{\partial x_k}= =\frac{\partial}{\partial x_k}\left(\left(\frac{\mu_t}{\mathrm{Pr}}+\frac{\mu_t}{\sigma_c}\right)\frac{\partial Y_n}{\partial x_k}\right);k=1,2,3 \qquad (5)$$

Where ρ, u_i, p, H are the density, velocity components, pressure and total enthalpy, respectively and $\mu=\mu_l+\mu_t$ is the total viscosity μ_l , μ_t being the laminar and turbulent viscosities and Pr is the Prandtl

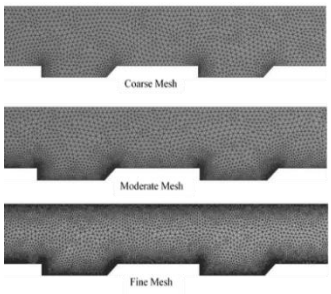

Figure 3. Different meshing scales.

number. The standard k-ε turbulence model [5] assumes that the turbulent viscosity is isotropic and the equation is:

$$\frac{\partial(\rho k)}{\partial t}+\frac{\partial(\rho k u)}{\partial t}= = \frac{\partial}{\partial x_j}\left(\frac{\mu_t}{\sigma_k}\frac{\partial k}{\partial x_j}\right)+2\mu_t E_{ij}E_{ij}-\rho t \quad , \qquad (6)$$

and

$$\frac{\partial(\rho t)}{\partial t}+\frac{\partial(\rho \in u_i)}{\partial t}= = \frac{\partial}{\partial x_j}\left(\frac{\mu_t}{\sigma_\epsilon}\frac{\partial \in}{\partial x_j}\right)+C_{1\epsilon}\frac{\in}{k}2\mu_t E_{ij}E_{ij}-C_{2\varepsilon}\rho\frac{\varepsilon^2}{k} \quad . \qquad (7)$$

Finite rate-eddy dissipation [7] species model [6] is used to complete the chemical kinetics. During fuel and air mixing, flow properties [8] such as wall pressure [9] is major influencing parameter in the reacting flow. Finite rate eddy dissipation model is more appropriate model over eddy dissipation [10] to solve complex chemical kinetics based [11] problems. Scramjet combustor of the present model utilizes single step reaction [12] and adequate to predict the results with less computational time [12]. Single step chemical reaction is as follows: $2H2 + O2 \rightarrow 2H2O$

III. BOUNDARY CONDITIONS

Table I describes the detailed description of selected boundary conditions of present model. Dirichlet boundary conditions are applied at inlet and Neumann boundary condition is selected for all values of outlet. For walls, no-slip and constant heat flux have been chosen [13]. The Courant Friedrichs Lewy number is taken as 0.5 [14]. Turbulent kinetic energy (k) and dissipation rate (ε) is taken same as given in the research paper of Gautam Choubey and K.M. Pandey [13].

TABLE 1. BOUNDARY CONDITION

S. No.	Variable	Air	Hydrogen
1	M_a	2.82	1
2	T_o (K)	1486	300
3	P_o (MPa)	1.6	0.8
4	Y_{O2}	0.232	0
5	Y_{N2}	0.736	0
6	Y_{H2O}	0.032	0
7	Y_{H2}	0	1

IV. VALIDATION

The chosen computational model for the tandem dual cavity scramjet combustor is verified by comparing its results with that of Yang et al. [2]. Qualitative validations of the results have been performed using the shadow image taken from the experiments. Fig. 4 shows the experimentally obtained shadowgraph image and computationally observed density contours. The shock wave generated at the fuel inlet is reflected by the upper wall and the intensity of wave decreases as it travels downstream of the flow. Fig. 5 represents graph of the pressure variation in the flow field and here both the experimental and computational results are plotted simultaneously and it can be seen that computational result show good resemblance with the experimental results.

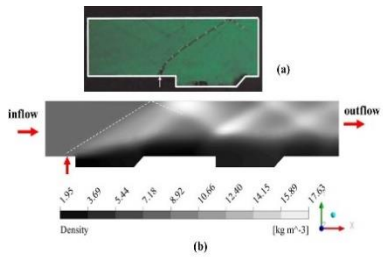

Figure 4. a) Shadowgraph image of fuel injection from experiment performed by Yang et al. [12], (b) Present computational model.

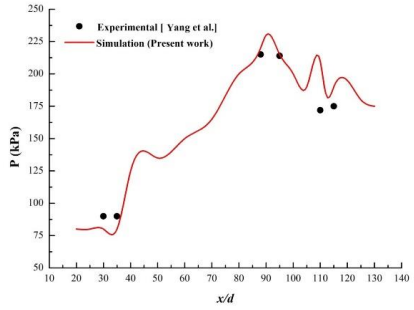

Figure 5. Comparison of wall pressure distribution for double cavity experimentally [2] with CFD simulation with k-$^{\varepsilon}$ turbulence model.

V. RESULTS AND DISCUSSION

As our primary objective of the present computational work is to study the effect of variation of hydrogen injection pressure and variation of inlet air total temperature on the flow-field of tandem cavity scramjet combustor. Contours and graphs obtained by changing Mach number and temperature of inlet air are discussed below nonetheless L/D ratio is also introduced and discussed below.

A. Variation of L/D ratio of combustor

Four L/D ratio of combustor cavity have been selected and analyzed to observe the effects.

a) Effect on mach number

Fig. 6 shows the variation of Mach number along the length of the combustor for various length-to depth (L/D) ratio. Here it is found that for lower L/D ratio 3, 5 and 7, the Mach number around the cavity remains limited to subsonic limit whereas in case of higher L/D ratio 9, the Mach no. around the cavity as well as in between the cavities remains subsonic. As it can be observed from the graphs (Fig. 7) between Mach no and position that in all the cases Mach no is highest at the fuel inlet and it decreases around the cavities but in case of lower L/D ratios 3, 5, 7 the Mach number around the combustor wall in between the cavities increases while in case of higher L/D ratio of 9, the Mach number in between the cavities is also very less.

b) Effect on pressure

Fig. 8 shows the variation of pressure along the length of the combustor for different L/D ratios. With the increase in L/D ratios the movement of shock waves becomes effective in the downstream of the flow. For lower L/D ratios 3, 5, 7 the shock waves gets reflected from the upper walls multiple number of times. The pressure around the cavities in case of lower L/D ratios is also very high. But in case of high L/D ratio 9, the pressure around the first cavity is somewhat lower compared to the other three. Also, here the pressure in the upper wall is significantly higher than the other three L/D ratios, which is not desirable from design point of view. So there must be optimal values of L/D ratios for which combustion efficiency will be more. From the graphs (Fig. 9), it is observed that in case of low L/D ratios of 3, 5 and 7, the pressure around the cavities increases abruptly and decreases abruptly in the region between the cavities. Whereas in case of L/D ratio of 9, the pressure around the cavities increases but also the pressure in the walls in between the cavities is also very high.

c) Effect on temperature

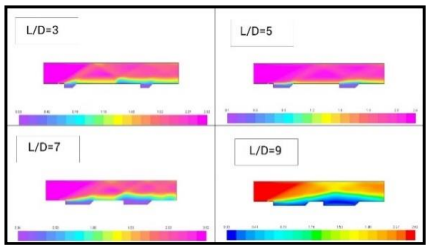

Figure 6. Mach no variation for different L/D ratio.

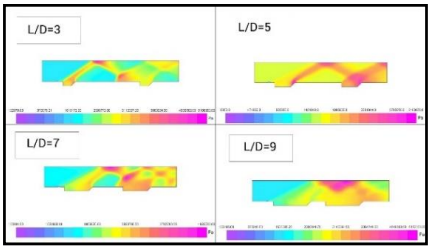

Figure 8. Pressure variation for different L/D ratio.

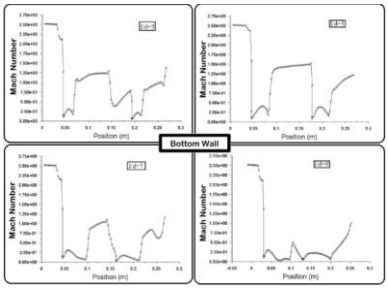

Figure 7. Mach number v/s position graph for L/D.

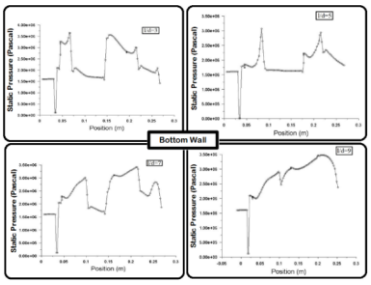

Figure 9. Static pressure vs position graph. for L/D ratio

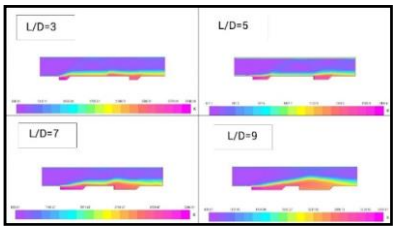

Figure 10. Temperature variation for different L/D ratio.

Fig. 10 shows the variation of temperature along the length of the combustor for different L/D ratios. For L/D ratios of 3, 5, 7 and 9, the temperature around the cavity is the highest. But in case of L/D= 3, the temperature around the bottom walls in between the cavities is also high.

Whereas in case of L/D = 5 and 7, the temperature around the bottom walls in between the cavities is somewhat lower than the other two cases remains confined around the cavities. In case of L/D = 9, the temperature around the bottom walls in between the cavities is also very high which means that combustion also takes place in that region. From the obtained graphs (Fig. 11), it can be observed that temperature is highest around the first cavity in all the four cases. It starts decreasing downstream of the flow that is in between the first and second cavity. Again, the temperature around the second cavity becomes significantly high in case of L/D=5.

Whereas in case of L/D = 3,7,9, the temperature around the second cavity takes a slight peak, which means that combustion occurs with a very good manner in case of L/D =5 compared to the other three cases.

B. Variation of inlet air temperature

a) Effect on static pressure

Fig. 12 shows the variation of pressure along the length of the combustor for different values of temperature. Here the oblique shock wave is generated because of the fuel injection is reflected by the upper wall and the intensity of shock decreases as it travels downstream of the flow for 1300 K and 1500 K, but for 1700 K the shock wave diminishes midway and the pressure at the region where the shock wave strikes is very high which may damage the material.

b) Effect on temperature

Fig. 13 shows the variation of temperature along the length of the combustor for various inlet air temperatures.

For inlet air temperatures 1300 K and 1500 K, the temperature around the cavity is very high i.e., the combustion region remains limited mainly around the cavity though some amount of combustion also occurs in the region between the cavities, But for 1700 K, the temperatures around the cavities is very less which means that combustion did not occur effectively in the

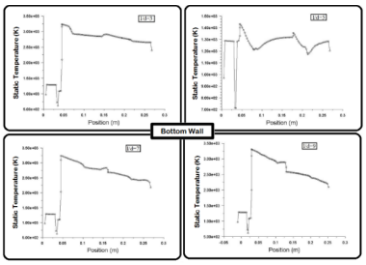

Figure 11. Static temperature vs position graph for L/D ratios.

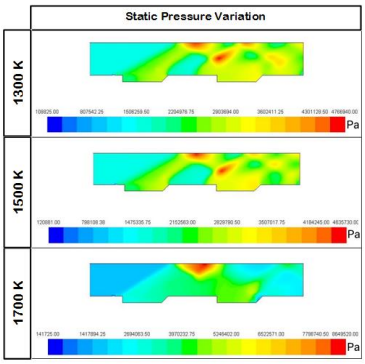

Figure 12. Static Pressure variation for different inlet air static temperature.

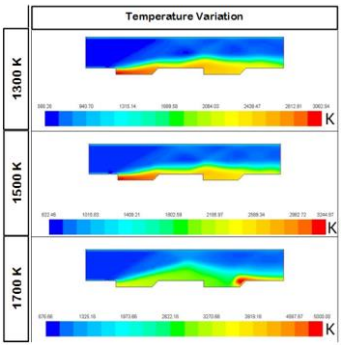

Figure 13. Temperature variation for different inlet air static temperature.

cavities.

C. *Variation of air inlet mach number*

a) *Effect on static pressure contour*

Fig. 14 represents the variation of static pressure for different Mach numbers along with the length of the combustor. Here the oblique shock waves are generated because of the fuel injection is reflected by the upper wall and the intensity of shock wave decreases as it travels downstream of the flow. It can be seen from the figure that for higher Mach numbers like 2.75 and 3, the shock wave distribution is good and hence it results in better mixing of fuel and air. So, combustion efficiency is more. Moreover, the pressure inside the cavity in case of Ma=2.75 and 3 is more than that of lower Ma=2 and 2.25. The pressure distribution in the upper wall for lower Mach number is high which may damage the surface of the upper wall.

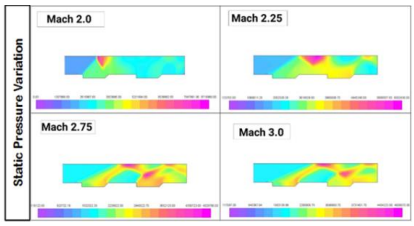

Figure 14. Static Pressure and Temperature variation for Various Mach numbers.

VI. CONCLUSION

The following conclusions are drawn on the basis of computational results:

- The effect of length-to-diameter (L/D) ratio variation shows that there are the best results for L/D=7 and also quite satisfactory results are there for L/D=3 and 5. But the results for L/D=9 are not at all acceptable.
- For temperature variation desirable characteristics are achieved for 1300 K and 1500 K but not for 1700 K.

Thus it is noticed that the present computational model concludes the results fairly satisfactorily while employing minimum computational facilities as compared to model like Large Eddy Simulation. The obtained Mach number profile, temperature profile as well as the pressure is very well matching with the experimental results whereas the predicted shock waves are also shown nicely. The computational outcomes show good agreement with the available experimental results.

REFERENCES

[1] WHITE, M., Drummond, J., Kumar, A. “Evolution and status of CFD techniques for scramjet applications”. In 24th Aerospace Sciences Meeting 1986, pp. 160.

[2] Yang Y, Wang Z, Sun M, Wang H, Li L. “Numerical and experimental study on flame structure characteristics in a supersonic combustor with dual-cavity”. Acta Astronautica, vol. 117, 2015, pp. 376-389.

[3] “Ansys Fluent 14.0 theory guide” Canonsburg: Ansys Inc. 2011.

[4] Launder, B. E., and Spalding, D. B. “The numerical computation of turbulent flows”. In Numerical prediction of flow, heat transfer, turbulence and combustion. Pergamon. 1983, pp. 96-116.

[5] Jones, W. P., and Launder, B. E. “The prediction of laminarization with a two-equation model of turbulence. International journal of heat and mass transfer, vol. 15, no. 2, 1972, pp. 301-314.

[6] Tu J, Yeoh G, Liu C. “Computational fluid dynamics a practical approach”. Oxford, UK: Elsevier, Butterworth-Heinemann, 2008.

[7] Oevermann, M. “Numerical investigation of turbulent hydrogen combustion in a SCRAMJET using flamelet modeling.” Aerospace science and technology, vol. 4, no. 7, 2008, pp. 463-480.

[8] Smirnov, N. N., and Nikitin, V. F. “Modeling and simulation of hydrogen combustion in engines.” International Journal of Hydrogen Energy, vol. 39, no. 2, 2014, pp. 1122-1136.

[9] Huang, W., Wang, Z. G., Li, S. B., Liu, W. D. “ Influences of H2O mass fraction and chemical kinetics mechanism on the turbulent diffusion combustion of H2–O2 in supersonic flows”, Acta Astronautica, vol. 76, 2008, pp. 51-59.

[10] Huang, W., Wang, Z. G., Yan, L., Li, S. B., and Ingham, D. B. “Variation of inlet boundary conditions on the combustion characteristics of a typical cavity-based scramjet combustor”. Proceedings of the Institution of Mechanical Engineers, Part G: Journal of Aerospace Engineering, vol. 228, no. 4, 2008, pp. 627-638.

[11] Smirnov, N. N., Betelin, V. B., Shagaliev, R. M., Nikitin, V. F., Belyakov, I. M., Deryuguin, Y. N., ... and Korchazhkin, D. A. “Hydrogen fuel rocket engines simulation using LOGOS code. International Journal of Hydrogen Energy”, vol. 39, no. 20, 2008, pp. 10748-10756.

[12] Kumaran, K., and Babu, V. “Investigation of the effect of chemistry models on the numerical predictions of the supersonic combustion of hydrogen”, Combustion and Flame, vol. 156, no. 4, 2009, pp. 826-841.

[13] Choubey, G., and Pandey, K. M. “Effect of variation of inlet boundary conditions on the combustion flow-field of a typical double cavity scramjet combustor”, International journal of hydrogen energy, vol. 43 no. 16, 2018, pp. 8139-8151.

[14] Erdem, E., and Kontis, K. “Numerical and experimental investigation of transverse injection flows”, Shock Waves, vol. 20, no. 2, 2010, pp. 103-118.

Producing of Microbial Oil Using Waste Glycerol from Biodiesel Production – From By-product to Raw Material

Jovan Ćirić[1], Nikola Stanković[2], Marko Živković[1], Đorđe Lazarević[1]

[1]Research and Development Center "ALFATEC", Niš, Serbia, jovan.ciric@alfatec.rs
[2]Faculty of Sciences and Mathematics, University of Niš, Niš, Serbia

Abstract — **Comparatively, with the great increase in the industrial production of biodiesel worldwide in the last decade, huge reserves of glycerol have been created and the price of pure and waste glycerol in the world market has fallen significantly. While the pure glycerol is an important commercial raw material with wide application in the pharmaceutical, cosmetic, chemical and food industry, waste glycerol presents a promising raw material for some new processes. One of the potential possibilities is to use it as a carbon source in nutrient media for microbial growth in industrial fermentation and the production of commercially important products. Results of studying the possibility of waste glycerol, obtained in sunflower oil-based biodiesel production, utilization by microalgae in order to produce microbial oil as a raw material for biodiesel are presented in this paper.**

Keywords – microalgae, oil, waste glycerol, biodiesel

I. INTRODUCTION

Many studies are focused on the production of inedible oils for energy purposes, especially for biodiesel production [1]. As one of the solutions, there are microorganisms (yeasts, fungi, and algae) and their biomass that can be used as a feedstock for biodiesel production. Microalgae are suitable promising producers of oil, favorably for biodiesel production. Microalgae can grow very fast [3] and very quickly can accumulate oil in biomass (up to 77 % of dry biomass with oil productivity up to 122 mg/l daily [4]). Compared to conventional crop cultivation, nearly 100 times more biodiesel can be obtained per unit area of algal cultivation [2]. Also, microalgae respond to the less favorable growing conditions (freshwater, seawater, wastewater, sewage, and uncultivated land) but as well they can be grown under controlled conditions (farms and bioreactors) [2]. One of the main byproducts in biodiesel production is glycerol (closely 10 % w/w of biodiesel amount) [5, 6]. Waste glycerol obtained in that way is of lower quality and it contains a lot of impurities that make it less suitable for conventional uses but purification is not necessary for microbial conversions. A lot of researches is focused on the microbial utilization of waste glycerol. Many microorganisms can successfully grow and convert glycerol into valuable products, such as 1,3-propanediol, n-butanol, ethanol, lactic acid, citric acid and others [7-10]. It is reported that some strains of algae may utilize heterotrophic pathways and grow successfully on organic carbon sources without a light source [11]. Several studies have reported that microalgae can effectively produce microbial oil using waste glycerol [12, 13]. Algae offer a dual solution in biodiesel production because they are very good producers of oil as raw material [14-17] but they also offer a solution for the utilization of large amounts of waste glycerol as a by-product [18, 19].

II. EXPERIMENTAL

Four isolated strains of microalgae, identified as members of the *Chlorococcum*, *Chlorella*, *Desmodesmus* and *Scenedesmus* genera, were used for the experiments. The strains were isolated from the samples of South Serbian swamps and ponds in the Laboratory for Microbiology and Food Technology of the

ISBN: 978-86-80616-04-9

Faculty of Technology in Leskovac [20]. Media used for growing of microalgae were as follows: Bolds Basal Medium (pH 6.6) ($NaNO_3$ 0.249 g/l; $CaCl_2$ x 2 H_2O 0.025 g/l; $MgSO_4$ x 7 H_2O 0.075 g/l; K_2HPO_4 0.072 g/l; KH_2PO_4 0.175 g/l; NaCl 0.025 g/l; EDTA 0.16 g/l; KOH 0.077 g/l; $FeSO_4$ x 7 H_2O 0.012 g/l; H_3BO_3 0.028 g/l; $ZnSO_4$ x 7 H_2O 0.019 g/l; $MnCl_2$ x 4 H_2O 0.004 g/l; MoO_3 0.002 g/l; $CuSO_4$ x 5 H_2O 0.004 g/l; $Co(NO_3)_2$ x 6 H_2O 0.001 g/l). Pure (Sigma Aldrich, 99.5 %) and waste glycerol, obtained in sunflower oil-based biodiesel production, were added to the BBM medium in quantity of 15 g/l. Waste glycerol was obtained in Laboratory for chemical engineering of Faculty of Technology in Leskovac, (University of Niš). Under the constant light, during the 30 days, isolated microalgae were grown in 1000 ml modified BBM media, on a rotary shaker (140 min-1) at a temperature of 22 °C. After inoculation, an absorbance value was approximately 0.05 (measured at λ = 620 nm) [21]. The growth of algae was monitored spectrophotometrically by measuring optical density (OD620), and the concentration of dry biomass was determined at the end of the process, after the entry of the algae into the stationary phase. The change in glycerol concentration was determined using the HPLC method. Dry algal biomass content was determined gravimetrically [22]. The content of algal oil was determined using the Bligh-Dayer method [23, 24].

III. Results And Discussion

The results of studying the possibility of microalgae cultivation in media with pure and waste glycerol obtained in sunflower oil-based biodiesel production are shown in Table I. The kinetics of microbial growth and glycerol consumption during the cultivation are shown in Fig. 1-4 shows the growth of isolated strains of *Chlorella*, *Chlorococcum*, *Desmodesmus*, and *Scenedesmus* in pure glycerol BBM medium. All strains were growing slower in the first 3 to 6 days and they have entered a stagnant phase after 27 days, except *Chlorococcum* which had constant growth until the end of the process. The highest concentration of biomass (1.7 g/l) was obtained with the *Chlorococcum* strain, followed by the *Desmodesmus* and *Chlorella* strains (1.4 g/l and 1.1 g/l), while the lowest concentration of biomass (1 g/l) was obtained with *Scenedesmus* strain (Table I). Glycerol had a stimulating effect on *Chloroccocum* growth, neutral effect on *Scenedesmus* strain and slightly negative effect on the *Desmodesmus* and *Chlorella* strains.

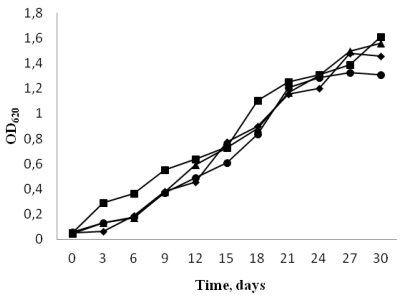

Figure 1. Changes of optical density (biomass content) during the cultivation of isolated microalgae from the genera *Chlorella* (♦), *Chlorococcum* (■), *Desmodesmus* (▲) and *Scenedesmus* (●) in BBM media with pure glycerol.

The lower growth was achieved by growing microalgae in media with waste glycerol than it was a case with pure glycerol. The obtained values of dry biomass content of isolated strains *Chlorella* and *Scenedesmus* were 10 % lower and the values for the *Chlorococcum* and *Desmodesmus* strains were 18 % and 15 % lower, respectively. The highest concentration of biomass was achieved with *Chlorella* (1.4 g/l) followed by *Desmodesmus* and *Chlorella* (1.2 g/l and 1 g/l). The same was the case of media with pure glycerol, the lowest amount of biomass was obtained with *Scenedesmus* (0.9 g/l). The growth kinetics of microalgae in waste glycerol media are shown in Fig. 2.

It was noticed that *Chlorella* sp., *Desmodesmus* sp. and *Scenedesmus* sp. strains grow weaker in the first 6 days (the restrained growth phase), and after they enter an exponential growth phase. *Desmodesmus* sp. and *Scenedesmus* sp. strains enter the stationary phase after 21 and 22 days while *Chlorococcum* grows continuously until the end of the process. The relatively long period of restrained growth phase can be explained as the necessary period for adaptation on the negative impact of impurities from waste glycerol. Same as in the medium with pure glycerol, *Chlorococcum* grows constantly until the end of the process.

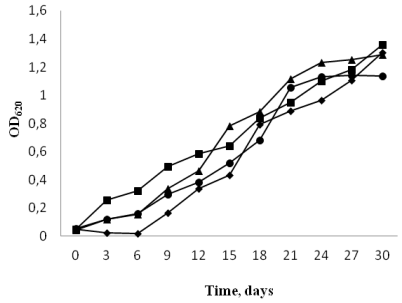

Figure 2. Changes of optical density (biomass content) during the cultivation of isolated microalgae from the genera Chlorella (♦), Chlorococcum (■), Desmodesmus (▲) and Scenedesmus (●) in BBM media with waste glycerol.

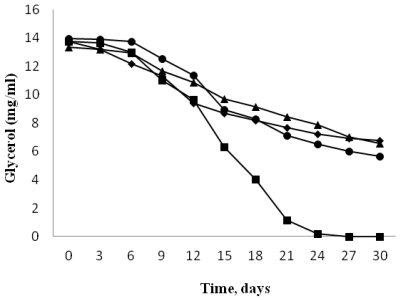

Figure 3. Change in glycerol concentration during the cultivation of isolated microalgae from the genera Chlorella (♦), Chlorococcum (■), Desmodesmus (▲) and Scenedesmus (●) in BBM media with pure glycerol.

Fig. 3 and Fig. 4 show the kinetics of glycerol consumption in media with pure and waste glycerol. During the cultivation of algae, it was observed that all isolated strains consumed glycerol, that is, the concentration of glycerol decreased during the process. The greatest glycerol consumption, with some variations, is observed in pure glycerol substrates. It is noticed that algal growth is not in accordance with glycerol consumption and thus confirming the fact that an organic carbon source is not required for the growth of algae [25]. Compared to the other studied strains, *Chlorococcum* sp. consumes the most glycerol in both media. Until the end of the process, it spends all available quantity. The significant glycerol consumption was observed only after 6 days, whereby in medium with pure glycerol it was consumed after 24 days and in medium with waste glycerol, although in a very small amount, it was present until the end of the process. Isolated strain *Scenedesmus* sp. has also consumed a higher amount of pure glycerol (59 %) compared to waste glycerol (47 %). The significant decrease of glycerol content was observed after 6 days and after that, it was declining steadily until the end of the process (Fig. 3). In pure glycerol medium, *Chlorella* and *Desmodesmus* strains consumed approximately the same amount of glycerol, 51 % of the total available amount (Table I). In both cases, the glycerol concentration decreased slightly in the first 3 to 6 days and then it was decreasing significantly by the end of the process.

Isolated strains produce different amounts of oil during the growth in glycerol media, unrelated to the microbial growth rate. It is well known that algae accumulate oil reserves in

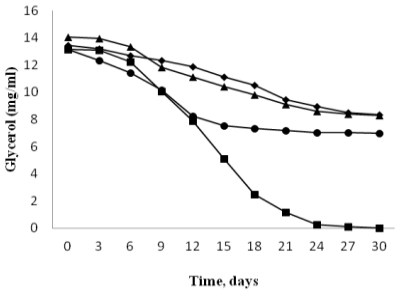

Figure 4 Change in glycerol concentration during the cultivation of isolated microalgae from the genera Chlorella (♦), Chlorococcum (■), Desmodesmus (▲) and Scenedesmus (●) in BBM media with waste glycerol.

unfavorable growth conditions. Despite the weaker growth in all media, compared to *Chlorococcum* sp. and *Desmodesmus* sp., *Chlorella* sp. produced the highest amount of oil. The oil content of the biomass obtained in pure glycerol medium was 34 %, slightly higher (35 %) was obtained in medium with waste glycerol. In these two cases, the productivity of the oil was 0.4 and 0.2 g/l.

The oil content in dry biomass obtained by cultivating in pure and waste glycerol media was higher than it was obtained by autotrophic cultivation in the basic BBM medium which was 33 % [20], and all obtained values are in accordance with the results obtained in similar studies where some strains of *Chlorella*

TABLE I. ACHIEVED MAXIMUM VALUES OF DRY BIOMASS (DBM), CONSUMPTION RATE OF GLYCEROL (ΔGLYC), YIELD ($Y_{P/X}$) AND OIL CONTENT IN DRY BIOMASS CONTENT, DURING THE CULTIVATING OF ALGAE IN PURE AND WASTE GLYCEROL MEDIA

CHARACTERISTICS OF BIOPROCESS										
	Pure glycerol					***Waste glycerol***				
Isolated strain	DBM	Δglyc		Oil		DBM	Δglyc		Oil	
	g/l	mg/ml	%	$Y_{P/X}$ g/l	%	g/l	mg/ml	%	$Y_{P/X}$ g/l	%
Chlorella sp.	1,1	6,97	51	0,4	34	1,0	5,11	38	0,3	35
Chlorococcum sp.	1,7	13,77	100	0,3	17	1,4	13,14	100	0,2	15
Desmodesmus sp.	1,4	6,80	51	0,3	22	1,2	5,76	41	0,3	22
Scenedesmus sp.	1,0	8,31	59	0,3	27	0,9	6,20	47	0,3	31

produced 26 – 47 % of oil under the autotrophic conditions [27]. Unlike strain *Chlorella* sp., *Scenedesmus* sp. strain produced 31 % of oil in medium with waste glycerol which is higher than it was obtained in pure glycerol medium (27 %). Although less favorable for growth, waste glycerol had a positive effect on oil production increase. This value is higher than it was obtained in studies with *Scenedesmus* growing under the autotrophic conditions (12 – 29 %) [27]. The strains of *Chlorococcum* and *Desmodesmus* showed the best growth in both media but they did not produce a significant amount of oil. *Chlorococcum* sp. produced twice less oil compared with *Chlorella sp.* (17 respectively 15 % of dry biomass). *Desmodesmus* sp. produced 22 % of oil in both media.

IV. CONCLUSIONS

During the study of the microbial utilization possibility of waste glycerol obtained in sunflower oil-based biodiesel production using the microalgae for oil production, it was concluded that the obtained results are encouraging for further research and they are consistent with the data reported in the literature.

The isolated strains, members of the *Chlorella* and *Scenedesmus* genera, have grown weaker and consumed less glycerol, but they have produced a significant amount of oil (27 – 35 % in DBM) by growing in media with waste glycerol, thus confirming that under less favorable conditions algae produce greater amount of oil.

In general, waste glycerol obtained in sunflower oil-based biodiesel production has proved to be suitable for the microbial processes and can be used without purification.

ACKNOWLEDGMENT

This work has been funded by the Ministry of Education, Science and Technological Development of the Republic of Serbia (Projects III 44006 and III 45001).

REFERENCES

[1] T.M. Mata, A.A. Martins, N.S. Caetano, "Microalgae or biodiesel production and other application" A review, Renew Sust. Energy Rev, vol. 14 no. 1, 2010, pp. 14 217–232.

[2] B. Danilović, J. Avramović, J. Ćirić, D. Savić, V. Veljković, "Production of biodiesel from microalgae" Chem Ind, vol. 68, no. 2, 2014, pp. 213–232.

[3] K. Vijayaraghavan and K. Hemanathan, "Biodiesel production from freshwater algae" Energ Fuels, vol. 23, 2009, pp. 5448–5453.

[4] J. Pruvost, G. Van Vooren, B. Le Gouic, A. Couzinet-Mossion, J. Legrand, "Systematic investigation of biomass and lipid productivity by microalgae in photobioreactors for biodiesel application" Bioresource Technol, vol. 102, 2011, pp. 150–158.

[5] M. Pagliaro, R. Ciriminna, H. Kimura, M. Rossi, C. Della Pina, "From Glycerol to Value-Added Products" Angewandte Chemie International Edition, vol. 46, no, 24, 2007, pp. 4434-4440.

[6] D.T. Johnson and K.A. Taconi, "The glycerin glut: Options for the value-added conversion of crude glycerol resulting from biodiesel production" Environmental Progress, vol. 26, no. 4, 2007, pp. 338-348.

[7] V.K. Garlapati and U. Shankar, A. Budhiraja, "Bioconversion technologies of crude glycerol to value-added industrial products" Biotechnol Reports vol. 9, 2016, pp. 9–14.

[8] S. Konstantinović, B. Danilović, J. Ćirić, S. Ilić, D. Savić, V. Veljković, "Valorization of crude glycerol from biodiesel production" Chem Ind Chem Eng Q, vol. 22, no. 4, 2016, pp. 461−489.

[9] M.R. Nanda, Z. Yuan, W. Qin, M.A. Poirier, X. Chunbao, "Purification of crude glycerol using acidification: Effects of acid types and product characterization" Austin Chem Eng vol. 1, 2014, pp. 1004-1011.

[10] E. Wilkens, A. Ringel, D. Hortig, T. Willke, K.D. Vorlop, “High-level production of 1,3-propanediol from crude glycerol by *Clostridium butyricum* AKR102a” Appl Microbiol Biotechnol, vol. 93, no. 3, 2012, pp. 1057-1063.

[11] P. Garcia, F.M. Escalante, L.E. de Bashan, Y. Bashan, “Heterotrophic cultures of microalgae: Metabolism and potential products” Water Research, vol. 45, no. 1, 2011, pp. 11-36.

[12] H.J. Choi and S.W. Yu, “Influence of crude glycerol on the biomass and lipid content of microalgae” Biotechnol Biotechnol Equip, vol. 29, no. 3, 2015, pp. 506-513.

[13] J.P. Denver, R.A. Garcia, Z. Wen, “Producing Docosahexaenoic Acid (DHA)-rich Algae from Biodiesel-Derived Crude Glycerol: Effects of Impurities on DHA Production and Algal Biomass Composition” J Agric Food Chem, vol. 56, 2008, pp. 3933–3939.

[14] S.N. Naik, V.V.Goud, P.K. Rout, A.K. Dalai, “Production of first and second-generation biofuels” A comprehensive review, Renew Sust Energ Rev vol. 14, 2010, pp.578–597.

[15] Y. C. Sharma, B. Singh, J. Korstad, “A critical review on recent methods used for economically viable and eco-friendly development of microalgae as a potential feedstock for synthesis of biodiesel” Green Chem, vol. 13, 2011, pp. 2993-3006.

[16] K. Vijayaraghavan and K. Hemanathan, “Biodiesel production from freshwater algae” Energ Fuels, vol. 23, 2009, pp. 5448–5453.

[17] J. Pruvost, G. Van Vooren, B.L. Gouic, A. Couzinet-Mossion, J. Legrand, “Systematic investigation of biomass and lipid productivity by microalgae in photobioreactors for biodiesel application” Bioresource Technol, vol. 102, 2011, pp. 150–158.

[18] H.J. Choi and S.W. Yu, “Influence of crude glycerol on the biomass and lipid content of microalgae” Biotechnol Biotechnol Equipment, vol. 29, no. 3, 2015, pp. 506-513.

[19] Y.H. Chen and T.H. Walker, “Biomass and lipid production of heterotrophic microalgae *Chlorella* protothecoides by using biodiesel-derived crude glycerol” Biotechnol Lett, vol. 33, 2011, pp. 1973-1983.

[20] B. Danilović, J. Cvetković-Rakić, J. Ćirić, J. Simeunović, V. Veljković, D. Savić, “The isolation and screening of microalgae for the production of oil” Chem Ind, vol. 71, no. 1. 2017, pp. 69–74.

[21] A.I. Reda, I. Matter, A. Abou-Shanab, S.N. Kim, Y.O. Kwan, J. Choi, B.H. Jeon, “Characterization and identification of lipid-producing microalgae species isolated from a freshwater lake” Biomass Bioenergy, vol. 35, 2011, pp. 3079-3085.

[22] M. Takagi, S. Karseno, T. Yoshida, “Effect of salt concentration on intracellular accumulation of lipids and triacylglyceride in marine microalgae *Dunaliella* cells” J Biosci Bioeng, vol. 101, 2006, pp. 223-226.

[23] S.J. Iverson, S.L.C. Lang, M.H. Cooper, “Comparison of the Bligh and Dyer and Folch methods for total lipid determination in a broad range of marine tissue” Lipids, vol. 36, 2001, pp. 1283–1287.

[24] P. Kumari, C.R.K. Reddy, B. Jha, “Comparative evaluation and selection of a method for lipid and fatty acid extraction from macroalgae” Anal Biochem, vol. 415, no. 2, 2012, pp. 134-144.

[25] V. Makareviciene, V. Skorupskaite, M. Gumbyte, “Biomass and oil content of *Chlorella* sp., Haematococcus sp., Nannochloris sp. and Scenedesmus sp. under mixotrophic growth conditions in the presence of technical glycerol” J Appl Phycol, vol. 26, 2014, pp.83–90,

[26] A. Sarmidi, “Review on biofuel oil and gas production processes from microalgae” Energy Convers Manage vol. 50, 2009, pp. 1834–1840.

[27] H.M. Amaro, A.C. Guedes, F.X. “Malcata, Advances and perspectives in using microalgae to produce biodiesel” J Appl Energ vol. 88, 2011, pp. 3402–3410.

Advances on LVRT Implementation at LV Networks in the Prospect of Mass Penetration of DERs

Dionisis Voglitsis, Aristotelis Tsimtsios, Ioannis Perpinias, Christos Korkas, Nick. P. Papanikolaou*

Democritus University of Thrace, Xanthi, Greece, *npapanik@ee.duth.gr

Abstract — **This paper summarizes the recent advances on Low Voltage Ride Through (LVRT) implementation at Low Voltage (LV) networks, in the prospect of mass penetration of Distributed Energy Resources (DERs). The reported advances are the outcomes of DGRES-Pro project, focusing on the transformation of typical LV feeders into contemporary flexible electric apparatus, with the use of power electronics conversion unitsthat will able to accommodate mass penetration of DERs in a safe and effective manner.**

Keywords – low voltage ride through, distributed energy resouces, power electronics, distribution networks

I. INTRODUCTION

The mass integration of Distributed Energy Resources (DERs) into distribution networks has necessitated the adoption of Low Voltage Ride Through (LVRT) requirements by relevant distribution networks codes over the last years [1]. LVRT is defined as the capability of generation units to remain connected to the electricity network (Transmission or Distribution level) during faults, providing voltage support, for a time duration that depends on the voltage drop at the point of common coupling (PCC). This distribution network transformation requires smart and flexible power electronic conversion units to implement all the operation/protection principles that LVRT scheme suggests.

In this context, a research project has been successfully conducted by the authors, namely "Application of advanced power electronic systems for the implementation of innovative protection schemes at LV distribution networks, in the prospect of mass penetration of DERs (DGRES-Pro)". The project is funded by the Operational Program "Human Resources Development, Education and Lifelong Learning" and is co-financed by the European Union (European Social Fund) and Greek national funds.

In order to highlight the main aspects of the alterations that mass DER penetration and LVRT implementation bring on the operation of LV networks. the project had the following main research activities:

- Investigation of the adaptation of line protection means to LVRT requirements in LV distribution feeders with photovoltaic generators (PVs) [2].
- Study on harmonic injection anti-islanding techniques under the operation of multiple DER-inverters [3].
- Study on the loss of neutral in low voltage electrical installations with connected DERs – consequences and solutions [4].

In the following section, a summary of the outcomes of DGRES-Pro project is presented.

II. SUMMARY OF RECENT ADVANCES ON LVRT IMPLEMENTATION AT LV NETWORKS, IN THE PROSPECT OF MASS PENETRATION OF DERS

A. Investigation of the adaptation of line protection means to LVRT requirements in LV distribution feeders with PVs

In LV distribution feeders with DG units, a major challenge to meet LVRT requirements is the coordination with the feeder protection means. Typically, LV distribution feeders are protected by a fuse, which implements a non-

ISBN: 978-86-80616-04-9

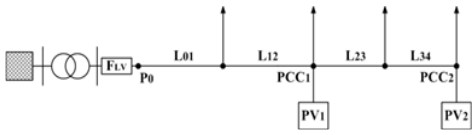

Figure 1. Test distribution feeder.

settable time-overcurrent characteristic curve. As such, the fuse cannot be reconfigured after its installation, failing to meet line protection and DG LVRT requirements at the same time.

This issue is examined with the aid of Fig. 1, which depicts a typical 50 Hz; 0.4 kV;, LV distribution feeder which is modeled with DIgSILENT Power Factory; all the segments of this feeder consist of 150-mm2 NAYY cable. Segments L01 and L12 are 25-m long, whereas segments L23 and L34 are 20-m long. The external grid is represented by an equivalent source with a maximum short-circuit power of 200 MVA at 20 kV. The feeder departs from a 20/0.4 kV transformer. The total system load is 140 kVA (133 kW). Finally, two 20 kW PV units are considered connected to points PCC1 and PCC2,PV1 and PV2, respectively (the simulation is based solely on PV units, being the predominant DER-units in LVRT networks). It is noted that the maximum steady-state short-circuit contribution of each PV-unit is limited to its nominal load current. Also note that PV1 and PV2 units operate according to the LVRT scheme of [5]. This LVRT characteristic is

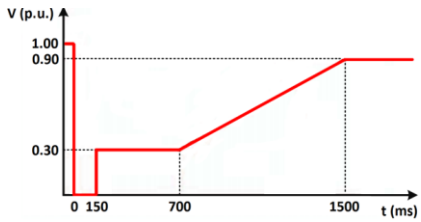

Figure 2. Adopted LVRT characteristic.

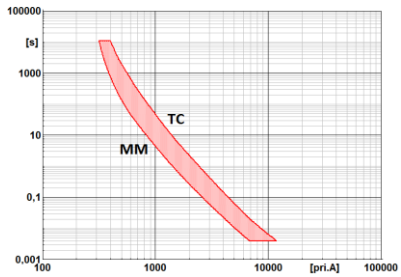

Figure 3. Time-overcurrent characteristic of fuse F_{LV}.

shown in Fig. 2, where a common 250 A gL fuse (FLV in Fig. 1) is installed for the feeder protection; fuse current rating is selected according to the maximum load current in the examined feeder. Fig. 3 illustrates both the minimum-melting (MM) and the total-clearing (TC) time-overcurrent characteristics of fuse FLV. Considering the case of a short-circuit occurs at the above line, the LVRT operation of PV-units might be interrupted by the fuse, leading the system into an islanding operation [6-9].

In order to better demonstrate the above-described problem, fault-simulations have been performed for all common fault types: line-line-line (LLL), double-line (LL), double-line-ground (LLG), and single-line-ground (SLG). According to the results in Table I, in all the examined fault-cases, LVRT requirements are violated, since fuse F_{LV} melts (or even starts melting) before the required time duration of PV-connection expires. These indicative results

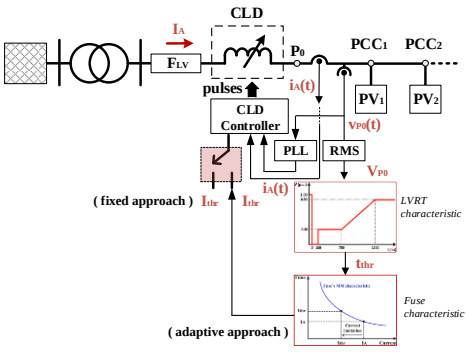

Figure 4. The proposed solution for flexible (power electronic-based) fault current limitation.

highlight the potential conflict of line protection (fuse) and LVRT requirements in LV networks.

TABLE I. INDICATIVE SIMULATION RESULTS

		t_{MM}/t_{TC} (in ms) of F_{LV} in each fault-case		
Fault position		**P_0**	**PCC_1**	**PCC_2**
Fault type	**LLL**	7/41	13/79	21/133
	LL	11/65	20/128	32/216
	LLG	7/40	12/76	21/138
	SLG	7/40	22/144	50/357

In order to avoid reconsideration of the LV distribution networks protection, a solution to the above problem would be the limitation of the short-circuit current that flows through the LV

fuse, so as for the latter to be suitably delayed, allowing the PV-units to stay connected for the time intervals that LVRT requirements impose. In the frame of DGRES-Pro project, a power electronic-based current-limiting device (CLD) solution has been developed, presented in Fig. 4, to limit the short-circuit current that flows through the LV fuse. The control diagram of the proposed CLD is depicted in Fig. 4 and implements a dual current-limiting approach (fixed or adaptive); $i_A(t)$ and $v_{P0}(t)$ represent the instant values of current and voltage at fuse location P_0, respectively, . The CLD device therefore resables a controllable impedance, placed in series with the fuse, as in Fig. 4.

In terms of hardware (power electronics) implementation, CLD is an ac-chopper which regulates the fundamental current component. Many topologies can be utilized to implement the ac-chopper. A particularly appealing topology though is the one proposed in [10]. Nevertheless, regardless the chosen topology, the design should meet the following two requirements:

a) The efficiency of CLD should be as high as 98%.
b) The power density of CLD should match current density of power grid-tied inverters (> 5 kW/kg).

Modern wind bandgap semiconductors (such as Silicon Carbide-SiC and Gallium Nitride-GaN) constitute an excellent solution to meet the above requirements.

B. Study on harmonic injection anti-islanding techniques under the operation of multiple DER-inverters

Apart from the LVRT scheme implementation at LV distribution networks, an additional critical issue that raises from the mass penetration of DERs is the effective anti-islanding protection. Although anti-islanding protection is well established in grid-tied PV inverters, all commercial solutions are designed for inverter sole operation [3]; thus, the effectiveness of commercial anti-islanding protection schemes in case of parallel inverters operation at the same PCC is poorly investigated [6, 9].

In this context, our work in the frame of DGRES-Pro project has also taken into consideration the impact of mass penetration of DERs on anti-islanding protection schemes. Our

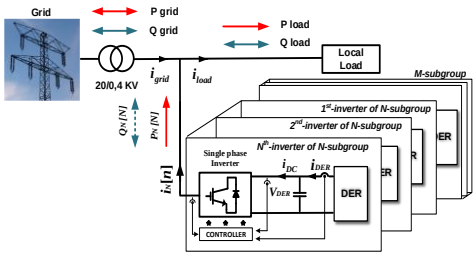

Figure 5. General description of the system under

main focus was on harmonic injection-based techniques, because they are referenced in literature as an appealing solution for anti-islanding protection of interconnected DER-systems [7, 8]. Those schemes do not disturb the output active-power of grid-tied inverter, they have reduced NDZ and provide fast island detection [7, 8]. Moreover, those schemes are highly dedicated to implementation in both high penetration levels of DERs and weak grid conditions, being the main theme of this work. According to those schemes, anti-islanding detection is based on the injection of selected harmonic current components and the evaluation of grid-response, typically through the comparison with a predefined threshold value.

The general description of multiple DRES-inverters connected at the same PCC is illustrated in Fig. 5. It consists of a subgroup of N-inverters that utilize a harmonic injection scheme, a subgroup of M-inverters (connected to the same PCC) that may or may not utilize an anti-islanding scheme, the local load, and the LV utility grid [9]. The power flow of each subsystem is also depicted in Fig. 5.

Considering the general system in Fig. 5, in the frame of this research activity, we proposed an advanced harmonic injection-based anti-islanding protection algorithm, illustrated in Fig. 6; the main idea is the introduction of an external integrator to cumulate the harmonic voltage components that have been induced by each inverter [9]. As such, the cumulative integral

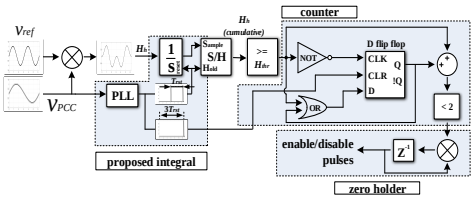

Figure 6. Proposed anti-islanding solution in the prospect of mass penetration of DERs at LV networks.

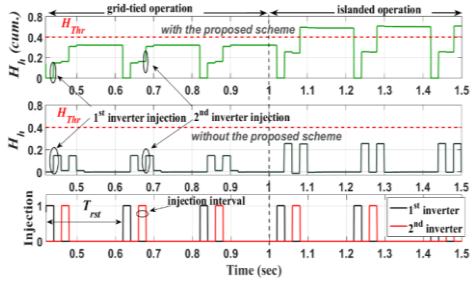

Figure 7. Demonstration of the proposed solution (grid-tied and islanded operation).

index will consider the individual impact of each inverter. It should be noted that a reset has to be performed periodically in this case, based on the periodicity of the harmonic injection of each inverter [9]. Consequently, the harmonic injection periodicity of each inverter (T_{rst} in Fig. 6) must be acknowledged beforehand, and be the same for all inverters, which is the main requirement of our proposed solution. Furthermore, the order of the harmonic injection should be an integer number, whereas the harmonic injection should be activated with respect to an agreed time-delay of PCC voltage; thus, the injected current components will not cancel each other. The time-delay could be agreed among the inverter manufacturers and included in the relevant prototyping standards.

The operation of the proposed (cumulative) technique is presented in Fig. 7. The case of two inverters has been considered, supporting the effectiveness of our solution.

C. *Study on the loss of neutral in low voltage electrical installations with connected DERs – consequences and solutions*

Another critical issue that raises from the mass penetration of DERs at LV networks (i.e. building DER installations) is the loss of neutral conductor, which is directly related to the safety of both human life and the electrical installation. The interruption of neutral conductor is a known issue in distribution networks, yet not fully addressed in view of the forthcoming massive installation of DERs and storage units (including Vehicle-to-Grid concept). Such a condition may result in serious repercussions for the connected electrical installations and consumers. The consequences of neutral conductor loss depend mainly on the load balance conditions in a three-phase system, but also on the type of earthing system used and the location of neutral interruption (relatively to the load). Worst-case scenarios may include both damages to

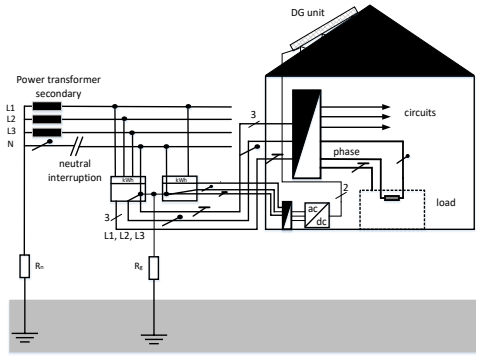

Figure 8. System under examination.

connected loads (due to overvoltages on single-phase circuits) and the creation of hazardous touch voltages on exposed conductive parts [11-13].

In the frame of DGRES-Pro project, the loss of neutral conductor under mass penetration of DERs has been thoroughly investigated; Fig. 8 presents the considered typical electrical building installation understudy, employing TN grounding system. A four-pole cable inserts to the energy meter of the building installation, where the neutral is connected to the grounding system of the installation to be protected. All the exposed-conductive-parts of the installation are connected to the protective earth conductor (PE). In addition, a DER (i.e. a PV system, namely DG-unit) is installed on the rooftop of the building, injecting the generated electrical energy to the network.

As an initial step, a sensitivity analysis for the developed voltages on the protective conductor is carried out, considering the following parameters:

- the generated electric power by the DG-unit (5A, 10A, 15A)
- the local load (1kW, 4kW, 6kW)
- the grounding resistance of the installation (1Ω, 2Ω, 5Ω, 10Ω, 15Ω, 20Ω).

Fig. 9 depicts the obtained results in the case that a DER is installed; in this case, the power coming from the DER and the absorbed power by the load, are key factors that influence the developed potential on the protective conductor. If the injected (by the DER) and the absorbed (by the load) energy are almost equal, then the developed voltage on the protective conductor does not exceed the safety limit of 50V (see load 1kW, DER-unit current 5A and load 4kW, DER-

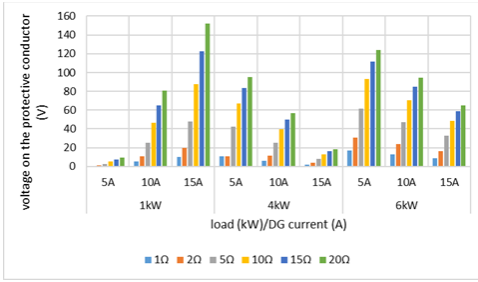

Figure 9. Developed voltages on the protective conductor in the case where a DG unit (a) is not installed, (b) is installed.

unit current 15A) for all the grounding resistance values. It is worth mentioning that even for low grounding resistance values the developed voltages can exceed the safety limit, due to the difference between the generated and the absorbed energy (see load power 1kW, DG unit current 15A, grounding resistance 10Ω).

The proposed loss of neutral conduction method (in the frame of DGRES-Pro project) is depicted in Fig. 10 and 11. The proposed neutral conductor loss detection scheme is based on the estimation of both zero-sequence impedance $z_{0,rms,50Hz}$ and voltage $v_{0,rms,50Hz}$ at the fundamental frequency of 50 Hz. The measuring point of the line to neutral voltages, v_{abc}, and neutral current, i_n, is indicated in Fig. 10. The zero-sequence voltage is calculated by summing the three-line to neutral voltages, as it is depicted in Fig. 11.

As Fig. 11 depicts, $z_{0,rms,50Hz}$ is compared with a predetermined threshold value $z_{0,thr}$ and if $z_{0,rms,50Hz} \geq z_{0,thr}$ then a neutral conductor interruption fault is indicated. It is noted that the impedance estimation method is not solely based on this proposed scheme, due to the incorrectly calculated values that arise under very high values of $z_{0,rms,50Hz}$ (in cases that $i_n \to 0$). For this reason, the impedance estimation scheme is activated only when the current of the neutral wire is above a threshold value, $i_{n,thr}$ (Switch1 at position 2). An overvoltage protection scheme operates complementary with the impedance estimation scheme and it is activated when the zero-sequence voltage is above the limit of 50V. This ensures the protection against hazardous touch voltages on exposed conductive parts.

Fig. 12 illustrates the loss of neutral conductor detection with the aid of the proposed methodology, considering the system in Fig. 10 with the technical characteristics of Table II (simulation results). The initialization time of the system is determined at 0.45s in order for the PV-Inverter to reach its nominal power value. When the neutral conductor interruption occurs a notable arise of the zero-sequence voltage $v_{0,rms,50Hz}$ emerges, while neutral current drops. The proposed scheme detects the fault by accurately estimating the grounding resistance value (z0,rms,50Hz = Rn+Rg = 10 Ω, in Fig. 12).

TABLE II. SYSTEM TECHNICAL PARAMETERS

$\mathbf{P_{pv\text{-}inv}}$	4 kW
$\mathbf{P_{Load}}$	6 kW
$\mathbf{z_{tr}}$	0.001 + j1e-6 Ω
$\mathbf{R_n}$	1 Ω
$\mathbf{R_g}$	9 Ω
$\mathbf{V_{abc}}$	230 V_{rms} (line to neutral)
$\mathbf{t_{disc}}$	0.5 s
$\mathbf{i_{n,thr}}$	0.5 A
$\mathbf{z_{0,thr}}$	5 Ω

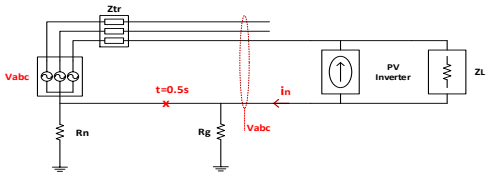

Figure 10. Equivalent system model.

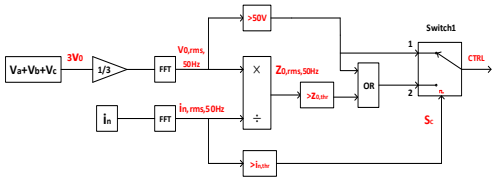

Figure 11. Proposed loss of neutral conductor detection scheme.

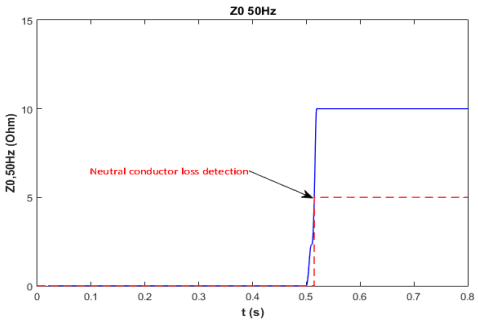

Figure 12. Loss of neutral conductor detection according to the proposed methodology.

III. CONCLUSIONS

This paper summarizes the recent advances on LVRT implementation at LV networks, in the prospect of mass penetration of DERs, in the frame of DGRES-Pro project. The main research activities of this project regarded a) the investigation of the adaptation of line protection means to LVRT requirements in LV distribution feeders with photovoltaic generators (PVs), b) the study on harmonic injection anti-islanding techniques under the operation of multiple DER-inverters, and c) the study on loss of neutral in low voltage electrical installations with connected DERs – consequences and solutions. All these research activities have concluded to successful technological solutions that contribute to the main goal of transforming the typical LV feeders into contemporary flexible electric apparatus, by means of power electronics conversion units, able to accommodate mass penetration of DERs in a safe and effective manner.

ACKNOWLEDGMENT

This research has been co-financed by the Operational Program "Human Resources Development, Education and Lifelong Learning" and is co-financed by the European Union (European Social Fund) and Greek national funds, in the context of the project "DGRES-PRO" (MIS 5006210).

REFERENCES

[1] D. Eltigani, S. Masri, "Challenges of integrating renewable energy sources to smart grids: A review," Renew. Sustain. Energy Rev. vol. 52, 2015, pp. 770–780 D.

[2] A. Tsimtsios, D. Voglitsis, I. Perpinias, C. Korkas, N. Papanikolaou, "Investigating adaptation of line protection means to low-voltage-ride-through requirements in low-voltage distribution feeders with photovoltaic generators," in 25th Int. Conf. on Electricity Distribution, June 3–6, Madrid, Spain, 2019.

[3] D. Voglitsis, F. Valsamas, N. Rigogiannis, N. Papanikolaou, "On harmonic injection anti-islanding techniques under the operation of multiple DER-inverters," IEEE Trans. on En. Conv., vol. 34, 2018, pp. 455–467.

[4] S. Frantzeskakis, D. Voglitsis, N. Papanikolaou, C. Christodoulou, I. Gonos, "Loss of neutral in low voltage electrical installations with connected DG units – consequences and solutions," in 25th Int. Conf. on Electricity Distribution, June 3–6, Madrid, Spain, 2019.

[5] BDEW (2008). *Technical guideline–Generating plants connected to the medium-voltage network–Guideline for generating plant's connection to and parallel operation with the medium-voltage network*. Available at:http://grouper.ieee.org/groups/scc21/1547a/email/pdfkz5Zov6vtg.pdf

[6] F. Valsamas, D. Voglitsis, N. Rigogiannis, N. Papanikolaou, and A. Kyritsis, "Comparative study of active anti-islanding schemes compatible to MICs in the prospect of high penetration levels and weak grid conditions," IET Gener. Transmiss. Distrib., vol 12, no. 20, 2018, pp. 4589 – 4596.

[7] D. Voglitsis, N. P. Papanikolaou, and A. Kyritsis, "Incorporation of harmonic injection in an interleaved flyback inverter for the implementation of an active anti-islanding technique," IEEE Trans. Power Electron., vol. 32, no. 11, 2017, pp. 8526–8543.

[8] D. Voglitsis, N.P. Papanikolaou, A. Kyritsis, "Active cross-correlation anti-islanding scheme for PV module integrated converters in the prospect of high penetration levels and weak grid conditions," IEEE Trans. Power Electron., vol 34, no. 3, 2019, pp. 2258-2274.

[9] D. Voglitsis, F. Valsamas, N Rigogiannis, N.P. Papanikolaou, "On harmonic injection anti-islanding techniques under the operation of multiple DER-inverters," IEEE Trans. Energy Convers., vol. 24, no. 1, 2019, pp. 455–467.

[10] S. Shibata, H. Yamada, T. Tanaka, M. Okamoto, "AC-chopper-based inrush current suppressor in a wind power generation system with squirrel-cage induction machines," Energies, vol. 11, 2018, pp. 1–14.

[11] V. Cohen. (2002). *Loss of neutral in low voltage distribution systems - consequences and solutions*. Available at: https://cbi-lowvoltage.co.za/sites/default/files/downloads/TechPapers/Loss%20of%20Neutral.pdf.

[12] M.H. Xivambu, "Impact of floating neutral in distribution systems," in 19th Int. Conf. on Electricity Distribution, May 21–24, Vienna, Austria, 2007.

[13] I. Lepadat, E. Helerea, S. Abagiu, "Effect on Neutral Interruption on the Unbalanced Three-Phase Consumers," in 14th Int. Conf. on Optim. of Electrical and Electronic Equipment, May 22–24, Brasov, Romania, 2014, pp. 192–197.

Analysis of a Hybrid Energy System for Supplying a Remote Critical Load in Onshore Coastal India

Momenul Islam[1], Arunava Chatterjee[1,2,*]

[1]Electrical Engineering Deptt., Meghnad Saha Institute of Technology, Kolkata, India,
[2]Electrical Engineering Deptt., Raghunathpur Government Polytechnic, W.B., India.
[*]arunava7.ju@gmail.com

Abstract — **This paper presents a technical analysis of a solar-photovoltaic based hybrid energy system for its use in a remote health center. The health center is setup in eastern coastal India. The aim of the paper is mainly to check the viability study for the energy system for its setup in the said region. *HOMER* (Hybrid Optimization Model for Electric Renewables) software-based technical analysis study is also presented for the purpose. An economic analysis for the setup is also presented in the paper. The study shows that even without the use of conventional fuels, the system is capable of sustaining a health center load effectively with low cost.**

Keywords – wind-PV hybrid, critical load, optimization.

I. INTRODUCTION

There is a continual increase in energy demand with growing population, which has led to depleting fossil fuel reserves. Also, fossil fuel usage has detrimental effects on the environment. Thus, there is always a need for a cleaner source of energy which will also be cost-effective. The use of renewable energy is therefore the need of the hour. Amongst different renewable energy sources, wind, solar, geothermal and tidal are mostly used for electricity generation in larger scales [1, 2]. However, most of the renewable energy sources are sporadic in nature and therefore requires appropriate control measures for sustained generation and use. In most of the cases for larger scale generations, hybrid renewable sources are therefore proposed. Among such generations, wind-PV [3-6] or solid oxide-based battery [7] are also used for supplying isolated and grid unreachable loads.

Some of such isolated loads are critical in nature and thus unavailability of power even for fraction of seconds need avoidance. Such a load is a health center/hospital load which needs constant power supply. In most such cases, fossil fuel-based generation sources are used with a backup source like storage battery [8]. These cases mostly increase the cost of the system over long run and also increases its carbon footprint which in turn affects the environment.

In a country like India, the electrification of the remote shoreline is difficult due to geographical barriers. Such places need an alternate and reliable source of power even for supplying small domestic loads.

This paper proposes a technical and economic analysis of a remote health center which is setup in such a coastal Indian location. The proposed generation system uses photovoltaic (PV)-wind generation for supplying the loads. The system viability is studied and found to be economical than diesel-based generations in a system projection of 25 years.

II. DESCRIPTION OF THE SYSTEM

The proposed hybrid generation-based system, supplying a health center is to be set up in a remote and grid-secluded area in eastern coast of India. The wind and solar data for the place can be obtained from surface metrological data using *HOMER* software. It uses NASA (USA) surface metrological data for the same. The generation scheme is shown in Fig.1.

The system is installed in a remote onshore place in eastern India which receives good solar insolation and good wind kinetic energy all over the year. The location of the proposed plant setup is shown in Fig.2.

ISBN: 978-86-80616-04-9

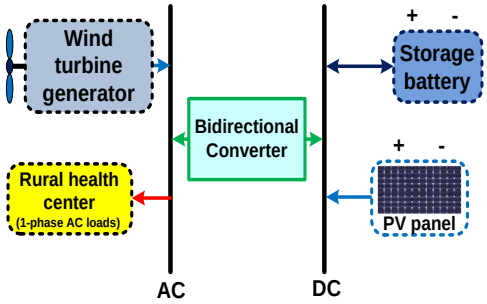

Figure 1. Proposed generation system.

Figure 2. Proposed system installation location (marked with red-pin, Courtesy: Google maps).

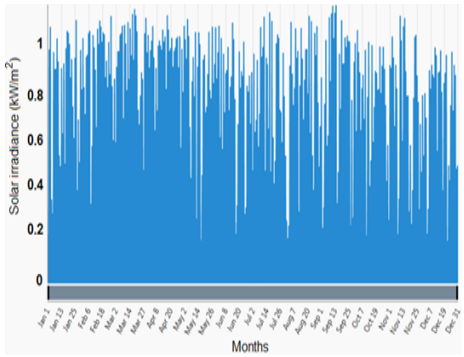

Figure 3. Solar daily radiation data of the chosen location.

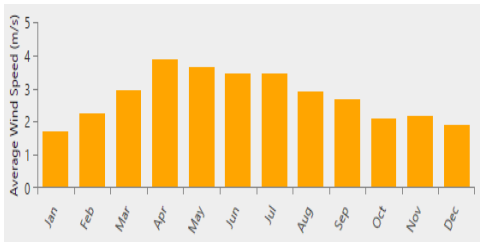

Figure 4. Average wind speed data of the chosen location.

The solar irradiance data as obtained from the simulation is shown in Fig.3 which is taken from the surface metrological data of NASA, USA. As observed from Fig.3, the area receives good solar radiation throughout the year.

The wind data is shown in Fig.4 below. It can be seen that the place also receives good amount of wind which is suitable for installation of a wind turbine generator (WTG).

III. System Setup

The health-center load is chosen as a critical load i.e. a load which is to be continually supplied without interruption. The health center has LED bulbs (2 nos.) which are used mostly in the nighttime. It also has ceiling fans (2 nos. used continuously), a refrigerator of 160W which is used continuously, a centrifuge and an incubator each of about 120W but used intermittently. The peak load of the system is 400W during a typical day. The overall load supplied in the day is 1.00kWh. The load is estimated similarly for simulation purpose also in software study. The system uses a 1kW induction generator-based wind turbine and a 500W-peak PV panel for the generation purpose. The system also uses a lead acid storage battery for supplying during also for storage during lean loads and later retrieval. The battery is rated at 77Ah and 24V.

The operating cost of the system including all components is given as,

$$C_o = C_{wtg}P_{wtg} + C_{pv}P_{pv} + \\ +C_cP_c + C_{batt}P_{batt} + C_{oc}, \quad (1)$$

where P represents power and C represents the cost of individual systems such as wind turbine generator (*wtg*), PV panel (*pv*), converter (*c*) and battery (*batt*). Other constant costs are represented as *oc*.

The Net Present Cost (*NPC*) of the generation system is derived using the cost of power sources in its lifetime and subtracting the discounted costs from them,

$$NPC = C_i + NPC_{om} + NPC_{rc} - (NPC_e + NPC_{svg}), \quad (2)$$

where NPC_{om} is the cost of operation and maintenance and is presumed as 2% of initial cost C_i. NPC_{rc} is the replacement cost given as [9],

$$NPC_{rc} = \sum_{i=1}^{N} C_{rc_k} \frac{(1+g_k)^{iN_k}}{(1+IR)^{iN_k}} \cdot \qquad (3)$$

IV. Simulation and Experimental Results

The proposed system is simulated using *HOMER* (*Hybrid Optimization Model for Electric Renewables*) software [10]. The software based study provides an insight in to the technical and economic analysis for the system. The system is scaled up for the techno-economic study using the software. In the simulation, the system is considered with an electric load of 1.00kWh/day with a peak load of 0.25kW. A storage battery of 48V, 77Ah, is considered with the PV module rated at 500 Watts-peak. The wind turbine is rated at 1kW. The simulated system in *HOMER* is shown below in Fig.5.

The power output of the PV panel installed for the system is shown in Fig.6.

The wind turbine generator output for the month of May is shown in the Fig.7 below. This is quite the average generated power from the system.

The system is simulated for a period of 25 years. It is observed that the cost of the system is around US$3120 for initial installation, however, the system running cost is reduced to around US$1720. The net present cost (*NPC*) of the system is US$3340. The cost of the system is on the higher side but on an average, the system cost decreases as the system simulation time is high.

A comparative analysis for the economic aspect with respect to a similar diesel-PV-based [11] generation system is shown in Fig.8. It is seen that the system cost is decreased as expected initial cost of the system will generally be recovered [12]. Also, the proposed system is 100% renewable. The system is observed to be a reliable source of power for supplying such a critical load and is independent of fossil fuel sources. Thus, the system is much more reliable than a diesel-PV based system which also has some environmental concerns. Similar techno-economic analytic studies [13-15] help in finding

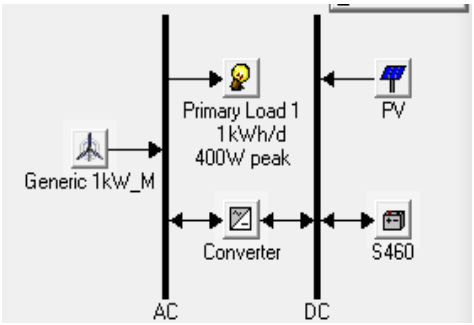

Figure.5. Simulated system.

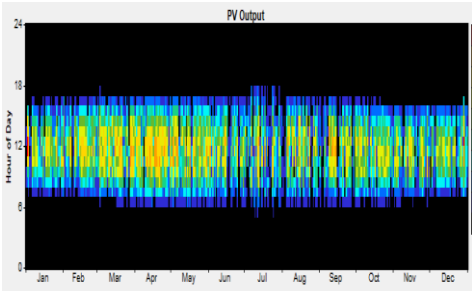

Figure.6. PV panel power output.

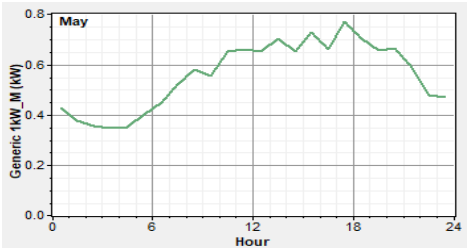

Figure 7. Wind turbine generator power output for month of May.

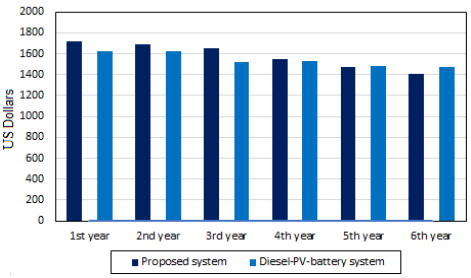

Figure 8. Comparisonal analysis of proposed system with diesel-based system as regards system cost

an optimized solution for hybrid source-based generation systems as regards system cost and viability.

The experimental setup is shown in Fig. 9. The experimental voltage and composite current profile for the system is shown in the Fig. 10(a) with the voltage harmonics profile is shown in Fig. 10(b). It shows that the system generates voltage suitable to meet the connected load demand. The system voltage THD is also within 5% which meets IEEE standards.

V. CONCLUSION

This paper presents a study on a hybrid PV-wind based generation source. It supplies power to an isolated critical load. The proposed study is carried out using HOMER software-based simulation backed up by suitable laboratory experiments. It was found that such a system can be easily setup in a remote onshore area with good viability as regards system cost and operating costs. It can be run with minimal maintenance with 100% renewable fraction. The running cost of the system is minimal than a fossil fuel-based source for similar kind of loads. The system reliability is also increased as regards availability of power throughout the day.

ACKNOWLEDGMENT

The Authors acknowledge the assistance of Electrical Engineering department, Meghnad Saha Institute of Technology for carrying out the research work in current form.

REFERENCES

[1] M. R. Patel, "Wind and solar power systems: Design, analysis and operation," 2nd ed. Boca Raton, USA: CRC Press; 2006.

[2] A. Khaligh, O. Onar, "Energy harvesting: Solar, wind and ocean energy conversion systems", 1st ed. Boca Raton, USA: CRC Press; 2010

[3] M. H. Nehrir, B. J. LaMeres, G. Venkataramanan, V. Gerez, L.A. Alvarado, "An approach to evaluate the general performance of stand-alone wind/photovoltaic generating systems", IEEE Trans Energy Convers, vol. 15, no. 4, 2000, pp.433–439.

[4] T. Hisrose and H. Matsuo, "Standalone hybrid wind-solar power generation system applying dump power control without dump load," IEEE Trans Ind Electron, vol. 59, no. 2, 2012, pp. 988–997.

[5] R. G. Wandhare and V. Agarwal, "Novel integration of a PV-wind energy system with enhanced efficiency," IEEE Trans Power Electron, vol. 30, no.7, 2015, pp. 3638-3649.

[6] A. Chatterjee and D. Chatterjee, "Analysis and control of photovoltaic-assisted three-phase induction machine operating as single-phase micro-wind

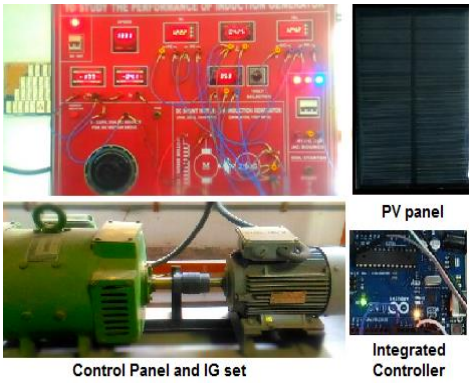

Figure 9. Photograph of experimental setup.

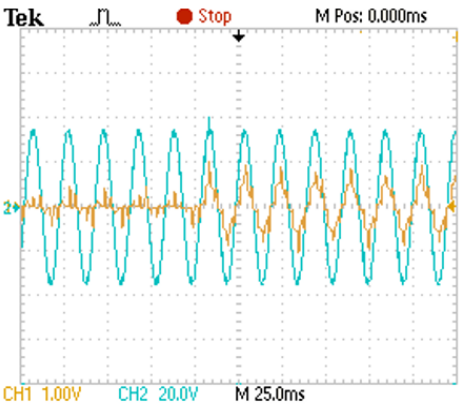

(a)

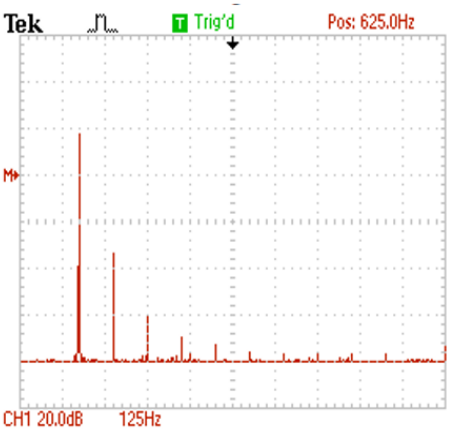

(b)

Figure 10. (a) The experimental voltage and composite current profile for the system (Scale:CH1: 2A/div., CH2: 200V/div.) and (b) voltage harmonics profile (THD = 4.87%).

generator," IET Generation, Transmission & Distribution, vol.10, no.9, 2016, pp.2165-2176.

[7] E. Reznicek and R. J. Braun, "Techno-economic and off-design analysis of stand-alone, distributed-scale reversible solid oxide cell energy storage systems," Energy Convers Manage, vol. 175, 2018, pp. 263-277.

[8] S. M. Shaahid and M. A. El-hadidy, "Economic analysis of hybrid photovoltaic–diesel–battery power systems for residential loads in hot regions—A step to clean future," Renewable and Sustainable Energy Reviews, vol. 12, 2012, pp. 488-503.

[9] R. Dufo-Lopez, J. L. Bernal-Augustin and F. Mendoza, "Design and economical analysis of hybrid PV-wind systems connected to the grid for the intermittent production of hydrogen," Energy Policy, vol. 37, 2009, pp. 3082-3095.

[10] NREL. HOMER User Manual. Golden, CO, USA: National Renewable Energy Laboratory, 2002.

[11] U. Bawah, K. E. Addoweesh and K. M. Eltamaly, "Comparative study of economic viability of rural electrification using renewable energy resources versus diesel generator option in Saudi Arabia," J Renewable Sustainable Energy , vol. 5, 2013, 042701.

[12] A. Chatterjee and D. Chatterjee, "PV-assisted microgeneration scheme with single-phase induction generator suitable for wide speed range application," IET Power Eelctronics, vol.10, no.14, 2017, pp.1859-1869.

[13] M. Mehrpooya, M. Mohammadi and E. Ahmadi, "Techno-economic-environmental study of hybrid power supply system: a case study in Iran," Sustainable Energy Technol Assess, vol. 25, 2018, pp. 1–10.

[14] G. Liu, M. Li, B. Zhou, Y. Chen and S. Liao, "General indicator for techno-economic assessment of renewable energy resources," Energy Convers Manage vol. 156, 2018, pp. 416–426.

[15] A. Chauhan and R. P. Saini, "Techno-economic optimization based approach for energy management of a stand-alone integrated renewable energy system for remote areas of India," Energy, vol. 94, 2016, pp. 138–156.

Computation of the Lightning Energy Spectral Density

Vesna Javor

University of Nis, Faculty of Electronic Eng., Nis, Serbia, vesna.javor@elfak.ni.ac.rs

Abstract — **Spectral analysis of the lightning discharges currents is important for the choice of protective devices and measurement equipment in the cases of fast transients in power systems. This paper gives results of the computation procedure for frequency spectrum of typical lightning discharge currents according to the IEC 62305 standard and of the measured lightning discharge currents.**

Keywords - frequency spectrum analysis, lightning discharge current, very fast transients

I. INTRODUCTION

Lightning discharges induce overvoltages, disturbances and damages in electric power systems. Characteristics of the typical lightning currents are given in IEC 62305 standard [1] and results of the measurements from [2-3] are usually referred to. Various mathematical functions are used [4-7] for the approximation of such currents. One of those is Multi-peaked analytically extended function (MP-AEF), proposed by the author in [8]. This function may better reproduce lightning currents pulse waveshapes using lesser number of parameters than other functions for the same accuracy. Marquardt least-squares method (MLSM) gives better results than Least-squares method if used for the calculation of MP-AEF parameters [9, 10]. Frequency analysis of the approximated lightning channel-base currents for measured and typical IEC 62305 standard waveshapes is given in this paper.

II. APPROXIMATION OF THE LIGHTNING DISCHARGE CURRENTS BY MP-AEF

If we denote function as 1P-AEF (1, 1) for the representation of current waveshapes, with zero value at $t=0$, one current peak I_m at t_m and two parameters of the function a_1 and a_2, as the following

$$i(t)=\begin{cases} I_m\left[(t/t_m)\exp(1-t/t_m)\right]^{a_1}, & 0\le t\le t_m, \\ I_m\left[(t/t_m)\exp(1-t/t_m)\right]^{a_2}, & t_m\le t<\infty, \end{cases} \quad (1)$$

then MP-AEF with N peaks may be defined as NP-AEF (k_1, k_2, …, k_{n+1}) given by

$$i(t)=\begin{cases} I_{m1}\sum_{i=1}^{k_1} b_{1i}\left[\frac{t}{t_{m1}}\exp\left(1-\frac{t}{t_{m1}}\right)\right]^{a_{1i}}, & 0\le t\le t_{m1}, \\ \sum_{j=1}^{n-1} I_{mj}+I_{mn}\sum_{i=1}^{k_n} b_{ni}\left[\frac{t-t_{mn-1}}{t_{mn}-t_{mn-1}}\exp\left(1-\frac{t-t_{mn-1}}{t_{mn}-t_{mn-1}}\right)\right]^{a_{ni}}, & t_{mn-1}\le t\le t_{mn}, \\ & n=2,\ldots,N, \\ \left(\sum_{j=1}^{N} I_{mj}\right)\sum_{i=1}^{k_{N+1}} b_{N+1i}\left[\frac{t}{t_{mN}}\exp\left(1-\frac{t}{t_{mN}}\right)\right]^{a_{N+1i}}, & t_{mN}\le t<\infty. \end{cases} \quad (2)$$

Its parameters are a_{ni} and weighting coefficients b_{ni}, so that for the n-th interval is $\sum_{i=1}^{k_n} b_{ni}=1$, for k_n the selected number of terms in the n-th interval between the peak at t_{mn} and previous peak at t_{mn-1}. Index m refers to the minimum, maximum or any other value at a chosen time moment. I_{mn} is the difference between the n-th and the previous peak.

III. FOURIER TRANSFORM OF LIGHTNING CURRENTS REPRESENTED BY MP-AEF

Using MLSM for parameters estimation of the function 2P-AEF (1, 4, 4), the first positive stroke discharge current is represented by the waveshape normalized to the maximum value I_m =35kA, and it is given in Fig. 1.

Real and imaginary parts of the Fourier transform of this current are given in Fig. 2, and its amplitude in dB versus frequency is given in Fig. 3.

Using also MLSM for parameters estimation of the function 2P-AEF (2, 1, 2), the first

negative stroke discharge current is represented by the waveshape normalized to the maximum value I_m=12kA, and it is given in Fig. 4. Real and imaginary parts of its Fourier transform are given in Fig. 5, and the amplitude in dB versus frequency in Fig. 6. The approximation of the typical subsequent negative stroke discharge current [3] is obtained by the function 2P-AEF (1, 2, 5) using MLSM for its parameters estimation. The obtained waveshape normalized to the maximum value I_m=30kA is given in Fig. 7. FFT results are obtained by program Origin [11] using rectangular window. FFT real and imaginary parts are given in Fig. 8, and the amplitude in dB versus frequency in Fig. 9.

The approximation of the measured negative stroke current [12] is obtained by 13P-AEF (Fig. 10). Its FFT results are given in Figs. 11 and 12.

IV. Energy Density of the Lightning Strokes Represented by MP-AEF

Specific energy of the lightning discharge stroke is defined as energy *W* per unit resistance *R*. According to the Parseval's theorem, this energy can be calculated for aperiodic functions in two ways: one way is to calculate the integral of the square of the current or voltage (in time domain), and the other way is to calculate the integral of the square of the Fourier transform module of current/voltage over all frequencies (in frequency domain). This energy is important in estimation of mechanical and thermal effects of direct lightning strikes. For the positive strokes, the total energy is the greatest due to the highest currents values.

If it is calculated in frequency domain as the square module of the Fourier transform (3), the energy spectral density is given in Fig. 13 for the positive stroke current.

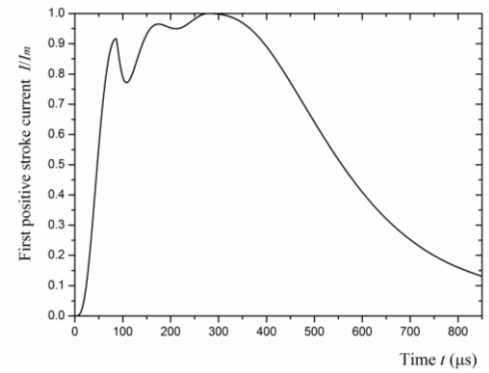

Figure 1. An example of the first positive stroke current normalized to the maximum value and approximated by 2P-AEF (1, 4, 4)

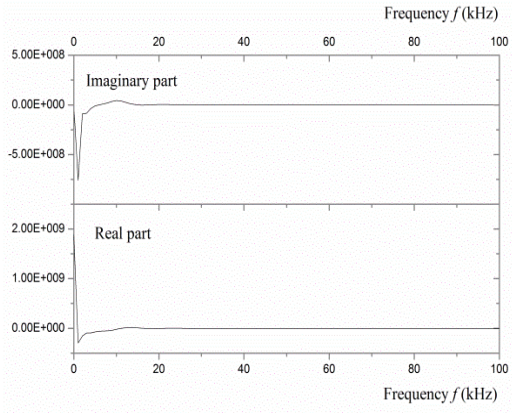

Figure 2. Real and imaginary parts of the Fourier transform of the first positive stroke current.

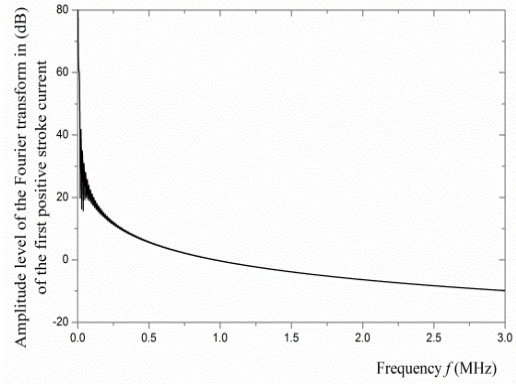

Figure 3. Amplitude level (in dB) of the Fourier transform of the first positive stroke current versus frequency.

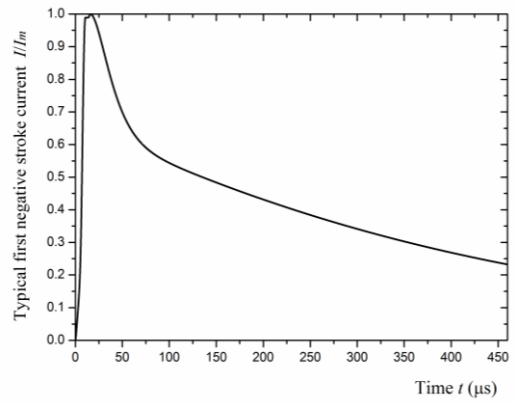

Figure 4. An example of the first negative stroke current normalized to the maximum value and approximated by 2P-AEF (2, 1, 2).

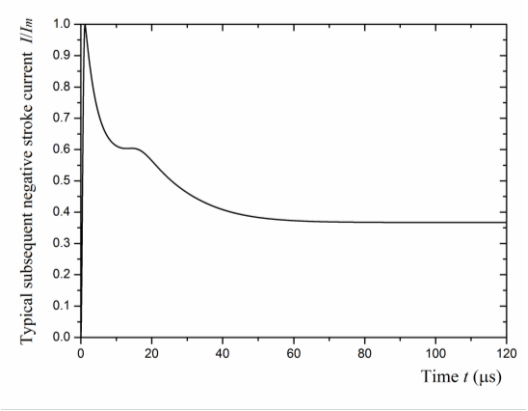

Figure 7. Subsequent negative stroke current normalized to the maximum current, approximated by 2P-AEF (1, 2, 5)

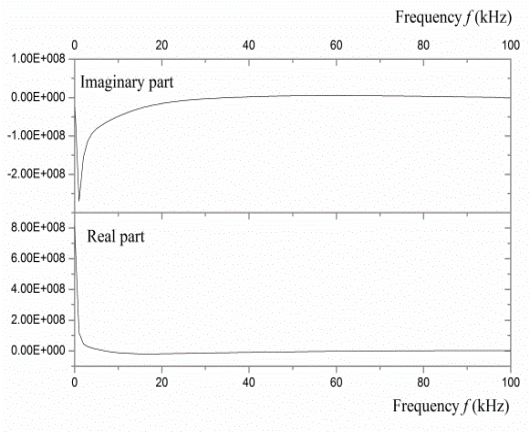

Figure 5. Real and imaginary parts of the Fourier transform of the first negative stroke current.

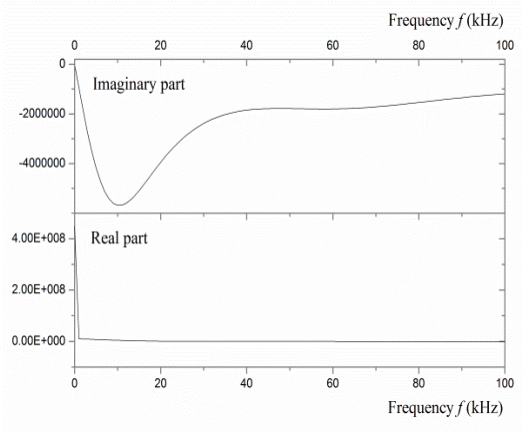

Figure 8. Real and imaginary parts of the Fourier transform of subsequent negative stroke current.

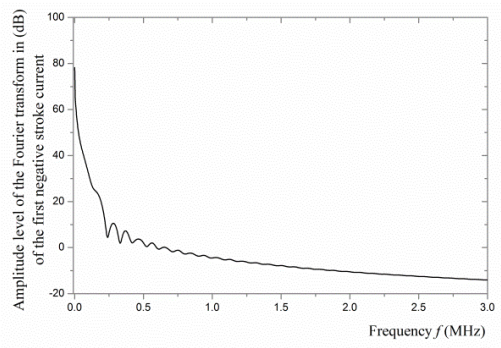

Figure 6. Amplitude level (in dB) of the Fourier transform of the first negative stroke current versus frequency.

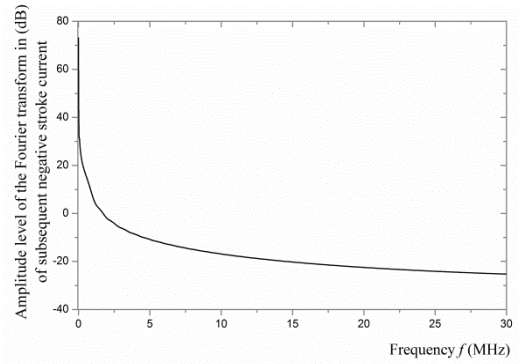

Figure 9. Amplitude level (in dB) of the Fourier transform of subsequent negative stroke current versus frequency.

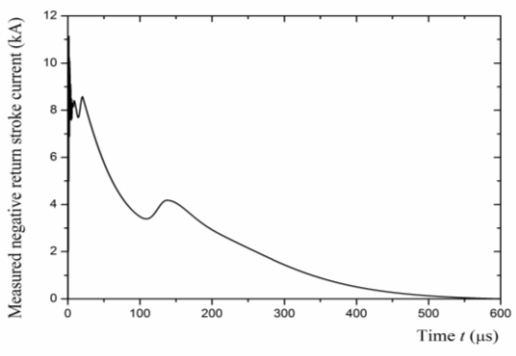

Figure 10. Measured negative return stroke current, approximated by 13P-AEF.

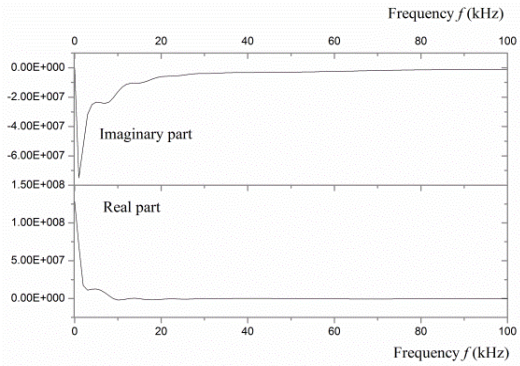

Figure 11. Real and imaginary parts of the Fourier transform of subsequent negative stroke current.

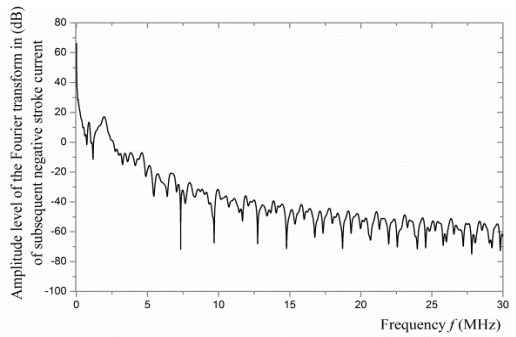

Figure 12. Amplitude level (in dB) of the Fourier transform of the measured negative stroke current versus frequency.

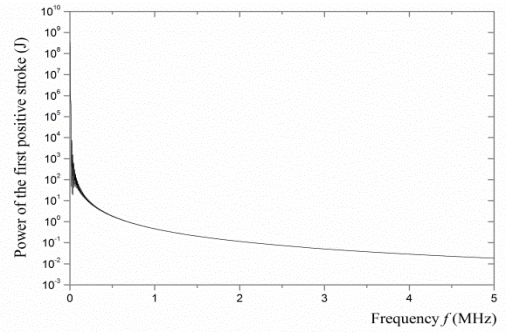

Figure 13. Energy density of the first positive stroke.

Due to simplicity, in this paper is given the Fourier transform of the current approximated just by one-peaked function 1P-AEF (k_1, k_2)

$$I(f) = I_m t_m \sum_{i=1}^{k_1} b_{1i} \frac{\exp(a_{1i})}{(a_{1i} + j2\pi f t_m)^{a_{1i}+1}} \gamma(a_{1i}+1, a_{1i} + j2\pi f t_m) + \\ + I_m t_m \sum_{i=1}^{k_2} b_{2i} \frac{\exp(a_{2i})}{(a_{2i} + j2\pi f t_m)^{a_{2i}+1}} \Gamma(a_{2i}+1, a_{2i} + j2\pi f t_m) \quad ,(3)$$

for Gamma function $\gamma(a+1,x) = \int_x^\infty t^a e^{-t} dt$ and

$$\Gamma(a+1,x) = \int_x^\infty t^a e^{-t} dt \quad . \qquad (4)$$

V. CONCLUSION

For the lightning negative stroke currents, rising times are shorter than for positive, so that frequencies of interest are higher for negative discharges. In cases of negative strokes, rising times are shorter for subsequent than for the first strokes, due to existence of previously defined discharge path in the atmosphere. Thus, frequencies important for the analysis of these signals are up to tens of MHz for subsequent strokes, whereas up to a few MHz for the first strokes. In that range the attenuation of currents is about 100 dB. Frequency domain analysis is important for the choice of measurement equipment and also for the choice of protective devices in power systems.

REFERENCES

[1] IEC 62305-1 standard, Protection against lightning - Part 1: General principles, Ed. 2.0, 2010-2012.

[2] K. Berger, R. B. Anderson, and H. Kroninger, "Parameters of lightning flashes," Electra, no. 41, 1975, pp. 23–37.

[3] Y. T. Lin, M. A. Uman, J. A. Tiller, R. D. Brantley, W. H. Beasley, E. P. Krider, and C. D. Weidman, "Characterization of lightning return stroke electric and magnetic fields from simultaneous two-station measurements," J. of Geophys. Research, vol. 84, 1979, pp. 6307-6314.

[4] C. E. R. Bruce and R. H. Golde, "The lightning discharge", J. Inst. Electr. Eng., vol. 88, 1941, pp. 487-520.

[5] V. A. Rakov and A. A. Dulzon, "Calculated electromagnetic fields of lightning return strokes (in Russian)," Tekh. Electrodinam. no.1, 1987, pp. 87-89.

[6] F. Heidler, "Travelling current source model for LEMP calculation," Proc. 6th Int. Zurich Symp. EMC, Zurich, Switzerland, March 1985, pp. 157-162.

[7] Z. Feizhou and L. Shange, "A new function to represent the lightning return-stroke currents," IEEE Trans. Electromagn. Compat., vol. 44, no. 4, 2002, pp. 595-597.

[8] V. Javor, "New functions for representing IEC 62305 standard lightning currents," USB Proc. of Papers, 30th Int. Conf. on Lightning Protection ICLP 2010, Sep. 2010, Cagliari, Italy.

[9] V. Javor, K. Lundengård, M. Rančić, and S. Silvestrov, "Analytical representation of measured lightning currents and its application to electromagnetic field estimation," IEEE Trans. on Electromagn. Compat., vol. 60, no. 5, October 2018, pp. 1415-1426..

[10] K. Lundengård., M. Rančić, V. Javor, and S. Silvestrov, "Estimation of Parameters for the Multi-peaked AEF Current Functions," Methodology and Computing in Applied Probability, vol. 19, no. 4, June 2016, pp. 1107-1121.

[11] Original lab. Available at: https://www.originlab.com

[12] F. Delfino, R. Procopio, M. Rossi, and F. Rachidi, "Prony series representation for the lightning channel-base current," IEEE Trans. Electromagn. Compat., vol. 54, no. 2, 2012, pp. 308-315.

Low Cost Electronic Calorimeter

Elson Avallone[1], Paulo César Mioralli[1], Pablo Sampaio Gomes Natividade[1], Paulo Henrique Palota[1], José Ferreira da Costa[1], Jonas Rafael Antonio[1], Thomas August Colombo[2], Sílvio Aparecido Verdério Junior[1]

[1]Federal Instituteof Education, Scienceand Technology of Sao Paulo, Catanduva-SP, Brazil, elson.avallone@ifsp.edu.br; mioralli@ifsp.edu.br; pablo.sgn@ifsp.edu.br; palota@ifsp.edu.br; joseferreira@ifsp.edu.br; jonas.antonio@ifsp.edu.br; silvioverderio@ifsp.edu.br

[2]Engineering Student-Federal Instituteof Education, Scienceand Technology of Sao Paulo, Catanduva-SP, Brazil, thomasaugust35@gmail.com

Abstract — **Calorimeters are thermally insulated devices that measure the heat exchanged between two bodies of different temperatures. The present work proposes to construct an electronic calorimeter with an average cost of US $ 60.00 using two ATMega328P microcontrollers and DS18B20 temperature sensors in order to measure the liquid specific heat. The mass of the liquid to be measured is typed on a matrix keyboard, thus eliminating post-measurement weighing for greater accuracy. The thermal capacity of the calorimeter was obtained from the use of a known liquid of known specific heat (water). Using the calorimeter allows specific heat values to be obtained from other liquids or mixtures. Application in the disciplines of heat and mass transfer, thermodynamics and electronics fosters the scientific knowledge of engineering, physics and chemistry students.**

Keywords - electronic calorimeter, ATMega328P, arduino.

I. INTRODUCTION

Calorimetry is a branch of physics that studies the problems involving heat exchange in different temperature systems. Calorimetry was already used by both Galileo Galilei and Isaac Newton, as well as current researchers. The calorimeter is a thermally insulated device that measures heat exchanged between two bodies of different temperatures [1-3] and is a simple and inexpensive way to determine specific heat [4]. The authors [5] define the calorimeter as a device to measure the heat produced in a time interval, where the equipment reservoir has the known thermal capacity.

In the research developed by [6], the calorimetric technique using a calorimeter for liquids in a mixer reservoir is presented. The authors [7] used a calorimeter to determine the thermal capacity of flammable liquids such as ethanol and benzene at low temperatures (298.15 K) and the results showed that there was a small difference in specific heat, not representing good accuracy of the equipment compared to literature.

The authors [8] present a didactic calorimeter built with a stainless steel thermos flask fitted with a glass thermometer and an electrical resistance. The thermal capacity of the device is 126 J/K and 2% accuracy.

In their work [9], the authors constructed an agriculturally applied calorimeter to measure the specific heat of various soil types using an Arduino UNO microcontroller.

The researchers [10] used Matlab software to model heat transfer on a calorimeter.

In the research of [11], a cone-shaped calorimeter was studied to identify the ignition point of wood products.

The authors [12] measure the specific heat of citrus juices and their derivatives using a thermos flask calorimeter.

In their work [13-14], the authors built a didactic calorimeter using the Arduino platform but did not present the electronic circuit, the graphs of the results obtained and the time between the measurements. There is also no

ISBN: 978-86-80616-04-9

information that the electronic system is capable of storing the data.

Calorimeters for normal applications are median instruments in the range of $ 100.00, but devices that use electronic systems for automatic control and measurement achieve significant values.

The main objective of this work is to construct an electronically controlled calorimeter using two ATMega328P [15] microcontroller to measure the specific heat of liquids and store the reading data on an SD card. The assembly and adjustment of the mechanical components, integration of the sensors to the assembly and the microcontrollers, programming in C ++ language, analysis of the experimental data and calculation of the experimental specific heat of the water and thermal capacity of the calorimeter, are the specific objectives of the project.

The work is justified because, besides being an accurate and reliable device, its construction promotes the learning of electronics, instrumentation, thermology and heat transfer for students of engineering courses.

II. MATERIALS AND METHODS

The reservoir is constructed with two aluminum pan of diameters 220 mm and 160 mm. To keep the smaller pan with the same spacing on the walls, a wooden spacer is installed at the bottom of the larger pan as shown in Fig. 1.

Figure 1. Spacing between pans.

The 30 mm annular space (Fig. 2.) is filled with expanded polyurethane, with thermal conductivity $k = 0.007W / m \cdot K$ and specific mass $\rho = 55kg / m^3$.

Figure 2. Annular space filled with expanded polyurethane.

A thin layer of polyester resin is applied to the surface of the annular space to protect the polyurethane (Fig 3.) when the calorimeter is in operation.

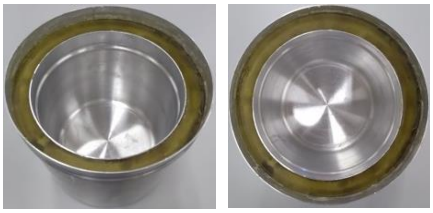

Figure 3. Polyester resin applied to the surface of expanded polyurethane.

The calorimeter lid is internally lined with 50 mm thick Styrofoam and it has a 1.47 W stirring rod motor, a DS18B20 temperature sensor thermowell and a 808.3 W electric heater according to Fig. 4.

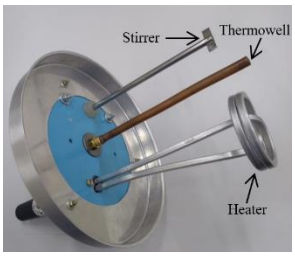

Figure 4. Instruments installed on the calorimeter lid.

The internal surface temperatures of the calorimeter are also measured with Dallas DS18B20 sensors, as well as the external surface and ambient, according to Fig. 5.

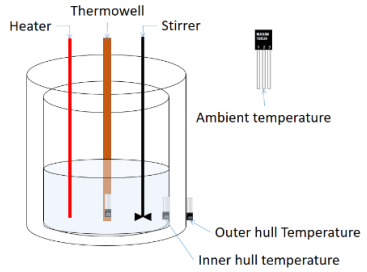

Figure 5. Sensors installed in the thermowell, stirrer, inner hull, outer hull, and ambient.installed on the calorimeter lid.

The electronic circuit consists of two ATMega328P. The first microcontroller acts as a master, connecting a matrix keyboard, where is typed the mass of liquid that will be inserted into the reservoir. The second ATMega328P works in slave mode. Upon receiving the mass information and pressing the "on" button, the program starts the motor and starts reading the internal temperature by the DS18B20 sensor and displayed on the LCD display. When there are no more variations in the internal temperature, the "start" button is pressed by the operator. At this time, the 808.3 W electric heater is turned on and the last mix temperature is locked on the left side of the LCD display. On the right side, the increasing temperature variation is shown by the same DS18B20 sensor installed in the thermowell. The chronometer is displayed on the upper left side of the LCD de 16x2 [15].

When the operator presses the "stop" button, the electrical resistance is turned off. At this moment, the cooling process begins. The stirrer is driven by only a few revolutions at 1-minute intervals so that there is no increased shaft work in the mix. The temperatures of the liquid, the inner and outer wall of the calorimeter hull and the ambient temperature are recorded on an SD card [16] throughout the cooling process. When the internal temperature of the liquid equals the external temperature of the hull, the equipment automatically shuts off and the data is analyzed in an electronic spreadsheet. If the operator needs to restart the readings, the reset button can be pressed.

The master electronic circuit is presented in Fig. 6 and 7.

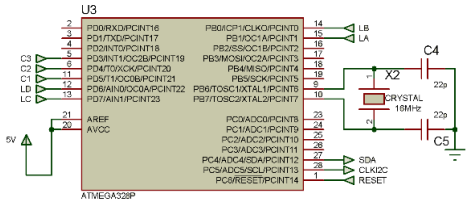

Figure 6. Sensors Master Electronic circuit.

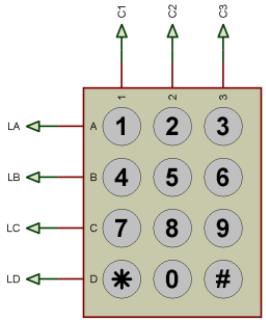

Figure 7. Master Electronic circuit.

The slave circuit consists of Fig. 8-14.

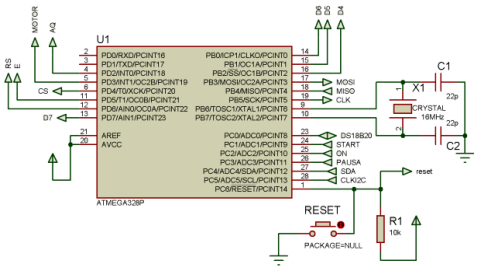

Figure 8. Slave electronic circuit.

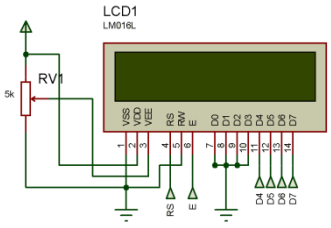

Figure 9. LCD - Slave electronic circuit.

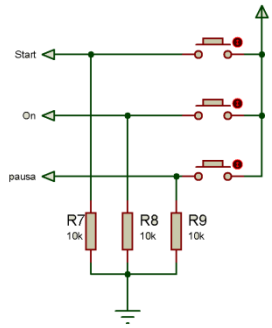

Figure 10. Buttons - Slave electronic circuit.

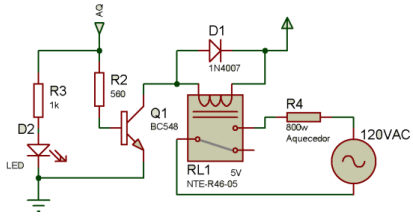

Figure 11. Heater - Slave electronic circuit.

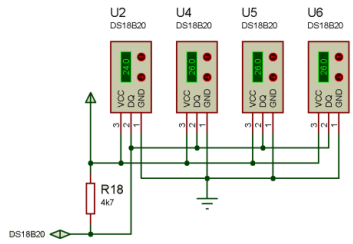

Figure 12. 4 DS18B20 - Slave electronic circuit.

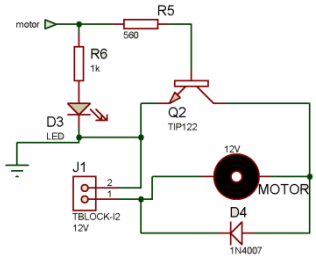

Figure 13. Motor - Slave electronic circuit.

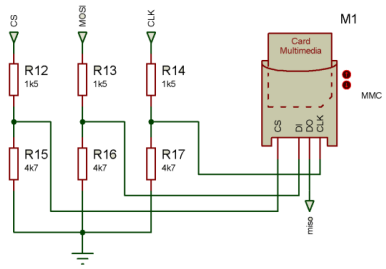

Figure 14. SD Card - Slave electronic circuit.

The First Law of Thermodynamics postulates that energy in the initial state (E_1) by adding or subtracting any portion of energy from the system is equal to the energy in the final state (E_2). This principle can be used in a calorimeter.

The summary of the First Law of Thermodynamics (1) is used in the calorimeter to calculate the specific heat of a substance.

$$Q = C_{assembly} \cdot (T_{final} - T_{initial}) . \qquad (1)$$

The thermal capacity of the calorimeter and water assembly $(C_{assembly})$ is measured by the angular coefficient of the mean accumulated heat line as a function of the variation of T_{final} temperatures and the $T_{initial}$ water temperature.

The thermal capacity of the calorimeter is calculated by the difference between the thermal capacities of the assembly and the water, according to (2).

$$C_{calorimeter} = C_{Assembly} - C_{water} . \qquad (2)$$

The thermal capacity of water (C_{water}) is calculated using (3).

$$C_{water} = m_{water} \cdot cp_{water} , \qquad (3)$$

where cp_{water} was obtained from the average temperature of $43.03^{o}C$ of the heating process of the experiment and m_water is the mass of water inserted in the calorimeter.

III. Results and Discussions

The liquid chosen for the calorimeter thermal analysis is water because it has known physical properties. After temperature homogenization, the “start” button is pressed, initiating the healing process, verifying that the external and ambient hull temperatures are similar. Temperature profiles as a function of time in seconds are shown in Fig. 15.

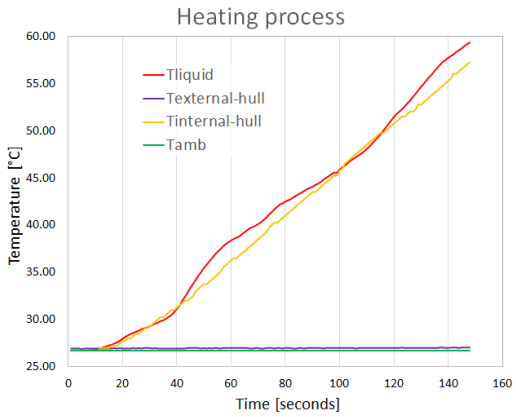

Figure 15. Temperature profiles of the heating process.

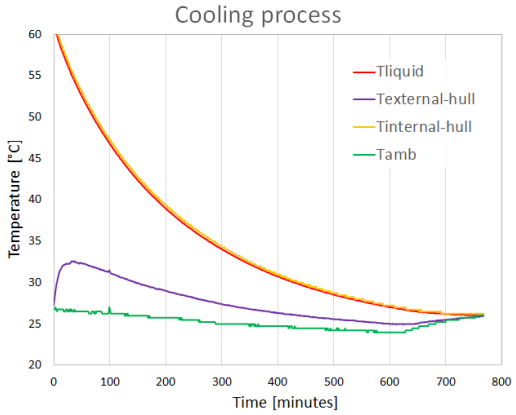

Figure 16. Temperature profiles of the cooling process.

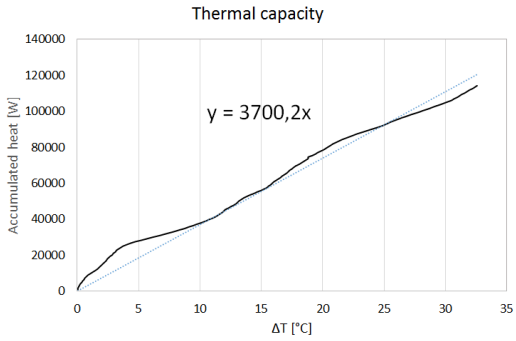

Figure 17. Accumulated heat curve x ΔT and thermal capacity.

The temperature profiles of the cooling process as a function of time in minutes are shown in Fig. 16.

The thermal capacity of the calorimeter is measured using the angular coefficient of the mean straight line of the accumulated heat during the heating process, and sum of the stirrer motor power, as a function of the temperature variation $T_{final} - T_{initial}$, where T_{final} is transient and $T_{initial}$, measured at the beginning of the experiment, presented in Fig. 17.

Equation $y = 3700.2 \cdot x$, taken from Fig. 17., presents the value $3700.2 J/^{o}C$ representing the thermal capacity of the assembly (water + calorimeter).

To calculate the thermal capacity of the assembly the distilled water masses, stirrer rod, thermometric well, heater and reservoir were considered with the respective values of 0.671322 kg, 0.046000 kg, 0.044000 kg, 0.046000 kg and 0.077000 kg.

The thermal capacity of the calorimeter was calculated using Equation 2 with a result of 894.59 $J/°C$. With this known value, from new experiments, it is possible to obtain the specific heat of other liquids.

IV. CONCLUSION

The built calorimeter has an average cost of US$ 60.00. The electronics using two ATMega328P microcontrollers in conjunction with the matrix keyboard and DS18B20 digital sensors not only make mounting easier but also give precision to the equipment. From a simple procedure, it is possible to estimate the specific heat of liquids or mixtures. Application in the disciplines of heat transfer, thermodynamics and electronics fosters the scientific knowledge of engineering, physics and chemistry students.

ACKNOWLEDGMENT

To the Federal Institute of Education, Science and Technology of Sao Paulo, Catanduva-SP, Brazil for the support and incentive.

REFERENCES

[1] F. Ramalho Jr, G. F. Nicolau, e P. A. Toledo Soares, Física II, 9º ed, vol. 2, 3 Brasil: Moderna, 2007.

[2] R. Resnick e D. Halliday, Física: Mecânica - Acústica - Calor, 2º ed, vol. 1, 2 vols. Rio de Janeiro: Ao Livro Técnico S/A, 1969.

[3] G. Cibinetto, "Calorimetry", Istituto Nazionale di Fisica Nucleare, Italia, Lecture 4, 2011.

[4] M. P. Hoffmann e B. C. S. Grandi, "Laboratório caseiro: Um calorímetro alternativo", Caderno Brasileiro de Ensino de Física, vol. 5, no. 1, 1988, pp. 47–49.

[5] H. Gupta e S. Roy, "Chapter 6 - ASSESSMENT AND EXPLOITATION", in Geothermal Energy, H. Gupta e S. Roy, Orgs. Amsterdam: Elsevier, 2007, pp. 121–164.

[6] J. Jeener, "Low Temperature Mixing Calorimeter for Liquids", Review of Scientific Instruments, vol. 28, no. 4, 1957, pp. 263–265.

[7] J.-L. Fortier, G. C. Benson, e P. Picker, "Heat capacities of some organic liquids determined with the Picker flow calorimeter", The Journal of Chemical Thermodynamics, vol. 8, no. 3, 1976, pp. 289–299.

[8] J. H. Vuolo e C. H. Furokawa, "Calorímetro didático (Didactic calorimeter)", Revista Brasileira de Ensino de Física, vol. 17, no. 2, 1995, pp. 140–151.

[9] R. O. Moreno, R. A. Armindo, e R. L. Moreno, "Development of a low-cost automated calorimeter for determining soil specific heat", Computers and Electronics in Agriculture, vol. 162, 2019, pp. 348–356.

[10] J. Lerchner, G. Wolf, C. Auguet, e V. Torra, "A simple tool for the modeling of heat flow calorimeters", Thermochimica Acta, vol. 415, no. 1–2, 2004, pp. 9–13.

[11] G. Marryweather e M. J. Spearpint, "Flame spread measurements on wood products using the ASTM E 1321 LIFT apparatus and a reduced scale adaptation of the cone calorimeter", Fire Materials an International Journal, vol. 34, no. 3, 2009, pp. 109–136.

[12] S. C. S. R. Mura, V. C. L. Franca, e Á. M. C. B. Leal, *Propriedades termofísicas de soluções-modelo similares a sucos: parte II*. Available at: http://www.scielo.br/scielo.php?script=sci_abstract&pid=S0101-20612005000300011&lng=pt&nrm=iso. [Acessado: 08-maio-2018].

[13] J. P. de Oliveia, S. Pereira, e T. I. M. de Souza, "Uso da plataforma Arduino no desenvolvimento de calorímetro didático", apresentado em CONTECO - Congresso Técnico Científico da Engenharia e da Agronomia, Foz do Iguaçu - PR - Brazil, 2016.

[14] J. P. de Olivera, S. Pereira, e T. I. M. de Souza, "Uso da plataforma Arduino no desenvolvimento de calorímetro didático", Revista Técnico-Científica, vol. 0, no. 0, 2016.

[15] Vishay, "LCD Module". Vishay, 01-out-2002.

[16] H. Bench, *Arduino LC Studio SD Card Tutorial, Arduino Low Cost SD Card, 11-fev-2016*. Available at: http://henrysbench.capnfatz.com/henrys-bench/arduino-output-devices/arduino-lc-studio-sd-card-tutorial/. [Acessado: 01-dez-2018].

CFD Simulations of Fireworks Blast Activity During Music Festival in Serbia, Model Development and Assessment

Rastko Jovanović[1], Ivan Lazović[2], Marija Živković[1], Miloš Davidović[3], Nataša Sarap[3], Renata Kovačević[4], Milena Jovašević Stojanović[3]

[1]Vinca Institute of nuclear sciences, Laboratory for Thermal Engineering and Energy, Belgrade, Serbia, virrast@vinca.rs; marijaz@vinca.rs
[2]Vinca Institute of nuclear sciences, Department of Engines, Vehicles and related Technologies, Belgrade, Serbia, lazovic@vinca.rs
[3]Vinca Institute of nuclear sciences, Department of Radiation and Environmental Protection, Belgrade, Serbia, davidovic@vinca.rs; natasas@vinca.rs; mjovst@vinca.rs
[4]Mining and Metallurgy Institute, Bor, Serbia, renata.kovacevic@irmbor.co.rs

Abstract — **Increasing occurrence of firework events represents a major contributor to air pollution caused by particulate matter, released as a result of an intensive fragmentation after firework explosion. The main aim of this paper is to suggest a novel model able to simulate fireworks' particulates spatial and temporal evolution. The main model feature is its ability to simulate both fireworks' particulates and air behavior in a single framework. The obtained results showed that, although significant part of particulate matter is concentrated on the ground area surrounding firework's event site, the majority of fine particles, with aerodynamic diameter of 10 μm and lesser, is taken by the wind flow, into upper levels of atmospheric boundary layer.**

Keywords – fireworks, numerical modeling, particulate matter

I. INTRODUCTION

Fireworks are becoming increasingly important air pollution source due to their frequent use during different celebration events: festivals, national holidays, sports matches, and other public events. Pollutants, resulting from fireworks explosion, are found both in gaseous phase and in Particulate Matter (PM)[1]. Fireworks blasts produce large quantities of PM consisting mainly of metal elements. Metal elements suspended in PM, with the highest detected concentrations after fireworks activities are aluminum (Al), zinc (Zn), lead (Pb), cadmium (Cd), copper (Cu), iron (Fe), manganese (Mn), cobalt (Co), and vanadium (V)[2, 3]. PM fragments consist largely of fine particles with aerodynamic diameter smaller of 2.5 μm (PM2.5) and with aerodynamic diameter in range between 2.5 and 10 μm (PM10)[4, 5]. These fine particles show flow patterns similar to the gaseous phase and can be inhaled during spectators' exposure [6]. Once inhaled, PM penetrates respiratory and cardiovascular system. Known consequent negative health effects, according to the World Health Organization (WHO), include: asthma, bronchitis, respiratory irritations and infections, and chronic obstructive pulmonary disease [7].

It is hard to fully access the impact of fireworks activities on air pollution and human health using traditional experimental technics. A large number of sampling sites and, often expensive, measurement equipment is necessary to determine fireworks blast front and PM concentration temporal and spatial distributions. Moreover, sampling campaign is time-consuming and requires highly trained professional staff in the field [8, 9]. Because of this, numerical simulations emerge as cost and

ISBN: 978-86-80616-04-9

time effective tool for fireworks activity modeling.

Most of the existing models rely on a hybrid approach for tracking massless Lagrangian parcels on Eulerian fixed three-dimensional grids. Although this approach proved useful for calculation of fireworks PM forward and backward trajectories it has significant shortcomings. First, it is an effective tool only for modeling of particle trajectories in upper levels of Atmospheric Boundary Layer (ABL). Second, it does not take into account important particle features (mass, density). Moreover, it can be used only on pre-existing Eulerian grids and, most importantly, it does not take into account particle-air interactions [10].

Van der Kamp and coauthors calculated trajectories from an elevated fireworks source at 300 m using 40 km resolution (EDAS) data to drive the simulations. It was concluded that it is difficult to verify the accuracy of modeled plume trajectories at plume height, other than to conclude that they are broadly consistent with the appearance of the plume at the ceilometer location and visual observations, but likely contain some error [11].

Feng and coauthors calculated back trajectories using HYSPLIT [10] model, where the initial height of 500 m above ground level was used. The obtained results indicated directions at which serious air pollution occurred after firework event [12].

Miller and co-authors calculated the 48 h backward trajectories terminating at the study site at a height of 500 m every hour. Possible source areas of particles were identified, based on the simulation results, pointing out firework influence on Pb species concentration in the air [13].

Zohdi developed a mathematical model to qualitatively simulate the progressive time-evolution of a blast from a simple firework. The model computes the trajectory of the material under the influence of the drag, gravity, and buoyancy forces. However, the suggested model does not take into account dynamics of the surrounding air. The necessity for further model development with implementation of fully coupled (two-way) particle–fluid interaction models was underlined[14].

The main aim of this study is the development and evaluation of novel numerical model for simulation of fireworks activity. The suggested model uses hybrid approach. Fireworks PM is calculated in Lagrangian frame, tracking large number of computational particles termed parcels. Surrounding medium – air is represented using Eulerian approach on arbitrary three-dimensional finite volume grid. The main equations for air flow are solved numerically, using Computational Fluid Dynamics (CFD) user-developed code.

The main novelty of the proposed model is that it can calculate parcel trajectories not only on pre-existing Eulerian grids but rather on user-generated computational grids with user-defined fineness. This allows to define and solve desired air wind flow and to take into account interactions between the wind flow and parcel trajectories. These interactions are modeled in a two-way manner, meaning that both particles – air and air –particles influences are simulated. Particle size, density, mass, and velocity are built in the model as user-specified variables, which can be easily altered.

The main hypothesis of this work is that the wind flow has a strong influence on the fine firework PM trajectories consisting of particles with aerodynamic diameter up to 10 μm. Thus, the fluid flow rate has to be simulated in order to quantitatively access firework blast front development and firework PM concentration distribution.

The subject of this work is three-dimensional CFD modeling of PM spread after firework event during a music festival in Belgrade, Serbia.

II. NUMERICAL MODEL

A. Governing equations for fluid flow

The three-dimensional, unsteady, turbulent flow field is described by the set of partial differential equations for mass, momentum, and turbulent quantitates (turbulent kinetic energy k, and its dissipation ε) conversion. Conversion equations in Reynolds Averaged Navier-Stokes (RANS) averaged form are given in the text below.

Mass conversion equation has the following form:

$$\frac{\partial \rho}{\partial x_i} + \frac{\partial}{\partial x_i}(\rho u_i) = S_m \ , \qquad (1)$$

where ρ is fluid (air) density, x_i is Cartesian coordinate in direction i, u_i is fluid flow velocity component in direction i, and S_m is source term due to mass exchange with particulate (PM) phase.

Momentum conversion equation is given by the following expression:

$$\frac{\partial(\rho u_i)}{\partial x_j}+\frac{\partial}{\partial x_j}(\rho u_i u_j)=-\frac{\partial_p}{\partial x_i}+\frac{\partial}{\partial x_j}\left[\mu\left(\frac{\partial u_i}{\partial x_j}+\frac{\partial u_j}{\partial x_i}-\frac{2}{3}\delta_{ij}\frac{\partial u_i}{\partial x_i}\right)\right]+\frac{\partial}{\partial x_j}\left(\overline{-u_i' u_j'}\right)+\rho g_i+\rho F_i \quad (2)$$

where ρ is fluid (air) density, x_i is Cartesian coordinate in direction i, u_i is fluid flow velocity component in direction i, x_j is Cartesian coordinate in direction j, u_j is fluid flow velocity component in direction j, p is the static pressure, μ is fluid (air) dynamic viscosity, ρgi is source term, which describes influence of gravity force, and ρFi is source term which describes momentum exchange with particulate (PM) phase.

Term $\overline{-u_i' u_j'}$ is the result of RANS averaging procedure and represents influence of turbulence on main flow field. This term is known as Reynolds stress tensor and can be expressed using the Boussinesq hypothesis, which relates Reynolds stress tensor and fluid deformation (velocity gradient) using the following relation [15]:

$$\overline{-\rho u_i' u_j'}=\mu_t\left(\frac{\partial u_i}{\partial x_j}+\frac{\partial u_j}{\partial x_i}\right)-\frac{2}{3}\left(\rho k+\mu_t\frac{\partial u_k}{\partial x_k}\right)\delta_{ij} \quad . \quad (3)$$

Unknown quantities in equation (3) are solved using an appropriate turbulence model.

B. Turbulence modeling

Realizable k-ε two-equation turbulence model is used for turbulence modeling in this work[16].The equation for turbulent kinetic energy has the following form:

$$\frac{\partial}{\partial_t}(\rho k)+\frac{\partial}{\partial x_i}(\rho k u_i)=\frac{\partial}{\partial x_j}\left[\left(\mu+\frac{\mu_t}{\sigma_k}\right)\frac{\partial k}{\partial x_j}\right]+ +G_k+G_b-\rho\varepsilon-Y_M+S_k \quad . \quad (4)$$

The equation for turbulent dissipation is given by the following expression:

$$\frac{\partial}{\partial_t}(\rho\varepsilon)+\frac{\partial}{\partial x_i}(\rho\varepsilon u_i)=\frac{\partial}{\partial x_j}\left[\left(\mu+\frac{\mu_t}{\sigma_\varepsilon}\right)\frac{\partial\varepsilon}{\partial x_j}\right]+ +\rho C_1 S_\varepsilon-\rho C_2\frac{\varepsilon^2}{k+\sqrt{v\varepsilon}}+C_{1\varepsilon}\frac{\varepsilon}{k}C_{3\varepsilon}G_b+S_\varepsilon \quad , \quad (5)$$

where k is turbulent kinetic energy and ε is turbulent dissipation. In equations (4) and (5), C_1 is determined using the following relations:

$$C_1=\max\left[0.43,\frac{\eta}{\eta+5}\right] \quad , \quad (6)$$

$$\eta=S\frac{k}{\varepsilon} \quad . \quad (7)$$

Unknown term μ_t – turbulent viscosity, necessary to close system of equations (1) – (3) is given by:

$$\mu_t=\rho C_\mu\frac{k^2}{\varepsilon} \quad . \quad (8)$$

In the equations (4) and (5), G_k represents the generation of turbulence kinetic energy due to the mean velocity gradients, G_b is the generation of turbulence kinetic energy due to buoyancy, Y_M represents the contribution of the fluctuating dilatation in compressible turbulence to the overall dissipation rate, and S_k and S_ε are source terms. Model constants are: $C_{1\varepsilon}$ = 1.44, C_2 = 1.9, σ_k = 1.0, and σ_ε = 1.2.

C. Particulate phase governing equations

PM trajectories are calculated by integrating the force balance acting on the computational particle (parcel), which is written in a Lagrangian reference frame[17, 18]. The force balance equates the particle inertia with the forces acting on the particle: drag force, gravity force, and buoyancy force:

$$\frac{d\vec{u}_p}{dt}=F_D(\vec{u}-\vec{u}_p)+\frac{\vec{g}(\rho_P-\rho)}{\rho_P} \quad , \quad (9)$$

where u_P is particle velocity vector, g is gravity acceleration vector, ρ_P is parcel density, and F_D is drag force. Drag force per unit mass is calculated using the following expression:

$$F_D = \frac{18\mu}{\rho_p d_p^2}\frac{C_D \mathrm{Re}}{24} \ , \qquad (10)$$

where d_P is particle diameter and Re is relative Reynolds number, calculated as:

$$\mathrm{Re} = \frac{\rho d_p \left|\vec{u} - \vec{u_p}\right|}{\mu} \ . \qquad (11)$$

Quantity C_D in equation (10) is the drag coefficient given by the following expression, with the assumption that all PM firework fragments have spherical shape:

$$C_D = a_1 + \frac{a_2}{\mathrm{Re}} + \frac{a_3}{\mathrm{Re}^2} \ . \qquad (12)$$

Coefficients necessary for drag coefficient calculation are given in Table 1.

TABLE I. COEFFICIENTS FOR DRAG COEFFICIENT CALCULATION

a_1	a_2	a_3	Re
0	24	0	$Re < 0.1$
3.69	22.73	0.0903	$0.1 < Re < 1$
1.222	29.1667	-3.8889	$1 < Re < 10$
0.6167	46.5	-116.67	$10 < Re < 10^2$
0.3644	98.33	-2778	$10^2 < Re < 10^3$
0.357	148.62	$-4.75 \cdot 10^4$	$10^3 < Re < 5 \cdot 10^3$
0.46	-490.546	$57.87 \cdot 10^4$	$5 \cdot 10^3 < Re < 10^4$
0.5191	-1662.5	$5.4167 \cdot 10^6$	$10^4 < Re < 5 \cdot 10^4$

D. Particulate phase turbulent dispersion

PM turbulent dispersion takes into account the effects of the particle velocity fluctuations caused by the flow field velocity fluctuations. Assuming that these particle velocity fluctuations are random, the following expression is obtained:

$$u_p' = \zeta \sqrt{\overline{u'^2}} \ , \qquad (13)$$

where u_P' is particle velocity fluctuation, ς is randomly sampled number from Gaussian distribution, and u' is fluid (air) velocity fluctuation[19]. Fluid velocity fluctuation is obtained using the Boussinesq assumption [15]:

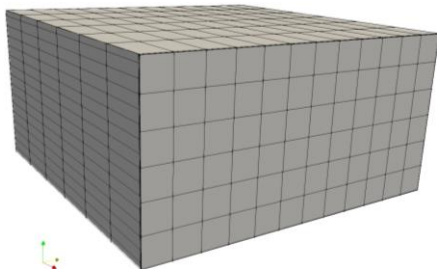

Figure 1. Computational domain.

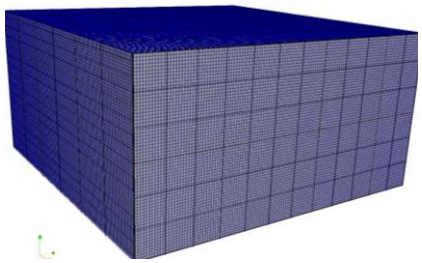

Figure 2. Computational grid.

$$\sqrt{\overline{u'^2}} = \sqrt{\frac{2k}{3}} \ . \qquad (14)$$

III. COMPUTATIONAL GRID AND GRID INDEPENDENCE STUDY

The main dimensions of the computational domain are 600 m in the x-direction, 600 m in the y-direction, and 300 m in the z-direction, as shown in Fig. 1. The domain dimensions are chosen to represent area at which spectators are located. The computational domain is divided in the finite number of control volumes giving computational grid consisting of totally 1576080 computational cells. A computational grid is locally refined in the region of firework explosion in order to ensure solution numerical stability. The generated grid consists of all hexagonal elements in order to lower numerical diffusivity and to increase solution stability, Fig. 2.

Grid independence study is conducted first lowering the number of computational cells for 50% and then refining original grid for 50%. As solution did not change more than 3% with increase in computational cell number, original computational grid was adopted for further simulations.

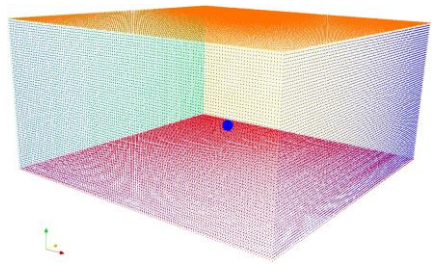

Figure 3. Boundary surfaces: green – inlet, light blue – side outlets, red – bottom wall (ground), orange – upper level of ABL, and dark blue – firework explosion position (enlarged for better viewing).

IV. Boundary Conditions

Boundary conditions are specified as follows: one wall representing the ground surface, three side outlets representing the open atmosphere, one inlet surface, and top surface representing the upper limit of ABL (Fig. 3).

The logarithmic velocity profile is specified at the inlet surface for velocity in order to simulate ABL[20]:

$$u_{inlet} = \frac{u^*}{k} \ln\left(\frac{z}{z_0}\right), \qquad (15)$$

where u_{inlet} is the fluid velocity at the inlet surface, u^* is frictional velocity, z is reference height, and z_0 is roughness height. Frictional velocity is calculated, by the solver using the following expression:

$$u^* = \sqrt{v \left.\frac{\partial u}{\partial z}\right|_{ground}}, \qquad (16)$$

where v is air kinematic viscosity, and $\partial u/\partial z$ is velocity gradient (shear stress) at the ground wall level.

The boundary condition for pressure is set to zero gradient at the inlet surface.

The boundary condition for turbulent kinetic energy is set using the following expression, which represents ABL properties:

$$k_{inlet} = \frac{u^{*2}}{\sqrt{C_\mu}}, \qquad (17)$$

where μ is dynamic viscosity of air and Cμ = 0.03 is model constant chosen according to[21].

The boundary condition for turbulent dissipation is also set to represent ABL properties:

$$\varepsilon_{inlet} = \frac{u^{*3}}{kz}. \qquad (18)$$

Boundary conditions at the outlet surfaces are set to zero gradient of the corresponding quantity if the flow is directed out of the surface, and to zero value if the flow is directed into the surface in order to prevent backflow in the computational domain.

The boundary condition for velocity is set to zero at the ground wall surface (no-slip wall). Zero gradient boundary condition is used for pressure at the wall ground surface. Modified wall functions, which take influence of ground roughness, are set as boundary conditions for turbulent kinetic energy and turbulent dissipation at the ground wall surface[22].

V. Firework Simulation Parameters

The main model input quantities for the firework activity simulation are taken into account using characteristics of the same type fireworks (shell size, shell shape, and detonation energy) as one applied during Belgrade music festival. These fireworks characteristics are adopted from[23].All other necessary data for the firework simulation is incorporated into model in accordance with regulations given in[24]. Summarized view of all input parameters used for the firework activity modeling in this work is given in the text below:

- shell size: 0.0508 m;
- initial shell velocity: (0 0 28) m/s;
- time to detonation after lunch: 3 s;
- detonation energy: 100 000 J;
- PM fragment size: 10 μm;
- material density: 1000 kg/m^3;
- total firework mass: 0.5 kg;
- total number of particles: 10000.

VI. RESULTS AND DISCUSSION

Prelaminar simulation of the ABL wind flow was conducted first. This was done in order to enable firework injection into already developed flow field corresponding to physical meteorological wind profile at the time of the event. Contour view of logarithmic wind profile averaged in vertical cross-sections of computational domain is shown in Fig. 4.

Plot view of ABL wind profile obtained at the back outlet surface (normal to wind direction) at the end of wind flow simulation is shown in Fig. 5. It can be seen that good agreement with the theoretically defined ABL profile at the inlet was achieved, pointing out accuracy of the performed initial simulation.

Firework material packed into the initial shell is injected in computational domain in the center

of the ground plane, at the second phase of simulation, as shown in Fig.6 (shell radius is enlarged due to visual purposes). The initial time corresponds to simulation time t = 0 s.

Injected particle material after lunch moves vertically until it reaches defied explosion time of 3s, Fig.7 (shell radius is enlarged due to visual purposes). It can be seen that PM stays in the compact spherical shell shape, identical to its initial shape. This is expected since the explosion is not yet occurred and all fragments move with identical initial lunch velocity.

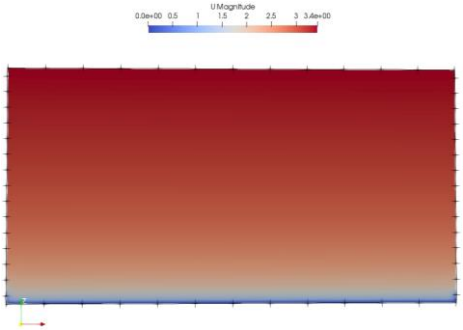

Figure 4. Contour view of averaged ABL wind profile, plane y = const.

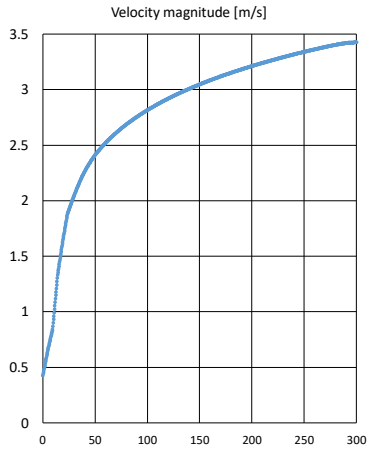

Figura 5. Plot view of ABL wind profile at domain outlet.

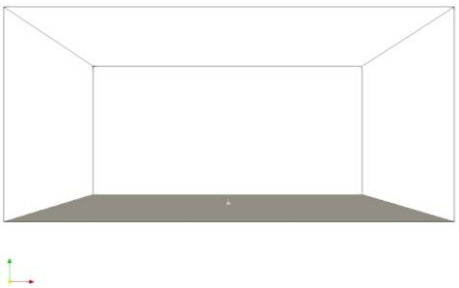

Figure 6. Firework initial shell starting position at the beginning of the simulation.

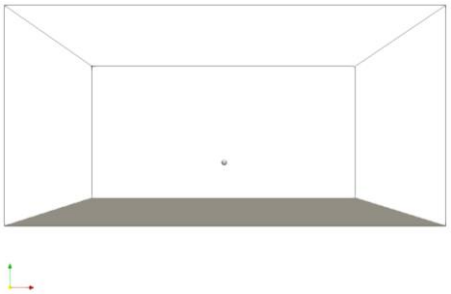

Figure 7. Firework shell position during vertical movement, moment before explosion t = 3 s.

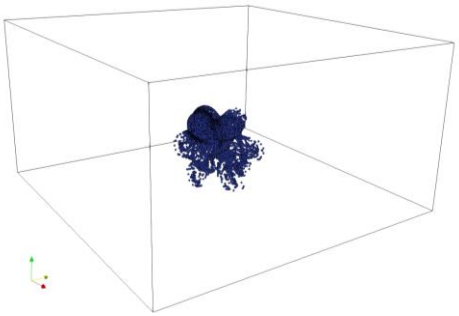

Figure 8. Firework plume development after explosion, simulation time t = 10s.

PM matter distribution at the time of 10 s after the explosion is shown in Fig. 8. It can be seen that PM10 particles spread radially outward from the initial shell center, due to high-velocity impulse given to the particles by the detonation of explosive firework content. It is important to note that particle positions are not completely spherical. This is caused by random turbulent particle dispersion which is still very intensive. It can be concluded that the PM10 particles' positions are predominately governed by the high-velocity explosion impulse at simulation time 10 s after explosion.

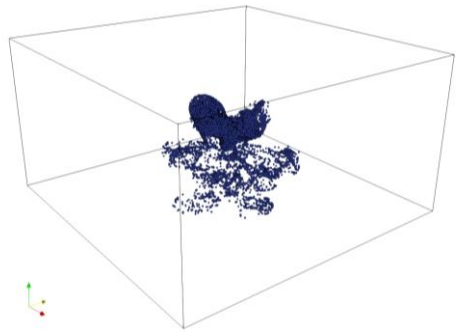

Figure 9. Firework plume development after explosion, simulation time t = 20s.

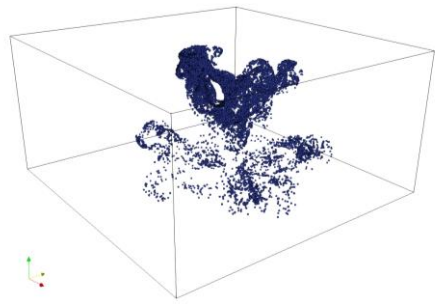

Figure 10. Firework plume development after explosion, simulation time t = 40s.

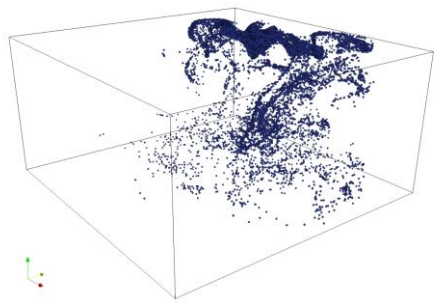

Figure 11. Firework plume development after explosion, simulation time *t* = 100s.

PM10 particle distribution 20 s after the firework explosion is shown in Fig. 9. It can be seen that PM10 particles, under gravity influence generally move towards ground surface. Influence of initial velocity is still present, although to the minor extent compared with the previous case, causing further spread of particles in radial directions.

PM10 particle distribution at the simulation time of 40 s is shown in Fig. 10. It can be seen that about one-third of the injected firework PM fragments are fallen on the ground surface, covering area of about 450 x 450 m. However, about two-thirds of the particles are directed in upper half of computational domain. This can be explained by the small PM10 particles mass. Initial velocity impulse has higher influence on the small size PM compared with gravity acceleration. Moreover, drag force is also lower for smaller particles. All of this allows significant portion of the total injected PM to remain in the upper half of the domain 40 s after injection.

Remaining particles, which were not stuck to the ground wall, at simulation time of 100 s after injection, are shown in Fig. 11. It can be clearly seen that the initial velocity impulse does not have any significant impact on PM10 particle trajectories anymore. Although gravitational force influence is still present, ABL wind flow has the prevailing impact on the particle distribution. PM10 particles are mainly concentrated in the upper zones of the domain and move in the direction of wind flow.

VII. Conclusions and Future Work

A novel hybrid model for simulation of fine PM distribution after fireworks activity was suggested. Model is able to simulate both fluid flow (wind) and particle behavior. The suggested model was applied to the firework event during musical festival in Belgrade, Serbia. The obtained simulation results showed that the PM matter is predominantly influenced by the explosion velocity impulse in the beginning stages, by the gravity in the middle stages, and by the ABL wind flow profile in the final stages of simulation. About one-third of PM10 particles are stuck on the ground surface in the area occupied by spectators, while the two-thirds of PM10 particles are carried by wind flow in upper ABL levels. The future simulations will include different sizes, different

wind flow conditions, and computational domain sizes.

ACKNOWLEDGMENTS

This work was carried out within the framework of research projects: III42010, TR33050, and III42008, financed by the Ministry of Education, Science and Technological Development of Serbia.

REFERENCES

[1] R.Vecchi, V.Bernardoni, D.Cricchio, A.D'Alessandro, P.Fermo, F.Lucarelli, S. Navad, A. Piazzalungab and G. Vallia, "The impact of fireworks on airborne particles," Atmos. Environ., vol 42, 2008, pp. 1121–1132.

[2] H.ten Brink, R.Otjes andE.Weijers, "Extreme levels and chemistry of PM from the consumer fireworks in the Netherlands," Atmos. Environ.,vol 212, 2019, pp. 36–40.

[3] A.Retama, A.Neria-Hernández, M.Jaimes-Palomera, O.Rivera-Hernández, M.Sánchez-Rodríguez, A.López-Medina andE. Velasco, "A major source of inorganic and organic aerosols during Christmas and New Year in Mexico City," Atmos. Environ., vol 2, 2019, pp.100013.

[4] A.Fortelli, N.Scafetta and A.Mazzarella, "Influence of synoptic and local atmospheric patterns on PM10 air pollution levels: a model application to Naples (Italy)," Atmos. Environ., vol 143, 2016, pp. 218–228.

[5] M.M. Scerri, K. Kandler, S. Weinbruch, E. Yubero, N. Galindo, P. Prati, L. Caponi, and D. Massabò, "Estimation of the contributions of the sources driving PM2.5 levels in a Central Mediterranean coastal town," Chemosphere,vol. 211, 2018, pp.465–481.

[6] C.A.Pope andD.W.Dockery, "Health effects of fine particulate air pollution: Lines that connect," J. Air Waste Manag. Assoc.,vol 56, 2006, pp.709–742.

[7] Air Quality Guidelines for Europe, Second Edition. Copenhagen, Denmark, 2000.

[8] L. Yao, D. Wang, Q. Fu, L. Qiao, H. Wang, L. Li, W. Sun, Q. Li, L. Wang, X. Yang, Z. Zhao, H. Kan, A. Xian, G. Wang, H. Xiao, and J. Chenaf, "The effects of firework regulation on air quality and public health during the Chinese Spring Festival from 2013 to 2017 in a Chinese megacity", Environ. Int., vol. 126, 2019, pp.96–106.

[9] Lv D, D. Lv, Y. Chen, T. Zhu, T. Li, F. Shen, X. Li, and T. Mehmood, "The pollution characteristics of PM10 and PM2.5 during summer and winter in Beijing, Suning and Islamabad," Atmos. Pollut. Res.,vol.10, 2019, pp. 1159–1164.

[10] Hybrid Single-Particle Lagrangian Integrated Trajectory (HYSPLIT). Available at: http:// www.arl.noaa.gov/ready/hysplit4.html n.d.

[11] D.van der Kamp, I.McKendry, M.Wong, and R.Stull, "Lidar ceilometer observations and modeling of a fireworks plume in Vancouver, British Columbia," Atmos. Environ., vol.42, 2008, pp.7174–7178.

[12] J. Feng, H. Yu, X. Su,S. Liu, Y. Li, Y. Pan andJ.-Hui Sun. "Chemical composition and source apportionment of PM 2.5 during Chinese Spring Festival at Xinxiang, a heavily polluted city in North China: Fireworks and health risks," Atmos. Res., vol. 182, 2016, pp. 176–188.

[13] J.Zhang, X.Huang, Y.Chen, B.Luo, J.Luo, W.Zhang, Z. Rao and F. Yang. "Characterization of lead-containing atmospheric particles in a typical basin city of China: Seasonal variations, potential source areas, and responses to fireworks," Sci. Total Environ., vol 661, 2019, pp. 354–363.

[14] T.I.Zohdi,"On firework blasts and qualitative parameter dependency," Proc. R. Soc. A Math. Phys. Eng. Sci., 2016, pp. 472.

[15] J. O. Hinze, Turbulence. New York.: McGraw-Hill Publishing Co, 1975.

[16] T-H.Shih, W.W.Liou, A.Shabbir, Z.Yang andJ.Zhu, "A newk-єeddy viscosity model for high :reynolds number turbulent flows," Computers Fluids,vol. 24, 1995, pp. 227–238.

[17] C.T. Crowe, J.D. Schwarzkopf, M. Sommerfeld and Y. Tsuji, Multiphase Flows with Droplets and Particles. 2nd ed. Boca Raton: CRC Press; 2012.

[18] S.Subramaniam, "Lagrangian-Eulerian methods for multiphase flows," Prog. Energy Combust. Sci.,vol. 39, 2013, pp.215–245.

[19] Q. Zhou and M. A. Leschziner. Technical report. Munich,1991.

[20] P.J. Richards, and Hoxey RP, "Appropriate boundary conditions for computational wind engineering models using the k-ε turbulence model," J. Wind Eng. Ind. Aerodyn., vol 47, 1993, pp. 145–153.

[21] P.A.Taylor andH.W.Teunissen, "The Askervein Hill project: Overview and background data," Boundary-Layer Meteorol, vol. 39, 1987, pp 15–19.

[22] A.Ricci, M.Burlando, M.P.Repetto andB.Blocken, "Simulation of urban boundary and canopy layer flows in port areas induced by different marine boundary layer inflow conditions," Sci. Total Environ., vol. 670, 2019, pp.876–892.

[23] K.L. Kosanke and BJKosanke, "Selected Pyrotechnic Publications of K. L. and B. J. Kosanke, Part 4 (1995 through 1997)," 1st ed. Whitewater, USA: Journal of Pyrotechnics, Inc., 1999.

[24] T.J. Poulton and KLKosanke, "Fireworks and their Hazards," Fire Eng.,vol. 148, 1995, pp. 49–66.

Performance Analysis of a Photovoltaic Array(15.936 MWc) at Ain Skhouna PV Power Station (Saida, Algeria)

Razika Ihaddadene[1,2*], Jed Mohamed El Hacen[1,] Nabila Ihaddadene[1,2], Mema Hneini[1]

[1]Mechanical engineering department, Med Boudiaf University, M'sila, Algeria, tassekurt1@gmail.com; hassenjid9@gmail.com; MAZ1dz@gmail.com; memahneini@gmail.com

[2]Laboratory of renewable energy and sustainable development, Constatine 1 University, Constantine, Algeria

Abstract — **The present paper shows the performance analysis of a photovoltaic system of 15.936 MWc (loop 1), a part of the 30 MWc photovoltaic power station of Saida (a province of Algeria). This investigation concerns one month of study (April 2019). The analysis done was evaluated according to IEC 61724. The parameters studied are the reference efficiency (Yr), the PV field yield (Ya), the final yield of the photovoltaic plant (Yf), the performance ratio (PR), the efficiency of the PV module (ηpv), the efficiency of the inverter (ηinv), and the efficiency of the photovoltaic system (ηsys).The results show that the monthly reference yield, the photovoltaic field yield, and the final yield of the photovoltaic plant are 6.83 h/d, 5.98 h/d, and 5.81 h/d respectively. They are proportional to the energies Eac and Edc. The average monthly efficiency of the field and system are 13.74% and 13.33%, respectively. The monthly-standardized performance index (PR) presents an average value of 85.75%, which is greater than 80%. This means that the performance of this PV plant approaches the ideal performance in the STC conditions. Therefore, Ain Skhouna photovoltaic power plant is in good operating condition, without degradation.**

Keywords - photovoltaic array, standardized performance analysis, grid connected PV.

I. INTRODUCTION

Global demand for energy has climbed up over the past 100 years, in parallel with population growth and industrial development. This demand for energy should continue to increase by at least 50% by 2030 [1]. To meet these energy needs, renewable energies are used as an alternative to conventional ones. Renewable energies such as solar, wind, hydropower, biomass, and geothermal have recently gained acceptance because of their ability to provide clean and inexhaustible energy production. They are now widely recognized as a sustainable solution to protect the atmosphere by reducing the greenhouse effect and control the air rising temperature. Solar energy is one of these five sources of alternative energy and the most significant. Worldwide installed solar capacity has grown exponentially over the past decade in both developed and developing countries due to collective research and development efforts in addition to government policies that encourage energy production from clean and renewable sources.

There are two different kinds of technologies, named solar thermal and solar electricity, employed in solar applications. Solar thermal energy is used for the production of thermal energy intended for industry and housework. Two technologies named concentrated solar power (CSP) and Photovoltaic (PV) are utilized for solar electricity production. The CSP uses solar radiation to generate high temperatures and, from that, electricity and heat are derived. Photovoltaic PV is a simple device based on the

ISBN: 978-86-80616-04-9

photo effect. It directly generates electricity from sunlight. The physical of the PV cell is very similar to that of the classical diode with a PN junction formed by the semiconductor material. The European PV Industry Association reported that the total global PV cell production worldwide in 2002, with the Integrity of the specifications, is over 560 MW, and it is growing with a rate of 30% annually in recent years [2].

Photovoltaic systems are basically composed of PV modules, charge controllers, storage batteries, and converter devices, namely DC to DC converters and DC to AC inverters.

Algeria has one of the largest solar deposits in the world. The duration of sunstroke on almost the entire national territory exceeds 2000 hours annually and reaches 3900 hours (especially in the highlands and the Sahara).Since Algerian renewable energy potential is strongly dominated by solar energy, Algeria considers this latter as an opportunity and a lever for its economic and social development, particularly through developing industries that create wealth and jobs. Among all the renewable energies, photovoltaic solar is of particular interest in Algeria, seen its very important solar field. Algeria's energy strategy is based on reinforcing and encouraging the development of solar energy. Indeed, the government plans to launch several solar photovoltaic projects with a total capacity of about 800 MWp by 2020. Other projects with a capacity of 200 MWp per year should be carried out over the period of 2021-2030. Moreover, there are currently 23 photovoltaic plants in the country. Among them, the photovoltaic power station of Ain Skhouna (Saida) with a capacity of 30 MWp, which is connected to the national grid.

The aim of this study is to analyze, for the first time, the performance of Saida 1 photovoltaic array of 15.936 MWp capacity during April (2019) month according to the standardized norms IEC 61724 (International Electro-technical Commission).Various studies have been conducted on the performance parameters of installed PV power plants in different geographical locations in the world and under different climatic conditions [3-8].

This investigation is divided into three parts as follows; the first one is devoted to the description of the photovoltaic power station of Ain Skhouna, namely its geographical location and its constituents, in addition to the parameters used to study its performance according to the IEC 61724 standard. The second part is reserved for the results and discussion. Finally, a conclusion and references end this paper.

Figure 1. Location of Saida province in Algeria [9].

II. Methods and Materials

A. Location

Ain Skhouna photovoltaic power plant is located in Saida (a province of Algeria) at a latitude of 34°48'43" North, a longitude of 4 °10'58" East, and an altitude of 900 m in a desert plain. It is situated between the two provinces of Saida (80 km) and Tiaret (150 km south) (Fig.1). This mega project covers an area of 42 ha with a construction cost estimated at 50 million Euros.

B. System description

Ain Skhouna photovoltaic solar power plant has a capacity of 30 MWp. It supplies Algeria's high-voltage national grid (60 kV).

The solar field of Ain Skhouna plant is composed of 119520 photovoltaic panels, type CS6P-250P made of polycrystalline silicon. These panels are supplied by the BELECTRIC group, a German operator. Each panel is characterized by a peak power of 250 Wc. Table I summarizes the PV module characteristics.

Ain Skhouna solar plant consists of two fields (called also loops), namely Saida 1 (loop 1) and Saida 2 (loop 2). The two loops supply power of 15.936 MWp and 13.944 MWp respectively. Saida 1 has 8 subfields (Skide), while Saida2 has 7 subfields. Thus, this photovoltaic plant is composed of 15 subfields. Each subfield has a peak power of 1.992 MWp, containing two (2) inverters, four

TABLE I. PV MODULES SPECIFICATIONS

PV Module	Specification
Type	CS6P-250P
Maximum power (Pmax)	250W
Maximum power voltage (Vpm)	30,1V
Maximum power current (Ipm)	8,30A
Open circuit voltage (Voc)	37,2V
Short circuit current (Isc)	8,87A
Temperature coefficient of Pmax	-0,43%
N° of module	60
NOCT	47°C

(4) central boxes, and a transformer. Every inverter regroups 3984 panels. The technical specifications of the inverters used (Sunny Central 850CP XT) are given in Table II. These photovoltaic panels are oriented towards the south, with an inclination of 15°.

C. Performance analysis methodology

Performance parameters have been specified by the International Energy Agency (IEA) and described in the IEC 61724 standard [10] to analyze the performance of a PV solar system. These parameters are the reference efficiency (Y_r), the yield of the PV field (Y_a), the final yield of the PV system (Y_f), the performance ratio (*PR*), the system losses of (*LS*), and the various losses (*LC*) [6, 8, 11].

TABLE II. INVERTER SPECIFICATIONS

Inverter	Specification
Type	Sunny Central 850CP XT
Maximum dc power	954 kW
Maximum dc voltage	1000 V
Maximum dc current	1400 A
Maximum ac power	935kVA
Nominal ac power	850kVA
Nominal ac voltage	386 V/50 Hz
Maximum efficiency	98,6 %
Euro-efficiency	98,4 %

Energy generated by the PV array system (E_{dc}). The total daily recorded value of DC power output ($E_{dc,d}$) is given by the following equation:

$$E_{dc,d} = \sum_{t=1}^{t=Trp} P_{dc} \times T_r \ , \qquad (1)$$

Where:

T_{r^0} is the recording time interval;

T_{rp} is the reporting period;

P_{dc} : is the DC power, it is given as:

$$P_{dc} = V_{dc} \times I_{dc} \ , \qquad (2)$$

Where:

V_{dc^o} is the DC voltage;

I_{dc} is the DC courant.

Energy output or Energy fed to the utility grid (E_{ac}) is the measure of the energy output across the inverter terminals, recorded every 5-min by the data logger. The total daily value of AC power output ($E_{ac,d}$) is obtained as follows:

$$E_{ac,d} = \sum_{t=1}^{t=Trp} P_{ac} \times T_r \ . \qquad (3)$$

AC poweris givenas follows:

$$P_{ac} = V_{ac} * I_{ac} \, , \qquad (4)$$

Where:

V_{ac} : is the AC voltage;

I_{ac} : is the AC courant.

The reference efficiency (Y_r) is the ratio between the total amount of solar radiation H_t (kWh/m^2) intercepted by the PV solar panels surface and the amount of reference radiation G_0 (1 kW/m^2). It depicts the number of hours during which the illumination is equal to that of the reference. Y_r defines the solar resource for the PV system. It is given by:

$$Y_r = \frac{H_t}{G_0} \, . \qquad (5)$$

The efficiency of the PV field (Y_a) is defined as the ratio between the total energy generated E_{dc} (kWh) by the PV rows for a defined period (day, month or year) and the nominal power P_0 (kWc) of the rows under the standard conditions (For STC: irradiation: 1000 W/m^2, 25 °C ambient temperature and AM 1.5-G reference

spectrum). The daily efficiency of the PV field ($Y_{a,d}$) is given by the following equation:

$$Y_{a,d} = \frac{E_{dc,d}}{P_{pv(rated)}} . \quad (6)$$

The final efficiency (Y_f) corresponds to the total energy produced by the PV system, E_{ac} (kWh) per the installed nominal power P_0 (kWp). This quantity represents the number of hours during which the PV field should operate at its rated power. The daily final efficiency ($Y_{f,d}$) is given by:

$$Y_{f,d} = \frac{E_{ac,d}}{P_{PV(rated)}} . \quad (7)$$

The module efficiency (η_{pv}) presents the effective energy generated by a module with respect to the available radiation. The daily PV array efficiency is given by the following equation:

$$\eta_{pv,d} = \frac{E_{dc,d}}{G \times A_m} \times 100 . \quad (8)$$

Where:

$E_{dc,d}$: is the dc energy generated by PV array system;

G: presents the global solar irradiation;

Am: presents the area of PV array system.

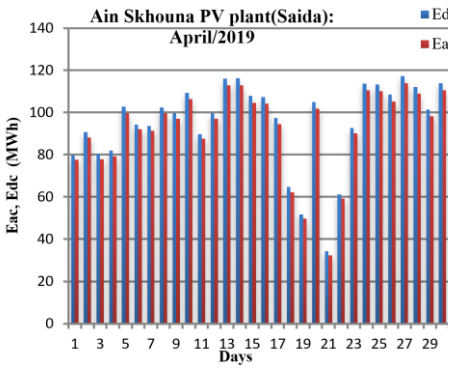

Figure 2. Daily evolution of *Edc*, *Eac* energies of Ain Skhouna PV plant.

Inverter efficiency (η_{inv}) supposed to be higher than both the module and the system efficiencies. It is also called conversion efficiency, expressed as the ratio between the AC power generated by the inverter and the DC power produced by the photovoltaic panel system. The daily inverter efficiency is given by:

$$\eta_{inv,d} = \frac{E_{dc,d}}{E_{ac,d}} \times 100 . \quad (9)$$

The photovoltaic system efficiency (η_{sys}) is related to the efficiencies of the PV module and the inverter. The monthly system efficiency can be calculated by applying the following the following equation:

$$\eta_{sys,m} = \eta_{pv} \times \eta_{inv} . \quad (10)$$

Standardized performance ratio (*PR*) indicates the overall effect of the energy production losses of the rows of a PV system. The *PR* values indicate how far a PV system approaches the ideal performance under real-world operating conditions. *PR* is defined as the ratio between the final yield and the reference yield. It is a dimensionless quantity, given as follows:

$$PR = \frac{Y_f}{Y_r} . \quad (11)$$

System losses by conversion (L_s) are due to the inverter conversion losses (DC-AC current) and are defined by the difference between the yield of the PV field Y_a and the final yield Y_f . They are given by:

$$L_s = Y_a - Y_f . \quad (12)$$

The array capture loss (L_c) is defined by the difference between the reference yield and the array yield of the PV field. It represents the losses due to panel temperatures, wiring, partial shading, spectral losses, soiling, errors in finding the maximum power point, conversions (DC-AC), etc. It is given as follows:

$$L_c = Y_r - Y_a . \quad (13)$$

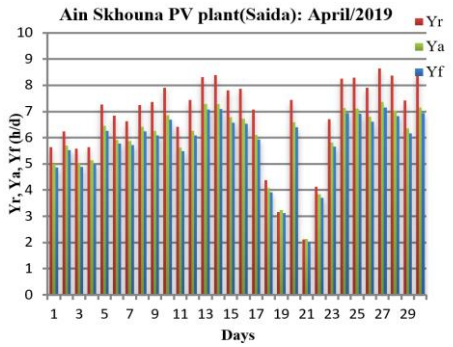

Figure 3. Daily evolution of *Yr, Ya, Yf* in Ain Skhouna PV plant.

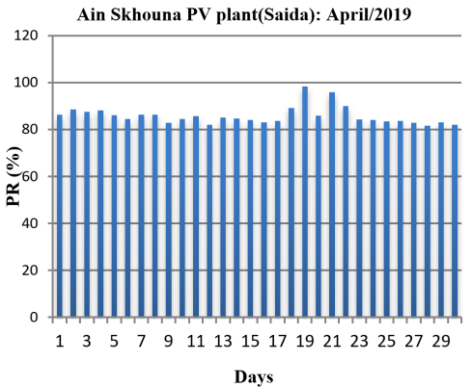

Figure 4. Daily evolution of PR in Ain Skhouna PV plant.

The current investigation focuses on the study of the photovoltaic field loop 1(15.936MWp) of capacity of the Ain Skhouna power station. This study is performed in one month (April 2019) according to the standard of the International Energy Agency (IEA).

III. RESULTS AND DISCUSSION

Fig. 2 illustrates the daily evolution of the energy generated by the photovoltaic field (E_{cd}) and the energy supplied to the distribution network (E_{ac}) during April's month (2019) by the photovoltaic power station of Ain Skhouna (Saida). These two energies (E_{dc} and E_{ac}) follow the same trend. In addition, the energy generated by the photovoltaic field (E_{dc}) is greater than that supplied to the distribution network (E_{ac}).

The daily energy generated by the photovoltaic field (E_{dc}) has a maximum value of 117.29 MWh recorded during the 27th day of the month and a minimum value of 34.18 MWh noted during the 21st day of the month. The average monthly energy generated is 95.30 MWh. The daily energy supplied to the grid (E_{ac}) has a maximum value of 113.93 MWh recorded on the 27th day of the month and a minimum value of 32.36 MWh registered on the 21st day of the month. The average monthly energy supplied to the grid is 92.51 MWh.

The daily evolution of April month yields, namely reference efficiency (Y_r), photovoltaic field efficiency (Y_a), and the final yield of the photovoltaic system, are shown in Fig. 3. These yields returns evolve in the same way. The reference yield varies between 2.12 hrs/d noted on the 21st April, and 8.64 hrs/d recorded on the 27th of April. Moreover, the average monthly value of the reference yield is 6.83 hrs/d. The yield of the photovoltaic field has a maximum value of 7.36 h/d recorded on the 27th of April and a minimum value of 2.14 h/d noted on the 21st day of April month. The average monthly value of the photovoltaic field output for April month is 5.98 h/d. The final yield has a maximum value of 7.15 h/d and a minimum value of 2.03 h/d recorded on the 27th and the 21st day of April respectively. The monthly value of the photovoltaic field yield for the studied month is found to be 5.81 h/d. It is noted that all these yields are proportional to the E_{ac} and E_{dc} energies, which is explained by the same trends observed for these yields (reference yield, photovoltaic field yield, and the final yield), and the energies illustrated in Fig. 2.

The daily evolution of the performance index for April month is illustrated in Fig. 4. The normalized performance index (PR) during this month is almost stable. It varies between 98.39% (recorded on 19th April) and 81.60% (registered on 28th April), with an average value of 85,75% for April month. Noting that a performance index greater than 80% corresponds to a system whose performance approaches the ideal performance under STC conditions. Hence, Ain Skhouna plant has a very interesting performance index. It is in good operating condition, with no degradation. This result is similar to that found in Marroco [6], when the performance ratio varies between 58% and 98%. The PR on monitored PV system in

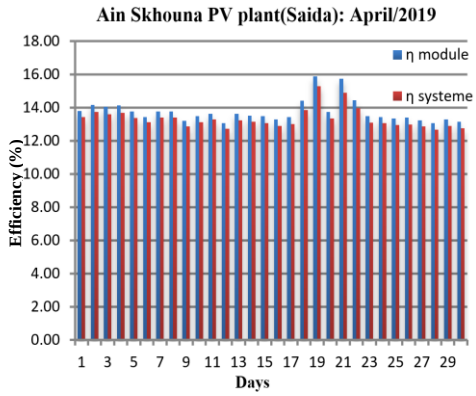

Figure 5. Daily efficiency evolution in Ain Skhouna PV plant.

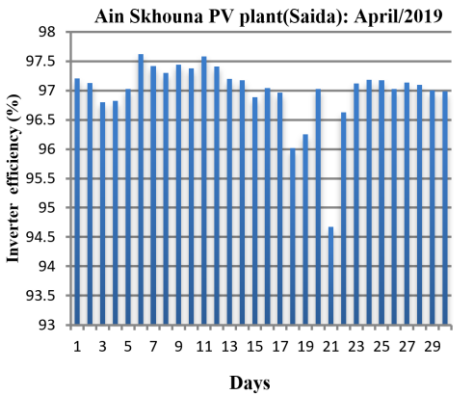

Figure 6. Daily evolution of inverter efficiency in Ain Skhouna PV plant.

Thailand ranged from 70% to 90% [12]. These values are in the same order as our study. The PR in Sheikh –Zaid power station in Nouakchott, Mauritania [8] is ranged between 61% and 71%. It presents an average monthly value of 66%. The PR in this solar power station is lower than that noted in Ain Skhouna solar plant.

The daily evolution of the module and system efficiencies of Saida1 is illustrated in Fig. 5. These two efficiencies follow the same pace. The efficiency of the system is less than that of the module. In addition, the daily efficiency of the module varies between 15.88% and 13.06% noted on the 19th day and 28th day of April month, respectively. The average monthly efficiency of the module is found to be 13.74%. On the other hand, the daily system efficiency varies between a maximum of 15.29% and a minimum of 12.68% recorded during the same dates as the effectiveness of the module. The average daily efficiency of the system is 13.33%.

Fig. 6 presents the daily inverters efficiency evolution of Saida1 field. It varies between a minimum of 79.62% noted on the 6th day of April, and a maximum of 94.67% noted on the 21st day of the same month. The average daily inverter efficiency value is 96.99%, which agrees with the results of the daily losses of the system by conversion. Noting that the inverter efficiency is in the range of (95% -98%) at actual operating conditions, as reported in [3]. This value is similar to that found by Attari et al. [6]. It is presents an average annual value of 96,7%. Similar results are found in [8].

IV. CONCLUSION

Ain Skhouna PV plant with a capacity of 30 MWc is located in Saida (a province of Algeria). It is one of 23 stations built across the highlands and the south of Algeria to produce 400 megawatts as part of the national program to promote the use of renewable energies. It was commissioned in 2017. This paper aims to study the performance analysis of Saida1 photovoltaic field with a capacity of 15.936MWc during April month of the current year (2019). This study allowed us to remember the following:

The generated energy (EDC) and the energy supplied to the grid (EAC) are of 95.30MWh and 92.51MWh, respectively;

The reference, photovoltaic and final fields are 6.83 h / d, 5.98 h / d and 5.81 h / d, respectively. They are also proportional to the energies E_{ac} and E_{dc};

The monthly standardized performance index (PR) has an average value of 85.75%. This value is greater than 80%, which corresponds to a system whose performance approaches the ideal performance in the STC conditions. Therefore, Ain Skhouna plant has a very interesting performance index. It is in good working order with no degradation;

The average daily efficiency of the field and system are 13.74% and 13.33%, respectively;

The efficiency of the inverters in Saida1 field has an average value of 96.99%, which agrees with the results of the daily losses of the system by conversion;

After 2 years of service, no degradation observed in the functioning of this installation

(remains in very good working condition). Noting that this plant ranks first in the ranking of photovoltaic power plants in Algeria.

ACKNOWLEDGMENT

The authors would like to acknowledge Mr. Saadi Idir, SKTM Human Resources Department Head, for giving access to Ain Skhouna PV plant. We would like to think all Ain Skhouna PV plant personnel particularly Hamel Cheikh for they help.

REFERENCES

[1] EPA, *Integrated Risk Information System*, Available at: http://www.epa.gov/iris/toxreviews/1022tr.pdf

[2] K. K.Vijay, and B. Mahadevi, "PV Based Switched Boost Inverter with Simultaneous DC and AC Outputs," International Research Journal of Engineering and Technology (IRJET), vol. 03, 2016.

[3] L. M. Ayompe, A. Duffy, S. J. McCormack, and M. Conlon,"Measured performance of a 1.72kW rooftop grid connected photovoltaicsystem in Ireland," Energy Convers. Manag., vol. 52, no. 2, 2011, pp. 816–825.

[4] D. Micheli, S. Alessandrini, R. Radu, and I. Casula, "Analysis ofthe outdoor performance and efficiency of two grid connected photovoltaicsystems in northern Italy," Energy Convers. Manag., vol. 80, 2014, pp. 436–445.

[5] M. Mpholo, T. Nchaba, and M. Monese., "Yield and performanceanalysis of the first grid-connected solar farm at Moshoeshoe I InternationalAirport, Lesotho," Renew. Energy, vol. 81, 2015, pp. 845–852.

[6] K Attari, A Elyaakoubi, and A Asselman, "Performance analysis and investigation of a grid-connected photovoltaic installation in Morocco" Energy Reports, vol. 2, 2016, pp. 261-266.

[7] M. Wichliński and J. Staszkiewicz., "Photovoltaic installation for aroofed car park in Egypt as an example of effective use of solar energy," E3S Web of Conferences, 2018, vol. 49, pp. 00127.

[8] J. M. El Hacen et al.,"Performance analysis of micro-amorphe silicon PV array under actual climatic conditions in Nouakchott, Mauritania," 10th International Renewable Energy Congress (IREC), Hammamet, Tunisia, March 26-28, 2019.

[9] Wilaya de Saida, Available at: http://www.andi.dz/PDF/monographies/SAIDA.pdf

[10] International Standard IEC 61724, Photovoltaic system performance monitoring guidelines for measurement, Data exchange and analysis. 1998.

[11] A Bouraiou, et al. "Experimental investigation of observed defects in crystalline silicon PV modules under outdoor hot dry climatic conditions in Algeria," Solar Energy, vol. 159, 2018, pp. 475-487.

[12] S. Chokmaviroj, R. Wattanapong, and Y. Suchart., "Performance of a 500 kWP grid connected photovoltaic system at Mae Hong Son Province, Thailand," Renewable Energy, vol.31, 2006, pp. 19-28.

Rain,Ice&Snow (RIS) Harvesting System for Supplying Homes with Free Soft Water to Decrease Water Bills and the Pressure on the Water Distribution System – SmartH2OHome

Sara Gračić

University of Novi Sad, Faculty of Economics, Subotica, Serbia, saritta4u@gmail.com

Abstract — **Only 3.5% of the Earth's water supplies are in fresh water necessary for survival of living beings. Development of industry, agriculture and human negligence caused that 3 out of 10 people do not have access to clean drinking water. To diminish overall water stress, science has offered rainwater harvesting systems for collecting, storing and using rain. But these systems depend on rainfall and their economic feasibility is questionable. To solve these problems, the author has designed primitive and sophisticated Rain, Ice & Snow (RIS) SmartH2OHome system and implemented its primitive version in 2011 in a ground-level home. Although primitive version covered only gardening, toilet, showering and washing needs, it has led to decreased water bills, since consumption from town's water supply system was often 1 cubic meter per month. The sophisticated RIS SmartH2OHome, although enabling even complete water self-sufficiency and high automation level, is very costly and for now not feasible, especially since primitive RIS SmartH2OHome solves both of the above stated problems.**

Keywords – rainwater harvesting systems, economic feasibility, water pollution, green home, sensors

I. INTRODUCTION

A. The Importance of Water and its Sources

Water is a constitutive element of all living beings, which need it for survival. Although water approximately covers 71% of the Earth's surface, majority of it, about 96.5%, is salt water in oceans and seas. Only a small percentage of the Earth's water supply is in form of freshwater, which could be found as vapor and in streams, rivers, lakes, icecaps, glaciers, groundwater and rain [1].

Although surface water is more used as drinking water and for crop irrigation, groundwater, apart from maintaining levels of rivers and lakes, is a source of freshwater in places where freshwater supplies are scarce [1].

Also, the amount of groundwater is much higher than that in rivers and lakes, while glaciers and icecaps in the Polar regions represent a vast supply of freshwater. Out of 3.5% of freshwater supplies, 68% is "locked" in ice, while 30% is located in the ground [1].

B. Water Pollution as a Cause of Disruptions in the World's Ecosystem

The development of industry, farming and irresponsible human behavior towards nature, have led to, among other environmental problems, water pollution.

Since water is a universal solvent, which can dissolve a lot of substances, harmful chemicals or microorganisms can easily contaminate a stream, river, ocean or other form of water and degrade water quality, which then becomes toxic to humans and/or the environment [2].

ISBN: 978-86-80616-04-9

Groundwater, when polluted with pesticides, fertilizers or a septic system can be almost impossible or costly to clean and an aquifer may be unusable for tens, or even thousands of years. Contamination can spread far from the source onto streams, lakes and oceans. Almost one half of rivers and streams and one third of lakes in the USA are contaminated and unfit for swimming, fishing and drinking [2].

Agriculture uses about 70% of the Earth's surface water supplies. On the other hand, it is a serious water polluter and the leading cause of water quality degradation around the world. More than 80% of the world's wastewater returns to the environment without being processed [2], while oil spills and radiation are just increasing the overall problem.

Water pollution causes algae bloom, which suffocates plants and animals due to lack of oxygen, thus disturbing the complete ecosystem. As far as humans are concerned, when chemical polluters (e.g. heavy metals, pesticides, fertilizers) are ingested, they can cause cancer, hormone disruption, alter brain function and death (1.8 million deaths in 2015, according to a study published in The Lancet) [2].

C. Clean Water and Sanitation Accessibility

Since the 1980s, due to population growth, socio-economic development and changes in consumption patterns, usage of water has been increasing by approximately 1% yearly, worldwide. This rise in global water demand is expected to continue at a similar rate until 2050 and will be increased by 20% to 30% above the current level of water use, due to demand rise in the industrial and domestic sectors [3].

Over 2 billion people live in countries where water stress is very high. 4 billion people experience drastic water scarcity during at least one month per year. Water stress levels will continue to rise, because water demand is growing and the effects of climate changes are getting more serious [3].

3 out of 10 people cannot access clean drinking water. Almost half of people who consume water from unproven sources live in Sub-Saharan Africa. 6 out of 10 people do not have access to proper sanitation services. The fact is that these differences are not just between, but also within regions, countries, communities and even neighborhoods [3].

However, many efforts are taken to find alternative ways of providing people clean water for drinking, personal hygiene and decreasing water stress by using other source of water – rainwater.

II. RAINWATER HARVESTING SYSTEMS – PROS AND CONS

Rainwater is a desirable water alternative for agricultural, industrial and domestic sectors, with one major advantage – it is free, so scientific research has been focused on developing rainwater harvesting systems (RWHS) for collecting, storing and using rainwater in a cost-effective way to minimize the pressure on a country's water supply system.

A. Research Background and Problem Identification

Malaysia has successfully implemented RWHS [6]. RWHS can be applied in various occasions and surroundings. Implementation of these systems can cover urban [7, 8] and rural areas [9, 10], domestic sector [11] and agriculture [12].

One of the problems with RWHS is their economic feasibility, that is are benefits of using rainwater greater than costs related to collecting, filtering, storing and using rainwater. According to research conducted in Brunei, implementation of rainwater harvesting system is not feasible at the moment [4] for this country.

Another problem is the amount and frequency of rainfall in a region, although e.g. Australia has successfully implemented rainwater harvesting system [4], despite minimal 45 mm average monthly rainfall [5]. Rainfall is one of the factors for determining capacity of a rain tank (apart from a user's needs).

B. Research Focus

Due to the above presented issues, focus of this research is to determine whether an individual can implement a RWHS with minimal costs and are there other sources of water that can be harvested and how.

C. Research Objective

The objectives of this research are two-fold. Firstly, because of variations in amount and frequency of rainfall, the goal is to consider other suitable sources of freshwater that can be

harvested by adapting the primitive RWHS according to current needs; needs are correlated with the water source being collected (different water sources will also be incorporated in the sophisticated RWHS).

Secondly, the goal is to design two harvesting systems (HS) for collecting rain, hail and snow (a sophisticated SmartH2OHome and a primitive SmartH2OHome); implement the primitive SmartH2OHome in a home of an individual; determine its costs related to collecting, filtering, storing and wide usage of freshwater and compare those costs with monthly bills for water consumption from the Serbian water supply system.

III. Modeling the Rain, Ice&Snow (RIS) Harvesting Systems

A. Choosing the Environment for Primitive and Sophisticated RIS

"Think globally, act locally" is the main motto in the environment protection. That is why the author of this paper will be focused on developing RIS for domestic sector.

In the center of development of both primitive and sophisticated model for harvesting different types of atmospheric falls is an individual's ground-level home with pipelines and wavy roof extension.

Before use, the collected rainwater, hail and snow will be filtered to remove debris and treated adequately to their intended use. The idea is to use these atmospheric falls as much as possible in gardening, bathroom, kitchen and heating system in a residence.

Although collected water could be used as drinking water, this would mean the additional implementation of disinfection processes e.g. boiling water and chemical treatments (chlorine), which will make even the simplest system quite costly.

B. Primitive RIS

1) Set up and Implementation

Pipeline, which transfers the roof rainwater to sewage, is located on one part of the ground-level home, while the wavy roof extension, from which rainwater falls onto the ground, is on its other part.

Containers with capacity of 30 liters are placed below the wavy roof extension, while the ending of the pipeline is put into a container with capacity of 100 liters. Both parts, instead of generating a massive loss of rainwater, are now being used to direct rain to containers and preserve it for various needs. Containers and pipelines have to be cleaned with water and brush and dried, to prevent dirt from contaminating the rainwater. When not in use, containers should be closed and stored inside.

Collected rainwater has to be removed from the sunlight; otherwise the algae will form and limit the use of rainwater.

PET bottles can be used for storing rainwater for two reasons. Firstly, the FDA has declared PET as safe for storing food and drink. Secondly, people already get PET bottles when they buy drinks, so instead of throwing them and polluting the environment, they can be put to a good use.

If growing fruits and vegetables is the case, like with the home in focus, the rainwater does not have to be filtered at all. For toilets, rainwater has to be filtered to prevent e.g. leafs from clogging the sewage.

For showering and dishwashing, rainwater does not have to be treated, unless the object is located near factories or other source of pollution. Then the water has to be boiled as well, to kill microorganisms and become safe. Heating system and washing machine were not using rainwater in the observed household.

2) Avantages and Disadvantages

The primitive RIS has been in use in the observed household since 2011 and has brought many advantages, of which the main is drastic decrease in water consumption from the town's water supply system. This has led to lower water bill, since consumption is around 1 cubic meter per month. Investments are minimal. A household needs to get containers, if already does not have them and roof extension is not mandatory.

The main disadvantage is that the system is not automated in any segment, which means that everything has to be done by household residents. Another disadvantage is that boilers, washing machine and heating system are not using rainwater, so when they are used, monthly water bill is either 1 or 2 cubic meters per month, depending of the frequency of using washing machine and refilling heating system with water.

C. Sophisticated RIS

1) Set up

Pipeline, surrounding the roof of the ground-level home, transfers the roof rainwater to the first tank with the highest capacity of 5,000 liters. Before water enters this tank, it is being physically cleaned by a filter made of stainless surgical steal. This prevents leafs and other debris from the roof and the pipelines to enter and contaminate the first tank.

The first tank has three pipes that carry rainwater to three exit points. The first exit point is the faucet located in the garden. Connecting the water hose to the faucet covers needs for watering plants, vegetables and fruit. The second exit point is the toilet. These two pipelines eliminate the need to withdraw water from a town's water supply system. The third exit point sends water to a water cleaner, after which the cleaned water is sent to the second tank.

The second tank has capacity of 4,000 liters and supplies several points in the household with clean water. It transfers water to two points in the bathroom: the boiler, so rainwater can be used for showering and washing machine. Therefore, the second tank eliminates the need to use town's water supply system for showering and washing clothes. The second tank also supplies the kitchen: dish machine and boiler, thus eliminating water consumption for washing the dishes, hands, cleaning rooms etc. It also enables water refill for gas and/or solid fuel heating system.

The last pipe carries water to the third tank, with capacity of 2,000 liters, where the water is boiled and then chlorinated to kill bacteria and microorganisms. This process ensures that the collected rainwater is safe to drink and it is connected to a glass container with capacity of 30 liters, which is used to store drinking and cooking water.

Each tank's inside is made of stainless steel, isolated with glass wool (the author proposes isolation to protect the system from high and low temperatures) and covered with durable plastic and has to be cleaned occasionally.

Each tank and glass container have minimal water level supply. Tanks and the glass container have sensors which measure water levels. Every time water level in any of the tanks or glass container comes to minimum or below, sensors send a refill signal to the preceding tank. For example, if water level in glass container is equal to or lower than 10 liters, the sensor sends a signal to the preceding third tank, which then refills the glass container. If water level in third tank equals to or is less then minimum, the sensor sends request to the second tank. After receiving the refill, decontamination process is started in the third tank.

2) Advantages and Disadvantages

The main advantage is that the system is automated in collecting, storing and transferring water to different points, as well as regulating levels of water in all containers. Apart from garden and toilet, boilers, washing machine, heating system are now connected to rainwater tanks, compared to the primitive RWHS, so practically, monthly use of water from the town's supply system would either be minimal, or equal to nothing, if the system would be self-sufficient. This would lead to lower water bill, since consumption would be very low or even zero cubic meters per month.

The automation has its perks. This type of RWHS would be expensive to implement, because it needs investments in specialized tanks and water level sensors. It would reflect on the electricity bill, unless it is powered by a solar collector, which has to be purchased. Another problem is decontamination process, because it is necessary to store chlorine.

Although this system can allow a household to become independent from a town's water supply system, because of droughts and clime changes it is advised to stay connected on a town's water supply system in case of rainfall shortages or malfunctioning of the proposed system.

IV. ICE&SNOW IN RIS HARVESTING SYSTEM

Countries worldwide are facing dramatic climate changes, droughts and variations in amount and frequency of rainfall; winters are colder, summers are hotter. In 2019, many countries have recorded highest temperatures in the last few decades.

Therefore, assuming that rain will be a secure source of freshwater for decades to come is a risky strategy. However, there are two more sources of fresh water that were not taken into consideration by previous researchers. The first source is hail and the second is snow. Both of these forms of freshwater can be harvested by

adopting the novel Rain,Ice&Snow harvesting system RIS-HS.

A. *Collecting Hail in RIS Harvesting System*

Collecting hail is identical in both, primitive and sophisticated RIS-HS. The process of collecting hail includes spreading shallow containers in the yard and let the hail melt. Afterwards, the collected water is filtered and bottled in primitive RIS, while water is transferred to the first tank in sophisticated RIS.

B. *Collecting Snow in RIS Harvesting System*

Collecting snow in a primitive RIS system includes pipelines and wavy roof extension, which will transfer snow into the designated containers. The water will, afterwards, be filtered and bottled.

However, collecting snow with a sophisticated RIS is a bit different. Apart from pipeline snow transfer during melting, it includes one more tank with capacity of 5,000 liters for collecting snow during winter. Therefore, instead of just letting the snow melt, RIS-HS transforms it into a valuable water reserve. This "zero" tank, is connected to the first tank via pipeline, so that the remaining tanks could be refilled according to current needs.

V. IMPLEMENTING SMARTH2OHOME IN AN INDIVIDUAL'S HOMESTEAD

The first step in transforming homestead in focus of this research in SmartH2OHome was to develop an energy management strategy, which would provide relatively permanent access to clean water and cost savings for the homestead, while still preserving water resources and decreasing stress on the town's water supply system, especially during droughts.

The second step was implementation of energy management strategy, which was conducted in three stages. The first stage included setting up the environment, the second stage included processes of collecting, filtering, storing and using atmospheric falls for various needs and the third stage included evaluation of achieved results.

A. *First stage of implementation*

In the first stage, conditions for collecting atmospheric falls had to be created, which meant small construction changes on the roof and in the yard.

Two important construction segments of the house are pipelines and wavy roof extension. Their role is to transfer atmospheric falls (rainwater, snow and hail) to containers used for soft water collection.

Additional shallow containers are used for collecting and melting hail. 30 to 20 liter containers are located below the wavy roof extension, while the pipeline ending is located above a 100 liter container.

Both parts of construction are used for preservation of atmospheric falls, instead of generating a massive loss of soft water resources. Containers, wavy roof extension and pipelines have to be cleaned regularly, to prevent soft water contamination. When not in use, containers should be closed and stored inside.

B. *Second stage of implementation*

In the second stage, collected atmospheric falls are bottled, filtered and removed from the sunlight, because algae formation will limit the use of soft water.

PET bottles are used for storing soft water, because they were declared safe by the FDA and are already in the individual's possession. When bottles are filled, soft water is being filtered, to prevent debris from contaminating the water.

Soft water is used both for indoor and outdoor purposes. Indoor utilization of soft water in the observed home includes toilet, shower, dishwashing and hand washing.

Toilets are disconnected from the town's water supply system. Filtered soft water is used to prevent e.g. leafs or other debris from clogging the sewage.

Showers are also disconnected from the town's water supply system. Dishwashing is done manually (dishwasher is not used in the observed home) with soft water and soft water is also used for hand washing – town's water supply system is also eliminated. Soft water is filtered from debris to eliminate contamination and sewage clogging for these purposes as well.

Heating system and washing machine are not using soft water in the observed household – they are connected to the town's water supply system. Drinking and cooking water is provided from the town's water supply system. The home does not have air condition.

In the observed homestead, the individual is growing fruits, vegetables and plants and is completely independent of the town's water supply system and soft water used for this purpose is not filtered (outdoor usage).

C. Third Stage of Implementation

In the third stage, progress of the SmartH2OHome concept implementation in the observed home is monitored and evaluated. This system is in use since 2011 and the results will be presented in this chapter.

Firstly, this home already has an appropriate construction for collecting atmospheric falls, so no additional costs related to purchasing and mounting wavy roof expansion were generated.

Secondly, PET bottles for storing soft water are used, because drinks in stores are kept in this type of package, so basically, these bottles are free and are even changed after several usages. This is also beneficial for the environment, because bottles are reused several times and then sent to recycling.

Thirdly, containers for collecting soft water varied in capacity and their number has increased over the observed 8 years. Some of the 30 liter containers were bought as well as the 100 liter container. All purchases were affordable, so containers created insignificant cost.

Fourthly, toilet is refilled with soft water, so every flush saves 20 liters from the town's water supply system and decreases water bill significantly. E.g. if a person flushes 5 times a day, 30 days a month and with the current price of 123.2 dinars per cubic meter of water, cost savings will be 4,453,2 dinars per person per year. For 8 years, cost savings per one person is 35,481.6 dinars. For a family of four during 8 years, this cost savings will be 141,926.4 dinars.

Investing in a primitive RIS Smart H2OHome is feasible, because cost savings reflected through monthly water bill are higher than costs related to acquiring necessary equipment and changes in a home's construction

When water needs for showering, dishwashing, hand washing, gardening and growing fruit and vegetables are taken into consideration, cost savings generated by the primitive RIS in SmartH2OHome are measured in tens, even hundreds of thousands of dinars and will continue to rise in the future.

One of the key characteristics of this system is transformation of certain amount of soft water into supplies, which is important during years with low level of rainfall. Collecting rain and hail has contributed to the stability of soft water supplies.

This enables the homestead to be relatively independent from the town's water supply system – water is only used for drinking, cooking, washing machine and heating system. Very often it is 1 cubic meter, or 2 (which is determined by the number of washing cycles and number of boiler refill). The monthly water bill is between 220 and 350 dinars. Huge benefit for the town's water supply system is significantly lower water consumption from the observed homestead, which is of great importance during drought.

VI. DISCUSSION

Water is an important element of the living world. With the rapid development of industry, agriculture and irresponsible human behavior, many water sources have been polluted and thus unusable for swimming, let alone drinking.

Many people do not have access to clean drinking water and human actions have disrupted the natural chain in the Earth's ecosystem.

With the growing population, water stress on many countries' water supply system is higher every year. For decades, scientists have been searching for new sources of water and best ways to exploit them. As a result, rainwater harvesting system has been proposed and implemented.

One of the main problems with RWHS was frequency and the amount of rainfall. Other problem was economic feasibility of these RWHS.

In this paper, the author gives alternatives for solving these two problems. First problem was solved by introducing two more types of falls: hail and snow. The second problem was solved by creating a primitive, low cost system.

The primitive system RIS has been designed for collecting rain, hail and snow and has been implemented in a ground-level household in the summer of 2011 and is still in use in 2019. The most important advantage was decrease in monthly water bills (some water consumers were completely eliminated e.g. garden, toilet,

and shower) as well as the elimination of rainfall dependency, due to the incorporation of two new freshwater sources: hail and snow.

But there were two main disadvantages: some water consumers like washing machine and heating system could not use rainwater, (because that would need additional investments, and the goals is that this system stays affordable) and everything has to be manually done, which is sometimes tedious and time consuming.

The sophisticated system RIS SmartH2OHome has also been designed. This system, if implemented, would not be solely dependent of rainfall, but could also form water supplies from hail and snow. Huge advantage of this system is that it can enable water self-sufficient household, with high level of automation. However, acquiring a system of this magnitude is very expensive for now and the primitive RIS does what it is supposed to and it is also cheap.

VII. Conclusion

Rainwater harvesting systems have been in focus of scientific research, because rain is a free freshwater source that can be collected, stored and used in various ways. These systems depend on frequency and amount of rainfall and the more sophisticated they are, the more expensive they get.

The author has designed primitive and sophisticated Rain, Ice & Snow harvesting systems and has implemented the primitive RIS SmartH2OHome in a ground-level household. By enabling collection of not just rain, but hail and snow as well, the system is less dependent of rainfall.

Although gardening, growing fruit and vegetables, toilet, shower, dishwashing and hand washing were covered, this system has led to decreased water bill –generally monthly usage is 1 cubic meter. Depending on the frequency of usage of washing machine and number of boiler refills it can rise to 2 cubic meters).

There are two major disadvantages – RIS SmartH2OHome does require human intervention in collecting, filtering, storing and using soft water and some water consumers e.g. washing machine are not incorporated into the system.

The sophisticated RIS, although enabling even complete water self-sufficiency, is very costly. However, the author believes that technology necessary for its development will become affordable and will enable successful and feasible implementation of the sophisticated RIS SmartH2OHome in the future.

References

[1] USGS.gov (2019). *How Much Water is There on Earth?*. Available at: https://www.usgs.gov/special-topic/water-science-school/science/how-much-water-there-earth?qt-science_center_objects=0#qt-science_center_objects.

[2] Nrdc. (n.d.). Available at: https://www.nrdc.org/stories/water-pollution-everything-you-need-know

[3] Unesdoc digital library (n.d.). Available at: https://unesdoc.unesco.org/ark:/48223/pf0000367303

[4] A.E.P. Abas and T.M.I. Malia, "Techno-Economic and Sensitivity Analysis of Rainwater Harvesting System as Alternative Water Source", Sustainability vol. 11, 2019.

[5] Y. Dumit Gómez and L.G. Teixeira, Residential rainwater harvesting: Effects of incentive policies and water consumption over economic feasibility. Resour. Conserv. Recycl. vol. 127, 2017, pp. 56–67.

[6] K.E. Lee, M. , Mokhtar, M.M. Hanafiah, A.A. Halim and J. Badusah, "Rainwater harvesting as an alternative water resource in Malaysia: Potential, policies and development", J. Clean. Prod. vol. 126, 2016, pp. 218–222.

[7] A. Campisano, C. Modica, "Optimal sizing of storage tanks for domestic rainwater harvesting in Sicily", Resour. Conserv. Recycl. vol. 63. 2012.

[8] M. Ozcelik, G. Sarp, "Evaluation of sustainable water supply alternatives in karstified rock masses using GIS and AHP methodology for Antalya (Turkey) urban area", Environ. Earth Sci. vol. 77, 2018.

[9] J. Berbel, C. Gutierrez-Marín, A. Expósito, "Impacts of irrigation efficiency improvement on water use, water consumption and response to water price at field level", Agric. Water Manag. vol. 203, 2018, pp. 423–429.

[10] Y. Zhang, A. Grant, A. Sharma, D. Chen, L. Chen, "Alternative water resources for rural residential development in Western Australia", Water Resour. Manag. vol 24, 2009.

[11] A. Rahman, "Recent advances in modelling and implementation of rainwater harvesting systems towards sustainable development", Water 2017.

[12] D.P.S. Terêncio, L.F.S. Fernandes, R.M.V. Cortes, F.A.L. Pacheco, "Improved framework model to allocate optimal rainwater harvesting sites in small watersheds for agro-forestry uses", J. Hydrol. vol 550, 2017, pp. 318–330.

Electricity Storage in the Optimization of Energy Supply Systems

Caio Tácito Miranda Castro Bezerra de Melo[1], Monica Carvalho[2], Alberto J. Romero[2]

[1]Graduate Program in Mechanical Engineering, Federal University of Paraíba, João Pessoa, Brazil, caiotcastro@gmail.com
[2]Department of Renewable Energy Engineering, Federal University of Paraíba, João Pessoa, Brazil, monica@cear.ufpb.br
[3]Université Libre de Bruxelles, Bruxelles, Belgium, aromerof@ulb.ac.be

Abstract — **The study presented herein introduces electricity storage within a mathematical model based on Mixed Integer Linear Programming that optimizes the energy supply to a tertiary sector building located in Northeast Brazil. The energy demands considered were electricity, hot water, steam, and cooling. The study extended over one year, and each month was represented by two 24-hour representative days. A superstructure was built to include all possibilities of energy conversion pathways and technologies, along with economic and legal data. The model was solved to minimize the total annual costs, which included capital costs and operational costs. The results demonstrated the economic benefits of incorporating renewable energy sources in the energy mix. The optimal economic solution installed 200 photovoltaic panels and utilized biomass to drive boilers, but did not install electricity storage. A sensitivity analysis verified that electricity storage was only installed when its variable costs were reduced by almost 70 %. Although capital costs were higher for the optimized energy system, these were annuitized and added to operation costs, which yielded a total annual cost that was 22% lower than a reference system based on conventional equipment.**

Keywords - electricity storage, optimization, linear programming, solar energy, biomass.

I. INTRODUCTION

In the context of distributed energy resources, energy storage can play an important role, although the high capital costs are a disincentive to their adoption. It is widely accepted that energy storage is the appropriate complement to the uncertainties associated with renewable energy, so that surplus energy can be stored and consumed later when its use or cost is more beneficial [1-4].

Energy storage is not only beneficial when addressing renewable energy [5]. Regarding electricity, it is also vital to improve the stability and quality of the grid, as well as regulate voltage and frequency when electric generators cannot accommodate sudden load changes. Electricity storage also improves the overall efficiency of cogeneration plants with non-simultaneous heat and energy demands.

In contrast, the variability and intermittency of renewable energy sources still hinder their widespread adoption [6], and storage and transportation solutions still not straightforward. This complexity, which is inherent to spatial and temporal interdependencies, is a significant challenge in the synthesis of renewable energy systems and interferes with the adaptation to distribution systems. Energy storage systems are therefore employed to stabilize and help intermittent renewable technologies become more competitive.

Due to the high degree of integration and coupling, determining the optimal configuration and design of a polygeneration energy system is quite a challenging task, and there are still complex problems that have not been adequately confronted as of yet [7, 8], such as the integration with renewable energy technologies and energy storage. This will open up new opportunities for benefit and realized value, in the form of lower costs of energy supply for buildings, through the utilization of indigenous energy resources. Integration of storage technologies into the energy supply optimization process may introduce less constraint into the

ISBN: 978-86-80616-04-9

resulting energy supply system and consequently could lower energy supply cost, carbon emissions, or both. Many of the technical challenges in reformulating the mathematical optimization procedures to accommodate intermittent and variable renewable energy supply utilities may be reapplied in consideration of energy stores acting as energy supply components. For energy supply infrastructure connected consumers (grid-connected), energy storage facilities may offer substantial savings in exploiting the terms of supply tariffs.

The multifaceted nature of polygeneration systems (multiple energy resources, multiple energy products, and multiple technology options) requires a design procedure that provides flexible, efficient, and reliable energy systems. The project is even more complicated as new factors are taken into account, such as the regulation of energy exchanges with the grid, decreasing capital costs of photovoltaic panels and solar thermal collectors, subsidies for the implantation of renewables, and the increase of biomass availability [5].

The objective of this study is to adapt a model of electric storage and introduce it within a mathematical model based on Mixed Integer Linear Programming (MILP) that optimizes the supply of energy (in all forms) to a tertiary sector building.

II. METHODOLOGY

MILP is an example of mathematical programming that utilizes binary and integer variables to express quantity, decision, and logical relations. MILP can tackle the inherent complexity of optimizing polygeneration systems, and consists of three steps [9]:

- Establishment of a superstructure of available equipment and resources (representation of all possible alternatives). The choice of appropriate technologies depends on the need for different forms of energy (electric or thermal), available resources, existing demands, and current legislation;
- Formulation of a mathematical model that represents all possible forms of operation through discrete variables and that uses continuous variables to represent flows;
- Determination of the optimized solution, from the resolution of the mathematical model.

A. Demands, tariffs, energy utilities, and technologies

The case study is a 420-bed hospital, with an area of 49.000 m^2, located in João Pessoa, Northeast Brazil. The energy demands considered were electricity, hot water, steam, and refrigeration. The study extended over one year, where each month was represented by two typical days (working day and weekend), each divided into 24 hourly periods, resulting in 576 different operation periods. The annual energy demands are 2791 MWh for electricity, 1947 MWh for hot water (direct use and laundry), 138 MWh for steam (sterilization), and 2309 MWh for cooling.

Real data for electricity was used. Calculation of hot water and cooling demands utilized the degree-day method [10] along with climatic [11], occupancy [12], and energy auditing [13] data. Steam demand was considered constant during the operation period of the sterilization facility, between 6 am and 8 pm, with the contribution of a thermal counter in the restaurant during lunch and dinner hours. The demand for hot water has two contributors: the laundry, which operates between 8 am and 6 pm, and internal hospital use, without interruptions 24 hours.

The superstructure (Fig. 1) contains all the energy supply possibilities available on the site as well as energy conversion possibilities and demands.

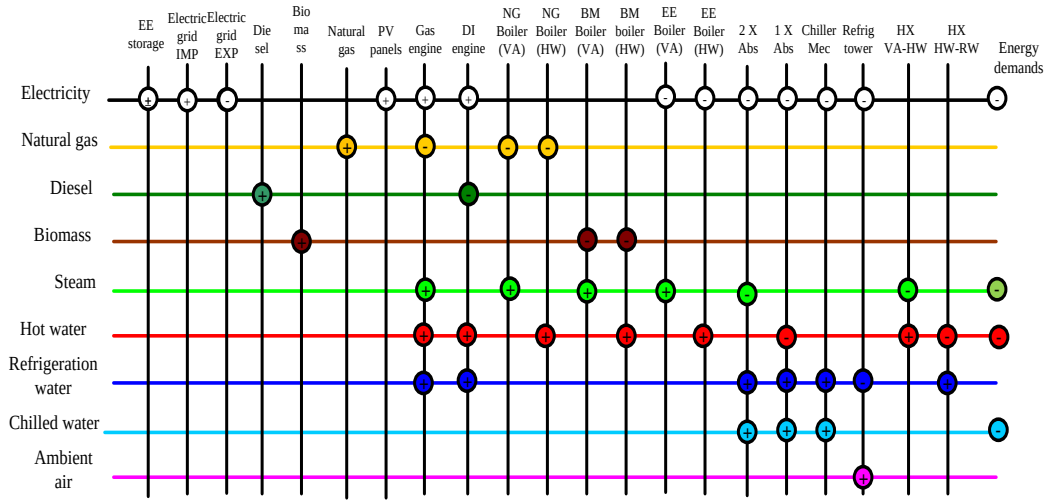

Figure 1 Superstructure for the studied polygeneration system (adapted from [14].).

The energy utilities (*j* index in the optimization model) available for purchase on site are electricity (EE), which can also be exported to the grid, natural gas (NG), biomass (BM) and diesel (DI). The intermediate forms of energy (also energy utilities) are steam (VA), hot water at 90ºC (AQ), refrigeration water (t_0 + 5ºC) (AR), and chilled water at 5ºC (AF). The ambient air (AA) is at t_0°C.

Tab. 1 and 2 show the technical and economic characteristics of the selected equipment to be part of the superstructure. In the optimization model, the index *i* refers to the equipment. The technical information was obtained from the manufacturers' catalogs, and their prices were obtained through direct consultation. Tab. 1 presents an energy balance of the production of each equipment, where positive and negative coefficients indicate, respectively, that the flow is produced or consumed. The bold number defines the energy flow that characterizes the equipment (the other coefficients were normalized).

As all technologies and equipment considered in the optimization are commercially available, the size and configuration of the system were determined in terms of quantities of equipment. Installation of multiple pieces of equipment of the same technology presents the advantage of modularity, especially regarding the commercial sector, providing flexibility to cover highly variable energy demands - daily and seasonal - with high efficiency. Also, the availability of energy supply is enhanced in case of equipment failure, and maintenance can be programmed for periods when power demand is lower, and some equipment is not in operation.

The current electricity tariff (2019) currently considers a value throughout the day (R$ 190/MWh), with a different "tip" time, between 18h and 21h (R$ 298/MWh) [15]. The natural gas tariff has a fixed value (R$ 398/MWh) [16]. The tariff considered for diesel (R$ 290/MWh), and the costs of installing diesel-powered equipment already include storage tanks. Biomass is a locally available energy resource, and here we chose to use sugarcane bagasse (R$ 52/MWh).

The solar energy resource considered herein is restricted to photovoltaic panels (1.64 m² each) for the production of electricity, following to the legal scenario established by the Brazilian Electricity Agency (ANEEL) [17], which enables the exports of self-generated electricity. In this way, the system was designed to interact with the electricity also through the exports of self-generated electricity, considering the credit compensation scheme established by ANEEL.

Regarding the economic and financial scenario, considering a 15-year lifetime for the system and an interest rate of 10 % y^{-1}, a depreciation factor (FAM) of 0.13 y^{-1} was obtained.

B. Mathematical model

The problem to be solved consists of two simultaneous steps: selection of equipment and operation mode during each of the defined time intervals, throughout the year.

Integer variables are employed for the determination of the number of equipment installed, and continuous variables represent energy, economic and environmental flows.

An economic objective function was defined to consider capital costs, purchase of energy utilities, and maintenance and operating costs. The solved employed in the optimization procedure was LINGO [18].

TABLE I. EQUIPMENT AVAILABLE FOR OPTIMIZATION: PRODUCTIVE DATA (ADAPTED FROM [19]).

	Technical production coefficients									
	Solar	GN	BM	DI	VA	AQ	AR	AA	AF	EE
Gas engine		-2.66				1.10	0.45			**1**
Diesel engine				-2.66		0.80	0.50			**1**
Steam boil (GN)		-1.18			**1**					
Steam boil (BM)			-1.40		**1**					
Steam boil (EE)					**1**					-1.15
HX (VA-AQ)					-1.10	**1**				
Hot water boil (GN)		-1.22				**1**				
Hot water boil (BM)			-1.25			**1**				
Hot water boil (EE)						**1**				-1.11
HX(AQ-AR)						-1.10	**1**			
Absorption chil (2x)					-0.77		1.77		**1**	-0.01
Absorption chil (1x)						-1.32	2.32		**1**	-0.01
Mechanical chiller							1.22		**1**	-0.22
Cooling Tower							-1.00	**1**		-0.02
Photovoltaic panels	6.67									**1**

TABLE II. EQUIPMENT AVAILABLE FOR OPTIMIZATION: ECONOMIC DATA (ADAPTED FROM [19]).

	Equipment		
	Cost CINV (10^3R$)	Cost O&M (R$/MWh)	Nom. Power PNOM (MW)
Gas engine	463.00	15.00	0.41
Diesel engine	227.00	15.00	0.40
Steam boil (GN)	47.90	2.00	0.30
Steam boil (BM)	51.00	8.00	0.25
Steam boil (EE)	42.50	2.00	0.15
HX (VA-AQ)	8.90	2.00	0.40
Hot water boil (GN)	49.30	2.00	0.30
Hot water boil (BM)	62.50	8.00	0.17
Hot water boil (EE)	28.20	2.00	0.15
HX(AQ-AR)	7.40	2.00	0.40
Absorption chil (2x)	465.20	10.00	0.45
Absorption chil (1x)	539.70	10.00	0.49
Mechanical chiller	217.40	4.00	0.27
Cooling Tower	28.00	10.00	1.00
Photovoltaic panels	1735.00	-	0.25

The economic objective was defined to consider the annual cost minimization, which includes fixed costs (capital costs) and variable costs:

$$Annual\ Cost = \left(Fixed\ costs\right) + \left(Variable\ costs\right), \quad (1)$$

$$Fixedcosts = FAM \cdot \left[\left(FCI \sum iCINV\_i\right) + Cost\ of\ PV\ panels + Cost\ of\ storage\right], \quad (2)$$

$$Variable\ Costs = \left(Cost\ of\ natural\ gas\right) + \left(Cost\ of\ electricity\ imports\right) - \left(Credit\ due\ to\ electricity\ exports\right) + \left(Cost\ of\ diesel\right) + \left(Cost\ of\ biomass\right) + \left(Operation\ and\ Maintenance\right). \quad (3)$$

$CINV_i$ is the number of equipment installed for each technology i multiplied by the individual cost, FAM is the depreciation factor, and FCI accounts for indirect costs involved in transportation, assembly, installation, supervision, engineering, service charges, and contingency, totaling 15 % of equipment investment costs. These costs are already included for solar panels and electricity storage.

In (2), the cost of storage is expressed as:

$$\left(Cost\ of\ storage_{ee}\right) = \left(Fixed\ cost\right)_{sto\ ee} + \left(Variable\ cost\right)_{sto\ ee}, \quad (4)$$

$$\left(Fixed\ cost\right)_{sto\ ee} = BSTEE \cdot c_{fix}\ , \qquad (5)$$

$$\left(Variable\ cost\right)_{sto\ ee} = STEE \cdot c_{\text{var}}\ . \qquad (6)$$

Equation (4) is linear and includes a fixed cost that is independent of the size of the battery bank to be installed and grows according to the variable cost, which depends mostly on the installed storage capacity.

Equation (5) defines the fixed cost of storage from the binary variable BSTEE, which defines the presence or not of electrical energy storage systems. BSTEE is multiplied by the cost of installation of the battery bank C_{fix} , which includes inverters,

With consideration of electricity storage, the energy balances for each equipment (*i*) and energy resource (*j*) in a given interval affect the subsequent intervals. In general, for each period of time, energy production is restricted to installed capacity, and the energy balance for each utility is obeyed:

$$\begin{aligned} &Production_j - Consumption_j + \\ &+Purchase_j - Demand_j - Surplus_j = 0 \end{aligned}\ . \qquad (7)$$

For electricity ($j = ee$) , the balance is modified to contemplate photovoltaic panels and storage:

$$\begin{aligned} &Production_{ee} - Consumption_{ee} + \\ &+Purchase_{ee} - Export_{ee} - \\ &-Demand_{ee} + EEPV_{ee} \pm Storage_{ee} = 0 \end{aligned}\ . \qquad (8)$$

The term EEFV includes considers the radiation absorbed by the installed panels, and thus (8) contemplates the possibility that electricity from photovoltaic panels (EEFV) can be used by the energy system. Thus, regarding electricity, there is the possibility of production above demand or below demand in each period of time, generating charge and discharge flows in the battery bank. The flow is considered negative when energy is being stored (charge), and positive when the battery bank is drawn upon (discharge). Fig. 2 shows the possibilities of electricity flows in the system, including storage.

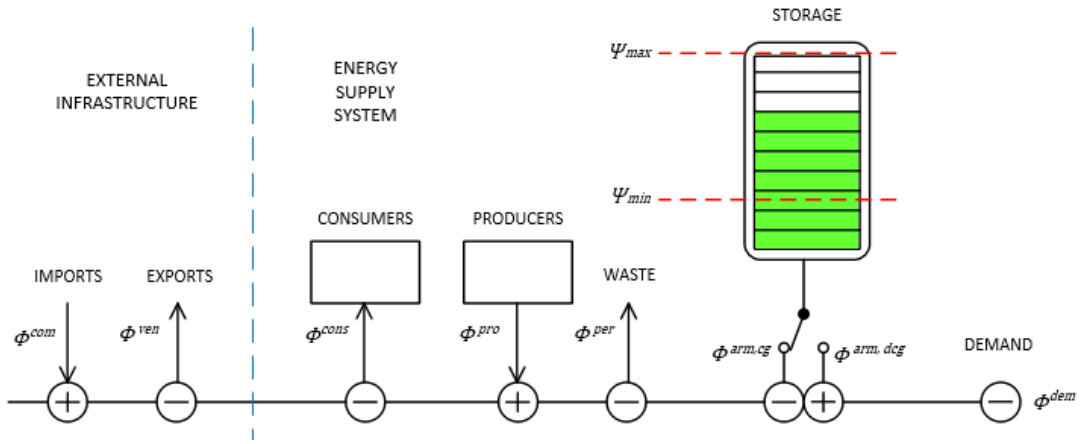

Figure 2 Storage scheme implemented in the optimization module (Translated from [2]).

The energy balance shown in Fig. 2 refers (8). Equations (9) – (13) indicate charge and discharge parameters of the storage system. Φ refers to energy flows, and the indices *arm*,*cg*, and *arm*, *dcg* refer to charge and discharge flows, respectively.

$$\phi_{u_{ij}}^{arm} = \phi_{u_{ij}}^{arm,cg} - \phi_{u_{ij}}^{arm,dcg}\ . \qquad (9)$$

$$\phi_{u_{ij}}^{arm} \le \delta_{u_{ij}}^{arm} \cdot HS_u\ . \qquad (10)$$

$$\phi_{u_{ij}}^{arm} \le -\left(1 - \delta_{u_{ij}}^{arm}\right) \cdot HS_u\ . \qquad (11)$$

$$\phi_{u_{ij}}^{arm,cg} \leq \phi_{u,\max}^{arm,cg} \quad . \tag{12}$$

$$\phi_{u_{ij}}^{arm,dcg} \leq \phi_{u,\max}^{arm,dcg} \quad . \tag{13}$$

Equation 9 is introduced to avoid non-linearity as the directions of the charge and discharge flows have different efficiencies, which require the definition of two different variables for the loading and unloading flows.

The values of these variables cannot be simultaneously higher than 0 and therefore, (10) and (11) are introduced, where $\delta_{u_{ij}}^{arm}$ is a binary variable that indicates the direction of flow (load 1, discharge 0) and HS_u is an integer, one order of magnitude higher than $\phi_{u_{ij}}^{arm}$.

HS_u is introduced to avoid non-linearity if a single decision variable is employed. The maximum flow and charge flow constraints are expressed in (12) and (13). $\phi_{u,\max}^{arm,cg}$ is the maximum charge rate that can be transferred to storage in a time interval.

$\phi_{u,\max}^{arm,cg}$ is defined as a fraction of the storage capacity $\left(\Psi_{\max}\right)$, which was called *STEE* in (6). The same applies to $\phi_{u,\max}^{arm,dcg}$ for the maximum discharge rate.

The optimization model compares all possible ways (within the superstructure) to meet the hospital's energy demands, either directly or through simple or multiple energy conversions, hour-by-hour, throughout the year, obtaining costs for each possible configuration and operation mode. Therefore all economic balances for all viable configurations contained in the superstructure are compared, yielding as a final result the minimum annual cost (optimal configuration and the optimal operation mode).

III. RESULTS AND DISCUSSION

A reference system was defined, where energy demands were satisfied conventionally, excluding the possibilities of cogeneration and the use of renewable energy sources. The economic optimal was obtained by solving the optimization model, minimizing the annual cost, with free selection of technologies. Regarding the PV panels, the area available at the hospital facility is sufficient for the installation of 200 panels, and priority is given to the installation of solar energy, which is then adjusted in function of the adjusted capacity. Tab. 3 shows the configuration and energy flows for the reference system and the economic optimal.

Tab. 3 shows that the reference configuration for the energy system relies on the installation of conventional equipment: an electric boiler producing steam, four electric boilers producing hot water, a hot steam-water heat exchanger, three mechanical chillers, and a cooling tower to evacuate excess heat. This system imports 5676 MWh of electricity from the grid annually and has a total annual cost of R$ 1,342,525.

When removing all restrictions on equipment installation, and leaving the optimization model free to minimize the total annual cost, the optimal solution benefits from a less traditional configuration. The optimal economic system employs biomass (2635 MWh/year) for the operation of a steam boiler and three hot water boilers. The system also includes the installation of 200 photovoltaic panels, covering part of the electricity demand (129 MWh), maintaining three mechanical chillers and a cooling tower, with a total annual cost of R$ 1,050,598.

There was an increase in capital cost (55.20 %), equivalent to R$ 536,107 in the optimal economic system, but there is a considerable annual benefit when considering the values of energy: with free choice of technologies and possibilities of using solar energy and biomass, R$ 291,947 is saved per year regarding energy resource acquisition and system operation and maintenance costs. This represents approximately -21.75 % in comparison with the reference system.

There was an increase in capital cost (55.20 %), equivalent to R$ 536,107 in the optimal economic system, but there is a considerable annual benefit when considering the values of energy: with free choice of technologies and possibilities of using solar energy and biomass, R$ 291,947 is saved per year regarding energy resource acquisition and system operation and maintenance costs. This represents approximately -21.75 % in comparison with the reference system.

The optimal economic solution did not include electricity storage, which was inserted in the optimization model to compensate, to some extent, for the characteristics of renewable energy sources (variability and intermittency). A sensitivity analysis verified that electricity

TABLE III. SOLUTIONS FOR THE REFERENCE SYSTEM AND THE ECONOMIC OPTIMAL.

	Reference system	Economic optimal
Composition of system	Number (installed power)	Number (installed power)
Steam boil (BM)	0 (0 MW)	1 (0.250 MW)
Steam boil (EE)	1 (0.150 MW)	0 (0 MW)
HX (VA-HW)	1 (0.400 MW)	1 (0.400 MW)
Hot water boil (BM)	0 (0 MW)	3 (0.510 MW)
Hot water boil (EE)	4 (0.600 MW)	0 (0 MW)
Mechanical chiller	3 (0.810 MW)	3 (0.810 MW)
Cooling Tower	1 (1.000 MW)	1 (1.000 MW)
Photovoltaic panels	--	200 units
Storage (EE)	--	0 MWh
Electricity imports	5676 MWh/year	3226 MWh/year
Biomass imports	0 MWh/year	2635 MWh/year
Capital costs	R$ 971,060	R$ 1,507,167
Annual cost of electricity imports	R$/year 1,174,722	R$/year 663,451
Annual cost of biomass imports	R$/year --	R$/year 137,045
Operation and maintenance costs	R$/year 41,585	R$/year 54,170
Annual cost of equipment*	R$/year 126,238	R$/year 195,932
TOTAL annual cost	**R$/year 1,342,545**	**R$/year 1,050,598**

* system lifetime 15 years, interest rate 10 %

storage was only installed when its variable costs were reduced by almost 70 %. The configuration of the optimal economic system was not very different from the conventional system (electric boilers were substituted by biomass boilers).

However, total annual costs were 22 % lower. Although the system is connected to the electric grid, surplus electricity was never exported to the grid.

In the current economic scenario, only extremely low prices for natural gas (half the current price) and diesel (around 30 % of the current price) led to the utilization of these fuels to drive cogeneration modules. Likewise, photovoltaic panels are only included spontaneously in the optimal configuration when capital costs are reduced by more than half (to values around R$ 944.10) or when the tariff of electricity imported from the grid increases considerably.

IV. CONCLUSION

Energy storage systems were considered herein as controllable, yet intermittent and variable generation technologies on the supply side of the system balance and also as dispatchable loads on the demand side of the system balance. The incorporation of storage equipment and renewable energies required the development of a more complex and specific model. Considering complementary or competing uses of renewable and stored energy increased the size of the optimization model significantly.

This study demonstrated the economic benefits of incorporating renewable energy sources in an optimized energy supply system. The ideal economical solution installed 200 photovoltaic panels and used biomass to power the boilers, but did not install electricity storage. When comparing the optimal economic solution with the reference system, the main modification the utilization of biomass boilers instead of electric boilers (benefiting from the technical and economic feasibility of this energy resource, considered very cheap and able to meet the energy demands).

Although the optimal economic solution presented higher capital costs, its total annual cost was 22 % lower than the reference system, based on conventional equipment.

This work can be extended by adding more equipment to the superstructure, such as biomass turbines, which could take advantage of the low price of the resource for the generation of electricity and steam, and diesel boilers for the generation steam and hot water. The use of solar collectors for the generation and accumulation of heat can also be incorporated. Another perspective to expand this work includes the consideration of environmental criteria, incorporating life cycle assessment to formulate and quantify reasonable environmental criteria, and thus identify which polygeneration systems are less aggressive to the environment.

ACKNOWLEDGMENT

CNPq (National Council for Scientific and Technological Development - Research Productivity Grant, nº 307394/2018-2), CAPES (Coordination for the Improvement of Higher Education Personnel – PhD. Scholarship), and the BATWAL project, funded by the Walloon Region (Belgium).

REFERENCES

[1] T. Kousksou, P. Bruel; A. Jamil, T. El Rhafiki, Y. Zeraouli, „Energy storage: Applications and challenges,“ Solar Energy Materials & Solar Cells, vol. 120, 2014, pp. 59 – 80.

[2] A. Romero, Optimal design and control of mine site energy supply systems. PhD Thesis (Faculty of Graduate Studies), Laurentian University, Sudbury, 2016.

[3] G. Zubi, R. Dufo-López, M. Carvalho, G. Pasaoglu, „The lithium-ion battery: State of the art and future perspectives,“ Renewable and Sustainable Energy Reviews, vol. 89, 2018, pp. 292-308.

[4] R. Fernandez, R. Chacartegui, A. Becerra, B. Calderon, M. Carvalho, „Transcritical Carbon Dioxide Charge-Discharge Energy Storage with Integration of Solar Energy,“ Journal of Sustainable Development of Energy, Water and Environment Systems, vol. 7, no. 3, 2019, pp. 444-465.

[5] E. A. Pina, M. A. Lozano, L. M. Serra, „Opportunities for the integration of solar thermal heat, photovoltaics and biomass in a brazilian hospital,“ In: international conference on solar energy for buildings and industry, 12., Rapperswil, Suiça. Proceedings… Rapperswil: HSR University of Applied Science, 2018.

[6] M. Carvalho, D. Delgado, „Potential of photovoltaic solar energy to reduce the carbon footprint of the Brazilian electricity matrix,“ LALCA-Revista Latino-Americana em Avaliação do Ciclo de Vida, vol. 1, no. 1, 2017, pp. 64-85.

[7] A. Romero, M. Carvalho, D. L. Millar, „Optimal design and control of wind-diesel hybrid energy systems for remote Arctic mines,“ Journal of Energy Resources Technology, vol. 138, no. 6, 2016.

[8] D. Delgado, M. Carvalho, L. M. C. Junior, R. Abrahão, R. Chacartegui, „Photovoltaic solar energy in the economic optimisation of energy supply and conversion,“ IET Renewable Power Generation, vol. 12, no. 11, 2018, pp. 1263-1268.

[9] I. E. Grossman, J. A. Caballero, H. Yeomans, „Advances in mathematical programming for the synthesis of process systems,“ Latin American Applied Research, vol. 30, no. 4, 2000, pp. 263-284.

[10] D. G. Erbs, S. A. Klein, W. A. Beckman, „Estimation of degree-days and ambient temperature bin data from monthly-average temperatures,“ ASHARE Journal, vol. 25, no. 6, 1983, pp. 60-65.

[11] Climaticus 4.2 - *Software version beta. Database of climate data.* Available at: <www.usp.br/fau/pesquisa/laboratorios/labaut/conforto/Climaticus_4_2.xls>, 2019.

[12] M. H. A. Nepote, I. U. Monteiro, E. Hardy, „Association between surgery indices and occupation rates of a surgical center,“ Rev. Latino-Am. Enfermagem, vol. 17, no. 4, 2009.

[13] M. M. D. Araújo, Methodological contribution to the exergy diagnosis of terhaml and electrical systems-study case at the Lauro Wanderley University Hospotal, Dissertation (MSc. in Mechanical Engineering) – Federal University of Paraíba, João Pessoa, 2004.

[14] M. Carvalho, D. L. Millar, „Concept development of optimal mine site energy supply,“ Energies, vol. 05, 2012, pp. 4726–4745.

[15] Energisa, 2018. *Electricity tariffs*. Available at: <https://www.energisa.com.br/empresa/Paginas/pequenas-e-medias-empresas/taxas-prazos-e-normas/tipos-tarifas.aspx>, 2019.

[16] PBGÁS – *Gas Company of Paraíba*. *Tariffs*. Available at: <http://www.pbgas.com.br/?page_id=1477>, 2019.

[17] ANEEL (BRAZIL). *Resolution nº687, of November 24, 2015. Establishes the general conditions for the access of distributed microgeneration and minigeneration, the electricity compensation system, and gives other providences.*

[18] Diário Oficial da União: seção 1, Brasília, DF, n. 230, p. 45, 2 dezembro 2015. Available at: <http://www2.aneel.gov.br/cedoc/ren2015687.pdf 2019.

[19] LINGO. *Lingo: the modeling language and optimizer*, 2019. <http://www.lindo.com>, 2019.

[20] B. C. T. Carvalho, C. T. M. C. B. Melo, M. Carvalho, „Multicriteria optimization of the energy supply for a northeast Brazil hospital, considering solar photovoltaic energy,“ in Congresso Brasileiro de Engenharia Mecânica, 24, 2017, Curitiba. Proceedings […]. Curitiba: ABCM, 2017.

Experimental Investigation of SiO_2/Thermal Oil Nanofluid Application in a Cylindrical Cavity Receiver

Reyhaneh Loni[1], Gholamhassan Najafi[1], Saša Pavlović[2], Velimir Stefanović[2], E. Askari Asli-Ardeh[3], Barat Ghobadian[1]

[1]Department of Mechanic of Biosystems Engineering, Tarbiat Modares University, Tehran, Iran, loni@modares.ac.ir; g.najafi@modares.ac.ir; ghobadib@modares.ac.ir

[2]Faculty of Mechanical Engineering, Thermal Engineering Department, University in Nis, Nis, Serbia, sasa.pavlovic@masfak.ni.ac.rs; veljas@masfak.ni.ac.rs

[3]Department of Mechanic of Biosystems Engineering, University of Mohaghegh Ardabili, Ardabil, Iran, ezzataskari@uma.ac.ir

Abstract — **In this study, a parabolic dish concentrator using a cylindrical cavity receiver was experimentally investigated. The effect of nanofluid application as the solar working fluid was studied in this research. The nanofluid of SiO2/thermal oil was examined in concentration of 0.8% Volume Fraction (VF) and volume flow rate of 10 ml/s. The designed experimental setup was included a parabolic dish concentrator, cavity receiver, and hydraulic circuit system. The main aim of this study was experimentally investigated the thermal performance of the cylindrical cavity receiver using silica/thermal oil nanofluid. The results indicated that the receiver heat gained and the thermal efficiency had a similar trend compare to the difference temperature. Finally, it was resulted that the application of the silica nanofluid didn't have an effective influence for improving the thermal performance of the investigated cylindrical cavity receiver compare to the pure thermal oil. Consequently, the application of the pure oil is recommended as the solar working fluid of the cylindrical cavity receiver instead of the silica/thermal oil nanofluid due to its less cost.**

Keywords - experimental study, silica/thermal oil nanofluid, cylindrical cavity receivers, thermal performance

I. INTRODUCTION

One effective solution for reducing alleviating environmental problems due to fossil fuel consumption such as emissions of CO, CO_2, global warming, and ozone depletion is application of renewable energy technologies. Solar energy is a kind of the renewable energy. The hourly solar irradiation on the Earth's surface being greater than all of the human consumption of energy in a year [1]. The concentrator solar collector as an efficiently type of solar collector, can concentrate, absorb and convert the solar radiation to heat. In the recent years, the researchers have increased on the concentrated solar energy systems as a high-quality technology [2]. The most common type of high-temperature solar thermal system is the parabolic dish collector [3].

There are different types of the receiver for dish concentrator that includes the volumetric, particle, tubular cavity and spiral absorber receivers [4, 5]. The tubular cavity receivers because of especial structure have a higher efficiency compared to external receivers [6]. Some researches were experimentally and numerically studied thermal performance of the dish concentrator with cavity receivers [7-11]. In [7] was numerically and experimentally considered a linear Fresnel heliostat collector

ISBN: 978-86-80616-04-9

using a conical cavity receiver with the spiral tube. Authors simulated the investigated solar system in a three-dimensional Computing Finite Dynamics (CFD) model. The water and Therminol VP-1 used as the solar working fluid. Their results indicate that the optimal conical angle equal to 100° has the maximum thermal performance with minimum cavity heat losses. Azzouzi et a. [8] experimentally and numerically evaluated the thermal performance of a dish collector using a cylindrical cavity receiver and the water as the solar working fluid. They received a good agreement between their experimental results and their calculated numerical study. Pavlovic et al. [5] numerically and experimentally considered the thermal performance of a dish collector using a spiral receiver. They numerically investigated different solar working fluid such as water, Therminol VP-1 and air. They concluded that water is most appropriate at low temperature application, and the Therminol VP-1 is the suitable at higher application temperature.

Skouri et al. [9] theoretically and experimentally researched on the optical, geometric and thermal performance of a parabolic dish concentrator as a case study. They experimentally investigated the thermal performance of the optimized system. Mawire and Taole [10] experimentally considered the energy and exergy performance of a new design of a dish collector using a cylindrical cavity receiver. Their investigated concentrator consists of heliostat reflecting mirrors that tracking the sun through a day. Then the reflected solar radiation is input in a parabolic dish concentrator. Finally, the total reflected solar radiation absorbed by the cylindrical cavity receiver that setup at the focal point of the dish collector. In their proposed design of the solar system, the dish collector is stable and the heliostat reflecting mirrors tracking the sun light. They studied the heat loss factor and optical efficiency of the considered setup. afeeu and Kadir [11] experimentally evaluated a dish concentrator in the different dimension using water as the solar working fluid. Their results revealed that the higher thermal efficiency is achieved using higher concentrator depth and applying the efficient reflective materials.

On the other hand, the thermal properties of the common working fluid can be enhancement by adding ultra-fine solid particles suspended. The suspension of nano-sized particles (1–100 nm) in a conventional base fluid is called a nanofluid. Choi first used the term ‘‘nanofluid’’ in 1995 Therefore, nanometer sized particles will not clog flow passages, but will improve the thermal conductivity of the fluids [12]. Some researches were conducted thermal performance of the application of the nanofluid in the solar [13-19]. He et al. [13] evaluated the thermal performance of a vacuum tube solar collector using two nanofluids including water/TiO2 and water/carbon nanotube, under sunny and cloudy weather conditions. They concluded that the water/carbon nanofluid shows higher performance compare to water/TiO2. Taylor et al. [14] considered the influence of the nanofluid application in the concentrating solar thermal system. The results indicate the thermal efficiency of the based concentrating solar thermal system could be increased by 10% in the application of nanofluid as the working fluid.

Yousefi et al. [15] experimentally considered the thermal efficiency of the flat plate collector using the MWCNT–water nanofluid as the working fluid of the solar collector. They studied the effect of the PH variation of the investigate nanofluid during their study. The results show a bigger difference between the nanofluid pH and isoelectric point pH caused the higher efficiency. Mahian et al. [16] studied the effect of the alumina/water-ethylene glycol nanofluid application as the solar working fluid in a flat plate minichannel-based solar collector. The influence of the different shape of nanoparticles on the energy and exergy analysis was evaluated. They concluded that the outlet temperature increased by application of the nanofluids independent of nanoparticle shape. Meibodi et al. [17] experimentally considered a flat-plate solar collector using SiO2/ ethylene glycol–water nanofluids as the solar working fluid. The influence of the different parameters such as nanoparticle volume fractions, mass flow rate, and solar radiation was evaluated in their study. The results show the exergy efficiency is higher at higher nanoparticle volume fraction.

Meibodi et al. [18] experimentally investigated the thermal performance of a flat plate collector using the SiO2/ethylene glycol (EG)–water nanofluid as the solar working fluid. The effect of the nanofluid mass flow rate was evaluated on the collector thermal performance. They concluded that the thermal efficiency of the solar collector improved by nanofluid application as the solar working fluid.

Mahian et al. [19] numerically and experimentally evaluated the thermal performance of a solar still using the nanofluids as the heat exchanger working fluid. The influence of the of the nanoparticle size, water depths in the solar still basin and mass flow rate of the nanofluid was investigated in their study. They resulted that the SiO2/water nanofluid shows a higher thermal performance compare to the Cu/water nanofluid in higher temperature.

It can be observed from the literature review that there is no reported paper of experimental investigation of a cylindrical cavity receiver using the nanofluid. Therefore, the novelty of the current study is the thermal performance investigation of the cylindrical cavity receiver using the silica/thermal oil nanofluid experimentally during the experimental tests. In this research, the thermal performance of the investigated solar system using the silica/thermal oil nanofluid in the concentration of 0.8% Volume Fraction (VF) and volume flow rate of 100 ml/s. The designed experimental setup was included a parabolic dish concentrator, cavity receiver, and hydraulic circuit system.

II. EXPERIMENTAL SETUP

The experiments were carried out in the Renewable Energy Research of the Tarbiat Modares University, Tehran, Iran (located at 35.68° N latitude and 51.42° longitude). The developed setup was included a parabolic dish concentrator, cylindrical cavity receiver, a heat exchanger system, and a hydraulic circuit (see **Error! Reference source not found.**). The characteristics of the parabolic dish concentrator are reported in Table shows the investigated parabolic dish concentrator with the cavity receiver.

Figure 1. The investigated parabolic dish concentrator with cavity receiver.

TABLE I. PARAMETERS OF THE INVESTIGATED DISH CONCENTRATOR [20].

Parameters of the dish	Data
Aperture diameter	1.9 m
Focal length	0.693 m
Reflectivity	0.84
Tracking error	1°
Rim angle	45°
Concentration ratio	165

Figure 1. The coated cylindrical cavity receiver.

The cavity receivers were constructed in three stages. In the first stage, the cavity receiver were built using wounded copper tubes. In the second stage, the black chrome (Cr-Cr2O3) coating was used on the cavity`s wounded copper tubes for the most absorption and lowest emissivity for the incoming solar radiation. Figure 1 shows the coated cavity receiver by the Mina Company, Tehran, Iran. Finally, for decreasing the heat losses, the outer walls of the coated cavity receiver, except for the aperture, were insulated with mineral wool.

Thermal oil was selected as the working fluid of the investigated solar system, because of its high heat transfer capacities and low viscosities. While it is recommended that the thermal oil is better in the higher temperature application in the solar collector systems such as dish concentrator [5]. The Behran thermal oil

was selected as the solar working fluid in this study. The thermal characteristics of the Behran thermal oil are obtained by Eq. 1 to 4 as below [21]:

$$k_f = 0.1882 - 8.304\times10^{-5}(T_f) \quad (\frac{W}{mK}), \quad (1)$$

$$c_{p,f} = 0.8132 + 3.706\times10^{-3}(T_f) \quad (\frac{kJ}{kgK}), \quad (2)$$

$$\rho_f = 1071.76 - 0.72(T_f) \quad (\frac{kg}{m^3}), \quad (3)$$

$$P_r = 6.73899\times10^{21}(T_f)^{-7.7127}. \quad (4)$$

For preparing the nanofluid, first the specified quantity of nanoparticles is added slowly to the thermal oil based on the 0.8% nanofluid concentration. In the next step, the suspension is well stirred by a stirrer in 400 rpm, and 150 °C for 1 h to separate the particle agglomerations. Finally, the suspension is inserted in an ultrasonic for about 1 h to break down the agglomeration between nanoparticles and minimizing the sedimentation. No sedimentation was observed for 9 month with naked eyes. It would be mentioned that 3 liter of silica/oil was prepared for experimental tests.

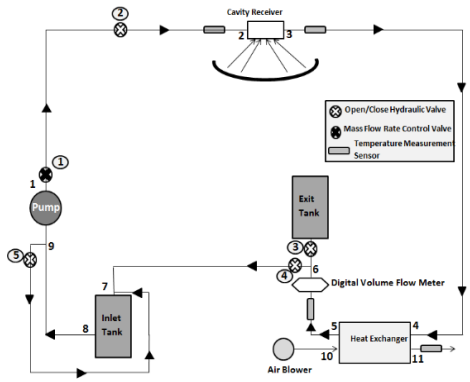

Figure 2. Schematic of the hydraulic circuit.

A. Instrumentation and measurement system

During the experimental tests, different parameters were measured that includes: (1) fluid situations (flow rate, temperature), (2) solar irradiation, and (3) weather situations (ambient temperature, wind speed). Volume flow meter FLUIDWELL model: F016-P was used for measuring the volume flow rate of the solar working fluid (oil). While the working fluid temperatures (at inlet and outlet of the cavities) and surface temperature (top wall and the side wall of the cavities), were measured by using K-type thermocouples (Chromel-Alumel).

TABLE II. ACCURACIES AND RANGES OF THE MEASURING INSTRUMENTS.

Instrument	Accuracy	Range
K-type thermocouples	±0.55 °C	0-800 °C
Solar power meter	±0.1 W/m^2	0-2000 W/m^2
Anemometer	±0.2 m/s	0.9 to 35.0 m/s
Volume flow meter	±0.05 mA	0-20 mA

The Omron data logger model: ZR-RX-45 was used to monitor and store the temperatures of the investigated setup at the different location. The radiation heat flux was measured by using Hukseflux Pyranometer, model SR12. The ambient temperature and wind speed were measured by a K-type thermocouple and anemometer CT model: AM-4220, respectively. Table explained the accuracy and ranges of the measuring instruments.

III. ENERGY ANALYSIS

An important parameter for thermal analysis is thermal efficiency. The thermal efficiency of the cavity receivers is defined as the receiver energy gained to the rate of the total incoming solar energy to the dish concentrator aperture and is expressed as:

$$\eta_{th} = \dot{Q}_{net} / \dot{Q}_{solar}, \quad (5)$$

$$\dot{Q}_{net} = \dot{m}c_p(T_{out} - T_{in}), \quad (6)$$

$$\dot{Q}_{solar} = I_{sun}\pi D_{conc}^2 / 4. \quad (7)$$

In these equations, η_{th} is the thermal efficiency, $\dot{Q}_{net(W)}$ is the receiver energy gained, $\dot{Q}_{solar(W)}$ is the total incoming solar energy, $\dot{m}(kg/s)$ is the mass flow rate of the solar working fluid, $c_p(\frac{J}{kg}.K)$ is the heat capacity of

the solar working fluid, $T_{out}(K)$ *and* $T_{in}(K)$ are the outlet and inlet temperatures of the solar working fluid, respectively, $I_{sun}(W/m^2)$ is the solar irradiation, and $D_{conc}(m^2)$ is the aperture dish concentrator.

A. Nanofluid properties

In this paper, the operation with nanofluids is investigated. The SiO2/thermal oil nanofluid is tested and its thermal properties are calculated according to the equations of this section. Table includes the thermal properties of the examined nanoparticle. It is obvious, that the nanoparticle present high density, high thermal conductivity and low specific heat capacity.

TABLE III: PROPERTIES OF NANOPARTICLE.

Property	**SiO_2**
Thermal conductivity (W/m K)	1.4
Heat capacity (J/kg K)	745
Density (kg/m3)	2220

Eq. (8-11) present the thermal properties of the nanofluids. The base fluid is symbolized with (bf), the nanoparticle with (np) and the nanofluid with (nf). The thermal conductivity of the nanofluid is calculated according to the suggested equation by Yu and Choi [22]:

$$k_{nf} = k_{bf} \cdot \frac{k_{np} + 2 \cdot k_{bf} + 2 \cdot (k_{np} - k_{bf}) \cdot (1+\beta)^3 \cdot \phi}{k_{np} + 2 \cdot k_{bf} - (k_{np} - k_{bf}) \cdot (1+\beta)^3 \cdot \phi} . \quad (8)$$

The parameter β in this equation is the ratio of nano-layer thickness to the nanoparticles diameter which is considered to be 0.1 in of this study [23]. The density of the mixture is given by equation (9) [24] and the specific heat capacity according to equation (10) [25]:

$$\rho_{nf} = \rho_{bf} \cdot (1-\phi) + \rho_{np} \cdot \phi , \quad (9)$$

$$c_{p,nf} = \frac{\rho_{bf} \cdot (1-\phi)}{\rho_{nf}} \cdot c_{p,bf} + \frac{\rho_{np} \cdot \phi}{\rho_{nf}} \cdot c_{p,np} . \quad (10)$$

The dynamic viscosity is calculated according to the Batchelor model [26]:

$$\mu_{nf} = \mu_{bf} \cdot (1 + 2.5 \cdot \phi + 6.5 \cdot \phi^2) . \quad (11)$$

IV. RESULTS AND DISCUSSION

Fig. 4 displays the variation of different parameters including the solar total radiation, ambient temperature, and the temperature difference between the inlet and outlet temperature of the working fluid on 23th September 2016 in Tehran, Iran. It shall be mentioned that the overall environmental and operational parameters for cylindrical cavity receiver were measured from 9:15 to 16:00 and the mass flow rate of the working fluid was 10 ml/s during the experimental tests. As shown, the temperature difference is ranged from 33.10°C at 16:00 to 66.18 °C at 12:10. And the solar total irradiance is varied in the range of 408.35 W/m2 at 16:00 to 706.65 W/m2 at 12:10. The temperature difference generally has a similar trend to the solar irradiation. The ambient temperature is ranged from 24.6 °C at 9:15 to 31°C at 14:00. As seen, the ambient temperatures are generally higher in the afternoon than the morning.

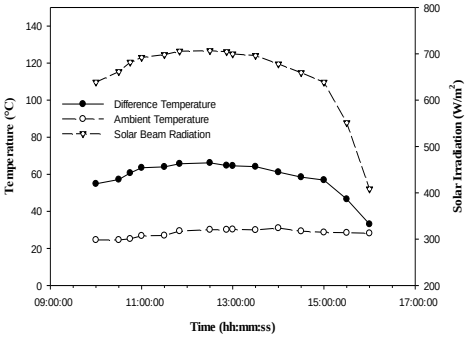

Figure 3. Variation of the solar irradiation, ambient temperature, and temperature difference between outlet and inlet of the cylindrical cavity receiver on 23th September 2016.

The receiver heat gained and thermal efficiency of the cylindrical cavity receiver are displayed in Fig. 5. It shows that the receiver heat gained is ranged from 566.71 W at 16:00 to

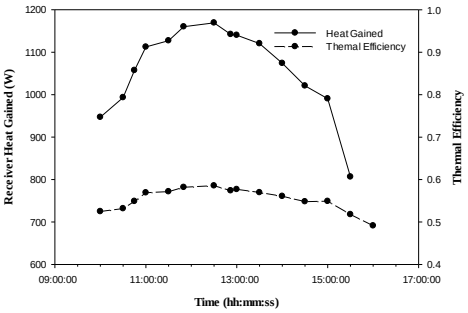

Figure 5. Variation of receiver heat gained ( ), and thermal efficiency of the cylindrical cavity receiver on 26th September 2016.

1169.2 W at 12:10. And the thermal efficiency is varied from 0.49 at 16:00 to 0.59 at 12:10. It can be concluded that the receiver heat gained and the thermal efficiency of cylindrical cavity receiver have a similar trend with the difference temperature. Consequently, the temperature difference is an effective parameter in the receiver heat gained and thermal efficiency of cylindrical cavity receiver. This result was also concluded by [10].

Finally, the investigated cylindrical cavity receiver was tested using the pure thermal oil as the based fluid of the silica/thermal oil nanofluid. Fig. 6 depicts a thermal performance comparison between the silica/thermal oil nanofluid and pure thermal oil as the solar working fluid for the investigated cylindrical cavity receiver. It can be seen from Fig. 6., the application of the silica nanofluid didn't have an effective influence for improving the thermal performance of the investigated cylindrical cavity receiver compare to the pure thermal oil. This issue is due to the thermal properties of the Silica nanoparticles. Consequently, the application of the pure oil is recommended as the solar working fluid of the cylindrical cavity receiver instead of the silica/thermal oil nanofluid due to its less cost.

V. CONCLUSIONS

In this study, a parabolic dish concentrator using a cylindrical cavity receiver was experimentally investigated. The effect of nanofluid application as the solar working fluid was studied in this research. The nanofluid of SiO2/thermal oil was examined in the nanofluid concentration of 0.8% Volume Fraction (VF) and volume flow rate of 10 ml/s. Comparison between the silica/thermal oil nanofluid and pure thermal oil as the solar working fluid for the investigated cylindrical cavity receiver was done. The results are extracted as followings:

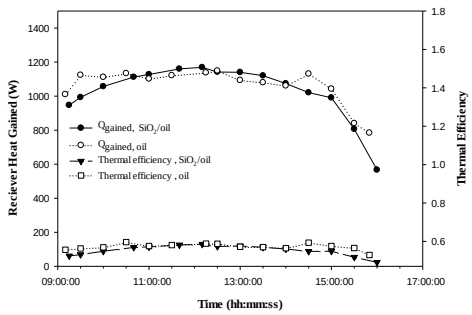

Figure 6. A thermal performance comparison between the silica/thermal oil nanofluid and pure thermal oil as the solar working fluid.

The temperature difference generally has a similar trend to the solar irradiation. Also, the ambient temperatures have generally higher amount in the afternoon compare to the morning.

It can be concluded that the receiver heat gained and the thermal efficiency have a similar trend compare to the difference temperature. Consequently, the temperature difference is an effective parameter in the receiver heat gained and thermal efficiency of cylindrical cavity receiver.

Finally, it could be resulted that the application of the silica nanofluid didn't have an effective influence for improving the thermal performance of the investigated cylindrical cavity receiver compare to the pure thermal oil. Consequently, the application of the pure oil is recommended as the solar working fluid of the cylindrical cavity receiver instead of the silica/thermal oil nanofluid due to its less cost.

ACKNOWLEDGMENTS

Authors are grateful to the University of Mohaghegh Ardabili (UMA), and the Tarbiat Modares University (http://www.modares.ac.ir) for financial supports given under IG/39705 grant for renewable Energies of Modares research group.

REFERENCES

[1] N.S. Lewis, "Toward cost-effective solar energy use," Science, vol. 315, 2007, pp. 798-801.

[2] M. Thirugnanasambandam, S. Iniyan, and R. Goic, "A review of solar thermal technologies", Renewable and sustainable energy reviews, vol. 14, 2010, pp. 312-322.

[3] S.A. Kalogirou, "Solar thermal collectors and applications", Progress in energy and combustion science, vol. 30, 2004, pp. 231-295.

[4] C.K. Ho, and B.D. Iverson, "Review of high-temperature central receiver designs for concentrating solar power", Renewable and Sustainable Energy Reviews, vol. 29, 2014, pp. 835-846.

[5] S. Pavlovic, A.M. Daabo, E. Bellos, V. Stefanovic, S. Mahmoud, and R.K. Al-Dadah, "Experimental and numerical investigation on the optical and thermal performance of solar parabolic dish and corrugated spiral cavity receiver," Journal of Cleaner Production, vol. 150, 2017, pp. 75-92.

[6] M. Günther, R. Shahbazfar, T. Fend, and M. Hamdan. (2007). *Solar Dish Technology, Advanced CSP Teaching Materials*, Available at: http://www.energy-

science.org/bibliotheque/cours/1361468083Chapter%2007%20dish.pdf

[7] X. Li, Y. Dai, and R. Wang, “Performance investigation on solar thermal conversion of a conical cavity receiver employing a beam-down solar tower concentrator,” Solar Energy, vol. 114, 2015, pp. 134-151.

[8] D. Azzouzi, B. Boumeddane, and A. Abene, “Experimental and analytical thermal analysis of cylindrical cavity receiver for solar dish,” Renewable Energy, 2017.

[9] S. Skouri, M.B. Salah, S. Bouadila, M. Balghouthi, and S.B. Nasrallah, “Optical, geometric and thermal study for solar parabolic concentrator efficiency improvement under Tunisia environment: A case study,” Energy Conversion and Management, vol. 75, 2013, pp. 366-373.

[10] A. Mawire, and S.H. Taole, “Experimental energy and exergy performance of a solar receiver for a domestic parabolic dish concentrator for teaching purposes,” Energy for sustainable development, vol. 19, 2014, pp. 162-169.

[11] Y. Rafeeu, and M. Ab Kadir, “Thermal performance of parabolic concentrators under Malaysian environment: A case study,” Renewable and Sustainable Energy Reviews, vol. 16, 2012, pp. 3826-3835.

[12] J. Eastman, U. Choi, S. Li, L. Thompson, and S. Lee, “Enhanced thermal conductivity through the development of nanofluids,” MRS proceedings, Cambridge Univ Press, 1996, pp. 3.

[13] Y. He, S. Wang, J. Ma, F. Tian, and Y. Ren, “Experimental study on the light-heat conversion characteristics of nanofluids,” Nanoscience and Nanotechnology Letters, vol. 3, 2011, pp. 494-496.

[14] R.A. Taylor, P.E. Phelan, T.P. Otanicar, C.A. Walker, M. Nguyen, S. Trimble, and R. Prasher, “Applicability of nanofluids in high flux solar collectors,” Journal of Renewable and Sustainable Energy, vol. 3, 2011.

[15] T. Yousefi, E. Shojaeizadeh, F. Veysi, and S. Zinadini, “An experimental investigation on the effect of pH variation of MWCNT–H 2 O nanofluid on the efficiency of a flat-plate solar collector,” Solar Energy, vol. 86, 2012, pp. 771-779.

[16] O. Mahian, A. Kianifar, S.Z. Heris, and S. Wongwises, “First and second laws analysis of a minichannel-based solar collector using boehmite alumina nanofluids: effects of nanoparticle shape and tube materials,” International Journal of Heat and Mass Transfer, vol. 78, 2014, pp. 1166-1176.

[17] S.S. Meibodi, A. Kianifar, O. Mahian, and S. Wongwises, “Second law analysis of a nanofluid-based solar collector using experimental data,” Journal of Thermal Analysis and Calorimetry, vol. 126, 2016, pp. 617-625.

[18] S.S. Meibodi, A. Kianifar, H. Niazmand, O. Mahian, and S. Wongwises, “Experimental investigation on the thermal efficiency and performance characteristics of a flat plate solar collector using SiO2/EG–water nanofluids,” International Communications in Heat and Mass Transfer, vol. 65, 2015, pp. 71-75.

[19] O. Mahian, A. Kianifar, S. Zeinali Heris, D. Wen, A.Z. Sahin, and S. Wongwises, “Nanofluids Effects on the Evaporation Rate in a Solar Still Equipped with a Heat Exchanger,” Nano Energy, 2017, pp. 71-75.

[20] S. Gorjian, B. Ghobadian, T.T. Hashjin, and A. Banakar, “Experimental performance evaluation of a stand-alone point-focus parabolic solar still,” Desalination, vol. 352, 2014, pp.1-17.

[21] A. Baghernejad, and M. Yaghoubi, “Thermoeconomic methodology for analysis and optimization of a hybrid solar thermal power plant,” International journal of green energy, vol. 10, 2013, pp. 588-609.

[22] W. Yu, and S. Choi, “The role of interfacial layers in the enhanced thermal conductivity of nanofluids: a renovated Maxwell model,” Journal of Nanoparticle Research, vol. 5, 2003, pp. 167-171.

[23] W. Duangthongsuk, and S. Wongwises, “An experimental study on the heat transfer performance and pressure drop of TiO 2-water nanofluids flowing under a turbulent flow regime,” International Journal of Heat and Mass Transfer, vol. 53, 2010, pp. 334-344.

[24] A.B. Kasaeian, “Convection heat transfer modeling of Ag nanofluid using different viscosity theories,” IIUM Engineering Journal, vol. 13, 2012.

[25] K. Khanafer, and K. Vafai, “A critical synthesis of thermophysical characteristics of nanofluids,” International Journal of Heat and Mass Transfer, vol. 54, 2011, pp. 4410-4428.

[26] G. Batchelor, “The effect of Brownian motion on the bulk stress in a suspension of spherical particles,” Journal of fluid mechanics, vol. 83, 1977, pp. 97-117.

Phase Change Materials for Thermal Energy Storage in Renewable Energy Systems in Rural Communities and Industries

Atul G. Bhave

Renewable energy consultant, Mumbai, India, agbhave@iitbombay.org

Abstract — **There is often a mismatch between availability of solar energy and the load profile of many applications. Latent heat thermal energy storage systems based on solid – liquid phase transformation offer benefits like compactness compared to sensible heat storage, low cost and availability of heat at constant temperature. This paper describes a few of the possible applications of such systems like drying, milk pasteurization and cooking among the numerous possible applications of such systems. It suggests a few phase change materials for the range 0^0C to 220 ^{0}C, which are suitable for these applications, based on the temperature needs and their properties.**

Keywords – solar thermal system, thermal storage, phase change material

I. INTRODUCTION

Renewable energy systems like those based on solar and biomass energy offer the advantage of reducing fossil fuel consumption and its negative effect of global warming. Solar energy availability peaks around noon, and is not available at night, leading to a mismatch between availability and load energy requirement in many applications.

Energy storages serve to ensure the supply on demand, to improve the performance and reliability of an energy system, to conserve energy and remove mismatch between energy availability and load requirement like in solar systems. Various types of energy storages are in use, like mechanical energy storage in flywheels, electrical energy storage as chemical energy in batteries, and thermal energy storage i.e. sensible heat, latent heat and thermochemical storages.

In sensible heat storages, thermal energy is stored as a temperature rise of the storage medium. The quantity of energy stored depends upon temperature difference, specific heat of the medium and amount of storage material. Possible materials include water, pebble beds, rocks and thermic oils. Their disadvantage is the large volume or mass needed to store the same quantity of heat as compared to solid-liquid phase change materials.

Latent heat storages store thermal energy as heat absorbed or released during change of phase of the storage material. The change of phase may be from solid to solid, solid to liquid, solid to gas and liquid to gas, or vice-versa. Solid-gas and liquid-gas systems (eg. water-steam) have high latent heat of phase change but have containment problems because of their high volume change during change of phase. This makes them unsuitable for most practical applications. In solid-solid phase transitions, heat is stored in the material as its crystal structure changes from one form to another. They have advantages like low volume change, but their energy storage density is low. An example is cross-linked HDPE with phase transition temperature in the range 125-146 ^{0}C and a latent heat of 167-201 kJ/kg [1].

In solid-liquid phase transitions, the volume changes are very low, and these phase change materials (PCMs) have been widely studied and used. Latent heat storages have advantages over sensible heat storages, like high energy storage per unit volume or unit mass, and largely isothermal heat transfer to the load near

ISBN: 978-86-80616-04-9

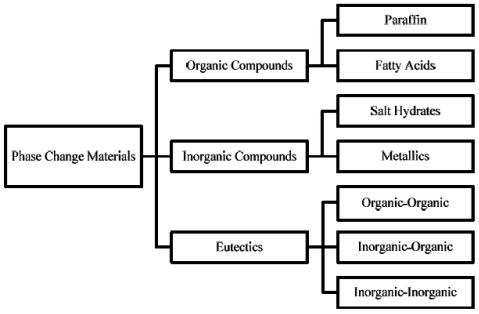

Figure 1. Solid-liquid phase change materials

the phase change temperature of the PCM (its melting point).

In thermochemical storage, energy is stored in the form of stored products of an endothermic reversible chemical reaction. The reaction absorbs heat in the forward direction and releases heat in the reverse direction. An example is steam reforming of methane in the presence of a catalyst to produce carbon monoxide and hydrogen.

The quantity of heat stored depends upon the quantity of reactants, enthalpy of reaction and the extent of reaction [1].

Phase change materials are classified into three categories as in Fig. 1 [1]. Salt hydrates are inorganic crystalline solids containing a salt and water. When it reaches phase change temperature, the water molecules are released and the salt dissolves in it, absorbing the necessary heat of fusion. When cooled, it recrystallizes, releasing the heat of fusion.

A eutectic is a mixture of two or more compounds which has a melting point lower than any of the components.

Desirable properties of solid-liquid phase change materials include a high latent heat of fusion, high thermal conductivity in both phases, high density, low vapour pressure, low volume change on melting, congruent melting, no super-cooling, chemical stability, low cost, and they should be non-corrosive to the container material, and non-hazardous.

II. APPLICATON AREAS

A few potential applications of PCMs for heat storage in renewable energy systems for rural areas and industries along with their temperature requirements are given in Table I.

Box type solar cookers for cooking involving boiling of food like rice and vegetables are commonly used around the world, especially in the developing countries of Asia and Africa, for domestic use. Cookers based on parabolic dish concentrators, with manual tracking of the sun, are useful in rural and semi-urban areas for cooking involving frying or high temperature cooking in the range 170 – 190 ^{0}C. They are available as family and community scale (large diameter paraboloid) systems.

Milk is pasteurised to destroy disease causing micro-organisms, and to increase its storage life by destroying spoilage micro-organisms and enzymes. Batch pasteurisation is used in small plants where milk is filled in a vat, heated to a temperature of 62.8 ^{0}C and held there for 30 minutes for pasteurisation to take place before cooling it. The most common process is the continuous pasteurisation process where milk is heated in a plate heat exchanger by hot water or steam. The continuous HTST (high temperature short time) process requires milk to be held at 71.7 ^{0}C for 15 seconds. Aseptic ultra high temperature pasteurisation requires the milk to be held at 135 – 150 ^{0}C for 4 – 15 seconds. [2]

TABLE I. POTENTIAL APPLICATIONS OF PCM THERMAL STORAGES

Area	**Application**	**Temperature requirement, ^{0}C**
Solar cookers	Cooking by boiling	100
	Frying	160- 180
Solar industrial process heat	Milk pasteurisation	60- 150
	Steam-sterilisation of vegetables, meat, fish	130- 150
Drying of crops	Solar, biomass fired, or hybrid solar-biomass fuelled driers for grains, fruits and vegetables.	40 – 70
Vapour absorption or adsorption solar cooling	Storage of heat:	Hot water/steam:
	-NH_3-H_2O system	Above 90
	-Silica gel- water System	Above 60
	Storage of cold	As per application

Solar energy can be conveniently used for low temperature hot air drying of agricultural produce. Due to the intermittent nature of solar energy, a uniform air temperature is not obtained, with the possibility of air above design drying temperature being obtained around noon, and no hot air in the evenings or overnight, which means the drying process of long drying cycle products gets interrupted. A PCM based energy storage can solve both these problems and smooth the supply air temperature and supply it when the sun is not available, if needed.

Heat driven solar cooling systems do not require a Freon refrigerant or a compressor, are comparatively quiet and do not consume fossil fuels [3]. They can be adapted for air conditioning as well as for storage of fruits and vegetables. Incorporation of a PCM for storage of heat or cold in such systems will make the cooling effect available whenever needed, as happens with chilled water storage in large central conventional air conditioning systems.

III. LATENT HEAT STORAGE MATERIALS AND CASE STUDIES

Table II summarises the important properties of selected PCM materials suitable for the applications mentioned in Table I.

A few applications with suitable latent heat storage materials are discussed below.

Reference [4] reports the design and experimental results of a parabolic dish based solar cooker with a thermal storage cum cooking device. The PCM used is 0.48 kg of magnesium chloride hexahydrate, which is melted in the device placed at the focus of the dish in direct solar radiation.

The PCM is placed in aluminium tubes which are immersed in thermic fluid in the thermal storage chamber. The device can be shifted to the kitchen, and used for cooking when desired, in the upper cooking cavity, with heat being transferred to the food from the PCM chamber below. The schematic of the system is shown in Fig. 2. It was possible to store one charge of heat in about 50 minutes, and prepare about 140 gm of rice in 30 minutes separately indoors from the stored heat. To store the same amount of sensible heat stored as latent heat in this system, in contrast it would need about 4-5 kg of rocks or pebbles at a temperature of 120 ^{0}C, which would cool to 100 ^{0}C (rice cooks by boiling) to release the heat.

TABLE II. SOLID-LIQUID PHASE CHANGE MATERIALS FOR THERMAL STORAGE

Name	Melting point, ^{0}C	Heat capacity, kJ/m^3	Latent heat of fusion, kJ/kg
C15- C16 paraffins [5]	8		153
Magnesium chloride hexahydrate ($MgCl_2.6H_2O$) [6]	117	244,470	168.6
Magnesium nitrate hexahydrate ($MgNO_3.6H_2O$) [6]	89	252340	162.8
Acetamide [7]	82	262,470	263
Paraffin wax [6]	64	137,144	173.6
Ice [8]	0	304,850	335
7% $NaNO_3$ + 53 % KNO3 + 40 % $NaNO_2$ by weight (eutectic, known as Hitec salt) [9]	142	164,968	83.74
60 % $NaNO_3$ + 40 % KNO_3 (eutectic, mol %, known as Solar salt) [10]	210 – 220 (range over which it melts)	217,340	108.67

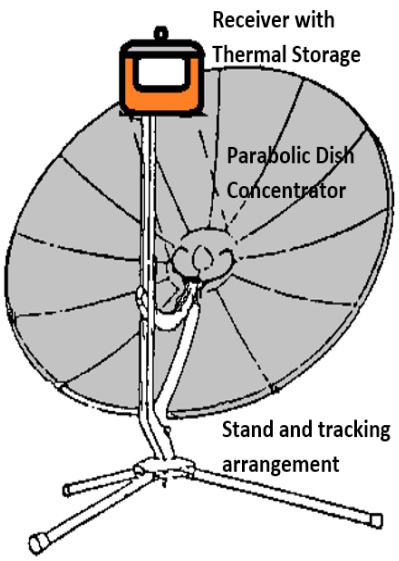

Figure 2. Thermal storage type solar cooker

In HTST pasteurisation of milk in plate heat exchangers, normally hot water 2 – 3 ^{0}C above desired milk temperature, i.e. at around 74 ^{0}C is used to heat the milk [11]. If the energy source is a solar flat plate or evacuated tube collector, surplus solar heat from noon collection could be stored in the hydrated salt magnesium nitrate hexahydrate or in the organic PCM acetamide (Table II). Both these materials have been used for heat storage in solar cookers by researchers [6, 7]. The thermal store can enable a hot water supply at constant temperature for 24 hours continuously.

A potential application of PCMs in rural areas is described in [12] for drying of agricultural produce (Fig. 3). It has a solar flat plate air heating collector which supplies hot air to the groundnuts to be dried in the drying trays during daytime. During the night wood is burnt in the biomass burner. The heat from flue gases is stored in the mass of bricks provided. The flue gases travel up along three sides of the drying cabinet from the outside, out of the chimney. They heat the chamber inside through the walls which draws in air through the collector inlet by natural convection, which removes moisture from the heated products and goes out through the vent. Heat storage in the bricks allows continuous drying to take place, e.g. for products which have a large drying cycle, and allows less frequent combustion of the fuel.

Use of a solid – liquid PCM in such a system will give a storage with less volume and weight than bricks, and in addition enable a constant drying air temperature to be obtained, giving optimum drying of the product.

The PCM needs to be chosen based on the drying temperature required by the product. Such a system could be adapted to a plain solar dryer, a plain biomass fuelled dryer or a mixed mode, hybrid dryer as in this case.

Suitable PCMs for this application could be paraffin waxes, which are available with melting points in the temperature range 40 – 60 0C [8], and acetamide (Table II). Paraffins have good thermal stability under repeated cycling [6], but have low volumetric storage capacity.

Materials that melt below 15 0C are used to store coolness in refrigeration and air conditioning systems, e.g. ice, as in Table II. PCMs that melt above 90 0C can be used to store heat to operate vapour absorption cooling cycles continuously, supplying heat at a constant optimum temperature depending on their melting point.

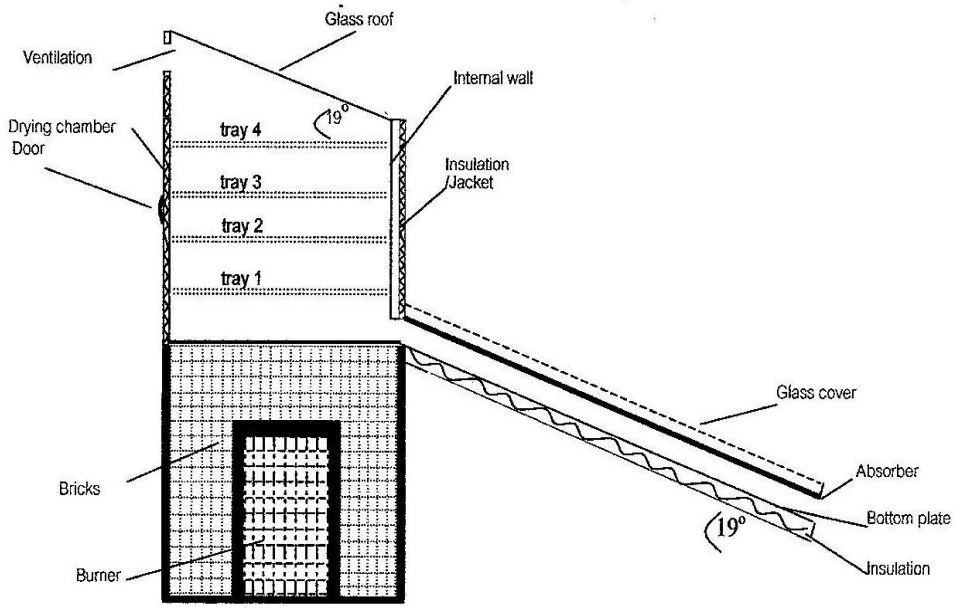

Figure 3. Mixed mode natural convection solar dryer [12]

As seen in Table II, C15 - C16 paraffin's with a melting point of about 8^0C appear to be well suited for thermal storage to cool the air, in air conditioning systems.

Hitec is a eutectic mixture of three inorganic salts that is used as a heat transfer medium. It has a high heat transfer coefficient, thermal stability and low cost. It is also suited for use as a latent heat storage medium in solar systems used for producing low pressure steam for industrial process heat.

The second binary eutectic mixture in Table II ($NaNO_3$ + KNO_3), known as Solar salt, has a higher melting point, and can be used as a storage and source of solar heat at a temperature of 210 – 220 ^{0}C, which may be adapted for applications like medium temperature steam production, and for sterilization operations in the food industry (Table I). Reference [10] have studied the thermal behavior of Solar salt using a differential scanning calorimeter and measured its specific heat in the range 32 – 496 ^{0}C. A solid-solid phase transition at 110-120 ^{0}C with a higher specific heat capacity, and solid-liquid phase change at 210- 220 ^{0}C with a high specific heat capacity (latent heat), when melting was occurring, were identified. They also tested a double reflector (two parabolic dishes, with the larger one of 1.2 m. diameter) solar concentrator with a stainless steel, slim cylindrical receiver containing Solar salt, at its focus. A copper plate which closed the top end of the container received the concentrated beam of light and transferred the heat into the PCM below through a single long copper fin attached to it. The fin serves to enhance the heat transfer rate as the thermal conductivity of PCMs is normally low. The top copper plate served as the solar absorber and during trials the full PCM melted within 2-2.5 hours and reached a temperature range of 230- 260 ^{0}C. This result met their objective of collecting and storing solar energy at a temperature for use for high temperature cooking like baking.

Another example of the potential application of Solar salt is the Fresnel paraboloid solar concentrator with pressurized hot water storage at 18 bar and 180 ^{0}C installed at Mahanand Dairy in India by [13] for meeting the thermal energy requirements of processes like milk pasteurization, milk chilling and sterilization.

Thermal storage in such applications can instead be carried out with reduced size and cost, and isothermal operation in a PCM such as Solar salt.

Reference [14] reports several research workers having worked on solar air heating flat plate collectors or solar dryers using PCM storage, especially paraffin based. He reports Fath (Egypt) having studied a solar air heater using corrugated tubes filled with paraffin wax as the absorber cum energy storage. His analysis showed that with an air flow rate of 0.02 kg/s, for an outlet air temperature of 5 ^{0}C above ambient, the daily average efficiency would be 63.35% compared to 38.7% for a normal flat plate air heater, and the hot air was available for 16 hours/day with the PCM as compared to 9 hours for the normal collector.

Reference [15] is an Indian company specializing in phase change materials, who offer solar drying systems with a PCM integrated with the flat plate air heater absorber, on its lower surface. 40 kg/sq.m. of an organic PCM with melting point of 55 ^{0}C and latent heat of 255 kJ/kg is used. Aluminum mesh is embedded in the PCM to improve its thermal conductivity. The PCM is capable of withstanding 3000 charge-discharge thermal cycles. Air flows between the absorber and glass cover and gets heated up by solar energy, or in its absence by heat transfer from the PCM below the absorber, and flows to the drying chamber. They report an increase in efficiency of the system, 24 hour drying instead of daytime only drying, and consistent air temperature leading to a better quality product.

Reference [16] are working on the development of a Screw Heat Exchanger in which the solid PCM is transported by two or more parallel screws. It is heated by steam from a linear Fresnel collector field, which flows through the hollow screw shaft, the screw flights and the trough. Molten PCM exits and is stored in a hot storage tank. The same heat exchanger can operate in reverse and evaporate water from heat of freezing of molten PCM, to run a steam turbine power plant. In this paper they have presented life cycle cost analysis of some configurations of a 50 MW direct solar steam based power plant with and without PCM storage. The PCM considered is sodium nitrate (melting point 306 ^{0}C).

IV. CONCLUSIONS

The review of a few typical renewable energy, mainly solar thermal systems being used

in rural communities and industries for process heat has identified areas where addition of thermal storage would be beneficial by making energy available over a longer duration beyond sunshine hours, and when needed. The advantages of solid-liquid phase change heat stores are higher energy density and consequent smaller size and cost, and availability of heat at constant temperature, which may be necessary to improve the quality of some processes. Materials identified include Solar salt for high temperature cooking or medium temperature industrial steam and process heat, magnesium nitrate hexahydrate, magnesium chloride hexahydrate and acetamide for low temperature cooking and storage of heat from flat plate or evacuated tube collectors, paraffins for lower temperature storage of heat or storage of "cool", and ice as a storage of "cold".

REFERENCES

[1] K.A. Thakare, A.G. Bhave, "Review on latent heat storage and problems associated with phase change materials," International Journal of Research in Engineering and Technology, vol 4, no. 10, 2015, pp. 176-182.

[2] www.milkfacts.info

[3] S. Mekhilefa, R. Saidurb, A. Safari, "A review on solar energy use in industries," Renewable and Sustainable Energy Reviews, vol. 15, 2011, pp. 1777–1790.

[4] A.G. Bhave, K.A. Thakare, "Development of a solar thermal storage cum cooking device using salt hydrate," Solar Energy, vol. 171C, 2018, pp. 784-789.

[5] A. Abhat, "Low temperature latent heat thermal energy storage: heat storage materials," Solar Energy, vol. 30, 1983, pp. 313-332.

[6] M. M. Farid, A. M. Khudhair, S. A. K. Razack, S. Al-Hallaj, "A review on phase change energy storage: materials and applications," Energy Conversion and Management, vol. 45, 2004, pp. 1597–161.

[7] S.D. Sharma, D. Buddhi, R.L. Sawhney, Atul Sharma, "Design, development and performance evaluation of a latent heat storage unit for evening cooking in a solar cooker," Energy Conversion & Management, vol. 41, 2000, pp. 1497–1508.

[8] S.P. Sukhatme, J.K. Nayak, Solar Energy- Principles of thermal collection and storage, New Delhi, India, Tata McGraw Hill, 2008.

[9] "HITEC Heat transfer salt", brochure of Coastal Chemical Co., L.L.C., USA.

[10] C. W. Foong, J. E. Hustad, J. Løvseth, O. J. Nydal, "Numerical Study of a High Temperature Latent Heat Storage (200-3000C) Using Eutectic Nitrate Salt of Sodium Nitrate and Potassium Nitrate," Excerpt from the Proceedings of the COMSOL Conference, France, 2010.

[11] www.dairyprocessinghandbook.com

[12] E. Tarigan, P. Tekasakul, "A Mixed-Mode Natural Convection Solar Dryer with Biomass Burner and Heat Storage Back-up Heater," ANZSES2005, New Zealand, 2005, pp. 1-9.

[13] www.cliquesolar.com

[14] S. M. Shalaby, M. A. Bek, A. A. El-Sebaii, "Solar dryers with PCM as energy storage medium: A review," Renewable and Sustainable Energy Reviews, vol. 33, 2014, pp. 110–116.

[15] http://www.pluss.co.in/solar-dryer/pluss-aagun-dryer-marketing-presentation.pdf

[16] V. Zipf, A. Neuhäuser, C. Bachelier, R. Leithner, W. Platzer, "Assessment of different PCM storage configurations in a 50 MWel CSP plant with screw heat exchangers in a combined sensible and latent storage – simulation results," Energy Procedia, vol. 69, 2015, pp. 1078–1088.

Wireless Android Power Consumer Monitoring System

Đorđe Kocić

Faculty of Electronic Engineering, University of Niš, Niš, Serbia,
seriousdjoka@gmail.com

Abstract — **This paper presents an overview of a working system, based on Android smart devices, for acquisition, processing and subsequent transmission of a single-phase consumer power (current) consumption data to a local Wi-Fi network, which can then be accessed by network clients. It allows the user to wirelessly monitor the consumer's power consumption, using any kind of personal computer.**

Keywords - andorid, wireless, HTTP, Power monitoring, Signal proccesing

I. INTRODUCTION

As the need for power consumption increases every day, and power distribution facilities grow in size, so does the need for ever more efficient and less space consuming measurement equipment. Modern digital data acquisition systems have had great improvements concerning these problems, and have made the process of monitoring and controlling very easy. Most recent developments are now enabling wireless connection between measurement systems, further reducing size, price and system complexity [1, 2]. The only currently visible drawback could be the increasing internal complexity of the computers used in these systems and lowered robustness of the systems. This paper covers one such application of a mobile computer device as a wireless measurement platform.

Basic functionality of the system described here is analog electric signal measurement, basic values displayed are amplitude and frequency. More complex values are also available like waveform, frequency spectrum and power measurement with 2 channel setup [3]. The intended functionality of the system is transmitting of the measured data to a local wireless network [1-3].

The system can be used for wireless reading of current data in the vicinity of the measurement device. Effective distance is determined by the topology of the site, and parameters of the Wi-Fi network hardware. Device can broadcast its own wireless network, eliminating the need for an access point router or other Wi-Fi equipment. Intended applications of this system are: dangerous environments, hardly accessible facilities, distance measurements, demonstration purposes.

There are many similar systems in use today [1, 4, 5]. Functionality of this system is similar to household smart plug [5]. Main difference is the use of audio card for A/D conversion. But the advantage of this system is that it is an open source platform for research and education and can also be implemented in industrial applications. It employs affordable devices that can be acquired easily. Other advantages of this system are: it is easy to use, easy to be put together, affordable components and free software, easy to be upgraded or expanded, an intuitive research platform with wide range of functionalities, independent power supply. Some future developments strive towards IoT and smart grid applications [6].

Disadvantages are: dependency on complex network system, may require maintenance or calibration from time to time, limited area of application, limited number of monitored consumers, limited distance of measurement.

II. OPERATIONAL PRINCIPLE

A. System overview

This system is based on the concept of soundcard oscilloscope, which enables digital computers to process analog input signals via the sound card [7].

ISBN: 978-86-80616-04-9

System hardware components are:

-current transformer

-Android smart device

System software components are:

-signal processing application

-data transmission application

Heart of the system is a smart device (smartphone, tablet, smart TV box, raspberry pi...) that runs on Android operating system. Electric current signal is acquired from the current transformer, which is then scaled down and transduced to a voltage signal by a low ohm resistor. That signal is then fed into the devices' audio port. The audio (sound) card of the Android device acts as a A/D converter (analog to digital), so the digital signal can now be processed by conventional signal processing software.

Next step is signal processing (waveform analysis, harmonic distortion, peak value, RMS value, frequency...) which is done by an Android application. There is a variety of applications that serve this purpose, and some of them are open source.

Finally, another Android application is used to convey the desired information to local clients. It transmits the signal information to local Wi-Fi network, so that users can log in and view the data.

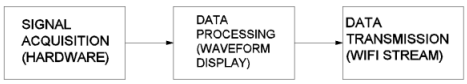

Figure 1. System block diagram.

B. *Hardware*

Hardware components used in this system are: current transformer (with built in resistor), an optional external audio card, connection cable with 3.5 mm audio jack and an Android device (Fig. 2).

Current transformer used is standard clamp type, with a built in resistor for transforming current into voltage signal, with a ratio of 50A/1V (Fig. 3). Output connector is 3.5mm audio jack. The transformer also isolates the measurement device from the high current, high voltage power grid.

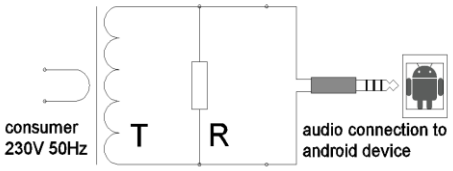

Figure 2. Hardware setup schematic.

Figure 3. Current transformer with 3.5mm output jack.

Applied Android device is a Smartphone (Meizu C9) who's audio card has ADC resolution of 24 bits, and a sample rate of min. 48 kHz. Standard audio stereo input supports 2 channels, that enables 2 signals to be processed. Usually current and voltage signals for 1 consumer, which yields complete power data needed for calculating consumption. In this example only one channel will be used, and that will be current measurement. Power can be calculated by multiplying the current value and voltage value (with a constant voltage assumption of 230V). It should be noted that standard integrated audio cards cannot detect DC component of a periodic sine wave signal, due to an input capacitor used for low frequency noise reduction. Which somewhat limits the use of such devices. But it is still fairly accurate when used for most low voltage electric consumers. Even more accurate for monitoring high voltage lines which have near perfect sine wave.

C. *Data acquisition and processing*

Electrical signal acquired from the transformer is processed as analog sound signal through the audio card system. Using already available and developed software, signal

properties (RMS, frequency, amplitude, spectrum...) are extracted and displayed (graphs, charts, tables...).

There are many applications used for this purpose, which have a variety of features. Some applications are open source, allowing further development and research. Commercial applications offer a wider set of options but are usually locked, and cannot be adjusted to various situations.

Application used in this instance is Smart scope, developed by LabNation [8]. It offers the ability to monitor the signal's waveform, amplitude and period (frequency) as shown in Fig. 4. The application was developed initially to be used with dedicated hardware from the same company, but it also allows the use of system microphone as signal input.

Other applications offer different possibilities for monitoring. Another very useful application that could be used in this case is Oscope by Sound-Base Audio [9]. It also has the oscilloscope function like the previous one, but additionally it displays the frequency spectrum of the signal, which allows the detection of dominant harmonics in the power signal, shown on Fig. 5.

D. Data transmission

For transmitting the data from the measurement device to the user interface device, another Android application is required. There is a lot of software that enables different kinds of data sharing through different communication protocols. Each protocol is suitable for some purpose. FTP (file transfer protocol) protocol is good for downloading entire datasets which have been recorded on the measurement device for prolonged periods of time. HTTP (hyper text transfer protocol) protocol can be used for real time event data supervision. MQTT (message queuing telemetry transport) protocol is often used in large IoT (Internet of Things) systems, with one main server and lots of sensor devices connected to it. All protocols support server hosting in local as well as on the global Network.

For the purpose of this paper an application called Screen Stream was used, working under the HTTP protocol [10]. The application

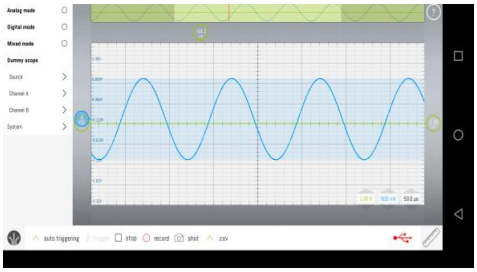

Figure 4. Smart scope Android application preview.

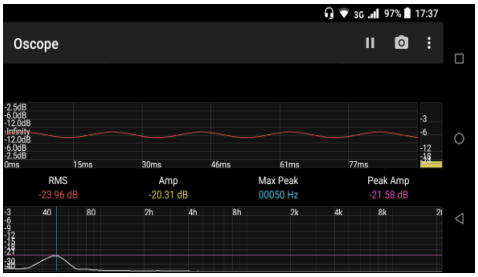

Figure 5. Oscope Android application preview.

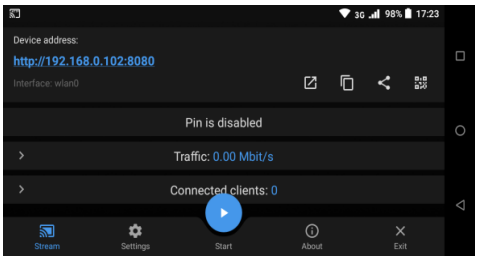

Figure 6. Screen Stream over HTTP application preview.

initiates a local server and transmits (streams) current data in real time (application preview shown in Fig. 6). All the client computers (devices) that are connected to the same wireless network can view that data. The connection between the client and the server can be established when the client device connects to the predefined IP (internet protocol) address of the server device (through a web browser). In this case shown here http://192.168.0.102:8080.

Alternative operation mode of the system is working without a Wi-Fi network. The measurement device can start its own access point, called a hotspot, and broadcast data on its own wireless network so clients can connect directly to the device and receive the data.

III. OPERATION EXAMPLE

In this section a simple example of operation will be presented for better understanding of the paper.

- 40W resistive load is connected to the 230V power outlet

- Current transformer is clamped to phase line of the load, for measurement

- Smart Scope application is started and it displays current waveform graph (Fig. 4)

- Screen Stream application is started and it broadcasts data (current display view) as a local server

- A windows desktop client is connected, and previewing the data stream through a web browser. (Fig. 7)

Device is broadcasting to a local Wi-Fi network, standard IEEE 802.11 b/g/n protocol for wireless transmission in real-time.

IV. EXPERIMENTAL DATA

Data acquired through experiments, using the above mentioned system is presented in this chapter. Some typical examples of load current waveforms can be seen in the following pictures.

First two samples were captured using the Oscope application. Upper graph shows current waveform (time-amplitude function) and lower shows frequency spectrum (frequency-amplitude function).

Fig. 8 represents data measured from a resistive load (incandescent light bulb) controlled by a triac, on a low firing angle setting. Low amplitude and characteristic waveform are present due to power electronic regulation. A wide spectrum of harmonic content can also be observed for the same reason.

Fig. 9 is the same load with the same regulator but on a different firing angle setting (greater angle). The waveform would be a sine wave but it has certain deformities due to faults in the triac regulator, which makes it more interesting for analytic display. A decrease in harmonic distortion is visible due to the firing angle of the triac.

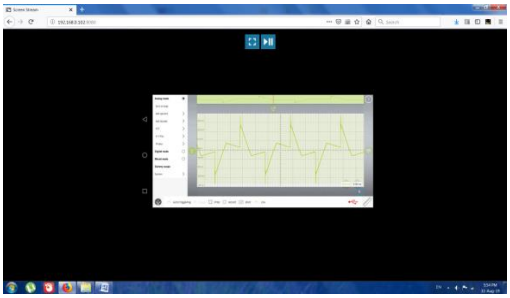

Figure 7. Windows desktop client displaying streamed data.

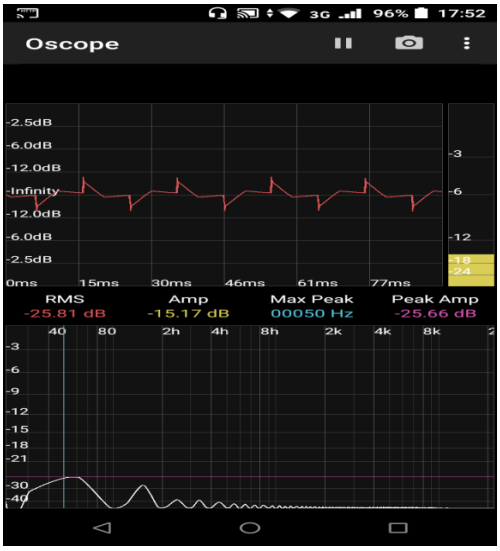

Figure 8. Resistive load low power - current waveform and frequency spectrum (Oscope).

Figure 9. Resistive load high power - current waveform and frequency spectrum (Oscope).

Next few samples were taken using the Smart Scope application, which has many options, but presented here are only signal waveform, amplitude and time base features.

Fig. 10 shows near perfect sine wave form of a resistive load.

Fig. 11 displays waveform of a CRT (cathode ray tube) television set. It owns some unique features because of the complex nature of the appliance.

Fig. 12 displays a waveform from the same type of load as in Fig. 9, a resistive load controlled by a triac on full power.

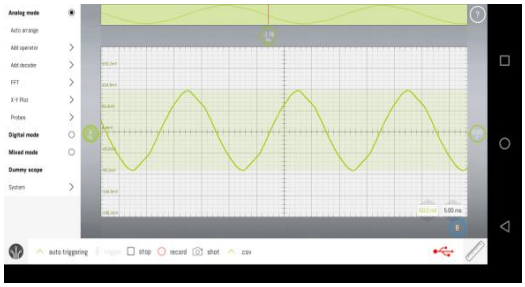

Figure 10. Resistive load (incandescent light bulb) current waveform (Smart Scope).

Figure 11. TV set current waveform (Smart Scope).

Figure 12. Triac controlled resistive load current waveform (Smart Scope).

V. CONCLUSION

This work presents a wireless power consumer monitoring system based on a Android smart device, along with an example of operation and some experimental results.

To conclude, a system for monitoring power consumers wirelessly, using an Android smart device through HTTP protocol has certain advantages. It allows power monitoring from a distance in dangerous and inaccessible environments and it is also suitable for academic presentations and scientific research.

The system can be compiled by anyone because it employs affordable devices that can be acquired easily. Some other differences of this system in comparison to other similar solutions are: it is easy to use, easy to be put together, affordable components and free software, easy to be upgraded or expanded, an intuitive research platform with wide range of functionalities and independent power supply.

Future improvements to the system may include data storage functions, data acquisition and monitoring over the internet protocol, from anywhere on the Globe and further connectivity with IoT measurement systems.

ACKNOWLEDGMENT

This work is partially supported by the Ministry of Education, Science and Technological Development of the Republic of Serbia, as part of the III44006 project. Special thanks to Research and Development Center “ALFATEC” Niš, Serbia.

REFERENCES

[1] J. A. Afonso, F. Rodrigues, P. Pereira, H. Goncalves, and J. L. Afonso, “Wireless Monitoring and Management of Energy Consumption and Power Quality Events”, WCE 2015, London, UK.

[2] J. Ferreira, J. A. Afonso, V. Monteiro, and J. L. Afonso, “An Energy Management Platform for Public Buildings”, MDPI Electronics, Basel, Switzerland, 2018.

[3] Đ. Kocić and N. Petrović, “Application of Android Based Devices in Analog Electric Signal Measurement”, YuInfo 2019, Kopaonik, Serbia.

[4] C. Meetoo, S. Bahadoorsingh, N. Ramsamooj and C. Sharma, "Wireless residential power monitoring system", IEEE Manchester PowerTech, Manchester, UK, 2017, pp. 1–6.

[5] M. Lee, Y. Park, K. Jung, and J. Yoo, “Wireless Electricity Monitoring System for Smart House using Smart Plug”, Trans Tech publications, USA 2011.

[6] N. Petrović, and Đ. Kocić, “Enabling Adaptivity in IoT-based Smart Grid Architecture”, ICEST 2019, Ohrid, North Macedonia, 2019, pp. 1-4.

[7] *Soundcard Oscilloscope*, C. Zeitniz, Available at: https://www.zeitnitz.eu, last accessed August 2019.

[8] *SmartScope*, Available at: https://www.lab-nation.com/, last accessed August 2019.

[9] *Oscope*, Available at: https://sbaud.io/oscope/, last accessed August 2019.

[10] *Screen Stream*, Dimitry Krivoruchko, Available at: https://github.com/dkrivoruchko/ScreenStream, last accessed August 2019.

Precision Electronic Weighing Scale System for Energy Conservation

Guilherme Lanzi Ernandes[1], Francisco Garcia Braghini[1], Paulo César Mioralli[2], Claiton Eduardo Luizete[2], Paulo Henrique Palota[2], Pablo Sampaio Gomes Natividade[2], Elson Avallone[2]

[1]Engineering Student-Federal Institute of Education, Science and Technology of Sao Paulo, Catanduva-SP, Brazil guilhermelanzi@hotmail.com; franciscobrag@hotmail.com
[2]Federal Institute of Education, Science and Technology of Sao Paulo, Catanduva-SP, Brazil, mioralli@ifsp.edu.br; claiton.eduardo@ifsp.edu.br; palota@ifsp.edu.br; pablo.sgn@ifsp.edu.br; elson.avallone@ifsp.edu.br

Abstract — **Scales are highly important equipments in academical and industrial environment, providing a number of methods and instruments to measurement, among them the use of load cells. This dispositive converts the deformation into an electrical sign, thus measuring the weight of an object. The present paper aims to construct a digital scale using a 3 kg load cell for liquid drip measurement. The proposed scale was built on steel and calibrated in another precision scale. Thus, was criated a calibration curve as much with the referred masses and the scale components as with the weighed scale, thus measuring only the masses' weight.**

Keywords – digital scale, strain gauge, load cell

I. INTRODUCTION

Scales are digital or analogical measurement instruments used in many knowledge areas, like in biological and exact sciences, among others. The measurement methods vary from comparison with standard weights to the application of electronic systems, which are of high accuracy, good calibration and simple construction [1].

The load cells work only with elastic deformations, a specific deformation region on the stress by strain diagram [2-4], restricting the maximum weight supported by the cell. The element that converts deformation into an electrical sign is a strain gauge (Fig. 1), which is a small resistive dispositive that turns small mechanical variations into an electrical resistance variation [5].

The strain gauge's resistance alteration follows the Second Ohm's Law [6], which states

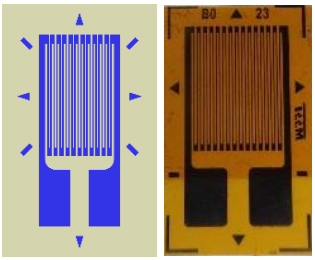

Figure 1. Strain gauge.

that the resistance of the material is directly proportional to the electrical conductor's length and inversely proportional to the cross-sectional area. Thus, the strain gauge's deformation is proportional to the load cell one.

Since the material of the strain gauge's filament is homogeneous, as much the length alterations as the cross-sectional area increase the resistance to current passage [6].

On [7] are shown some techniques for scale's use and construction using load cells.

According to [8], the strain gauge's output sign has a low voltage, in the millivolts range. In order to have a significative voltage variation and proportional to the weight variation, [8-9] it's used a Wheatstone Bridge model, according to Fig. 2.

ISBN: 978-86-80616-04-9

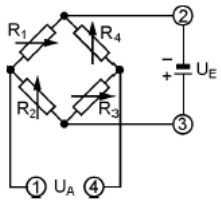

Figure 2. Wheatstone Bridge suggested by [9].

The present paper main goal consists on build a digital scale using a 3 kg load cell to liquid drip measurement. To achieve this, the balance assembly (hardware), circuit assembly and programming phases in Arduino (software), integration of the balance with the Arduino and the calibration of the balance are required.

II. MATERIALS AND METHODS

This research uses a 3 kg load cell, according to the Fig. 3.

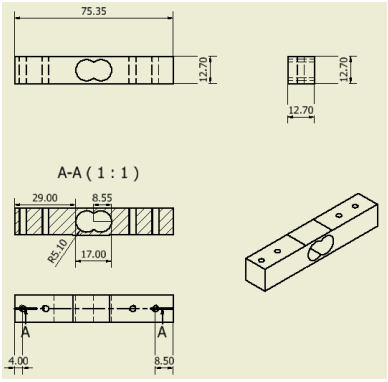

Figure 3. Dimensions of the load cell [mm].

The Fig. 4 presents isometric perspective and Fig. 5 the lateral view, respectively, with the scale's dimensions and the load cell installation. If the load cell surface is inclined, the measured value will be a weight component. Therefore, for the weight component and the normal force to be equal, it's necessary that the scale be leveled, in other words, zero slope. Thus, it was added three adjustable feet disposed in the base structure and the level kept with the assistance of water levels.

The Fig. 6 presents the scale final mounting, with the support plate, the spacer, the leveling screws and the load cell.

The load cell should be positioned so that one edge remains fixed to the structure and the other suspended. Thus, all the weight over the suspended edge promotes a uniform deformation. The metallic disc, installed on the suspended edge (Fig. 7), works like a scale tray.

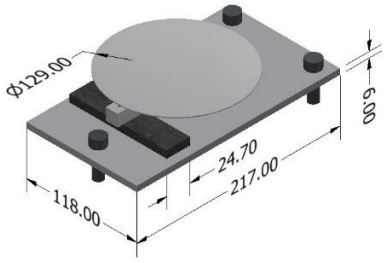

Figure 4. Scale's isometric perspective [mm].

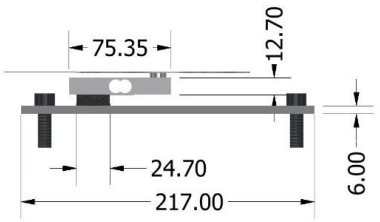

Figure 5. Scale's lateral view [mm].

Figure 6. Scale final mounting.

Figure 7. Metallic disc and load cell.

The electronic system used is an amplifier Analog-to-Digital Converter (ADC) designed for weigh scales and industrial control applications to interface directly with a bridge sensor, connected to the load cell, as shown on Fig. 8. The microcontroller Arduino do the data control and register it on a SD card [10].

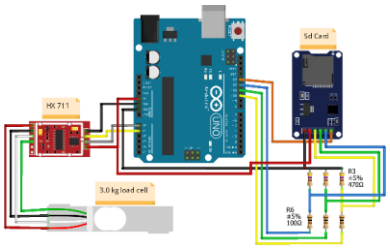

Figure 8. Load cell's schematic diagram connected to analog digital converter and to Arduino.

The generated load cell values are pure dimensionless values. Therefore, it's necessary to obtain a calibration factor for the conversion of the raw value ("get.units" function of the HX711 amplifier's library) to grams (g). Thus, was used a library to the HX711 [11], which the angular coefficient of the tendency straight is the scale's calibration factor and it's presented on Equation (1).

$$y = 733.42\,X - 31114 \quad . \qquad (1)$$

On Arduino programming [12] was observed that the scale has a linear behavior. Thus, if the scale is calibrated to a weight of 100 grams, the nearest values will have good precision.

III. RESULTS AND DISCUSSIONS

The Fig. 9 presents the values supplied by the load cell (y axis) in function of the mass. Those values was acquired by the function "get.units" from the computational program. The scale was calibrated with known masses generating the Fig. 9 graph.

The orange line represents the readings with known masses, screws, spacers and disc. The

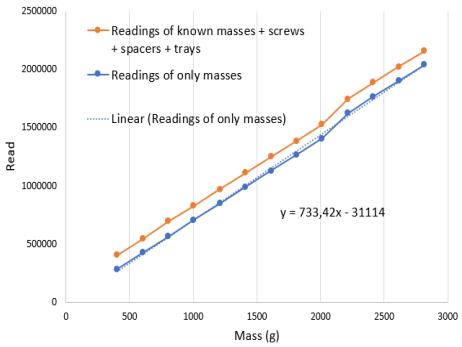

Figure 9. Acquired values by the cell in function of the mass.

blue line represents only known masses values. Analyzing the graph, it concludes that the tendency straight tends to be a linear function. The two lines are similar, but with a constant displacement between them. This displacement refers to a preload presence generated by the tray, screws and spacers.

Also was made simulations with a 29.43 N load, to verify the load cell's dynamic behavior, presented on Fig. 10.

IV. CONCLUSION

The built scale using load cell is simple and easy to build, presenting linearity on results, according to what is represented on Fig. 9. The calibration method using known masses showed itself efficient, with no significant alterations. The biggest advantage of this project is the use of Arduino platform in a simple mechanical dispositive, having an approximate cost of US$ 50,00, considering the machining. As the proposed scale has a high sensibility, it's highly applicable on the flow rate measurement, being possible to measure the small drops mass.

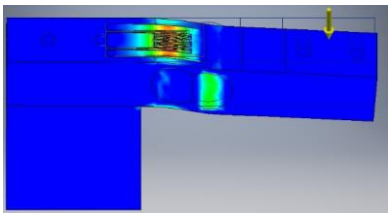

Figure 10. Load cell simulation under action of a flection force.

There's a lot of applications on the engineering environment and on scientific researches.

ACKNOWLEDGMENT

To the Federal Institute of Education, Science and Technology of Sao Paulo, Catanduva-SP, Brazil for the support and incentive.

REFERENCES

[1] R. B. Frost and C. A. Cass, "A Load Cell and Sole Assembly for Dynamic Pointwise Vertical Force Measurement in Walking", Engineering in Medicine, vol. 10, no. 1, 1981, pp. 45–50.

[2] D. Thomazini and P. U. B. Albuquerque, Sensores Industriais - Fundamentos e Aplicações, 4th ed, vol. 1, 1 vols. Brazil: Érica, 2011.

[3] H. B. Motra, J. Hildebrand, and A. Dimmig-Osburg, "Assessment of strain measurement techniques to characterise mechanical properties of structural steel", Engineering Science and Technology, an International Journal, vol. 17, no. 4, 2014, pp. 260–269.

[4] J. P. Holman, Experimental Methods for Engineers, 8th ed, vol. 1, 1 vols. Southern Methodist University: Mc Grall Hill, 2012.

[5] A. L. Silva et al., "A study of strain and deformation measurement using the Arduino microcontroller and strain gauges devices", Revista Brasileira de Ensino de Física, vol. 41, no. 3, 2019.

[6] H. D. Young and R. A. Freedman, Física III - Eletromagnetismo, 12th ed, vol. 1, Brazil: Pearson Education do Brasil, 2009.

[7] Agilent Technologies, "Resolvendo Problemas em Aplicações de Célula de Carga com a Solução de Conectividade Sem Fio da Agilent". Agilent Technologies, 2012.

[8] A. A. Zorob, "Building signal conditioning for strain gauge sensors", The Islamic University of Gaza, Gaza - Israel, 2010.

[9] K. Hoffmann, An Introduction to Measurements using Strain Gages, vol. 1, Darmstadt - Germany: Hottinger Baldwin Messtechnik GmbH, 1989.

[10] H. Bench, "Arduino LC Studio SD Card Tutorial", *Arduino Low Cost SD Card*, 11-fev-2016. [Online]. Disponível em: http://henrysbench.capnfatz.com/henrys-bench/arduino-output-devices/arduino-lc-studio-sd-card-tutorial/. [Acessado: 01-dez-2018].

[11] Avia Semiconductor, "HX711". Avia Semiconductor.

[12] Arduino, "Arduino UNO". Arduino, 2015.

Condition-Based Maintenance of Power Transformers

Sanja Stanković, Zoran Stajić, Milica Rašić

R&D Center "Alfatec", Niš, Serbia, sanja.stankovic@alfatec.rs; zoran.stajic@alfatec.rs; milica.rasic@alfatec.rs

Abstract — **Assessment of electrical equipment's condition is crucial for determining its overall health, remaining useful life, and most important, for implementing appropriate maintenance actions at the right moment in the lifetime of equipment. For power transformers, condition assessment is usually performed periodically, in certain time intervals, but this is not an insurance that failures won't occur between two overhauls. In order to prevent them, on-line condition monitoring systems are used worldwide, and different parameters are measured, alongside with standard tests and inspections done periodically. This paper reviews most important parameters that affect transformer's health condition, and different techniques used for its assessment.**

Keywords – power transformer, condition-based maintenance, health index, artificial intelligence, dissolved gas analyses

I. INTRODUCTION

Power transformer is the most important equipment in electrical energy system. In previous decades, electricity consumption has been increasing constantly, and electrical companies have been constantly challenged to improve their service, which means improving the quality and reliability of power system and power delivery. Power transformer also represents the greatest cost in electrical substation, in terms of initial investment costs, operational costs and appropriate periodical maintenance costs. If unexpected failure occurs, repair costs can be bigger than initial costs of power transformer. This is why appropriate maintenance actions must be performed according to the real condition of the transformer. This type of maintenance is called Condition-Based Maintenance (CBM). The most significant part of CBM is condition assessment and determination of required parameters, so that will be the main topic of this paper, along with overview of techniques used for this purpose.

Current practices in Serbia's electrical energy system (EES) consist mostly of periodical maintenance actions, called Time-Based Maintenance [TBM]. This practice consists of yearly overhauls of substations, when current condition of equipment is mostly evaluated subjectively during tests and inspections, and upon that, decisions about further maintenance actions are made. Another, worst case actions are performed when failure happens, and this is called Corrective Maintenance. The result and consequence of corrective and time-based maintenance is high overall costs during lifetime of transformer. These are not optimal maintenance methods, but because of the lack of on-line monitoring systems for collecting information about equipment's condition in Serbia, they are most often used methods [1-3].

This paper analyzes the most important parts and parameters of transformer which are subject to premature failures, and issues that occur and cause these failures. It also presents current practices of monitoring and diagnostic procedures of transformers, and reviews practical examples of methodologies widely used for transformer's condition assessment.

II. POWER TRANSFORMER'S CONDITION ASSESSMENT

A. *Factors that influence transformer's health condition and ageing*

The decision about revitalization or replacement of transformer can be made on the basis of information given by complete analyses of driving events, as well as diagnostics of its condition. Determination of the revitalization

ISBN: 978-86-80616-04-9

(replacement) priority depends on condition of transformer and its parts and their role in the electrical system. Because of the high investment costs in large power transformers, their replacement is conditioned by their age, or in other words, they are used for work as long as technically possible. Economic reasons, such as reducing losses in transformer, are almost never a reason for its replacement. Repairs of old transformers are also almost never practiced because the cost of repair is very high. Insulation is the most important part of transformer in term of failures, and ageing of transformer is proportional with ageing of insulation. The unexpected and premature failures of insulation can be caused due to electrical stresses, dielectric stresses, electromagnetic stresses, thermal stresses and chemical stresses. Ageing of transformer's insulation can be represented with "degradation" curve [5, 9], and it is shown in Fig. 1.

The following are the most important indicators of the end of transformer's insulation useful life [1, 10]:

- decrease in oil quality,
- increase in dissipation factor (tan δ),
- oil leakage at edges, valves and pipes,
- corrosion of the oil boiler, lid and auxiliary parts,
- damage of auxiliary devices such as thermometer, Buchholz relay, safety valves, cables etc.

Since the ageing of other individual transformer components, such as core, windings, cooling system, bushings, mechanical parts, control switches and other is not uniform and not simultaneously as insulation ageing, it is necessary to implement certain partial maintenance and monitoring activities for certain individual transformer's component.

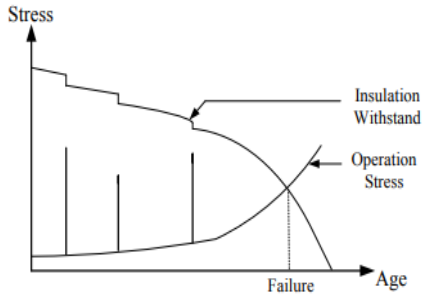

Figure 1. Degradation curve of power transfomer's insulation [5]

The ageing of transformer windings depends primarily on the operating conditions and events, especially on the duration and amount of overload during its use, and on thermal stress caused by a malfunction. The cause of the boiler ageing is corrosion, depending on transformer utilization period, external influences and maintenance. The insulation oil is subject to chemical reactions that cause its ageing, which happens faster if the oil temperature is higher. Inside long-term high-loaded transformers the heat is increasing, absorbed by the oil, and as a result its ageing accelerates. Important factors that affect transformer's characteristics are moisture and oxygen. Increasing the moisture content in the oil reduces its breakdown strength. Moisture, oxygen and heat can also damage the solid (paper) insulation of the windings of transformer. It can generally be concluded that the main impact on the aging of the transformer have moisture, oxygen and heat. The main causes of transformer aging most depend also on the operating conditions to which the transformer is exposed during its utilization. The most intense ageing processes in transformer happen at the point with the highest insulation temperature (Hot-spot temperature), which can be measured and calculated using a thermal model of transformer. Usually, thermography is used for monitoring and determining the hot-spot in transformer.

Life expectancy of large energy transformers according to available estimates ranges between 42 [11] years and 50 [10] years, assuming that they have been maintained regularly and that there have been no major failures that would permanently damage them. Different factors that affect life expectancy of power transformers are following [11]:

- installation of transformer and its commissioning;
- transformer's load rate;
- degradation of insulating paper and oil;
- exposure to system failures;
- availability of spare parts;

- system influence on transformer characteristics (apparent power);
- exposure to high temperatures;
- moisture content.

During the evaluation of power transformers' state and future availability, the following criteria are also used [12]:

- experience with similar units,
- power factor analysis,
- assessment of the condition of the control switch,
- condition of spare equipment,
- failure history.

Transformer's life can be extended by filtration of its oil which removes oxygen and other gases, water, dirt particles and acid, thus protecting hard-to-reach paper insulation of transformer windings. To evaluate the actual state of power transformers and estimate their useful remaining life, it is also necessary to record and analyze the following [12]:

- type, manufacturer and year of production,
- history of operating events (loads, voltages, short circuits),
- history of maintenance activities,
- results of diagnostic procedures.

B. Important parameters for condition assessment of power transformer

Various diagnostic procedures and tests are used to evaluate the transformer's condition such as oil analysis, dissolved gas analysis, moisture and temperature measurements, sample testing of paper insulation, furan analysis, frequency response measurements, vibration measurements and other procedures. One comprehensive list of mostly used diagnostic tests and parameters found in literature is presented in Tab. 1 [1-3, 5, 10-12, 14-21, 23-39].

Dissolved Gas Analyses (DGA) in oil is most frequently used procedure for obtaining information about transformer's insulation health and therefore information about condition of transformer itself. The distribution of each gas analyzed is related to different fault in transformer.

TABLE I. LIST OF PARAMETERS OBTAINED BY DIFFERENT TESTS AND DIAGNOSTIC INSPECTIONS OF TRANSFORMER

Test/Analyses/ Inspection/Records	**Parameter**
Dissolved gas analyses of oil and/or tap changer	Oxygen Carbon Monoxide Hydrogen Acetylene Carbon Dioxide Methane Ethan Nytrogene Ethylene
Other insulation tests Electrical tests Mechanical tests Visual inspection	Furan Dielectric losses in oil Power factor Dissipation factor Moisture Breakdown voltage Partial discharge analyses results (PDA) Hot-Spot temperature Overheating temperature Acidity Oil leakage Interfacial tension Degree of polymerization Color and feculence Corrosion Tensile strength Dielectric losses of windings Dielectric losses of bushings DC windings' resistance Insulation resistance Grounding current Vibration signals Short circuit impedance Frequency response analyses results (FRA)
Environment inspection Operation records Maintenance records Failure records	Commissioning year Installation year Operational year Load rate Overloading records Environmental temperature Environmental pressure Environmental humidity Average lifetime Cooling type Failure rate Overhauls records

On-line monitoring tools for DGA are usually photo-acoustic spectroscopy and gas chromatography with alarms to warn about high levels of any of mentioned gases in the table. Their rate can indicate the severity of deterioarition or failure. However, it is not always easy to understand the results of DGA, because a lot of other factors have impact on transformer's health and failures. Because of this, it is necessary to use other analyses, tests and different techniques beside DGA for obtaining the overall health condition of transformer [13]. Some of them are acoustic emission monitoring, thermography, winding's resistence tests, the Doble test, insulation resistence test and many other tests used for obtaining parameters from Tab. 1.

III. TECHNIQUES AND PRACTICAL EXAMPLES OF THEIR APPLICATION FOR TRANSFORMER'S CONDITION ASSESSMENT

A. Health Index Method

All previously mentioned tests, monitoring inspections and diagnostic procedures give results that need analyses and interpretation in order to get conclusions about transformer's health state. If monitoring is performed on-line continuously, and tests are carried out regularly, the collected results can be enormous and unclear, so-called "big data", and often must be analyzed with appropriate mining technique, which is called "data mining". This is done in order to extract useful information from collected data, primarily information about transformer's health condition. When on-line monitoring systems don't exist, or they are not common, like in Serbia's EES, tests can be carried out off-line or periodically, which in combination with environmental, operational and maintenance recorded data, give also useful information about current condition of transformer. This data also require some methodologies and techniques to be applied. Fig. 2 presents algorithm for condition-based maintenance, regardless of which technique or method is used.

The most commonly used and the simplest method is Health Index method (HI), and it uses different techniques to obtain overall health index of transformer. This method is often found in literature. References [14-21] explain HI methodology with practical application on power transformers to obtain their health state for the purpose of CBM.

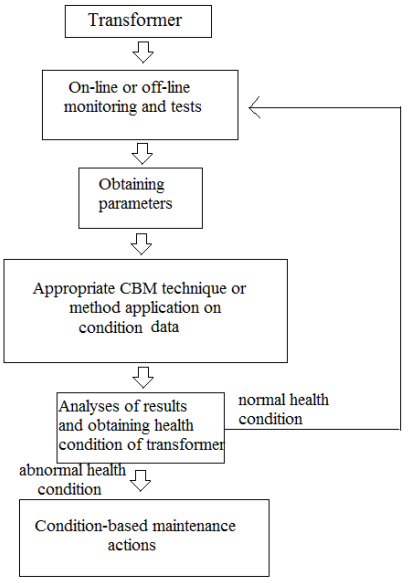

Figure 2. Condition-based maintenance algorithm

Health index method is based on ranking and scoring of different parameters that are obtained during condition monitoring and diagnostic tests. Appropriate weights are assigned to each parameter, and empirical equations developed by utilities and working groups in the domain of power engineering like CIRED, CIGRE, IEC, IEEE or others are used for health index calculation. The result of health index calculation is a number from various ranges, like 0-100, 1-10, 1-5, and 1-4 with each value having its meaning for condition of power transformer [14-16]. Evolution of mathematical formulations for health index of transformers is presented in [17]. In this paper, parameters that are observed and mostly used are reviewed with different weights from different references, and different equations used are presented. It is an excellent overview of excessive number of references, with brief explanation of some characteristic methods for health index calculation.

One good example of health index method is presented as a case study in [18]. Three transformers are analyzed, during the period from year 2003 to year 2015. Parameters that are used are condition monitoring and test data of oil, dissolved gases, electrical parameters, and records. With weights assigned to each parameter, condition rating of 4-0 (from very good to very bad) and mathematical equation applied, health indices are calculated for

previously mentioned period and each transformer.

Beside often used dissolved gases in oil and other parameters, tap changer gases as parameters can be used to complete analyses [19]. However, these parameters are not so often used, because it is difficult to determine gases content since it depends on many variables. Therefore, there are no general recommendations for tap changer gases analyses in terms of health index calculation.

Reference [20] is another good example that presents calculation of current health index of transformer based on oil parameters: breakdown voltage, acidity, moisture, color, interfacial tension, and seven gases dissolved in oil. After calculation of overall health index, it uses Markov chain model for prediction of current and future health index value.

It should be emphasized that nowadays HI methodology is most often used only because of its simplicity. However, the biggest disadvantage of this method is that subjective impact cannot be removed, so distribution utilities are challenged to replace this method with other that are less subjective. Such methods are based mostly on artificial intelligence (AI).

B. AI-based methods

In recent decades, computer science has progressed a lot, and as a branch of computer science, artificial intelligence stands out as the most applicable computational discipline in industry. Machine learning has been used since 1990s for the purpose of data mining, and in the early 21st century it started being massively used for optimization in industry and electrical engineering. In well-developed electrical energy systems, with on-line monitoring systems and sensors, condition-based maintenance is always performed with some of AI-based methods. Especially, if big data is used, condition assessment techniques are almost always AI-based.

The greatest benefit of using artificial intelligence methods over standard ranking and scoring HI method is that subjective perspective of diagnostic is totally excluded. On the other hand, HI method is very simple and practical if there is no on-line condition monitoring and if there is no big data for analyzing. Depending on complexity of the system and information collected, appropriate method can be chosen.

Reference [22] represents one excellent approach for application of AI-based techniques on condition-based maintenance. Author has developed Intelligent Fault Diagnosis and Prognosis System for CBM based on data mining techniques that are following: Supervised Back-Propagation Artificial Neural Networks, Self-Organizing Maps, Particle Swarm Optimization, Bee Colony Algorithm, Ant Colony Optimization and Association Rule. All these techniques can be generalized for any kind of equipment, including power transformer.

Concrete examples of AI-based methods applied to power transformers are presented in references [23-39]. Tab. 2 summarizes all methods applied in [23-39], in terms of method or technique that is used, number of input parameters, the type of output results and accuracy of applied method, if it is determined. It can be noticed that accuracy of each method depends a lot on number of used parameters.

In [23] artificial neural network (ANN) is applied to evaluate the health state of power transformer by using multilayer 2-tier neural network with back propagation. In the first-tier parameters that are used are dissolved gases in oil, furan, power factor, transformer's age and operation and maintenance history. In the second-tier, parameters that are used are turn ratio, short circuit impedance, DC winding resistance, frequency response analyses result and degree of polymerization. The results after training the network, verification and evaluation of test data show that this method can be accurate up to 99.5%.

References [24-26] use similar condition monitoring data and ANNs for determining the health condition of transformers. One of the oldest applications of ANN for transformer's fault diagnostics based on DGA is presented in [24]. Paper [25] is distinctive because it shows the example of estimation of remaining useful life by empirical equation based on degree of polymerization. In [26], a feed forward ANN is applied on 88 transformers for obtaining the health index.

Beside ANN, which is one of the most commonly used methods, some other AI-based methods can be found in literature. In [27], test data is classified into 8 datasets which are subjected to Support Vector Machine (SVM) method in combination with Particle Swarm Optimization and Genetic Algorithm. These two

TABLE II. REVIEW OF AI-BASED METHODS USED FOR CBM

Method/Technique	No. input parameters	Type of output	Accuracy	Ref.e
Multilayer 2-tier ANN	10	Health index [1-3] (1-poor, 2-warning, 3-good)	99.5 %	[23]
Back-propagation ANN	6	Fault class (normal, overheating, corona, arcing)	86.8-95 %	[24]
Structured ANN with Ensemble Technique	>5	Remaining useful life (in years)	96 %	[25]
Feed-forward ANN	11	Health index [0-1] (0-new transformer, 1-old transformer that should be replaced)	96.55 %	[26]
Support Vector Machine with Particle Swarm Optimization/Genetic Algorithm	13	Condition class (excellent, good, fair, poor) Fault class (normal, discharge fault, partial discharge fault, thermal fault)	93-95 %	[27]
Logistic Regression Model with Poisson Distribution	6	Condition class (good, moderate, bad)	83.3 %	[28]
Machine Learning Techniques with Particle Filtering Method	3	Remaining useful life (in years)	91.6-99.5 %	[29]
Fuzzy Logic	9	Health index [0-1] (0-good, 1-bad) Fault class (partial discharge, low discharge, high discharge, low thermal fault, medium thermal fault, high thermal fault)	Not determined	[30, 31]
Fuzzy Logic	10	Health index [0-1] (0-good/normal/excellent, 1-very poor/critical/severe)	Not determined	[32]
Fuzzy Logic	3	Condition class (poor, fair, good)	80%	[33]
Fuzzy Logic	30	Health index [0-1] (0-worst, 1-excellent) Condition class (excellent, good, poor, worst)	96 %	[34]
Neuro-Fuzzy System	8	Age of transformer (in years)	Not determined	[35]
Fuzzy Logic	4	Fault class (no fault, partial discharge, thermal fault)	70-80 %	[36]
Neuro-Fuzzy System	3	Age of transformer (in years)	89.3-99.3 %	[37]
Fuzzy Logic	5	Health index [0-1] (0-good, 1-deteriorated) Probability of failure and probability of maintenance [0-1] (0-low prob., 1-high prob.)	Not determined	[38]
Neuro-Fuzzy System	15	Condition class (very good, good, moderate, bad, very bad)	Not determined	[39]

algorithms are often used for optimization. In the case of [27] they are used for optimization of useful parameters for condition assessment. Reference [28] proposes a combination of Logistic Regression model with Poisson distribution to assess the health state of oil-immersed transformer, by using dissolved gases, breakdown voltage, furan and acidity content, moisture content and dissipation factor. Reference [29] proposes different machine learning techniques for condition assessment and lifetime predictions of power transformer. It presents good practical and software implementation of these techniques, and Extreme Gradient Boosted Regression Tree has been proven to be the most suitable and accurate prediction technique for concrete example. Another often used approach for condition assessment based on computational intelligence is Fuzzy Logic Systems method. Good theoretical background on fuzzy logic theory and applications can be found in [8]. An excessive number of references proposes this technique for overall health condition evaluation and remaining useful life prediction. References [30-39] are practical examples of fuzzy logic application on power transformers. [30] and [31] use DGA and FRA results, dielectric losses

and insulation resistance, insulation temperature, transformer's age and overheating temperature. Fuzzy logic system is generally comprised of input data, fuzzification, rule database, defuzzification and output data. Decisions about maintenance actions are made upon obtained results.

Reference [34] is very specific because it uses almost all parameters from Tab. 1 in order to obtain overall health condition of five transformers, by using fuzzy logic. This approach is one of the most comprehensive found in literature and has been proven to be very accurate.

It is worth mentioning that fuzzy logic method and ANN are sometimes used together, or in combination with ranking health index method. This approach improves these methods' accuracy, because some parameters need subjective assessment, and combination with fuzzy logic systems or ANN eliminates ambiguity. Examples of such methodology can be found in [21, 35, 37, and 39].

All previously mentioned references represent good examples of implementation of different advanced methodologies for transformer's condition assessment for the purpose of CBM.

IV. CONCLUSION

Condition-based maintenance represents "future" of maintenance practices worldwide, and so in Serbia's EES. Power transformer is the most important part of electrical substation's equipment, and it is necessary to improve its condition monitoring and diagnostics, especially if economic aspect is considered, which means that overall costs of maintenance must be minimized. This paper has presented the most important parameters that affect transformer's health condition and reviewed practical examples from scientific papers. It can be concluded that different techniques can be used for transformers' condition assessment, and the future work can be based on their practical implementation on power transformers in Serbia's EES.

ACKNOWLEDGMENT

This paper is a part of the research done within the project III 44006, supported by the Ministry of Education, Science and Technological Development of the Republic of Serbia within the framework of technological development.

REFERENCES

[1] R&D Center "Alfatec", "Racionalizacija rezervne opreme i poboljšanje pouzdanosti elektrodistributivnih objekata 110 kV i 35 kV", Niš, December 2017. (in Serbian)

[2] S. Stanković, M. Rašić, Z. Stajić, M. Stanković, "Electrical Equipment's Condition and Remaining Useful Life Assessment-a Review", Proceedings of 4th Virtual Conference on Science, Technology and Management in Energy, October 25-26, 2018, pp. 267-273.

[3] R. M. Ćirić, S. N. Mandić, "Održavanje elektroenergetske opreme", AGM knjiga, Belgrade, 2015. (in Serbian)

[4] E. L. Kokorin, A. I. Khalyasmaa, "Electrical Equipment Condition Based Maintenance Strategy," Proceedings of International Conference and Exposition on Electrical and Power Engineering (EPE 2016), October 20-22, 2016, Iasi, Romania, pp. 748-753.

[5] Q. Zhong, "Power Transformer End-of-Life Modelling: Linking Statistics with Physical Aging". Doctoral Thesis, 2011, The University of Manchester.

[6] X. Zhang, E. Gockenbach, V. Wasserberg, H. Borsi, "Estimation of the lifetime of the electrical components in distribution networks", IEEE Transactions on Power Delivery, vol. 22, no. 1, January 2007, pp. 515-522.

[7] Y. Zhang, X. Han, S. Zhang, S. Wang, "Decision-Making Methods of Condition-based Maintenance", Prognostics and System Health Management Conference, Beijing, October 21-23 2015, pp. 1-4.

[8] L.A. Zadeh, R. A Aliev, "Fuzzy Logic Theory and Applications", Part I and Part II, World Scientific, December 2018.

[9] C. Okoh, R. Roy, J. Mehnen, L. Redding, "Overview of Remaining Useful Life Prediction Techniques in Through-Life Engineering Services", Proceedings of 6th CIRP Conference on Industrial Product-Service Systems, Vindsor, Canada, May 1-2, 2014, pp. 158-163.

[10] D. Reichlet, A Frey, M. Schonneberg, "Life Expectancy of Power Systems Apparatus and Components", Cigre session 1996, Paris, 1996.

[11] CIGRE Working Group 37-27, "Ageing of the systems – Impact on planning", Paris, December 2000

[12] Edison Electric Insitute, Transmission Subject Area Subcommittee, "Round Table Discusision – Transformer Ageing", USA, 2005

[13] S. N. Hettiwatte, H. A. Fonseka, "Analysis and Interpretation of Dissolved Gases in Transformer Oil, A case study", IEEE International Conference on Condition Monitoring and Diagnosis, September 23-27, 2012, Bali, Indonesia, pp. 35-38.

[14] M. Wang, A. J. Vandermaar, "Review of condition assessment of power transformers in service", IEEE Electrical Insulation Magazine, vol. 18, 2002, pp. 12-25.

[15] A. N. Jahromi, R. Piercy, S. Cress, J. R. R. Service, W. Fan, “An approach to power transformer asset management using health index”, IEEE Electrical Insulation Magazine, vol. 25, no. 2, March-April 2009, pp. 20-34.

[16] A. Azmi, J. Jasni, N. Azis, M. Z. A. A. Kadir “Evolution of transformer health index in the form of mathematical equation”, Renewable and Sustainable Energy Reviews vol. 76, 2017, pp. 687-700.

[17] J. H. Jürgensen, A. S. Godin, P. Hilber, “Health Index as Condition Estimator for Power System Equipment: a Critical Discussion and Case Study”, Proceedings of 24th International Conference & Exhibition on Electricity Distribution (CIRED), Glasgow, Scotland, June 12-15, 2017, pp. 202-205.

[18] A. Naderian, S. Cress, R. Piercy, F. Wang, J. Service, “An Approach to Determine the Health Index of Power Transformers”, Conference Record of the 2008 IEEE International Symposium on Electrical Insulation, Vancouver, BC, Canada, June 9-12, 2008, pp. 1-5.

[19] T. Hjartarson, B. Jesus, D.T. Hughes, R.M. Godfrey “Development of Health Indices for Asset Condition Assessment”, Proceedings of IEEE PES Transmission and Distribution Conference and Exposition, Dallas, TX, USA, September 7-12, 2003, pp. 541- 544.

[20] M. S. Yahaya, N. Azis, M.Z.A. Ab Kadir, J. Jasni, M. H. Hairi, M. A. Talib**,** “Estimation of transformers health index based on the Markov chain”, Energies, vol. 10, 2017, 1824.

[21] R. D. Medina, J. P. Lata, D. P. Chacón, “Health Index Assessment for Power Transformers with Thermal Upgraded Paper up to 230kV Using Fuzzy Inference Systems”, International Caribbean Conference on Devices, Circuits and Systems (ICCDCS), Cozumel, Mexico, June 5-7, 2017, pp. 1-6.

[22] Z. Zhang, “Data Mining Approaches for Intelligent Condition-based Maintenance,” Doctoral Thesis at Norwegian University of Science and Technology, Trondheim, 2014

[23] P. H. Mukti, F. A. Pamuji, B. S. Munir, “Implementation of Artificial Neural Networks for Determining Power Transfomer Condition”, Proceedings of 5th International Symposium on Advanced Control of Industrial Processes, Hiroshima, Japan, May 28-30, 2014, pp. 473-477.

[24] Y. Zhang, X. Ding, Y. Liu, P. J. Griffin, “An artificial neural network approach to transformer fault diagnosis”, IEEE Transactions on Power Delivery, vol. 11, no. 4, October 1996, pp. 1836-1841.

[25] T. Matsui, Y. Nakahara, K. Nishiyama, N. Urabe, M. Itoh, “Development of Remaining Life Assessment for Oil-immersed Transformer Using Structured Neural Networks”, Proceedings of CROS-SICE International Joint Conference, Fukuoka, Japan, August 18-21, 2009, pp. 1855-1858.

[26] A. E. B. Abu-Elanien, M. M. A. Salama, M. Ibrahim, “Determination of Transformer Health Condition Using Artificial Neural Networks”, International Symposium on Innovations in Intelligent Systems and Applications, Istanbul, Turkey, June 15-18, 2011, pp. 1-5.

[27] Y. Cui, H. Ma, T. K. Saha, “Power Transformer Condition Assessment Using Support Vector Machine with Heuristic Optimization”, Australasian Universities Power Engineering Conference, AUPEC 2013, Hobart, TAS, Australia, 29 September - 3 October, 2013, pp.1-6

[28] S. Areffin, M. I. Hasan, B. A.Chowdhury, “Assessment of the Health Condition of OilImmersed Transformers Using Logistic Regression and Poisson Distribution”, 3rd International Conference on Electrical Information and Communication Technology (EICT), Khulna, Bangladesh, December 7-9, 2017, pp. 1-5.

[29] J. I. Aizpurua, S. D. J. McArthur, B. G. Stewart, B. Lambert, J. G. Cross, V. M. Catterson, “Adaptive Power Transformer Lifetime Predictions through Machine Learning & Uncertainty Modelling in Nuclear Power Plants”, IEEE Transactions on Industrial Electronics, vol. 66,no. 6, June 2019, pp. 4726– 4737.

[30] M. Žarković, Z. Stojković, “Analysis of artificial intelligence expert systems for power transformer condition monitoring and diagnostics”, Electric Power System Research 149, 2017, pp. 125-136.

[31] M. Žarković, “Monitoring and Diagnostics of Substation Based on Fuzzy Model of High Voltage Equipment Condition”, Doctoral Thesis, University of Belgrade, 2017.

[32] M. Arshad, S. M. Islam, A. Khaliq, “Fuzzy Logic Approach in Power Transformers Management and Decision Making”, IEEE Transactions on Dielectrics and Electrical Insulation vol. 21, No. 5, October 2014, pp. 2343-2354.

[33] G. C. Jaiswal, M. S. Ballal, D.R. Tutakne, “Health Index Based Condition Monitoring of Distribution Transformer”, International Conference on Power Electronics, Drives and Energy Systems (PEDES), Trivandrum, India, December 14-17, 2016, pp. 1-5.

[34] C. Ranga, A. K. Chandel, R. Chandel, “Fuzzy logic expert system for optimum maintenance of power transformers”, International Journal on Electrical Engineering and Informatics, vol. 8, No 4, December 2016, pp. 836-850.

[35] A. K. Kori, A.K. Sharma, A.K.S. Bhadoriya, “Neuro fuzzy system based condition monitoring of power transformer”, IJCSI International Journal of Computer Science Issues, vol. 9, no. 2, No 1, March 2012, pp. 495-499.

[36] C. Q. Su, “A New Fuzzy Logic Method for Transformer Incipient Fault Diagnosis”, IEEE International Conference on Fuzzy Systems (FUZZ-IEEE), July 24-29, 2016, pp. 324-327

[37] S. Forouhari, A. Abu-Siada, “Application of adaptive neuro fuzzy inference system to support power transformer life estimation and asset management decision”, IEEE Transactions on Dielectrics and Electrical Insulation, vol. 25, no. 3, June 2018, pp. 845-852.

[38] L. Rosero-Z, A. Pavas, I. C. Duran, “Analysis of Maintenance in Transformers Based on a Fuzzy Logic Method”, IEEE PES Transmission & Distribution Conference and Exhibition - Latin America, September 18-21, 2018, pp. 1-5.

[39] E. Kadim, N. Azis, J. Jasni, M. Talib, “Transformers health index assessment based on neural-fuzzy network“, Energies, vol. 11, 2018, 710, pp. 1-14.

Greenland Wolf Optimization Algorithm for Solving Optimal Reactive Power Problem

Kanagasabai Lenin

Prasad V.Potluri Siddhartha Institute of Technology, Kanuru, Vijayawada, Andhra Pradesh -520007.Email: gklenin@gmail.com

Abstract — **This paper proposes Greenland wolf optimization (GWO) algorithm to solve the optimal reactive power problem. Deeds of the Greenland wolf have been imitated to formulate the proposed algorithm. Greenland wolf is a breed of gray wolf which whiter in coloration, narrower braincase. Exploration & Exploitation ability of the algorithm has been improved by flag vector, position, velocity update property. Proposed Greenland wolf optimization (GWO) algorithm has been tested in standard IEEE 30 bus test system and simulation results show the projected algorithms reduced the real power loss considerably.**

Keywords - Optimal Reactive Power, Transmission loss, Greenland wolf optimization

I. INTRODUCTION

Reactive power problem plays an important role in secure and economic operations of power system. Numerous types of methods (Newton's method, interior point, successive quadratic programming method) [1-6] have been utilized to solve the optimal reactive power problem. However many scientific difficulties are found while solving problem due to an assortment of constraints. Evolutionary techniques gravitational search, Ant Lion Optimizer, symbiotic organism search algorithm) [7-16] are applied to solve the reactive power problem. This paper proposes Greenland wolf optimization (GWO) algorithm to solve the optimal reactive power problem. Greenland wolf is a variety of gray wolf and they possess average length of 155 cm. Naturally in a pack of Greenland wolf 3 to 4 will be there. Greenland wolf are in danger of extinction owing to their remarkably little densities, minor pack sizes, less reproduction, and inferior brood production. GWO algorithm is based on the actions of Green land wolf. Proposed Greenland wolf optimization (GWO) algorithm has been tested in standard IEEE 30 bus test system and simulation results show the projected algorithm reduced the real power loss considerably.

II. PROBLEM FORMULATION

Objective of the problem is to reduce the true power loss.

$$F = P_L = \sum_{k \in Nbr} g_k (V_i^2 + V_j^2 - 2V_i V_j \cos\theta_{ij}) . \quad (1)$$

Voltage deviation given as follows:

$$F = Power\ \ Loss + \omega_V \times VD . \quad (2)$$

Voltage deviation given by:

$$Voltage\ \ Deviation(VD) = \sum_{i=1}^{N_{pq}} |V_i - 1| . \quad (3)$$

Constraint (Equality)

$$P_G = P_D + P_L \ . \quad (4)$$

Constraints (Inequality)

$$p_{gslack}^{\min} \le P_{gslack} \le p_{gslack}^{\max} \ , \quad (5)$$

$$Q_{gi}^{\min} \le Q_{gi} \le Q_{gi}^{\max}, i \in N_g \ , \quad (6)$$

$$V_i^{\min} \le V_i \le V_i^{\max}, i \in N \ , \quad (7)$$

$$T_i^{\min} \le T_i \le T_i^{\max}, i \in N_T , \quad (8)$$

$$Q_C^{\min} \le Q_C \le Q_C^{\max}, i \in N_C \ . \quad (9)$$

III. GREENLAND WOLF OPTIMIZATION

Greenland wolf optimization (GWO) mimics the deeds of Greenland wolf in nature. The deeds of the Greenland wolf have been imitated to formulate the algorithm. Hunting procedure of the Greenland wolf is designed to formulate the algorithm. There are three fittest candidate solutions embedded as α, β and γ to lead the population toward capable regions of the exploration space in each iteration of Greenland wolf optimization. φ is named for the rest of Greenland wolf and it will assist α,β and γ to encircle, hunt, and attack prey; in order to find improved solutions. Encircling actions of Greenland wolves are:

$$\vec{Q} = \left| \vec{I}.\vec{G}_p(t) - \vec{G}(t) \right|, \quad (10)$$

$$\vec{G}(t+1) = \vec{G}_p(t) - \vec{G}.\vec{Q} \ . \quad (11)$$

Hunting actions of Greenland wolf are expressed by,

$$\vec{Q}_\alpha = \left| \vec{I}_1 \vec{G}_\alpha - \vec{G} \right|, \quad (12)$$

$$\vec{Q}_\beta = \left| \vec{I}_2 \vec{G}_\beta - \vec{G} \right|, \quad (13)$$

$$\vec{Q}_\gamma = \left| \vec{I}_3 \vec{G}_\gamma - \vec{G} \right|, \quad (14)$$

$$\vec{G}_1 = \vec{G}_\alpha - \vec{F}_1.\vec{Q}_\alpha \ , \quad (15)$$

$$\vec{G}_2 = \vec{G}_\beta - \vec{F}_2.\vec{Q}_\beta \ , \quad (16)$$

$$\vec{G}_3 = \vec{G}_\gamma - \vec{F}_3.\vec{Q}_\gamma \ , \quad (17)$$

$$\vec{G}(t+1) = \frac{\vec{G}_1 + \vec{G}_2 + \vec{G}_3}{3} \ . \quad (18)$$

Greenland wolf position is is modernized and discrete the position is given by,

$$flag_{i,j} = \begin{cases} 1 & G_{i,j} > 0.490 \\ 0 & otherwise \end{cases} \ . \quad (19)$$

where i , indicates the j^{th} position of the i^{th} Greenland wolf, $flag_{i,j}$ is features of the Greenland wolf.

Greenland wolf communications among them is augmented by,

$$\omega_i^d = G_i^d + \varphi_{id}(G_\alpha^d - z_i^d) + \varphi_{id}(G_j^d - G_k^d) \ . \quad (20)$$

Density of the Greenland wolf is given by,

$$\rho_i = \sum_{G \in T/\{i\}} e^{-\left(\frac{d_{ij}}{dc}\right)^2} \ . \quad (21)$$

"X" and "Y" intersection of sets is symbolized by "E":

$$E = X \cap Y \ , \quad (22)$$

$$E = \{e; e_i \in S, e_i \in X, i = 1,2,..,i\} \ . \quad (23)$$

Let "M" be the accumulate to stock the eradicated individuals,

$$M = \begin{cases} M_1, random > e^{(\frac{t}{t_{\max imum}})^2} \\ S[1;E], other \end{cases} \ . \quad (24)$$

Positions and velocities are modernized to advance the performance of the exploration & exploitation in the projected algorithm.

$$v_{t+1}^i = \omega_t.v_t^i + cg_1.Rm.(m_t^i - y_t^i) + \\ + cg_2.Rm_2.(m_t^g - y_t^i) \ . \quad (25)$$

$$y_{t+1}^i = y_t^i + v_{t+1}^i \ . \quad (26)$$

ω_t is updated by

$$\omega_t = (\omega_{\max} - \omega_{\min}).\frac{(t_{\max} - t)}{t_{\max}} + \omega_{\min} \ . \quad (27)$$

Maximum and minimum of ω_t is represented by $\omega_{\max}$ and $\omega_{\min}$; maximum number of iterations is given by $t_{\max}$

Fitness function will be calculated by,

$$Fitness = \alpha T + \beta \frac{N - P}{N} \quad . \qquad (28)$$

Where T define the accurateness, P is the length of chosen element division, N is the sum of all features, and α and β are the weight of classification and picking quality, $\alpha \in [0,1] and$

$\beta = 1 - \alpha$.

Initialization

$i = 1$: population size; $(j) = 1 : n$

When $(i, j) > 0.490; (i) = 1$; Else $(j) = 0$;

End if

Fitness function computed by;

$$Fitness = \alpha T + \beta \frac{N - P}{N}$$

Primary, secondary, third maximum fitness of the Greenland wolf is designated as "α", "β", "γ"

While k < maximum number of iteration

For $i = 1$: population size

Modify the position of Greenland wolf by

$$\vec{G}(t+1) = \frac{\vec{G_1} + \vec{G_2} + \vec{G_3}}{3}$$

Present Greenland wolf location has been modified episodically

End for

For $i = 1$: population size; For $i = 1 : n$

If $(i, j) > 0.490; (j) = 1$; Else; $(j) = 0$;

End for

Update the parameter values whenever necessary

Computation of fitness function;

$$Fitness = \alpha T + \beta \frac{M - G}{M}$$

Greenland wolf"α","β" and " γ" will be renewed

$t = t + 1$

End while

Return the best solution" α "

End

IV. SIMULATION STUDY

Projected Greenland wolf optimization (GWO) algorithm has been tested, in IEEE 30 Bus system. Table 1 shows the constraints of control variables, Table 2 shows the limits of reactive power generators and comparison results with particle swarm optimization (PSO), modified particle swarm optimization (MPSO), self-adaptive real coded Genetic algorithm (SAGRA), Evolutionary Programming (EP) are presented in Table 3.

TABLE I. CONSTRAINTS OF CONTROL VARIABLES

System	Variables	Minimum (PU)	Maximum (PU)
IEEE 30 Bus	Generator Voltage	0.95	1.1
	Transformer Tap	o.9	1.1
	VAR Source	0	0.20

TABLE II. CONSTRAINS OF REACTIVE POWER GENERATORS

System	Variables	Q Minimum (PU)	Q Maximum (PU)
IEEE 30 Bus	1	0	10
	2	-40	50
	5	-40	40
	8	-10	40
	11	-6	24
	13	-6	24

V. CONCLUSION

In this paper Greenland wolf optimization (GWO) algorithm successfully solved the optimal reactive power problem. Wolf embedded as α, β and γ to lead the population toward capable regions of the exploration space in each iteration of Greenland wolf optimization. φ is named for the rest of Greenland wolf and it will assist α, β and γ to encircle, hunt, and attack prey. .Proposed Greenland wolf optimization (GWO) algorithm has been tested in standard IEEE 30 bus test system and simulation results show the projected algorithms reduced the real power loss efficiently and percentage of real power loss reduction obtained is 18.11.

TABLE III SIMULATION RESULTS OF IEEE −30 SYSTEM

Cont. variables	Base case	MPSO [19]	PSO [19]	EP [19]	SARGA[19]	GWO
VG−1	1.060	1.101	1.100	NR*	NR*	1.020
VG−2	1.045	1.086	1.072	1.097	1.094	1.023
VG−5	1.010	1.047	1.038	1.049	1.053	1.054
VG−8	1.010	1.057	1.048	1.033	1.059	1.012
VG−12	1.082	1.048	1.058	1.092	1.099	1.031
VG-13	1.071	1.068	1.080	1.091	1.099	1.037
Tap11	0.978	0.983	0.987	1.01	0.99	0.912
Tap12	0.969	1.023	1.015	1.03	1.03	0.910
Tap15	0.932	1.020	1.020	1.07	0.98	0.914
Tap36	0.968	0.988	1.012	0.99	0.96	0.910
QC10	0.19	0.077	0.077	0.19	0.19	0.070
QC24	0.043	0.119	0.128	0.04	0.04	0.112
PG (MW)	300.9	299.54	299.54	NR*	NR*	298.76
QG (Mvar)	133.9	130.83	130.94	NR*	NR*	130.84
Reduction in PLoss (%)	0	8.4	7.4	6.6	8.3	18.11
Total PLoss (Mw)	17.55	16.07	16.25	16.38	16.09	14.370

NR* - Not reported

REFERENCES

[1] K. Y. Lee. “Fuel-cost minimisation for both real and reactive-power dispatches,” Proceedings Generation, Transmission and Distribution Conference, vol. 131, no. 3, 1984, pp. 85-93.

[2] N. I. Deeb. “An efficient technique for reactive power dispatch using a revised linear programming approach,” Electric Power System Research, vol. 15, no. 2, 1998, pp. 121–134.

[3] M. R. Bjelogrlic, M. S. Calovic, B. S. Babic.”Application of Newton’s optimal power flow in voltage/reactive power control”, IEEE Trans Power System, vol. 5, no. 4, 1990, pp. 1447-1454.

[4] S. Granville “Optimal reactive dispatch through interior point methods,” IEEE Transactions on Power System, vol. 9, no. 1, 1994, pp. 136–146. http://dx.doi.org/10.1109/59.317548

[5] N. Grudinin, “Reactive power optimization using successive quadratic programming method,” IEEE Transactions on Power System, vol. 13, no. 4, 1998, pp. 1219–1225.

[6] Ng Shin Mei, R.; Sulaiman, M.H.; Mustaffa, Z.; Daniyal, H. (2017) “Optimal reactive power dispatch solution by loss minimization using moth-flame optimization technique”, Appl. Soft Comput. No. 59, 2017, pp. 210–222.

[7] Chen, G.; Liu, L.; Zhang, Z.; Huang, S. “Optimal reactive power dispatch by improved GSA-based algorithm with the novel strategies to handle constraints” Appl. Soft Comput. vol. 50, 2017, pp. 58–70.

[8] Naderi, E.; Narimani, H.; Fathi, M.; Narimani, M.R, “A novel fuzzy adaptive configuration of particle swarm optimization to solve large-scale optimal reactive power dispatch”, Appl. Soft Comput. Vo. 53, 2017, pp. 441–456.

[9] Heidari, A.A.; Ali Abbaspour, R.; Rezaee Jordehi, A. “Gaussian bare-bones water cycle algorithm for optimal reactive power dispatch in electrical power systems”, Appl. Soft Comput. vol. 57, 2017, pp. 657–671.

[10] Mahaletchumi Morgan, Nor Rul Hasma Abdullah, Mohd Herwan Sulaiman, Mahfuzah Mustafa, Rosdiyana Samad, “Benchmark Studies on Optimal Reactive Power Dispatch (ORPD) Based Multi-objective Evolutionary Programming (MOEP) Using Mutation Based on Adaptive Mutation Adapter (AMO) and Polynomial Mutation Operator (PMO)”, Journal of Electrical Systems, 2017, pp. 12-1.

[11] Rebecca Ng Shin Mei, Mohd Herwan Sulaiman, Zuriani Mustaffa, “Ant Lion Optimizer for Optimal Reactive Power Dispatch Solution” , Journal of Electrical Systems, "Special Issue AMPE2015", 2016, pp. 68-74.

[12] P. Anbarasan ; T. Jayabarathi, “Optimal reactive power dispatch problem solved by symbiotic organism search algorithm”, Innovations in Power and Advanced Computing Technologies, 2017, DOI: 10.1109/IPACT.2017.8244970

[13] Gagliano A., Nocera F. “ Analysis of the performances of electric energy storage in residential applications”, International Journal of Heat and Technology , vol. 35, Special Issue 1, 2017, pp. S41-S48. DOI: 10.18280/ijht.35Sp0106.

[14] Caldera M., Ungaro P., Cammarata G., Puglisi G. Survey-based analysis of the electrical energy demand in Italian households, Mathematical Modelling of Engineering Problems, vol. 5, no. 3, 2018, pp. 217-224. DOI: 10.18280/mmep.050313

[15] M. Basu, “Quasi-oppositional differential evolution for optimal reactive power dispatch”, Electrical Power and Energy Systems, vol. 78, 2016, pp. 29-40.

[16] X.S. Yang. “Bat algorithm for multi-objective optimization”, International Journal of Bio-Inspired Computation, vol. 3, no. 5, 2011, pp. 267– 274.

[17] Y W. Yamany, E. Emary, and A. E. Hassanien, “Wolf search algorithm for attribute reduction in classification,” in Computational Intelligence and Data Mining (CIDM), 2014 IEEE Symposium, pp. 351–358.

[18] IEEE, *The IEEE-test systems*, (1993) Available at:, http://www.ee.washington.edu/trsearch/pstca/.

[19] Ali Nasser Hussain, Ali Abdulabbas Abdullah and Omar Muhammed Neda, "Modified Particle Swarm Optimization for Solution of Reactive Power Dispatch", Research Journal of Applied Sciences, Engineering and Technology, vol. 15, no. 8, 2018, pp. 316-327. DOI:10.19026/rjaset.15.591

Application of SWOT Analysis in the Energy Sector: A Case Study of a District Heating Plant

Ivana Veličkovska

Mathematical Institute SASA, Belgrade, Serbia, ivana.v.93@gmail.com

Abstract — **Strengths (S) Weaknesses (W) Opportunities (O) and Threats (T) analysis is one of the most well-known analyzes in strategic management. It is used to explore internal and external influencing factors on different questions. It plays a significant role in defining development strategies and can be applied in different sectors. In this paper, SWOT analysis is used in energy sector in the case of Public Utility Company "Toplana" Bor, which is responsible for the production and distribution of heat for the purposes of district heating. Based on the gathered information and interviews with employees of this company, strong aspects of the company are identified and those aspects where the company has problems. Opportunities that come from the external environment and threats that can put the company at risk are perceived. Results of the research identified 24 elements of SWOT analysis, 4 belonging to the company's strengths, 7 elements identified as weaknesses, 6 potential development opportunities and 7 environmental challenges seen as threats.**

Keywords – SWOT analysis, energy, district heating

I. INTRODUCTION

Energy development is an important task in achieving growth and development of an economy [1]. The reason for performing the analysis in an energy system is to define the existing situation in the system and beyond, which initiates the first step towards achieving sustainable development of the system and maximizing its energy efficiency.

The development of the energy system of the Republic of Serbia is defined in the Strategy for Energy Development of the Republic of Serbia until 2025 with projections to 2030 [2]. The strategic objectives of this strategy in terms of district heating systems are reflected in (1) Providing heat for a secure supply of consumers; (2) Increasing energy efficiency in production, distribution and use of thermal energy; (3) Increasing the use of renewable energy and (4) Sustainable business producers of heat. Further analysis described in the strategy shows main problems of district heating systems which are seen in the use of nonrenewable resources, obsolete infrastructure, high level of consumption and inadequate energy market.

The authors Mazhar et al., [3] conducted a detailed survey on the development of the district heating. In the research, they found that district heating was the most common way of heating urban areas. According to their research, modernized district heating systems require the use of renewable energy by using renewable technologies.

Similar study considers trends in modernizing district heating technology in Europe [4]. Results of the study indicate increased need for more flexible energy systems and greater share of renewable energy used in district heating.

The use of sustainable energy sources is present in district heating systems and it requires sustainable energy management [5]. SWOT analysis used in this paper is a powerful management tool which is usually used in the process of investigating a specific situation by observing it from multi-level perspective (internal and external influential factors) [1]. Therefore, it is the main reason for using this analysis. Internal and external factors are described by [6-9]. Internal factors include Strengths and Weaknesses which directly influence on the specific situation. While external factors are Opportunities and Threats

ISBN: 978-86-80616-04-9

that come from the environment and systems cannot directly influence on them but can adopt preventive measures and well-designed strategies to react. The main objective of this paper can be defined as an idea of implementing SWOT analysis in a specific energy system, based on listing all 4 elements of the analysis in order to identify current situation in the system, main problems and strengths so adequate development strategies could be defined.

The subject of this paper is reflected in the implementation of a SWOT analysis in the energy system involved in the production and distribution of thermal energy for district heating. Section II gives a brief overview of the company where the survey is being conducted. Section III presents the main results of the SWOT analysis and a detailed description of the individual influencing factors. Section IV summarizes the obtained results and recommendations for future research.

II. CASE STUDY

Public Utility Company "Toplana" Bor (PUC "Toplana" Bor) has been operating independently since 2002 when it was separated from the mining complex RTB Bor [10]. The main activity is the production of thermal energy for district heating in the city of Bor, located in Eastern Serbia [10].

Basic information about consumers can be found in Table I, which is compiled based on data from Business Association of the District Heating Companies of Serbia [11].

In order for a company to take corrective actions or devise a new strategy, first it must determine current internal resources and external possibilities. During interviews with company representatives, it was determined that there was no defined SWOT analysis which represents the base for further research. The task of implementing SWOT analysis in the PUC "Toplana" Bor is done in order to determine the internal forces on which the company can rely and disadvantages which must be familiar when implementing the process of planning the development of this energy system. The analysis is also conducted for external factors as each system represents one part of the environment and is exposed to exterior influences.

The research was realized in collaboration with the experts from the thermal power plant through interviews where they identified the most important development challenges. Table II shows different internal and external factors whose impact was analyzed.

TABLE I. GENERAL INFORMATION ABOUT DISTRICT HEATING IN BOR

	Total
Population	34,710
Number of households	12,420
Number of households connected to the district heating system	11,352
Percentage of households connected to the district heating system (%)	91.4
Total heating area of the residential units connected to the district heating system (m^2)	624,612
Total heating area of other establishments, institutions and business units connected to the district heating system (m^2)	134,819
Total heating area (m^2)	759,431
Total installed power of the heating units of residential units connected to the district heating system (MW)	105
Total installed power of the heating units of other units connected to the district heating system (MW)	24
Total installed power consumption (MW)	129

TABLE II. INTERNAL AND EXTERNAL INFLUENTAL FACTORS

Influence level	**Factor**
Internal	Technical resources
	Human resources
	Financial resources
External	Government
	Customers
	Competition
	Suppliers
	Environment
	Other stakeholders

III. FINDINGS

SWOT analysis results show the great potential that the environment provides and strengths that form the basis for further development. 4 elements of company's strength and 6 elements of opportunity that can be used in the environment have been identified. Furthermore, the analyzed threats from the environment indicate that there are a number of challenges and in this research, they cover 7 elements. Additional 7 elements represent the company's weaknesses. All of them are listed in Table III and described in the following part of the research.

TABLE III. SWOT ANALYSIS FOR PUBLIC UTILITY COMPANY "TOPLANA" BOR

	Strengths (S)	**Weaknesses (W)**
INTERNAL	A satisfactory level of production capacity	Obsolete Equipment
	Built district heating system	Low level of automation
	Large number of users	Many failures
	Expert staff	Lack of financial resources
		Inadequate maintenance system
		High preparation costs
		Use of nonrenewable energy sources
	Opportunities (O)	**Threats (T)**
EXTERNAL	Heating price regulation	Increase in energy prices
	Specialized funds	Reduction of coal use
	Renewable energy sources	Reducing the number of users
	Gasification	Change of legislation
	Public-Private Partnership	Lower investment by state
	Cooperation with the EU	Outflow of skilled labor and unemployment
		Climate change

Strengths. District heating plant consists of a new facility, a boiler room with 2 hot-water boilers for coal and one hot-water boiler for fuel oil, a separate facility for a pump-exchange station, a fuel station with a fuel oil tank, daily coal depots with an inclined conveyor from the landfill to the bunker of the boilers, chimney, substation, distribution electro technical facilities and cable network [12]. PUC "Toplana" Bor has 3 heat boilers with 58 MW individual capacity so total boiler capacity is 174 MW [12]. The current capacity of the company is sufficient for the existing heat demand. Two boilers use coal as a fuel and are currently active. Third boiler uses oil fuel and is not active with low number of working hours. Detailed characteristics of coal heat boilers [12] are shown in Table IV.

Type of transportation system of thermal energy consists of one-pipe and two-pipe heating network while branched and airy. The main network consists of 3 main lines: "A", "C" and "Veliki Krivelj" [10]. The longest line is "C", where the final consumer is 4,946.5 m away from the heat source and the shortest is "Veliki Krivelj" with a distance of 2,859 m.

TABLE IV. TECHNICAL CHARACTERISTIC OF THE COAL HEAT BOILER [12]

Power (MW)	58
Level of efficiency (%)	83
Maximum pressure (bar)	25
Working pressure at the outlet (bar)	18.4
Water temperature at the inlet (°C)	130
Water temperature at the outlet (°C)	190
Water flow (t/h)	804
Water pressure drop in the boiler (bar)	1.47
Fuel	Coal
Amount of flue gas (m^3/h)	210,000
Flue gas temperature (°C)	200

For the purpose of urban district heating system 235 substations have been installed, of which 86 have been modernized and their characteristic power is shown in Table V [11]. Total production capacity of thermal energy is adequate in relation to the consumption according to expert opinions.

TABLE V. INSTALLED SUBSTATION POWER [11]

Installed substation power	Total number of substations
>30 KW	7
30 KW – 100 KW	10
100 KW – 500 KW	125
< 500 KW	93

Another important internal advantage of the company was found in the total number of users in relation to the population of the city. Heat production in Bor is performed only in PUC "Toplana" Bor [13] which means that the thermal energy market in this area is established by the company. The company is in charge of heating over 11,000 customers each year, an average of 200 days a year, which can be deduced from Table I. In this area, there has been a dramatic decline in residential construction since the 1990s due to economic and political reasons [13] which leads to the fact that the heating network, which has already been built, is enough to power the city. Urban district heating system in the city is characterized by the large coverage of the city district heating network and is partly due to previously explained reasons. In other words, 91.4% of the city population uses heating services, which places Bor at the very top, perceived at the national level when the city's coverage of the district heating network is observed [10, 11]. According to internal statistical data about consumers the highest percentage of users is the local population for heating private facilities while heating services are also used for public buildings with various purposes such as schools, local administration and others.

Based on interviews with company experts, it was found that the company engages skilled workforce with extensive knowledge in its field of work based on education and extensive work experience.

Weaknesses. Boiler units and heating network have been in use more than 30 years [11] and for many years appropriate maintenance hasn't been realized. The total length of the distribution network is 37,000 m and of this length 11% of the network is above ground, 4% in the concrete channel and 85% underground [11].

Heating network is obsolete and during the heating season a number of breakthroughs occur due to damaged isolation, causing lower heating quality and energy losses at a share of 25%, which represents a major problem for the company [13]. Heating substation which are summarized above in Table V represent outdated technology and less than 40% of these substations are modernized in the last few years. The problem of outdated equipment along with outdated network and other supporting infrastructure leads to reduced efficiency of operations which results in high costs [10]. There are 4,500 m^3 of water in the system during the heating season [11], and when the pipes burst, there is an enormous loss of water because the water in the system is chemically prepared thereby is more expensive than regular. Company experts state that for a better heating service it is necessary to replace the old and damaged grid, which would also reduce the losses caused by the pipe burst.

Experts from the company cite a problem of financial nature in terms of insufficient degree of regular payment of heat consumption by the consumers where less than 50% of users pay their bills on time. They emphasize that poor collection of receivables results in a lack of own funds that would otherwise be utilized in the regular production and would not create company debts. It is necessary to use a more efficient system of collection of receivables. There are no investments by the private sector as this company is part of a public sector.

Energy source which is used for the production of thermal energy is coal and its average consumption is 46 466 tons per year [10]. The total production of thermal energy in the district heating system is based on the use of nonrenewable energy sources because the existing technology is inadequate for these energy sources as described Table IV. According to experts, the additional problem of the use of nonrenewable energy sources is the absence of electrostatic precipitators in the existing production process that would treat gases emitted into the atmosphere.

Opportunities. Experts from the company emphasized the problem of current payment system where monthly heating price is calculated for the heated area, expressed in m^2, which could be solved by installing a heat meter so that individual user could control own energy consumption and thus increase the efficiency of the heating system. By them, the problem of billing per square meter is reflected in the lack of isolation of public and private space belonging to the district heating system causing bad quality of heating even provided heat is on a satisfactory level. Therefore, new model of payment would regulate the price of district heating by charging according to the real energy consumption and affect the company's revenue.

Development of the energy system of the Republic of Serbia foresees a trend of increased use of renewable energy sources in the

considered period until 2030 [2]. One of the potentials arising from this regulation is the transition to renewable energy for urban heating. When it comes to renewable energy sources, the greatest potential in Serbia is biomass that is available throughout the country. Study on energy efficiency and analysis of biomass heating potential of public buildings in Bor already exists [14]. The study shows that the construction of several biomass boilers for heating is socially and economically justified and it ensures the supply of thermal energy which affects the stabilization of the price of heating.

Statistics on the share of renewable energy sources for cooling and heating purposes [15] in Serbia indicate that in 2017, approximately 25.5% of total energy produced for these purposes was produced from renewable energy sources, which is higher than the European average of approximately 19.5%. The leading countries are Sweden, Finland, Latvia and Estonia which use more than 50% of renewable energy for cooling and heating.

According to experts, the problem with introducing renewable energy in the company is financial. According to a performed study [14], significant financial resources are required for the purchase of new biomass boiler and implementation of reconstruction of facilities in order to create conditions for the transition to renewable energy sources. The existing 2 boilers, shown in more detail in Table IV, use coal as fuel, while the third boiler which is not currently in use uses fuel oil or gas. Therefore, it is necessary to apply to different funds and banks that allocate funds for renewable energy sources and to improve cooperation with the European Union in this field.

The organization of this type is the European Bank for Reconstruction and Development, which in 2018 alone invested in Serbia approximately € 396 million for 18 projects in various fields [16]. The Bank has launched the Renewable District Energy in the Western Balkans Program (the ReDEWeB Program) [17] to assist in the development of renewable energy sources by countries and municipalities located in the program area. This program applies to Serbia. Applicants are provided assistance in the process of preparing project documentation. Another program of the European Bank for Reconstruction and Development is the Green Economy Financing Facility [18] for financing energy-efficient technologies used by households in their homes as well as companies.

The concept of public-private partnership [19] can be implemented to search for a private partner who would provide the necessary financial resources for the installation of new boilers and the reconstruction of the grid and connected infrastructure in order to improve urban district heating service and move to renewable energy sources.

Natural gas has great potential to become a major energy source in the future that would be used for urban heating because its use can meet 80-85% of people's energy needs [20]. Experts at the company see this opportunity as a potential for transfering to gas heating. They point to the need to increase the use of gas in Serbia and emphasize the importance to construct gas pipeline which would increase the country's gasification in Eastern Serbia, as a development potential for decreasing the use of coal. According to them, with the construction of the gas pipeline, possibility to distribute natural gas in Bor would appear, considering that there are other large companies operating in the city that would express their needs for this type of energy.

Threats. Changing regulations on energy development of the Republic of Serbia [2] will cause a reduction in the use of nonrenewable energy sources in the coming period, which affects the future existence of the company and the need to consider the introduction of renewable energy sources because the investments in nonrenewable energy sources will be restricted. As stated by Energy Development Strategy [2] the production of coal will decrease in the next decade causing unstable supply for all consumers including coal thermal heating plants that use coal like PUC “Toplana” Bor. The aforementioned numerous technical problems in the area of weaknesses have a negative impact on consumer satisfaction, which creates the problem of reducing the number of users [10].

Due to the current optimization of number of employees in the public sector, which is active in Serbia [21], in PUC “Toplana” Bor, which is a part of the public sector for a long time there is no employment of new workers. Serbia is faced with the problem of brain drain as young unemployed people are leaving the country in search of work. Statistical data show that at the beginning of 2019 almost 32% of young people were unemployed [22]. Experts suggest that the

deposition of new employment creates a generation gap, and this represents a huge loss for the company because the knowledge of older and more experienced employees is not transferred to young people.

Another potential problem is global warming which is defined as an increase in average temperature over a long period of time [23]. According to a systematic review of papers related to the impact of climate change on energy systems, it can be concluded that, in the long term, an increase in global temperature results in a decrease in the output of thermal energy systems [23]. The study conducted in 2019 [24] shows the latest results in examining this problem and the conclusion is that global warming leads to decreasing in heating days and increasing in cooling days.

IV. Concluding Remarks

The paper discusses strengths, weaknesses, opportunities and threats of PUC "Toplana" Bor, whose main activity is production of thermal energy used in the city district heating system. According to the results of the analysis, the advantage of the company is that it has a large number of users arising from the built heat network that covers the entire city. However, there are a number of problems in the work process and the most important are outdated equipment and insufficient financial resources. Lack of investment has led to the inadequate maintenance of this large energy system and the increased number of network breaks during the heating season causing high costs and customer dissatisfaction. Threats from the environment are numerous and, above all, relate to an important issue today - the use of renewable energy. Bearing in mind that PUC "Toplana" Bor is an outdated energy system in terms of production technology which is used, it is necessary to devise a strategy of switching to the use of clean energy sources such as biomass, which will be further investigated by the author. At the same time, the use of renewable energy sources is the greatest potential the company has to harness which is in accordance with the Energy Development Strategy of the Republic of Serbia [2].

Results of this analysis provide the base for generating strategies that utilize opportunities, relying on the strengths of the company and take action against the identified threats and weaknesses. Defined SWOT analysis will be used in further author's research in improving investigated energy system using a multi-criteria decision method.

Acknowledgment

This work is supported by the Ministry of Education, Science and Technological Development of the Republic of Serbia through Mathematical Institute of Serbian Academy of Sciences and Arts (Project III 044006).

References

[1] B. Ervural, S. Zaim, O. Demirel, Z. Aydin and D. Delen, "An ANP and fuzzy TOPSIS-based SWOT analysis for Turkey's energy planning," vol. 82, no. Part 1, 2018, pp. 1538-1550.

[2] Ministry of Mining and Energy, *Energy Sector Development Strategy of the Republic of Serbia for the period by 2025 with projections by 2030*. Available: https://www.mre.gov.rs/doc/efikasnost-izvori/23.06.02016%20ENERGY%20SECTOR%20DEVELOPMENT%20STRATEGY%20OF%20THE%20REPUBLIC%20OF%20SERBIA.pdf. [Accessed 5 August 2019].

[3] A. Mazhar, S. Liu and A. and Shukla, "A state of art review on the district heating systems," Renewable and Sustainable Energy Reviews, vol. 96, 2018, pp. 420-439.

[4] M. Sayegh, J. Danielewicz, T. Nannou, M. Miniewicz, P. Jadwiszczak, K. Piekarska and H. and Jouhara, "Trends of European research and development in district heating technologies," Renewable and Sustainable Energy Reviews, vol. 68, no. Part 2, 2017, pp. 1183-1192.

[5] A. Zajacs and A. and Borodiņecs, "Assessment of development scenarios of district heating systems," Sustainable Cities and Society, vol. 48, 2019, pp. 101540.

[6] J. Nazarko, J. Ejdys, K. Halicka, A. Magruk, Ł. Nazarko and A. and Skorek, "Application of enhanced SWOT analysis in the future-oriented public management of technology," Procedia Engineering, vol. 182, 2017, pp. 482-490.

[7] G. Bell and L. and Rochford, "Rediscovering SWOT's integrative nature: A new understanding of an old framework," The International Journal of Management Education, vol. 14, no. 3, 2016, pp. 310-326.

[8] P. Falcone, A. Tani, V. Tartiu i C. and Imbriani, „ Towards a sustainable forest-based bioeconomy in Italy: Findings from a SWOT analysis," Forest Policy and Economics, 2019, pp. 101910.

[9] J. Huang, J. Fan and S. and Furbo, "Feasibility study on solar district heating in China," Renewable and Sustainable Energy Reviews, vol. 108, 2019, pp. 53-64.

[10] PUC "Toplana" Bor, "History of the development of the production and distribution system of PUC “Toplana” Bor," 2018.

[11] Business Association of the District Heating Companies of Serbia (2017), *Extract from general information for 2017* Available at: https://www.toplanesrbije.org.rs/sr/publikacije. [Accessed 6 August 2019].

[12] Energoprojekt, "Feasibility study of PUC “Toplana” Bor," 2002.

[13] *Sustainable Development Strategy of Bor Municipality for the period 2011-2021* Available at: http://bor.rs/documents/. [Accessed 6 August 2019].

[14] Eko Produkt - Technological machine bureau, "Energy Efficiency and Analysis of Biomass Potential," Novi Sad, 2012.

[15] Eurostat, *Share of energy from renewable sources* Available at: http://appsso.eurostat.ec.europa.eu/. [Accessed 10 August 2019].

[16] European Bank for Reconstruction and Development, Available at: https://www.ebrd.com/where-we-are/serbia/data.html. [Accessed 12 August 2019].

[17] European Bank for Reconstruction and Development, Available at: https://www.ebrd.com/work-with-us/projects/tcpsd/renewable-district-energy-in-the-western-balkans-redeweb-programme.html. [Accessed 12 August 2019].

[18] European Bank for Reconstruction and Development, *Green Economy Financing Facility* Available at: https://ebrdgeff.com/serbia/. [Accessed 12 August 2019].

[19] Government of Republic of Serbia, *The Law on public-private partnership and concessions, Official Gazette of the Republic of Serbia, No. 88/2011, 15/2016 and 104/2016* Available at: http://jpp.gov.rs/content/Datoteke/pravniokvir/Zakon%20o%20javnoprivatnom%20partnerstvu%20i%20koncesijama.pdf. [Accessed 13 August 2019].

[20] *SrbijaGas* Available at: http://www.srbijagas.com/sr_RS/specificnostiprirodnog-gasa/?script=lat. [Accessed 13 August 2019].

[21] *Republic of Serbia, Ministry of public administration and local self-government*, Available at: http://mduls.gov.rs/en/public-administration reform/?script=lat. [Accessed 14 August 2019].

[22] *Trading Economics*, Available at: https://tradingeconomics.com/serbia/youth-unemployment-rate. [Accessed 13 August 2019].

[23] N. Emodi, T. Chaiechi and A. and Beg, "The impact of climate variability and change on the energy system: A systematic scoping review," Science of the total environment, vol. 676, 2019, pp. 545-563.

[24] M. Berger and J. and Worlitschek, "The link between climate and thermal energy demand on national level: A case study on Switzerland," Energy and Buildings, 2019, pp. 109372.

Enhancing Production of Oil and Gas by Using Hydraulic Fracturing Process

Branko Leković

University of Belgrade, Faculty of Mining and Geology, Belgrade, Serbia,
branko.lekovic@rgf.bg.ac.rs

Abstract — **Hydraulic fracturing is a method of stimulating production of oil and gas in a well by the increase surface area between the reservoir and the wellbore. The fracturing fluid is squeezed at a high enough pressure to generate artificial fractures in reservoir rock. A large number of low-permeability oil and gas reservoirs in the world would not be in production at all if hydraulic fracturing had not been applied. The hydraulic fracturing method has been applied in Serbia since 1976, when it was first applied in the "Banatsko Karađorđevo" oil-gas field. In Serbia today, fracturing is used in oil and gas fields in accordance with Serbian legislation and all international standards. It is necessary to emphasize that hydraulic fracturing operations in Serbia are conducted by the world's largest service companies, Schlumberger and Halliburton, which use the latest efficient and safe technologies.**

Keywords - hydraulic fracturing, fracturing fluids, pressure, hydrocarbons

I. INTRODUCTION

The first experimental treatment to "Hydrafrac" a well for stimulation was performed in the Hugoton gas field in Grant County, Kansas, in 1947. by Stanolind Oil (Fig. 1). A total of 3785 l of naphthenic acid and napalm thickened gasoline was injected, followed by a gel breaker, to stimulate a gas producing limestone formation at depth 731,5 m. Deliverability of the well did not change appreciably, but it was a start. In 1948, the Hydrafrac process was introduced more widely to the industry in a paper written by J.B. Clark of Stanolind Oil. A patent was issued in 1949, with an exclusive license granted to the Halliburton Oil Well Cementing Company (Howco) to pump the new Hydrafrac process. Howco performed the first two commercial fracturing treatments, in Stephens County, Oklahoma, and the other, in Archer County, Texas, in 1949, using a blend of crude and gasoline. In the first year, 332 wells were treated, with an average production increase of 75%.

Applications of the fracturing process grew rapidly and increased the supply of oil in the worldwide far beyond anything anticipated. In 2008, more than 50000 frac stages were completed throughout the world. Some estimate that hydraulic fracturing has increased USA recoverable reserves of oil by at least 30% and of gas by 90% [1].

II. HYDRAULIC FRACTURING TECHNOLOGY

Hydraulic fracturing, enhances the recovery of oil and gas from wells by fracturing formation rocks to release the hydrocarbons, allowing them to flow more easily through the rocks to the wellbore. Not whole oil and gas fields or formations require such treatment to permit extraction of hydrocarbons. Certain rocks contain plentiful naturally fractures and linked pore space that allow fluids to move freely through them. Another formations, are not permeable, such as lots of shale gas

Figure 1. First fracturing job run 1947. by Stanolind Oil in Kansas [1].

ISBN: 978-86-80616-04-9

reservoirs, and have few pore space and natural fractures. Hydrocarbons caught in a trap inside such impermeable rock can only be removed by fracturing the rocks. During this process water containing sand and additives is then pumped at very high pressures, through the casing perforations into the neighboring rock. The excessive pressure apply by the water brake the rock, creating tiny fractures that propagate sometimes tens of meters away from the wellbore (Fig. 2). Fracturing activity are normally engineered to restrict the fractures to the desired formation. The sand is added as a "proppant", to support fractures open after the pressure is released. It allows hydrocarbons captured in the rocks to flow to the wellbore [1]. In Europe, fracturing is carried out in England, Croatia, Hungary, Romania, Poland, and Russia. Nearly all global companies use the method, including, among others: BP, Chevron, Exxon Mobile, Gazprom Neft, Lukoil, Rosneft, Shell, and Total. Around 50% of hydrocarbon produced in the USA is obtained from wells after fracturing [2].

A. Equipment and materials for hydraulic fracturing

The hydraulic fracturing procedure requires an array of specialized devices and materials for operations in vertical and horizontal wells. The devices needed to carry out a hydraulic fracturing procedure includes storage tanks for fluid, proppant transport equipment, blending equipment, pumping equipment, and all additional equipment such as hoses, piping, valves, and manifolds (Fig. 3). Service companies which perform hydraulic fracturing also provide specialized controlling equipment

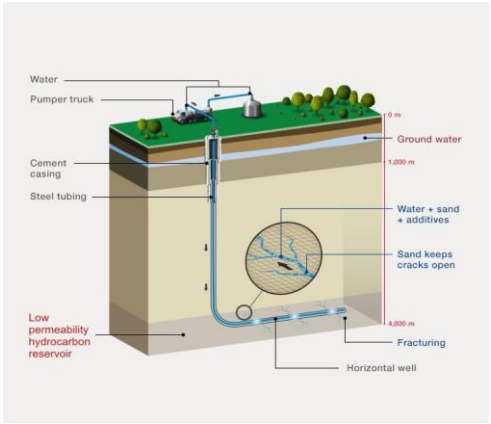

Figure 2. Hydraulical fracturing in a horizontal well [3].

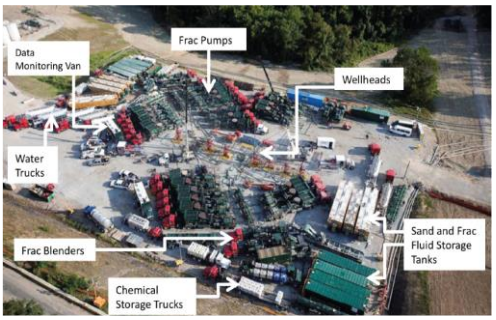

Figure 3. Huge numbers of tracks, equipment and large volume of fracturing fluid is need for staged hydraulic fracturing [5].

that is necessary in order to realize a successful treatment. Through the fracture treatment, from the various units data are being collected, and sent to monitoring equipment. Data being measured include fluid rate from the storage tanks, slurry from the high-pressure pumps, slurry density, wellhead treatment pressure, proppant concentration, chemical rate, etc. [4].

B. Fracturing fluids

In the first few years of hydraulic fracturing application was a common use of gelled crude and later gelled kerosene. These fluids were cheap, allowing greater volumes at lower price. Water started to be used in 1953 as a fracturing fluid, and numerous gelling agents was developed. To reduce emulsions generation with the formation fluid different surfactants were added. In the early 1970s, a major innovation in fracturing fluids was the use of metal-based crosslinking agents to enhance the viscosity of gelled water-based fracturing fluids for higher temperature wells [6].

The fluid used in fracturing is an essential constituent of hydraulic fracturing, not only because of its characteristics like rheology or formation compatibility but also for its potential environmental impact. In general, a fracturing fluid is the system of three main components: base fluid, additives and proppant. Mostly, water-based fluids are the simplest and most economical solution to fracture a hydrocarbon bearing formation [7].

C. Additives

The prevailing fluids presently used for fracture operations are water-based fluids blended with friction-reducing additives (called slick-water) to help pumping of the fluids and proppant at lower pressures and a higher rate at

than if water alone were used. Gelling agents, like as guar gum, aid suspend the proppant in the fluid. The gel-like fluid is more capable to transport the proppant than would a normal low viscous fluid. Crosslinked fluids as Borate crosslinked fluids were developed in order to improve the performance of gelling polymers without increasing their concentration. Supplementary chemicals are added to reduce friction, bacterial-growth, corrosion, and provide other benefits during the stimulation process [7].

D. Proppant types and properties

There are several group of proppants with different quality which must be appropriate to the type of well and reservoir in order to be hydraulically fractured. Proppants act properly in the support of opened cracks from fracking procedure. Proppants materials can be classify into three main categories: silica sand, resin coated sands, sintered and/or fused synthetic ceramic materials (Fig. 4). The proppants' main particle sizes are between 0,589 mm (30 mesh) and 0,297 mm (50 mesh), and typical density is between 2,65 and 3,56 g/cm³ [8].

III. New Developments in Hydraulic Fracturing Technology

Service companies create a new approach to fracturing that maximizes productivity, minimizes down time, and optimizes the operator's return on their service investment. Strategies for improving fracture production by optimizing conductivity have traditionally included: enhancing proppant roundness and strength, lowering proppant crush and gel loadings, improving gel breakers. These strategies are all based on improving flow through a porous proppant or sand pack.

A. HiWAY fracturing

The HiWAY™ technique fundamentally changes the way proppant fractures generate conductivity. It decouples fracture productivity from proppant permeability and creates flow

Figure 4. Scheme of proppant type [8].

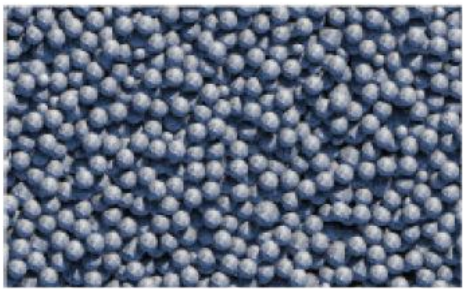

Figure 5. Conventional hydraulic fracturing methods rely on larger proppant sizes and resin coating to improve conductivity [9].

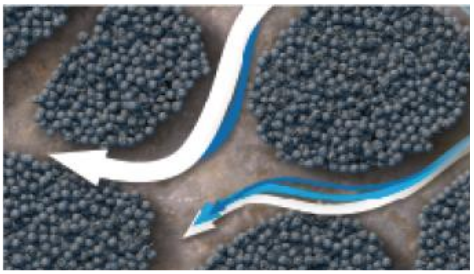

Figure 6. The HiWAY technique create stable, infinite-conductivity flow channels within fractures [9].

channels. So instead of flowing through the proppant in the pack (Fig. 5), hydrocarbons flow through channels, increasing conductivity by orders of magnitude (Fig. 6). Conductivity extends all the way to the tip of the fracture, allowing for longer effective fracture half-length, higher effective contact area, better fluid and polymer recovery, and less fracture face damage. These effects all mean optimized production and superior hydrocarbon recovery. By changing the way hydrocarbons flow, HiWAY channel fracturing ensures that traditional proppant pack conductivity losses are eliminated, including crushing, fines, fluid damage, multiphase flow, and non-Darcy effects. The stability of the flow channels is maintained by using a proprietary fiber that protects the structure from surface to reservoir until the fracture closes and the in situ stress takes over.

The average HiWAY flow-channel fracturing technique job increase production by more than 20%, on average, helps operators use 40% less proppant per job and compared to slick-water treatments uses 25% less water [9].

B. *BroadBand Shield - fracture-geometry control service*

BroadBand Shield™ fracture-geometry control service minimizes the risk of communicating with neighboring wells or fracturing into undesirable zones. It delivers engineered fracture stimulation treatments, constraining fracture growth with far-field diversion. The service uses a composite fluid system with a proprietary engineered far field diversion pill that bridges at the fracture tip to prevent excessive growth of fracture length and height.

Schlumberger engineers are able to model the fracture geometry using Kinetix Shale™ reservoir centric stimulation-to-production software and optimize the pumping schedule to prevent frac hits, increase fracture complexity by opening secondary and tertiary fractures, and optimize recovery without the detrimental effects of well-to-well communication. BroadBand Shield service is an environmentally friendly and easily deployed solution that provides maximum control of fracture geometry. Well-to-well communication can be monitored with WellWatcher Stim™ stimulation monitoring service, which uses high-frequency pressure data to analyze the risk of frac hits in real time, enabling operators to change the treatment design in the field and optimize hydrocarbon recovery.

With a properly engineered fracture design that limits fracture growth, BroadBand Shield service optimizes fracture geometry and increases fracture complexity in unconventional reservoirs. This helps improve reservoir drainage by maximizing reservoir contact within discrete areas and limiting pressure drops at the edge of (or outside) the desired drainage area [10].

IV. HYDRAULIC FRACTURING IN SERBIA

Method of hydraulic fracturing has been used in Serbia since 1976, when it was applied for the first time on the Banatsko Karđorđevo field. During the eighties, the method was used also on the oilfield Kikinda East. Modernization of the very process of hydraulic fracturing, but also possession of necessary assets for its application, have enabled more intensive use of this method since 2010. Successfulness of hydraulic fracturing project justified its further application. In addition to method of standard hydraulic fracturing, new technology is

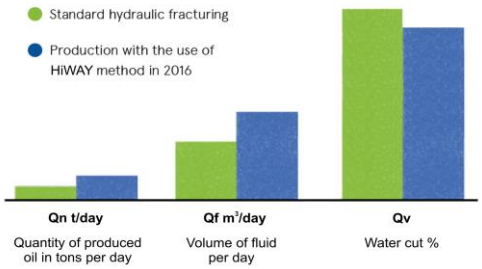

Figure 7. Diagram of production realized in the field "Itebej" in Vojvodina by different methods of fracturing [2].

performed on NIS-Gazpromneft's fields using methods of Fiber frac, Termo frac, Multistage frac, BroadBand Shield, HiWAY. Depending on collector features and general conditions in the reservoir, professional services analyses possibilities of implementation of different alternatives of hydraulic fracking. One of them is the HiWAY method. The method was proven successful on oil fields of Itebej, Elemir and Mokrin (Fig. 7). During 2016, hydraulic fracturing was done on 39 wellbores out of which more than half operations deployed HiWAY method, whereby additional production of 17,000 tons of oil was achieved. Fracturing is used these days in Serbia on five local fields [2].

V. CONCLUSION

Hydraulic fracturing has been used by the petroleum companies seven decades as a way to improve hydrocarbon production. Fracturing has been used in Serbia since 1976, when it was tested for the first time on the Banatsko Karđorđevo field.

The recent improvements in technology have allowed companies to extract oil and gas resources from formations that previously inaccessible. The newest generation of Schlumberger HiWAY technology combines simulation of formation productivity, optimized operation performance, selection of special fracturing fluids and monitoring, which enables creation of fractures with complex structure of their stable channels. This technology was proven successful on oil fields of Itebej, Elemir and Mokrin.

ACKNOWLEDGMENT

This article is the result of the Project № 33001 financed by the Ministry of Education, Science and Technological Development of the Republic of Serbia.

REFERENCES

[1] D.R. Suchy and K.D. Newell. (2012). *Hydraulic fracturing of oil and gas wells in Kansas*. Available at: http://www.kgs.edu/Publications/pic/pic32r1

[2] Energize, No 11, (2017). Available at: https://www.nis.eu/lat/korporativni-casopisi/energize-11

[3] Total, *Focus on hydraulic fracturing***.** Available at: https://www.total.com/en/infographics/focus-hydraulic-fracturing

[4] American petroleum institute. (2009). *Hydraulic fracturing operations - Well construction and integrity guidelines*. Available at: https://www.api.org/

[5] U.S. DOE and NETL. (2011). *Shale gas - Applying technology to solve America's energy challenges*. Available at: https://www.energyindepth.org/wp-content/uploads/2018/01/Shale_Gas_March_2011.pdf

[6] C.T. Montgomery and M.B. Smith. (2010). *Hydraulic fracturing: History of an enduring technology.* Available at: https://www.ourenergypolicy.org/wp-content/uploads/2013/07/Hydraulic.pdf

[7] L. Gandossi. (2013). *An overview of hydraulic fracturing and other formation stimulation technologies for shale gas production*. Available at: http://publications.jrc.ec.europa.eu/repository/bitstream/111111111/30129/1/an%20overview%20of%20hydraulic%20fracturing%20and%20other%20stimulation%20technologies%20%282%29.pdf

[8] V.P.P. de Campos, E.C. Sansone, G.F.B.L. e Silva. (2018). *Hydraulic fracturing propants.* Available at: https://www.researchgate.net/publication/324981761_Hydraulic_fracturing_proppants

[9] Schlumberger. *HiWAY fracturing.* Available at: https://www.slb.com/completions/stimulation/fracturing-services/hiway-fracturing-technique

[10] Schlumberger. *BroadBand Shield.* Available at: https://www.slb.com/broadband

Impact on the Grid of Bridgeless Interleaved Boost PFC Converter as the Front-edge Stage of an Onboard Charger

Tamara Ninković, Martin Ćalasan

Faculty of Electrical Engineering, Podgorica, Montenegro, tamara.ninkovic9@gmail.com; martinc@ucg.ac.me

Abstract — **As electric vehicles are becoming more mainstream every day, it is estimated that the stress on the utility grid will drastically increase. Hence, proper design of battery chargers must be taken into account. Generally, there are two types of EV battery chargers: onboard and off-board chargers. Owing to being seated inside the vehicle, onboard chargers are usually designed for lower kilowatts. On the other hand, off-board chargers are mounted on fixed locations outside the vehicle and thus can transfer higher kilowatts. Both onboard and off-board chargers are usually designed regarding two-stage approach, where AC-DC converter is followed by DC-DC converter. This paper proposes bridgeless interleaved boost PFC (Power Factor Correction) converter as a good candidate for the front-end stage of an onboard charger. The proposed converter shows a high power factor and low input current harmonics. Also, it can operate at power levels above 3.5 kW. Performances of this converter are simulated in MATLAB/Simulink environment, along with two more candidates for AC-DC stage of an onboard chargers. The simulation results show advantages of this convertor regarding low value of THD (total harmonic distortion) factor.**

Keywords – electric vehicle, onboard charger, AC-DC converter**,** bridgeless interleaved PFC converter.

I. INTRODUCTION

Even though it seems that electric vehicles are concept of 21st century, they have a much longer history. The first model electric vehicles were made in 1830s, but they didn't become commercial product until the end of 19th century. Due to popularity of internal combustion vehicles, regarding longer ranges and easier refueling, electric vehicles weren't able to gain huge success in the previous century. However, today's situation has drastically changed. Increasing concerns about environment, along with development in battery technology, has resulted in expanding use of electric vehicles.

Just as using IC vehicles was unimaginable without widespread gas station infrastructure, flexible use of electric vehicles requires development of EVSE (Electric Vehicle Supply Equipment) infrastructure. This will result in drastic increase of utility grid stress. Hence, huge efficiency of battery chargers is important to minimize negative aspects of electric vehicles charging.

Battery chargers are type of power converters that supply power to the battery from the utility grid. As it is presented in [1] these chargers usually create non-linear load in power systems, which causes a problem such as low power factor and excessive total harmonic distortion (THD) in grid. Thus, choosing proper deign of battery charger is one of the most important tasks regarding adoption of EV.

EV's chargers are designed into two forms: onboard and off-board chargers. Onboard charger is built in vehicle and, thus, adds significant weight to the vehicle. It is designed for lower kilowatts; but it provides flexibility to recharge at various places where electric outlet is available. In comparison to the onboard charger, off-board charger is mounted outside

ISBN: 978-86-80616-04-9

the vehicle, hence it is not limited by vehicle weight and can transfer higher kilowatts. On the other hand, off-board charger requires more sophisticated battery management system (BMS) and battery heating must be controlled during charging.

Onboard and off-board chargers are usually designed using two-stage approach. They consist of AC-DC front-end converter followed by DC-DC converter. The front-end stage is used to rectify input AC voltage and to transfer it to DC-DC convertor, where rectified voltage is converted into regulated DC voltage for battery charging [2, 3].

This paper deals with the impact on the grid of bridgeless interleaved boost PFC converter as the front stage of an onboard charger. Performances of this converter will be tested and simulated in MATLAB/Simulink environment, along with two more candidates for AC-DC stage of an onboard chargers. It should be noted that in [4] boost interleaved PFC converter and the bridgeless boost interleaved PFC converter is also analyzed. However, mentioned paper only deals with the converter efficiency of these converters.

This paper is organized as follows: three most common AC-DC topologies of onboard chargers will be presented in the second section and results of simulation in MATLAB will be presented in third section. The final remarks will be given in Conclusion section.

II. REVIEW OF DIFFERENT AC-DC FRONT END TOPOLOGIES

The front-end AC-DC converter represents a key component of charger. Rectifiers produce input current with rich harmonic content, which pollute the grid and cause overheating of power system components. Thus, AC-DC converter must meet regulatory standards of AC mains and must achieve high efficiency. According to those requirements, front-end converter is usually implemented as PFC (Power Factor Correction) stage.

Expressing distortion of certain waveform can be attained by using one of two different factors: distortion factor (K_d) or THD (Total Harmonic Distortion). The distortion factor represents the ratio of the fundamental root mean square (RMS) current to the total RMS current:

$$K_d = \frac{I_{1rms}}{I_{rms}} . \quad (1)$$

There is a unique relation between K_d and THD factors:

$$K_d = \sqrt{\frac{1}{1+THD^2}} , \quad (2)$$

so THD can be expressed as follows:

$$THD^2 = \sqrt{\frac{I_{rms^2} - I_{1rms^2}}{I_{rms^2}}} . \quad (3)$$

On account of having value close to unity even for noticeably distorted waves, the distortion factor could not be credible measure for practical use. On the other hand, value of THD varies in a huge range for different waveforms, and thus only this factor is used to express distortion.

According to IEEE 519-2014 [2] standard, THD factor must be lower than 7%.

Notable reduction of input current harmonics, and THD factor can be achieved by applying PFC convertors. These convertors are designed and controlled to imitate resistive load and thus produce very low input current harmonics. Three popular topologies of these converters: conventional boost PFC converter, interleaved boost PFC converter and bridgeless interleaved boost PFC converter (BLIL); will be presented in the next subsections.

A. *Conventional boost PFC converter*

The conventional boost PFC convertor is the most widely used topology for PFC stage. It includes full-bridge diode rectifier that is followed by conventional boost section, as it is shown in Fig. 1.

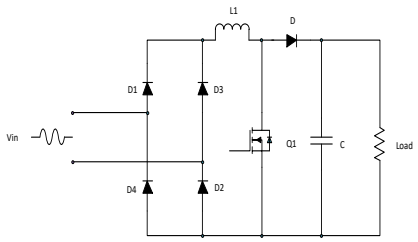

Figure 1. Conventional boost PFC topology

This topology is can be used for low to medium power ranges. However, as the power level increase, power losses in diode bridge reduce efficiency of this converter. Also, dealing with heat dissipation in limited can become complicated. Other disadvantages of this converter are high output capacitor ripple current and inductor volume at high power applications. Interleaved boost PFC converter

Fig. 2 presents the interleaved boost PFC topology. It consists of full-bridge diode rectifier and two boost sections in parallel, operating 180^0 out of phase. Interleaving topology has several advantages, as it is shown in [3]. The input current is sum of inductor currents L_1 and L_2 . The interleaving causes canceling of ripple currents of these two inductors, therefore it tends to drastically reduce high frequency input ripple current. As a result, input EMI (Electromagnetic Interference) filter can be smaller.

By paralleling semiconductors, conductions losses of this converter are reduced. Also, interleaving reduces high frequency output capacitor ripple current. On the other hand, the main disadvantage of this converter is use of diode bridge to rectify input AC voltage. As in previous case, due to power losses, diode bridge decreases efficiency of this convertor and introduce heat management problem.

B. Bridgeless interleaved boost PFC converter (Proposed topology)

The bridgeless interleaved topology addresses the problems connected to the diode bridge losses. In comparison to interleaved PFC boost converter, this topology eliminates need for input diode bridge by introducing two more MOSFETs and two fast diodes, as it is shown in Fig. 3. The gates of MOSFETs Q1 and Q2 are tied together, so the gating signals are identical for this pair of MOSFETs. The same principle applies to MOSFETs Q3 and Q4. These two gating signals (for MOSFETs Q1 and Q2; and for MOSFETs Q3 and Q4) are $180°$ out of phase, similar to interleaved boost converter.

This converter introduces many advantages comparing to previous two topologies. It shows high input power factor, low *THD*, low high frequency output capacitor ripple and high efficiency over the entire load range. Bridgeless interleaved topology is proposed for higher power applications, above $3.5kW$ and thus presents very good candidate for PFC stage of an onboard chargers [4].

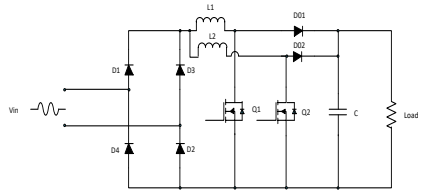

Figure 2. Interleaved boost PFC topology.

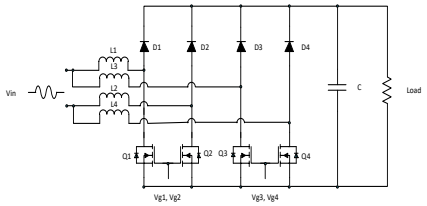

Figure 3. Bridgeless interleaved boost PFC topology.

In following section, superiority of this topology will be justified by simulation results.

III. SIMULATION RESULTS

In order to compare performances of these three convertors, each topology is implemented in MATLAB Simulink (Appendix 1). Controller implementation is based on average current control model.

The presented simulation results are obtained using the following parameters [5]: RMS value of input AC voltage $V_{in\_rms} = 230V$ (frequency $f = 50Hz$); desired output voltage is controlled around $V_{out} = 400V$; inductances $L_n = 300\mu H$; the DC capacitance and resistive load are set to $C = 7800\mu F$ and $R = 58\Omega$, respectively.

Fig. 4-6 show obtained values of THD factors for all three converters. The lowest value of THD is achieved by using bridgeless interleaved boost PFC topology. This value complies with IEEE 519 standard.

Other two converters create input current with larger harmonic content, thus, the value of THD is higher than the allowed one. Also, it is important that value of THD factor for interleaved boost PFC topology is slightly better than the value for conventional boost PFC converter, which shows advantages of interleaving.

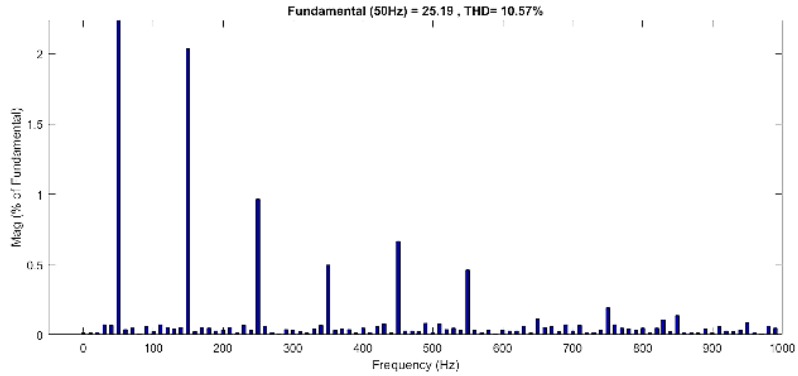

Figure 4. THD of conventional boost PFC converter.

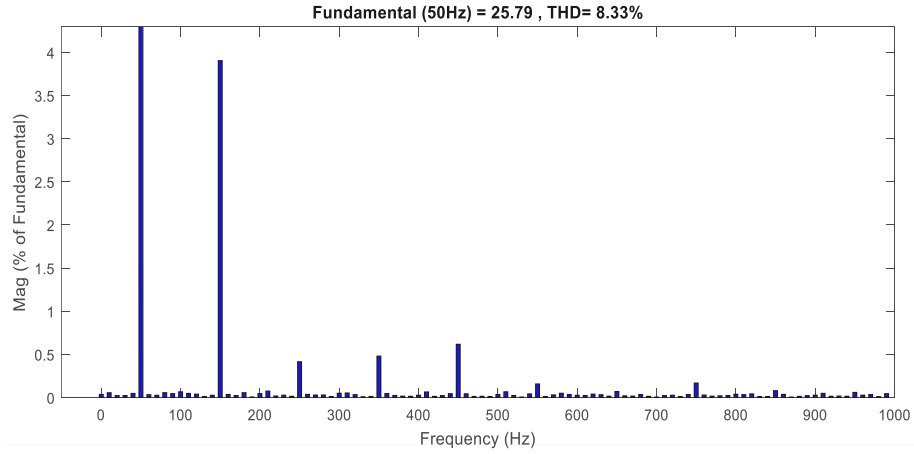

Figure 5. THD of interleaved boost PFC converter

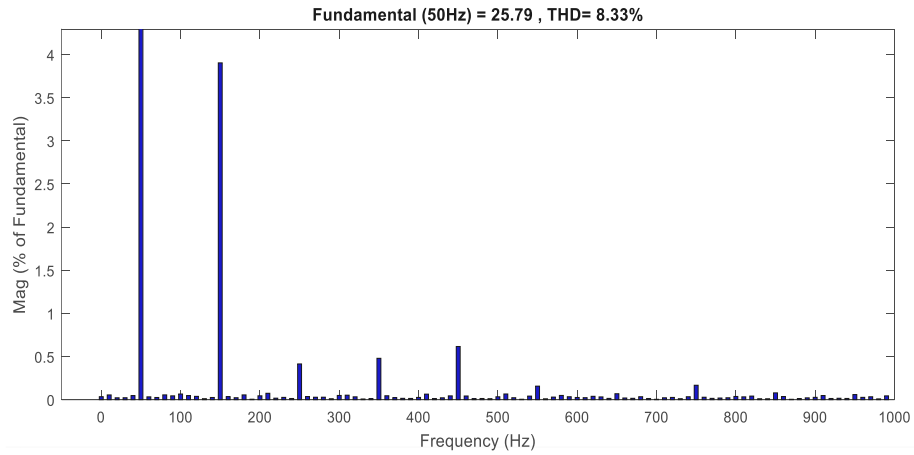

Figure 6. THD of bridgeless interleaved boost PC converter.

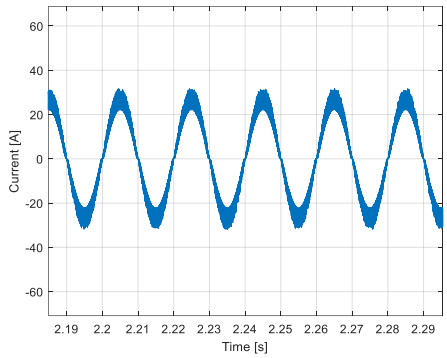

Figure 7. Zoom on input current of conventional boost PFC converter

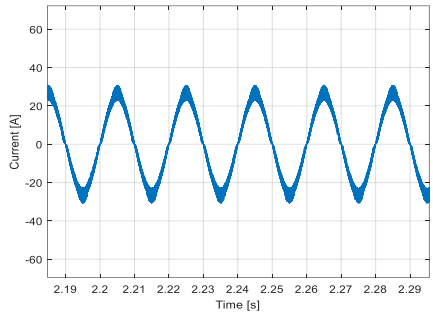

Figure 8. Zoom on input current of interleaved boost PFC converter.

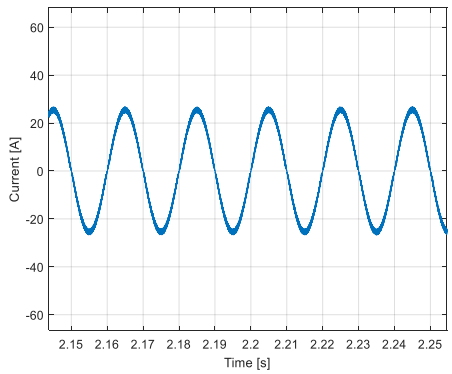

Figure 9. Zoom on input current of bridgeless interleaved boost PFC converter.

In compliance with *THD* factors, waveforms of input current are presented in Fig. 7-9. By observing these figures, it can be concluded that the input current of BLIL has waveform closest to sinusoidal input voltage. Wave shape is slightly distorted near the curves, but not as much as in case of interleaved and conventional boost topology. The other two input currents have sharper edges and waveform is obviously distorted. DC link voltages are illustrated in Fig. 10-12. In steady state, output voltage reaches set value (400V).

Even though output voltage of PFC stage is usually about 400 V (up to 700 V), higher values of voltage are chosen in order to show THD - voltage dependence. This dependence is illustrated in Fig. 13. Decreasing function shows that by increasing output voltage, input current harmonics reduces.

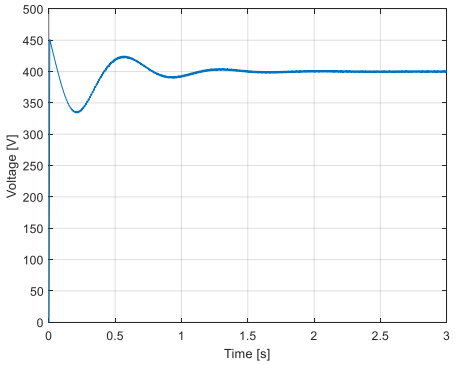

Figure 10. Output voltage of conventional boost PFC converter

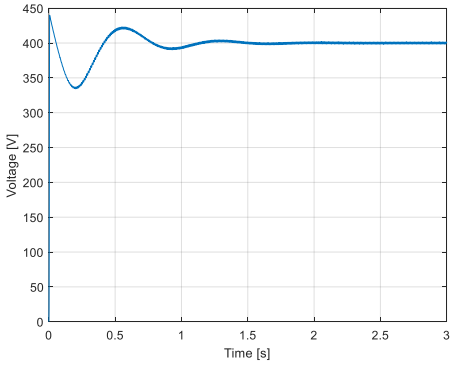

Figure 11. Output voltage of interleaved boost PFC converter.

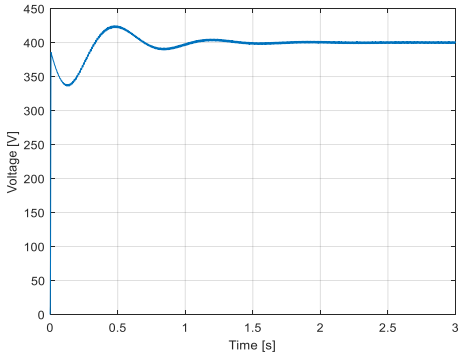

Figure 12. Output voltage of bridgeless interleaved boost PFC converter.

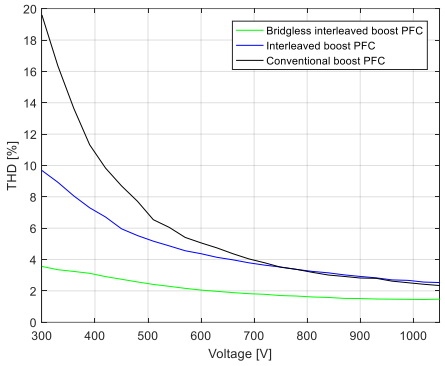

Figure 13. THD-Output voltage dependence.

IV. CONCLUSION

In process of electric vehicles future deployment, charging technology development will play a significant role; especially development of applied AC-DC and DC-DC converters.

This paper presents three different topologies: Bridgeless interleaved, Interleaved and conventional boost PFC converter; that can be used as front-end stage of onboard charger. Performances of these converters are analyzed and compared using MATLAB/Simulink. Simulation results, ran for the same operation mode, confirm that the bridgeless interleaved boost PFC converter is the best solution for PFC stage of onboard charger. Input current is in phase with input voltage and its shape is almost sinusoidal, in comparison to the other two topologies. Also, this topology eliminates need for diode bridge rectifier, which significantly improves its efficiency.

In conclusion, bridgeless interleaved boost PFC topology completely complies to regulatory standards and requirements. Also, it shows better performances comparing to the conventional and interleaved boost PFC converters, regarding value of THD factor and efficiency. Hence, this topology is excellent option for front-end stage of onboard charger.

REFERENCES

[1] Ö. Türksoy, U. Yilmaz, and A. Teke, “Overview of battery charger topologies in plug-in electric and hybrid vehicles,” 16th International Conference on Clean Energy (ICCE-2018), Famagusta, Cyprus, 2018.

[2] IEEE 519, “IEEE Recommended Practice and Requirements for Harmonic Control in Electric Power Systems,” 2018.

[3] A. Emadi, Advanced electric drive vehicles, Ontario, Canada: CRC Press, Taylor & Francis Group, 2015.

[4] M.C. Ancuti, M. Svoboda, S. Musuroi, A. Hedes, N.V. Olarescu, and M. Wienmann, “Boost Interleaved PFC versus Bridgeless Boost Interleaved PFC Converter Performance/Efficiency Analysis,” International Conference on Applied and Theoretical Electricity (ICATE), 23-25 Oct. 2014.

[5] G. Kanimozhi, and V.T. Sreedevi, “Modeling and Control of Bridgeless Interleaved PFC Boost Converter,” Transylvanian Review, vol. XXIV, no. 11, 2016.

APPENDIX 1

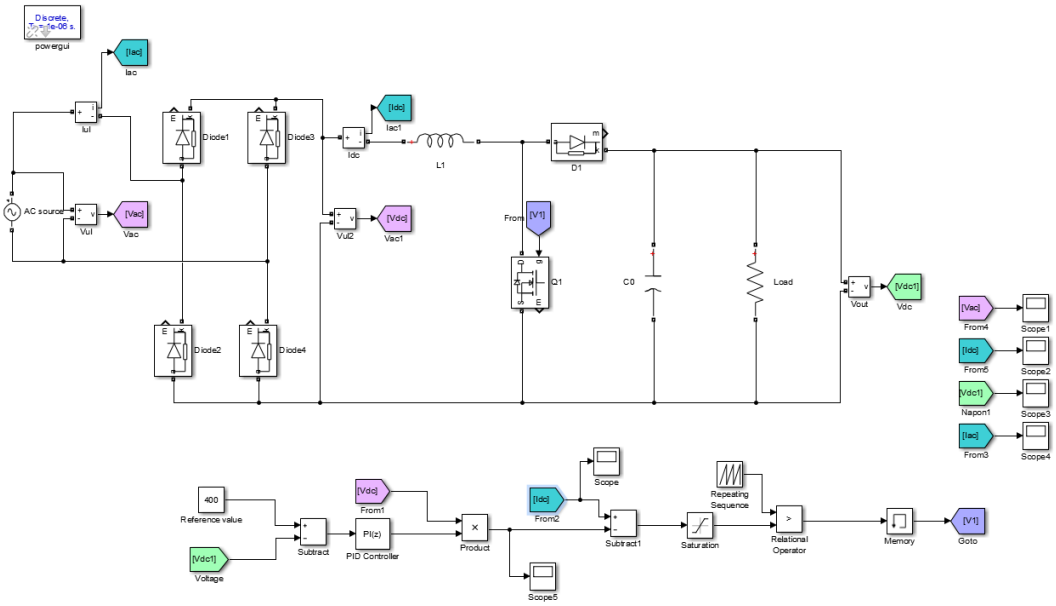

Figure A1. Implementation of conventional boost PFC converter in MATLAB Simulink

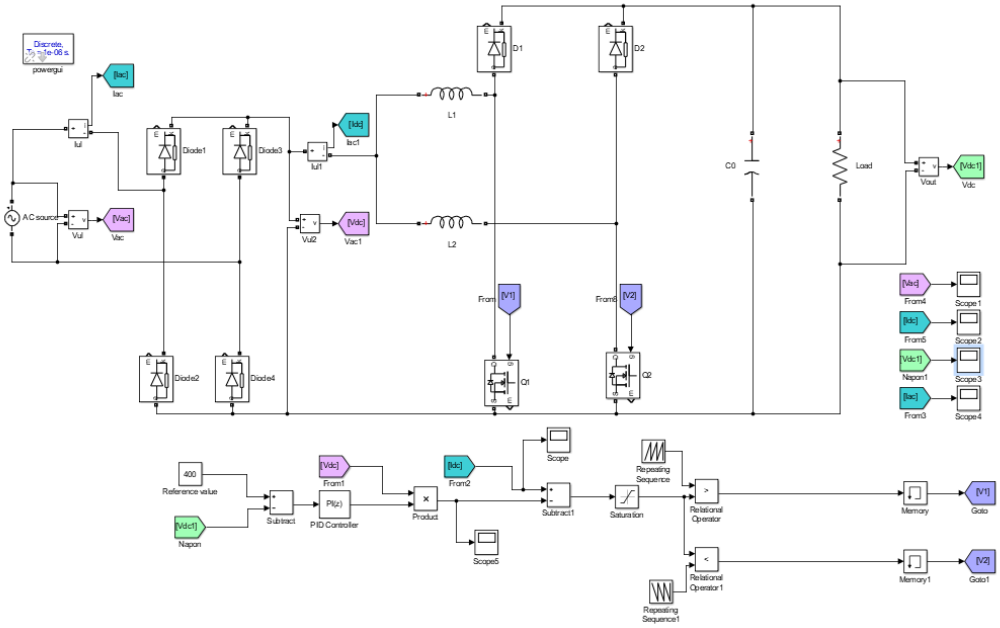

Figure A2. Implementation of interleaved boost PFC converter in MATLAB Simulink

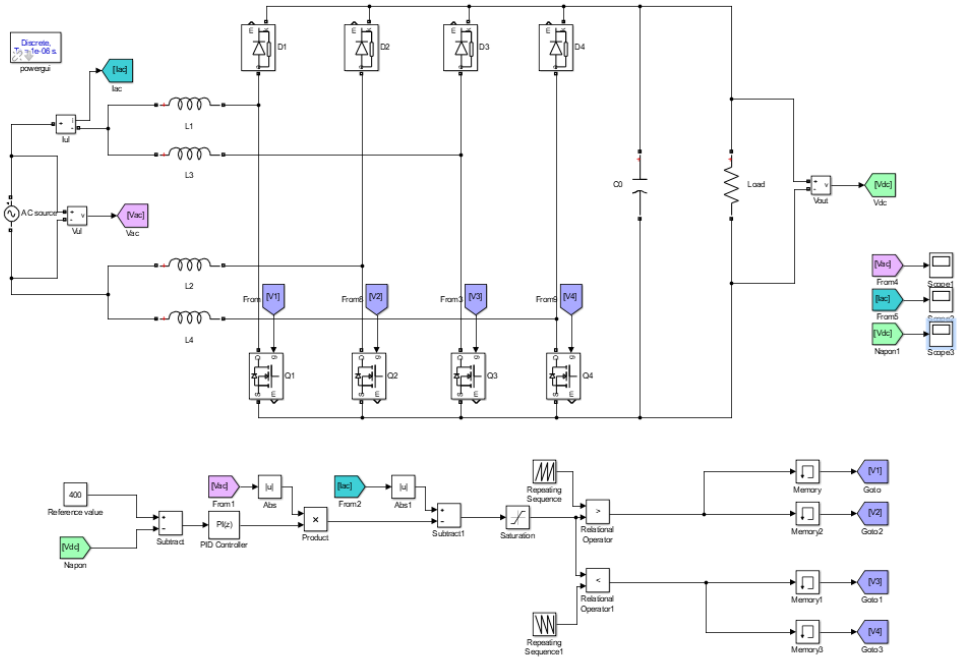

Figure A3. Implementation of bridgeless interleaved boost PFC converter in MATLAB Simulink

Wet Technology for the Production of Energy Briquettes with Binding Means, as an Example of the Energy Recycling of Waste Biomass from Husbandry

Bratimir Nešić[1], Dejan Vasović[2], Ljubiša Stajić[3]

[1]Technical College of Applied Sciences, Niš, Serbia, bratimir@gmail.com
[2] University of Niš, Faculty of Occupational Safety in Niš, Niš, Serbia, djnvasovic@gmail.com
[3] Research and Development Center "ALFATEC", Niš, Serbia, ljubisa.stajic@alfatec.rs

Abstract — **The paper presents the results of the "wet" technology for the production of energy briquettes from waste biomass ORIGINATING from HUSBANDRY with binders in the form of paper and semi-cellulose pulp. PRODUCED resulting energy briquettes have: energy, economic and environmental characteristics. Physical characteristics, technological conditions for production and categorization of produced energy briquettes are presented.**

Keywords - wet, briquette, waste, recycling, energy

I. INTRODUCTION

Man is a decisive factor in environmental change through his activities. All these activities are related to meeting the needs of life. Much of the need is created artificially and the question is whether we need so many different products that will become waste after use. Our civilization produces more and more pollution and nothing indicates a recent change in this trend. Yet, thanks to technological advances and the development of environmental awareness, the fight against pollution is becoming much more successful [1].

The development of cleaner technologies, increased energy efficiency and the use of renewable energy sources will certainly have the effect in reducing environmental pollution. Promoting renewable energies requires the introduction of incentive measures, which will encourage private investment in the energy sector and strengthen competitiveness in the energy and economy sectors in general [2].

There is a lot of agricultural residues which posses a disposal problem to most of the farmers. Energy briquettes are the most probable solution to this environmental threatening and rising cost of fossil fuels. This process involves compressing the residues into a higher density material than the original raw materials is called briquette formation and is also known as densification [3].

The small scale industries are the places where briquettes can be highly useful. The traditional ceramics and clay ware processing can also be improved with these energy briquettes due to their high calorific value; they can even power boilers to generate steam and electricity [4].

Advantages of using energy briquettes compared to other solid fuels (coal) [5]:

- Easy handling and transportation, compact in size;
- Ash content limits are below than 10% (coal: 25 to 40%) resulting in low boiler ash disposal problems;

ISBN: 978-86-80616-04-9

- Lower amount of sulphur-dioxide (compared to coal);
- Lower ignition point (compared to coal) and it burns easily;
- No corrosion effect on boiler equipment and low maintenance costs;
- Cleaner and cheaper fuel for energy production;
- No gas and effluents like coal - no bad effects on human health;
- High volume reduction during briquetting process;
- No fly ash during burning briquettes.
- High burning efficiency.

The main aim of this paper is to contribute to overcoming some of the limiting factors that come from the so-called dry briquetting technologies. These limiting factors prevent the mass use of different energy materials in the form of energy briquettes. The limiting factors include [6]:

- the requirement so far, that the particle granulation of the input energy material should be up to 3 mm;
- the humidity problem of the input energy material as a limiting factor;
- achieving a compact form, whose surface strength will not change during the storage period of energy briquettes;
- the problem of weakening the inter-particle bonding forces to prevent bursting and decay of energy briquettes.

II. MATERIAL AND METHOD

The paper presents the results related to:

- the physical characteristics of energy briquettes produced from crop biomass waste materials such as: wheat straw, tree, goblet and corn leaf and rice husk with binders in the form of paper and semi-cellulosic pulp;
- technical and technological possibilities of production;
- categorization of energy briquettes according to Serbian standard SRPS D.B9.021: 1987 - Energy briquettes made of lignocellulosic material [7].

The production process of briquetting and the quality of the produced energy briquettes is influenced by the type, quality, composition and technological parameters of the input materials i.e. the waste biomass from the husbandry, for energy recycling and binding mean. Materials' humidity is one of the most important parameters of the production process of briquetting, because the presence of moisture is necessary in the material preparation phase and the briquette forming phase. Briquettes as industrial products in our areas are not a news [6] and energy briquettes became actual for production and use.

"Wet" energy briquette production technology uses old waste paper in the form of lignocellulosic pulp in aqueous suspension as a base material with the addition of waste biomass from husbandry. In this case, energy briquettes are produced from such mixtures by pressing the mixture in a suitable tool with pressures in the range of 0.3 - 0.5 MPa [8]. Pressing removes most of the water and the rest is removed by air drying.

The advantages of an energy briquette produced by wet process with paper pulp as a binder compared to the dry briquette production process are: cheaper technical solution of briquetting equipment, possibility of briquetting materials with heterogeneous compositions and with particles larger than 10 mm (depending on the dimensions of the briquettes), prior drying of the waste biomass is not necessary, there are no strictly prescribed values of moisture content, the required surface pressure is much lower (0.3 - 0.5 MPa compared to 300 MPa) and possible storage without problems accompanying storage briquettes produced by the dry process (volume, swelling and decomposition) [6].

The disadvantages of the energy briquette produced by wet process with paper pulp as a binder in relation to the dry process of briquette production are: pre-preparation of paper pulp is required (a certain period of time is necessary for the paper to decompose in water and homogenization) and a certain time interval is also required for the drying process after forming a wet briquette, which is relatively long for drying in air (7 to 10 days) and if it is artificially dried then this is an additional cost [6].

Given that the paper is, in some way, strategic or better to say scarce material, it turned out that it was not suitable for this purpose, so, the possibility was sought to replace the paper with some other material. This material should meet the following conditions: preparation technology for the binder must be sufficiently simple, it is desirable for the process to be "wet" and that there is no condition for pre-drying the components, the material should be combustible and the combustion products should be equivalent in composition products obtained by combustion of biomass, the material must allow the installation of a wide range of waste biomass and the concentration of mass and energy in the volume unit of the energy briquette thus obtained, should be as high as possible [9].

The solution for such requirements was found in a new binder in the form of cellulose. To obtain the cellulose, a cooking solution consisting of a mixture of sodium sulphite and a sufficient amount of sodium carbonate is used to allow the solution to remain weakly basic until the cellulose is discharged from the autoclave. Depending on the end use, the yield ranges from 65% to 85%. Higher yield semi-cellulose has higher strength and thermal power [10]. The pulp of the cellulose is obtained from biomasses that are not attractive for crop, livestock or other purposes. The pressures required to form this briquette depend on a number of factors, but usually do not exceed 5 bars. This produces fuel, the production of which does not require the use of adhesive or filler, whose thermal power is substantially improved by various additives that can most often be treated as waste material. Additive material may be added to improve the mechanical, thermal, environmental or aesthetic properties of the energy briquettes. The energy briquettes thus produced, have a volume mass ranging from 720 to 830 kg/m^3, depending on the proportion of cellulose and surface pressure [11].

III. RESULTS

In Table 1, the values of the lower thermal power of the produced energy briquettes are shown.

TABLE I. LOWER THERMAL POWER OF THE PRODUCED ENERGY BRIQUETTES [6]

No.	Composition	H_d (MJ/kg)
1	Wheat straw	15,357
2	Corn tree	16,074
3	Corn goblet	16,917
4	Wheat straw / paper pulp	15,357
5	Rice husk / paper pulp	15,644
6	Semi-cellulose	17,35

Based on the classification of the Serbian standard for lignocellulosic material briquettes [7], the volume of the briquettes is at least 800 kg/m^3 at the permissible moisture content. Table 2 shows the classification of energy briquettes.

TABLE II. ENERGY BRIQUETTES CLASSIFICATION [7]

Class	Lower thermal power at least to (MJ/kg)
Extra	16,75
I	14,65
II	12,98
III	11,72

IV. CONCLUSION

It can be concluded that energy briquettes from corn goblet and semi-cellulose with lower thermal power values from 16,917 to 17,35 MJ /kg, subject to the extra class of energy briquettes and all others belong to I class. Based on testing of energy briquettes produced from waste biomass from husbandry, can be concluded that: ''wet'' production technology is relatively easy and inexpensive, it is possible to bind heterogeneous structure materials, it can be used for components that come from other technologies as waste materials, due to lower surface pressure this technology is much cheaper in relation to "dry" technology, the input components of the energy briquette should not be specifically prepared because the shredding is minimized.

There is another element that cannot be taken into account by any techno-economic analysis - from a global point of view, there is no profit that can justify environmental pollution and there is no cost to pay for clean air [12]. This paper presents the authors' contribution to obtaining a new type of environmentally friendly, economically viable energy fuel based on a wide variety of renewable biomass as their use substantially

eliminates categorical risks from the use of fossil fuels. The current tendency for the use of biomass (both in bulk and in the form of energy briquettes) in small and medium-sized thermal power plants and efforts to move into the organized use and production of energy biomass, should be supported. This is all the more so given the fact that fossil fuel reserves are problematic for use, from an environmental point of view as well as their resources are running low.

REFERENCES

[1] B. Nešić, "Upravljanje komunalnim otpadom i potencijali za reciklažu južne i jugoistočne Srbije," Centar za Razvoj građanskog društva Protecta, Niš, 2010, pp. 3-5.

[2] B. Nešić, "Generatori otpada i zagađivači južne i jugoistočne Srbije," Centar za Razvoj građanskog društva Protecta, Niš, 2010, pp. 4-15.

[3] A. Praneeth, P. Kumar, R. Ravikiran, P. Marimuthu, ''Evaluation of Briquettes made of Biodegradable materials as an alternate source of energy'', International Journal of Mechanical Engineering and Technology vol. 8 (11), 2017, pp. 977–983.

[4] A. Amarasinghe, D. Shyamalee, N. Senanayaka, ''Evaluation of different binding materials in forming biomass briquettes with saw dust'', International Journal of Scientific and Research Publications, 2016, pp. 1-8.

[5] A. Kau, A. Kumar, P. Singh, K. Kundu, ''Production, Analysis and Optimization of Low Cost Briquettes from Biomass Residues''. Advances in Research vol. 12, no. 4, 2017, pp. 1-10.

[6] B. Nesic, "Energy Briquettes," Ekološki pokret Novog Sada, Novi Sad, in press.

[7] Energetski briketi od lignoceluloznog materijala - tehnički uslovi, Srpski standard SRPS D.B9.021:1987, Institut za standardizaciju Srbije, Beograd, 1987.

[8] D. Mitic, B. Nesic, S. Jankovic: "Light Composite Biobriquettes - Physical Characteristics", Scientific Journal Facta Universitatis, Series: Working and Living Environmental Protection, vol. 1, no. 2, 1997, pp. 51-58.

[9] D. Mitic, B. Nesic, S. Jankovic: "Usability of Light Composite Biobriquettes", Scientific Journal Facta Universitatis, Series: Working and Living Environmental Protection, vol. 1, no. 2, 1997, pp. 43-50.

[10] Papir, karton, celuloza i srodni termini – Rečnik – Deo 2: Terminologija u oblasti celuloze, Srpski standard SRPS ISO 4046-2:2018, Institut za standardizaciju Srbije, Beograd, 2018.

[11] D. Mitic, E. Mihajlovic, B. Nesic, B. Milanovic: "Reduction of Environmental Pollution by using Biobriquettes", Scientific Journal Facta Universitatis, Series: Working and Living Environmental Protection, vol. 1, no. 3, 1998, pp. 41-49.

[12] D. Mitic, B. Nesic, E. Mihajlovic, B. Milanovic.: "Istraživanje mogućnosti izrade raznih vrsta biobriketa," Procesna tehnika i energetika u poljoprivredi, vol. 3, no. 1-2, 1999, pp. 29-32.

The Formation and Usage of the Neural Network

Enver Agić[1], Damir Šljivac[2], Bakir Agić[3]

[1]Forensic expert of the electrical profession, Tuzla, Bosnia & Herzegovina, enveragic99@gmail.com;
[2]Faculty of Electrical Engineering, University J.J. Strossmayer, Osijek, Croatia, damir.sljivac@etfos.hr;
[3]Faculty of Electricity, University of Tuzla, Tuzla, Bosnia & Herzegovina, bakir.agicc@gmail.com

Abstract — **The complex problems of the real world require owning a smart system that will combine the knowledge, techniques and methodologies from various sources. It is assumed that these systems have the ability to resonate as true experts in a particular field, to be flexible, to learn and to explain how they made a decision or taken any action. The integration of various complementary approaches, together with optimization techniques without seeking derivatives, as a result of putting a new discipline is called "soft computing"**.

Keywords - science, approximate reasoning, evolutionary computation, simulated annealing

I. HISTORY OF SOFT COMPUTING METODOLOGY

The founder of soft computing is Lofti Zadeh, and he presented a new way of constructing hybrid systems based on computer intelligence in which there are neural networks, fuzzy logic theory, approximate reasoning and optimization methods without searching of derivation such as evolutionary computation and simulated annealing [1].

Modern artificial intelligence is constantly progressing and the border between conventional artificial intelligence systems and soft computing methodologies is less expressed [2].

II. THE CHARACTER OF NEURO – FUZZY MODELING

The character of soft computing with neuro – fuzzy modeling as background can be looked as:

- Neuro – fuzzy models and controllers based on fuzzy logic use human experts as fuzzy if-then rules and conventional presentation of knowledge for getting a solution for some problems.
- Artificial neural networks are inspired by biologic neural networks [3]. Their application is in soft computing for perception, pattern recognition, non-linear regression and classification problems.
- Neural networks and fuzzy conclusion systems have the ability to form models using just samples of data of target system. Detail entry into the target system will help to form an initial structure of model, but it is not necessary.
- Neuro-fuzzy and soft computing methodologies rely on very fast numerous calculations to find rules, or to find regularity in data set. This is a common characteristic for all components of soft computing [4].
- Neural networks as well as fuzzy systems show the characteristics of tolerating the error [5]. Ejection of one neural from neural network or one rule form fuzzy conclusion system will not cause the destruction of system. In most cases the system continues to work, but weakened and with reduced level of efficiency because of its parallel structure.

Neural networks and fuzzy systems are important representatives of intelligent systems and both can be very successfully applied for getting a solution for various problems in practice. Using advantages of both sides, neural

network and fuzzy system are combined into homogeneous architectures, commonly called hybrid neuro-fuzzy models. Such system is a special neural network with fuzzy parameters or fuzzy system in parallel distributed form [6]. Adaptive neuro – fuzzy lock system – ANFIS is an example of that architecture, commonly formed by two separated parts which can be independently changed: causing and resulting part [7].

Both parts can be adjusted using various optimization methods such as hybrid procedure of learning that combines method of gradient decline and least square estimator. Causing part or If-part contains non–linear parameters of affiliation function which can be in various forms. The affiliation function can be any function in extent [0, 1], if an expert determines that it is a good way to present his knowledge.

The gradient decent method is used to configure non-linear parameters. The resulting part or then-part contains exiting linear parameters, which are being adjusted with least squares estimator [8].

Causing part or If-part contains non – linear parameters of affiliation function which can be in various forms. The affiliation function can be any function in extent [0, 1], if expert determines that it is a good way to present his knowledge.

The gradient decent method is used to configure non-linear parameters [9]. The resulting part or then-part contains exiting linear parameters, which are being adjusted with least squares estimator.

The possibility of using fuzzy conclusion system for getting solution for various engineering problems is illustrated in the application in creating load model of electric energy system [10]. This access can replace complex computer programs based on differential equations in time domain.

III. FORMING THE NEURAL NETWORK AND SOLUTIONS

In the work, the example of forming the neural network using data of 15-minute load of one electric energy system is presented.

The neural network is formed using given data from file “diario-setembro.xls”, in which are systemized 15-minute load of electric energy system of Portugal for month of September, for one year [11].

Into consideration are taken the changes of characteristics in network and in work will be described the solutions.

To get solution for the given task, the multilayer neural network with return propagating the error [12].

The data from file diario-setembro-xls are translated into file dd.dat. The data of load of electric energy system of Portugal are expressed in GW.

```
TSdata

» load tsdata.dat %load data from file tsdata.dat
t=tsdata(:,1); % define parameter t
x=tsdata(:,2); % define parameter x

% plot the data
figure(1)
plot(t,x)
xlabel('t(sec)')
ylabel('time series')
»
```

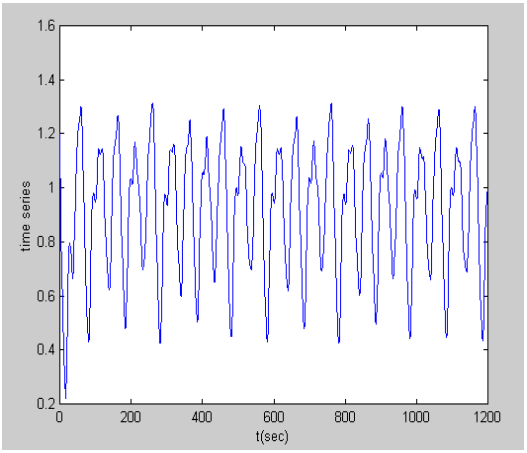

Figure 1. Diagram of data of load of electric energy system of Portugal

The first column is data of load two days ago, the second column is data of load from previous day, the third column is data of load in observed moment [13].

The fourth column presents the exit that is load in the next day, the result. To form the neural network the new function is used that creates feedforward network which syntax is:

net = newff(PR,[S1 S2...SNl],{TF1 TF2...TFNl},BTF,BLF,PF)
opis
NEWFF(PR,[S1 S2...SNl],{TF1 TF2...TFNl},BTF,BLF,PF) takes,
PR - Rx2 matrix of min and max values for R input elements.
Si - Size of ith layer, for Nl layers.
TFi - Transfer function of ith layer, default = 'tansig'.
BTF - Backprop network training function, default = 'trainlm'.
BLF - Backprop weight/bias learning function, default = 'learngdm'.
PF - Performance function, default = 'mse'.
and returns an N layer feed-forward backprop network.

In this case, minmax is matrix of minimal and maximal values of entering vector. Formed network has 3 layers: entering, hidden and output layer of neuron [14]. The process of training the neural network is being done by using the function train. For simulation of network exit the sim function is used [15]. Total number of data is 1000:

- First 500 data is used for training of network,
- Second 500 data is used for checking the validity of created model. This data are located in matrix from 500 data each: trndata and chkdata.

A few models will be analyzed, which are given next in work:

A. The First Model

```
load vremenska.dat
t=vremenska(1:2880,4);
x=vremenska(1:2880,5);
figure(1)
plot(t,x)
xlabel('Period from 1.9.-30.9.2004.')
ylabel ('15-o minut load for period 1.9.-30.9.2004.')
```

In the first model it is selected that the number of neurons in entering layer is 3, in hidden layer 5 and the number of neurons in output layer is 1. Portable functions in entering and hidden layer are ‘tansig’, while in the output layer the selected function is ‘purelin’. The training function is ‘trainlm’, and the learning function is ‘learngdm’. For the simulation the function ‘sim’ is used.

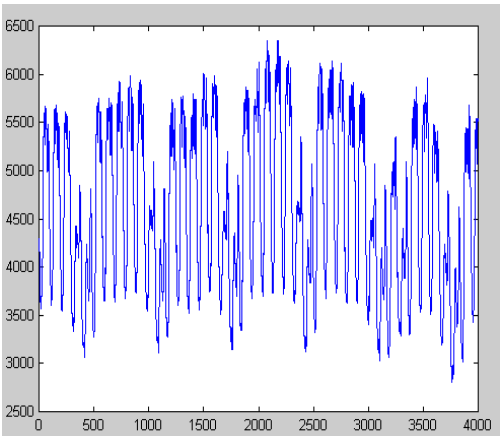

Figure 2. Time diagram of observed network

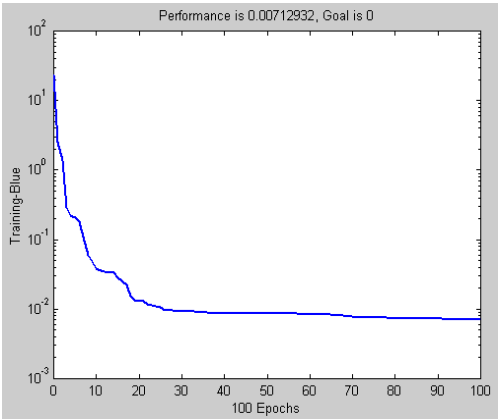

Figure 3. Training process of neural network

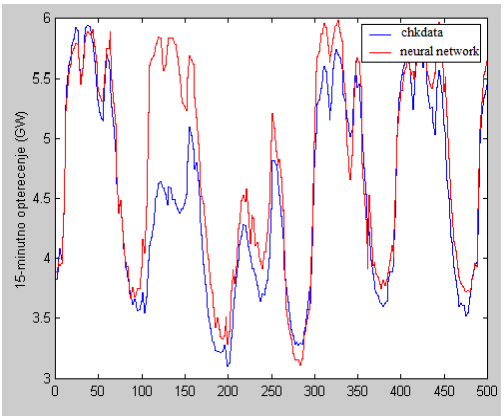

Figure 4. The comparison of desired and real response

B. The Second Model

In the second model, it is selected that the number of neurons in entering and hidden layer is 3 and, in the output, layer is 1. The number of epochs is 100.

C. The Third Model

In the third model it is selected that the number of neurons in entering layer is 3, in the hidden layer is 10 and, in the output, layer is 1. Portable functions are:

- in entering and hidden layer ‘logsig’,
- in output layer ‘purelin’.

The selected number of epoch is 100.

D. The Fourth Model

In the fourth model it is selected that the number of neurons in entering layer is 3, in hidden layer is 10 and in output layer 1 [1]. Portable functions in entering and hidden layer are ‘tansig’, while in the output layer the function ‘trainlm’ is selected. The training function is ‘trainlm’, while the learning function is ‘learngdm’. Simulation function is ‘sim’.

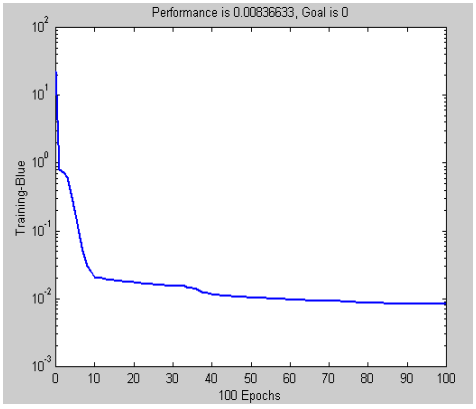

Figure 5. Training process of neural network

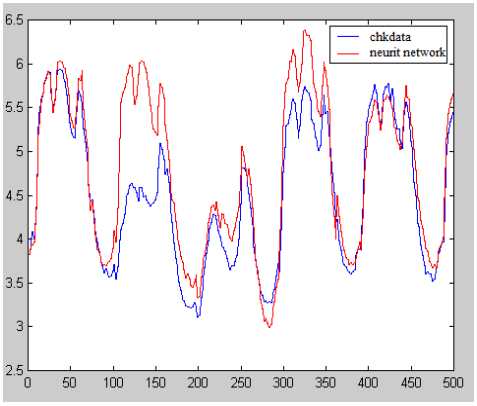

Figure 6. The comparison of desired and real response

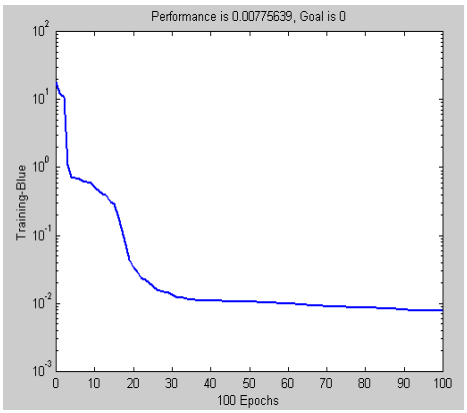

Figure 7. Training process of neural network

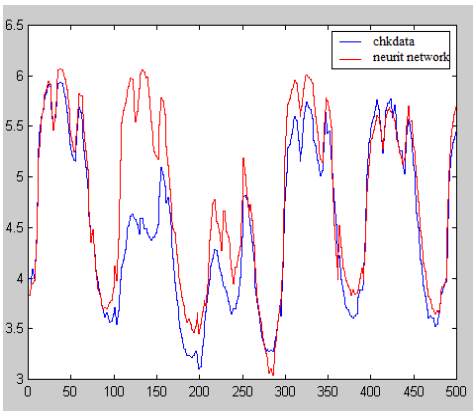

Figure 8. The comparison of desired and real response

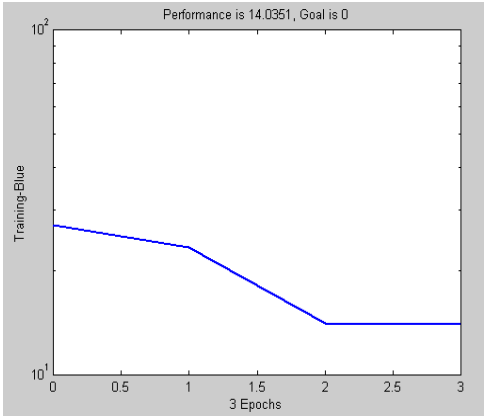

Figure 9. Training process of neural network

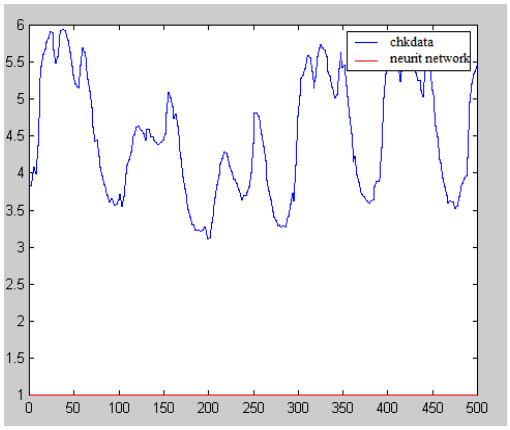

Figure 10. The comparison of desired and real response

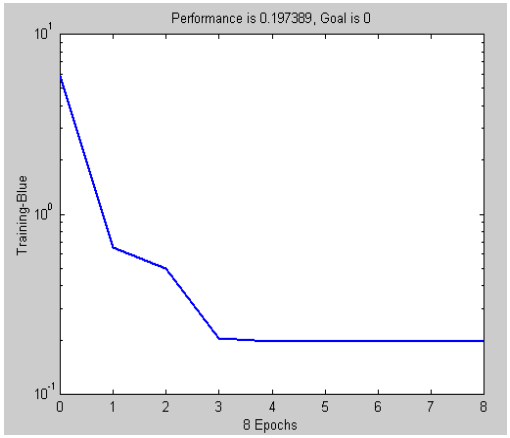

Figure 11. Training process of neural network

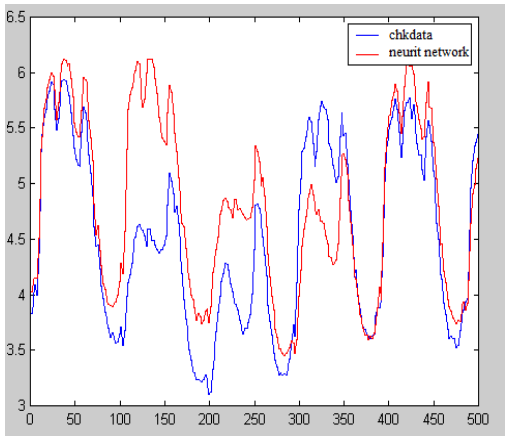

Figure 12. The comparison of desired and real response

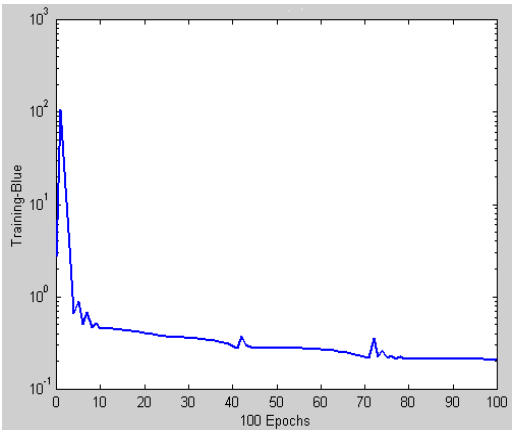

Figure 13. Training process of neural network

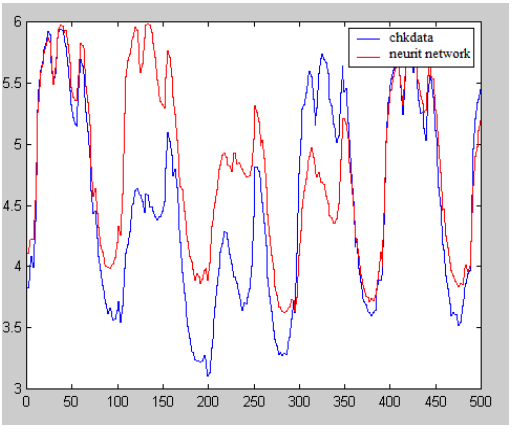

Figure 14. The comparison of desired and real response

E. The Fifth Model

In the fifth model it is selected that the number of neurons in entering layer is 3, in hidden layer is 10 and in output layer 1 [2]. Portable functions in entering and hidden layer are ‘purelin’, while in the output layer the function ‘trainlm’ is selected [3]. The training function is ‘trainlm’, while the learning function is ‘learngdm’ [4]. Simulation function is ‘sim’ [5].

F. The Sixth Model

In the sixth model it is selected that the number of neurons in entering layer is 3, in hidden layer is 10 and in output layer 1. Portable functions in entering and hidden layer are ‘purelin’, while in the output layer the function ‘trainrp’ is selected.

IV. CONCLUSION

Based on the results it is concluded that:

- In all of given examples the analyze of the neuron network with various number of neurons on the hidden layers is done.
- With the increase of the number of neurons the response is much better which is concluded based on the diagrams.
- With changing the training function trainlm and learngd the result of deviation is very little.
- In our concrete example the foresight for one day had been done, and the difference between observed working and non-working days is large.
- To solve that problem it is necessary to get the foresight for the working and non-working days based on the working and non-working days from the database.

REFERENCES

[1] P. E. Nikravesh, Computer Aided Analysis of Mechanical Systems, Upper Saddle River: Prentice-Hall, 1988, pp 32-34.

[2] R. Norton, Machine Design: An Integrated Approach, Upper Saddle River: Prent.-Hall, 1998.

[3] A. G. Erdman, G. N. Sandor, Mechanism Design: Analysis and Synthesis, Upper Saddle River: vol. 1, Prentice-Hall, 1997.

[4] G. Cybenko, „Approximation by superposition of a sigmoid function," Mathematics of Control, Signals and systems, no. 2, 1989, pp. 303-314.

[5] K. Hornik, M. Stinchcombe, H. White, „Multilayer feedforward networks are universal approximators," Neural Networks, no. 2, 1989, pp. 259-366.

[6] J.-S. R. Jang, Fuzzy Modelling Using Generalized Neural Networks And Kalman Filter Algorithm, Proceedings of 9th National Conference on Artificial Intelligence, 1991, pp.762-767.

[7] J.-S. R. Jang, „Self-learning Fuzzy Controller Based On Temporal Back-Propagation," IEEE Trans. Neural networks, vol. 3, 1992, pp. 714-723.

[8] J.-S. R Jang., „ANFIS – Adaptive-Network-Based Fuzzy Inference Systems," IEEE Trans. Man & Cybernetics, vol. 23, 1993, pp. 665-685.

[9] G. B. Wetherill, P. Duncombe, M. Kenward, J. Köllerstörm, S. R. Paul, B. J. Vowden, Regression analysis with applications - Monographs on Statistics and Applied Probability, Chapman and Hall Ltd., New York, 1986.

[10] M. S. Bazara, H. D. Sherali, C. M. Shetty, Nonlinear Programming – Theory and Algorithms, second edition, John Wiley&Sons, Inc., 1993.

[11] D. Nauck, F. Klawonn, R. Kruse, Foundation of Neuro-Fuzzy Systems, John Wiley&Sons, 1997

[12] J.-S, R. Jang, E. Mizutani, Levenberg-Marquardt Method for ANFIS Learning, Proc. Biennial Conference of the Computers, 1996, pp. 665-685.

[13] J. -S, R. Jang, C. -T. Sun, E. Mizutani, Neuro-Fuzzy and Soft Computing – A Computational Approach to Learning and Machine Intelligence, Prentice Hall, 1997.

[14] D. Sprečić, T. Konjić, E. Mujić, V. Miranda, Fuzzy Inference Systems Applied to the Analysis of Machine Mechanisms, IASTED – ASM, pp 25-28, Crete, 2002.

[15] W. E. Fang, F. Freudenstein, „The Stratified Representation of Mechanisms," Journal of Mechanical Design, vol. 112, no. 4, 1990, pp. 514.

Author Index

Bul. Nikole Tesle 63/5, 18000 Niš
Tel. 018 293 920; Fax: 018 293 921
e-mail: office@alfatec.rs; http://www.alfatec.rs
PIB: 104099234; m.b. 20090219; š.d. 73102
t.r.: 165-4863-06; 275-0010220587184-85

R&DC "ALFATEC" was founded in November 2005, with the purpose of enabling placement of innovative products and services developed by a group of researchers, who have worked as a part of the Section of Electric Machinery, at the Department of Energetics of the Faculty of Electronics in Nis.

R&DC "ALFATEC", upon being founded, worked in the field of measurement and control systems, where it has developed a substantial number of innovative products for the needs of various users.

In February 2008, R&DC "ALFATEC" became registered as a research and development centre by the Ministry of Science and Technological Development of the Republic of Serbia.

R&DC "ALFATEC" is currently the leader in:

- the number of realised innovative products and services which are successfully administered on the market of Serbia;
- the diversity of realised projects;
- the projecting and realisation of complex measurement and information systems, as well as measurement and control systems;
- savings of electric energy achieved by various users;
- innovative investment models for electric energy consumption reduction in small and medium-sized enterprises;
- software for decision support in emergency situations;
- design of electrical installations according to international standards.

www.energetics.cosrec.org

ISBN: 978-86-80616-04-9